Polygeneration in HCCI Engines: A kinetic and thermoeconomic analysis with focus on hydrogen production

Von der Fakultät für Ingenieurwissenschaften, Abteilung Maschinenbau und Verfahrenstechnik der

Universität Duisburg-Essen

zur Erlangung des akademischen Grades

eines

Doktors der Ingenieurwissenschaften

Dr.-Ing.

genehmigte Dissertation

von

Dominik Freund
aus
Oberhausen, Deutschland

Gutachter:
Univ.-Prof. Dr. rer. nat. Burak Atakan, Universität Duisburg-Essen
Univ.-Prof. Dr.-Ing. Francesco Contino, Université catholique de Louvain

Tag der mündlichen Prüfung: 03.04.2023

PREFACE

Before you lies the dissertation "Polygeneration in HCCI Engines: a Kinetic and Thermoeconomic Analysis with Focus on Hydrogen Production", which I wrote while working as a research assistant at the Chair of Thermodynamics at the University of Duisburg-Essen from 2018 to 2023. I was engaged in writing this cumulative dissertation from August 2022 to January 2023.

Since the beginning of my studies in 2009, I have been particularly interested in combustion engines in the context of energy supply and am therefore very pleased to be able to dedicate my dissertation to this topic.

My work was embedded in a FOR research unit project about polygeneration, including seven groups from the University of Duisburg-Essen and the Karlsruhe Institute of Technology. I very much enjoyed the collaboration and the exchange of data and results with our colleagues.

I would like to thank my supervisor, Burak Atakan, for his excellent guidance and support during the last five years, which will leave a positive mark on me for life. I appreciate that his door was always open for me to discuss my topic and current problems.
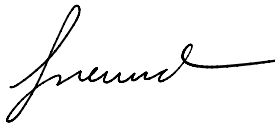
I would also like to thank all co-workers for their great cooperation, without whom I could not have done this work, namely Ali Güngör, Sebastian Kaiser, Kai Banke, Charlotte Rudolph, Christoph Horn, Dennis Kaczmarek, Julian Quenel, and Robert Hegner. I am also very grateful to Sebastian Grimm, Dimitrij Chudinzow and Yiqing Yan for proofreading and Francesco Contino for reviewing my thesis.

I would like to thank Charlotte Rudolph and Dennis Kaczmarek for not only sharing the same office but also their opinions on my work; I especially enjoyed our critical discussions about ideas and results and, of course, the many fun conversa-

tions we had. I would also like to thank the entire group of thermodynamics for accompanying me on this way, I consider you not only as colleagues but as friends.

My special thanks go to my beloved wife Domenica and my beloved son Emilian, who always support and motivate me, but also cheer me up when it is needed! Finally, I thank my parents who have paved the way for me for getting this far.

I hope you enjoy your reading.

Dominik Freund

Mülheim an der Ruhr, May 2023

ABSTRACT

Global greenhouse gas emissions should be reduced in the short term, and increasing efficiency in energy and material conversion is crucial for this. Therefore, novel conversion processes are required and polygeneration in engines poses a possible solution. However, these processes must also be competitive with the cost of conventional processes.

The aim of this thesis is to evaluate the efficiency and costs of fuel-rich operated homogeneous charge compression ignition engines for a simultaneous provision of work, heat, and base chemicals.

In literature fuel-rich operation of conventional spark-ignition engines have been proven. However, high fuel-air equivalence ratios are required for high yields of chemicals such as synthesis gas, but then spark-ignition causes misfires due to a reduced flame speed. In a few recent works, homogeneous charge compression igniting seemed promising for achieving high yields and high exergetic efficiencies. However, a comprehensive study of kinetically feasible and exergetically reasonable operating conditions in combination with an economic analysis has not yet been conducted.

Consequently, this thesis draws the question what operating conditions are feasible and reasonable, considering methane containing fuels, and reactive additives like dimethyl ether and ozone to decrease the required intake temperature and to control ignition timing. Furthermore, the exergetic efficiencies at those conditions are evaluated and the product costs calculated and compared to conventional production processes.

For this purpose, single-zone and multi-zone engine models have been developed in Python, as well as complete process concepts including hydrogen separation.

It was found that ozone is the most suitable additive since if used in small amounts, it decreases the efficiency only slightly, and can be produced on-site. With reactive additives, the engine can be operated at fuel-rich conditions, up to fuel-air equivalence ratios of 2. The exergetic efficiency reaches up to 82 % for the engine only and up to 68 % for a complete process with hydrogen purification and separation. The pressure swing adsorption process is suitable for the separation of hydrogen and the resulting hydrogen costs are found in a range of 2.7 €/kg to 7.2 €/kg, which is competitive to electrolysis processes. To date, conventional steam reforming costs less than all alternatives. The electricity is produced at low costs of 44 €/MWh to 98 €/MWh and is thus competitive to conventional and renewable power plants.

Biogas can also be converted, and CO_2 emissions are then net negative. At very fuel-rich fuel-air equivalence ratios of 6 and higher, promising amounts of the base chemical ethylene are also produced.

In conclusion, homogeneous charge compression ignition engines provide electricity at low costs and hydrogen at competitive costs. Therefore, it is promising to replace conventional steam reforming plants partially by engines in the near future. This could reduce the cost of the necessary CO_2 reduction and ensure base load in the power sector and chemical industry. The flexible operation of the engine could also contribute to grid stability as the share of renewable energy increases.

KURZFASSUNG

Die globalen Treibhausgasemissionen sollten kurzfristig gesenkt werden und ein entscheidender Faktor hierfür ist die Steigerung der Effizienz bei der Energie- und Materialumwandlung. Dazu sind neuartige Umwandlungsverfahren erforderlich und die Polygeneration in Motoren stellt eine mögliche Lösung dar. Allerdings müssen neue Verfahren auch mit den Kosten der konventionellen Verfahren konkurrenzfähig sein.

Ziel dieser Arbeit ist es daher, den Wirkungsgrad und die Kosten von brennstoffreich betriebenen Verbrennungsmotoren mit homogener Kompressionszündung (homogeneous charge compression ignition, HCCI) für eine gleichzeitige Bereitstellung von Arbeit, Wärme und Basischemikalien zu bewerten.

In der Literatur ist der kraftstoffreiche Betrieb von konventionellen Ottomotoren bereits erfolgreich nachgewiesen worden. Für eine hohe Ausbeute an Chemikalien wie z.B. Synthesegas sind jedoch hohe Brennstoff-Luft-Äquivalenzverhältnisse erforderlich, die bei fremdgezündeten Motoren zu Fehlzündungen aufgrund einer reduzierten Flammengeschwindigkeit führen. In einigen neueren Arbeiten schien die homogene Kompressionszündung vielversprechend, um bei diesen Bedingungen hohe Ausbeuten und hohe exergetische Wirkungsgrade zu erzielen. Eine umfassende Untersuchung der kinetisch relaisierbaren und exergetisch sinnvollen Betriebsbedingungen in Kombination mit einer wirtschaftlichen Analyse wurde jedoch noch nicht durchgeführt.

In dieser Arbeit wird daher der Frage nachgegangen, welche Betriebsbedingungen unter Berücksichtigung von methanhaltigen Kraftstoffen und reaktiven Additiven, wie Dimethylether und Ozon zur Senkung der erforderlichen Ansaugtemperatur und

zur Steuerung des Zündzeitpunkts, realisierbar und sinnvoll sind. Außerdem werden die exergetischen Wirkungsgrade unter diesen Bedingungen bewertet und die Produktkosten berechnet und mit konventionellen Produktionsverfahren verglichen.

Zu diesem Zweck wurden Einzonen- und Mehrzonen-Motormodelle in Python entwickelt, sowie komplette Prozesskonzepte einschließlich Wasserstoffabtrennung.

Es zeigte sich, dass Ozon das am besten geeignete Additiv ist, da es in geringen Mengen eingesetzt den Wirkungsgrad nur geringfügig verringert und vor Ort hergestellt werden kann. Mit reaktiven Additiven kann der Motor unter kraftstoffreichen Bedingungen bis zu einem Brennstoff-Luft-Äquivalenzverhältnis von 2 betrieben werden. Der exergetische Wirkungsgrad erreicht bis zu 82 % für den Motor und bis zu 68 % für einen vollständigen Prozess mit Wasserstoffreinigung und -abtrennung. Das Druckwechseladsorptionsverfahren eignet sich für die Abtrennung von Wasserstoff und die resultierenden Wasserstoffkosten liegen in einem Bereich von 2,7 €/kg bis 7,2 €/kg, was mit Elektrolyseverfahren konkurrenzfähig ist. Bislang ist die konventionelle Dampfreformierung kostengünstiger als alle Alternativen. Der Strom wird zu niedrigen Kosten von 44 €/MWh bis 98 €/MWh erzeugt und ist damit wettbewerbsfähig zu konventionellen und erneuerbaren Kraftwerken.

Auch Biogas kann umgewandelt werden und die CO_2-Emissionen sind dann netto negativ. Bei sehr brennstoffreichen Brennstoff-Luft-Äquivalenzverhältnissen von 6 und mehr werden auch vielversprechende Mengen der Basischemikalie Ethylen erzeugt.

Zusammenfassend lässt sich sagen, dass Motoren mit homogener Kompressionszündung Strom zu niedrigen Kosten und Wasserstoff zu wettbewerbsfähigen Kosten liefern können. Daher ist es vielversprechend, konventionelle Dampfreformierungsanlagen in naher Zukunft teilweise durch Motoren zu ersetzen. Dies könnte die Kosten der notwendigen CO_2-Reduktion senken und die Grundlast im Stromsektor und der chemischen Industrie sicherstellen. Der flexible Betrieb des Motors könnte außerdem zur Netzstabilität beitragen, wenn der Anteil der erneuerbaren Energien steigt.

CONTENTS

LIST OF FIGURES

LIST OF TABLES

INTRODUCTION

1.1 Motivation

The reduction of greenhouse gas emissions has become one of the most important tasks in the field of engineering in recent decades and thus, in the literature, many researches have addressed this topic. Some works cited more frequently than average are those of Nakicenovic et al. in 1993 [1], Yamasaki in 2003 [2], and Rogelj et al. in 2016 [3]. Motivated by scientific findings, policymakers have concluded several contracts to counteract the emissions-induced climate change. The first contracts were signed in the 1990s, such as the United Nations Framework Convention on Climate Change (UNFCCC) in 1992 [4] and the Kyoto protocol in 1997 [5], which set greenhouse gas emission reduction goals and established systems for emission trading between the participating countries. Until now, these agreements formed the basis for the further development of emission reduction targets. In 2015, the United Nations defined 17 sustainable development goals to address the most important challenges of human society [6]. One of these goals was defined as climate action [7], which includes the implementation of the UNFCCC in country policies.

In contrast to the increasingly restrictive emission targets, the global primary energy consumption has risen since then and with it greenhouse gas emissions [8]. The usage of fossil fuels increased from 71.4 TWh in 1980 by 94.4 % to 138.8 TWh in 2021 [8]. This includes mainly coal, oil, natural gas, and nuclear fuels. At the same time, the total primary energy consumption increased from 83.2 to 159.0 TWh (+91.1 %). The share of coal, oil, gas, and nuclear fuels consistently decreased, but they were still high in 2021 with a total of 87.3 %.

This ongoing development leads to increasing CO_2 emissions as well, which increased from 19.5 Gt in 1980 to 36.7 Gt in 2019 (+88.2%) [9]. The total greenhouse gas emission were 49.8 Gt (CO_2-equivalent) in 2019 [10]. According to the United Nations Environment Programme (UNEP) this number has to decrease at least to 39 Gt until 2030 to limit the global warming below 2.0 °C, while stating that without further countermeasures an increase to 55.0 Gt is expected until 2030 [11].

Consequently, greater efforts are needed to achieve a significant reduction. According to the Institute of Environmental Management and Assessment (IEMA) [12], the following steps should be conducted regarding greenhouse gas emissions, in

an hierarchical order: avoid, reduce, substitute, compensate. Avoidance of greenhouse gas emission means that, whenever possible, alternative or new operation methods or products should be developed. Moreover, the emissions should be reduced by increasing the efficiency of energy usage, and also technologies using fossil energy carriers should be substituted by renewable or low-carbon technologies. Finally, if these three measures are applied, residual or unavoidable emissions should be compensated, for instance by investing in projects which reduce greenhouse gas emissions equivalently.

Where avoidance is impossible, conventional processes should be improved in efficiency or replaced by novel low-carbon technologies. Hence, the expansion of technologies with so-called renewable sources, which utilizes energy sources such as solar radiation, wind energy, and biomass, is an ongoing process. However, according to the data previously presented, it is not expected that a large proportion of fossil fuels can be replaced by renewables in the short term. The global share of renewable energy sources (RES) in primary energy consumption was 5.7 % in 2021, up only slightly from 2.2 % in 1980. The highest rate of worldwide RES increase per year was recently in 2020 with an increase of 1.22%-pts [13]. With this rate, a 50 % share could be expected in 2032.

However, even in a very ambitious scenario in which global emissions are reduced by two-thirds in 2050 compared to 2020, full coverage by renewables is not feasible [14]. According to the International Renewable Energy Agency, in this scenario, 52 % of the emission reduction would be achieved through the expansion of renewable energies, but the authors also forecast a 27 % share through energy efficiency improvements in the energy, industry, transportation, and buildings sectors, and by switching fuels in the transport sector to electric power and blue and green hydrogen. Therefore, solutions must be found in the short term to increase the conversion efficiency of primary energy carriers.

As a countermeasure to reduce greenhouse gas emissions, improving energy efficiency has been studied for decades and significant progress has been made. For instance, the average efficiency of thermal power plants in the European Union improved by 7.5 %-points to 49.7 % from 1990 to 2016 [15]. Furthermore, cogeneration of heat and power increases energy efficiency, either in coal and natural gas power plants or by using stationary internal combustion (IC) engines. In this comparison, the advantages of IC engines are low costs and high flexibility, in terms of load change, and their on-site applicability. They also achieve energy efficiencies of more than 90 % [16]. Therefore, disused gas or oil boilers are often replaced by IC engines for combined heat and power generation, with the investment being amortized

within a few years [17].

To evaluate the potential of increasing conversion efficiency, the end energy usage of fossil fuels has to be known. According to the International Energy Agency (IAE) [18], five major end energies exist. In 2019, 40.4 % of the end energy were oil products like gasoline and diesel, 19.7 % electricity, 16.3 % natural gas, 10.4 % biomass and biofuels, and 9.5 % coal. The oil and natural gas share in the end energy use is significant with 56.7 %. However, oil and natural gas cannot be completely replaced by carbon-free sources since they are not only used for energy conversion to work and heat, but also for chemical conversion. In 2019 the chemical industry required 14 %, 8 %, and 2 % of the global oil, natural gas, and coal to produce base chemicals such as synthesis gas (a mixture of hydrogen and carbon monoxide), ethylene, propylene, methanol, and ammonia [19]. From that, plastics, resins, solvents, fertilizers, and most of all other chemicals for modern life are produced. Moreover, about 6.8 % of the global green house gas emission can be attributed to non-energy use [18]. Therefore, it seems reasonable to not only increase energy conversion efficiency, but also chemical conversion efficiency, since power-to-liquid technologies are not expected to replace fossil fuel feedstocks in the near future.

1.2 Polygeneration in fuel-rich operated engines

A promising approach to increase the conversion efficiency from primary energy carriers to end products, like electricity and chemicals, is to produce multiple products simultaneously, which can include different energy and material streams at the same time. This is in general called polygeneration and presents an emerging research field. Since 2005 publications including the keyword "polygeneration" rose consistently from 11 per year to a maximum of 302 per year in 2021 [20].

Dincer et al. state that the energy efficiency increases with the number of product outputs, e.g. a cogeneration of heat and power can be enhanced to a trigeneration system by producing hydrogen in an additional process step [21].

A comprehensive review about polygeneration was published by Calise et al. [22] in 2022. According to the authors, polygeneration systems discussed in the literature are mostly a combination of at least two energy or chemical conversion systems, in which one conversion system is the main component. Often, a combination of renewable technologies and conventional technologies is investigated, for instance using solar power to reduce the amount of fossil fuels needed. They also state that the most widely used components for small- and medium-scale energy conversion are internal combustion (IC) engines, since they are cheap, robust, and run with

various fuels (biogas, biodiesel, and different compositions of biogas). Additionally, for high energy efficiency, the heat must be utilized on-site, e.g. for heating or for driving adsorption chillers for cooling.

It must be noted that IC engines convert chemical exergy into exergy of heat and therefore lead to significant exergy losses. Sala et al. conducted an exergy analysis of a medium-scale diesel engine cogeneration plant with a power output of 903 kW in 2006 and found an exergetic efficiency of up to 47.3 % [23], which is a difference of up to 42.7 %-points to the energy efficiency. For a large-scale diesel engine with 5.76 MW power output Yildirim et al. found an even lower exergetic efficiency below 40 % [24].

Consequently, the chemical exergy of methane-based fuels should be converted more efficiently, e.g. by producing base chemicals like synthesis gas as an additional product of the IC engine process. Typically, steam reforming (SMR) is used for converting natural gas to synthesis gas, but also partial oxidation (POX) and autothermal reforming (ATR) is feasible [25]. In the case of steam reforming the exergetic efficiency reaches values of up to 63 % [26].

In 1956 Szeszich et al. proved that partial oxidation of methane for synthesis gas production in spark-ignition (SI) engines is feasible [27]. Over the years there have been a few other works showing that in principle synthesis gas can be produced from methane-containing fuels in SI engines [28, 29].

However, SI operation is limited by reduced flame propagation at high fuel-air equivalence ratios (ϕ). Wiemann et al. [30] found that SI engines engines work at equivalence ratios of up to 1.56, but a further increase in the equivalence ratio leads to misfires. Since homogeneous charge compression ignition (HCCI) engines were already well known from fuel-lean operation [31], it was assumed that they might present an alternative for fuel-rich processes, since they are not dependent on flame propagation, but on chemical kinetics. Therefore, Wiemann et al. investigated the engine in HCCI mode experimentally and achieved stable operation at equivalence ratios of up to 2.4. A comprehensive review about recent progress in fuel-reforming in IC engines was provided by Tartakovsky et al. in 2018 [32].

It must be considered that HCCI operation also poses challenges. The operation of spark-ignition engines is limited by flame propagation and thus controlled by the ignition timing of the spark-plug. On the contrary, HCCI depends solely on the chemical kinetics for autoignition of the fuel-air mixture. Therefore, achieving ignition and controlling ignition timing was investigated thoroughly in the literature, especially for fuel-lean operated HCCI engines. Several solutions exist: exhaust gas recirculation, preheating, pilot injection, turbocharging, fast thermal management,

variable compression ratio, and the usage of reactive additives [33]. Wiemann et al. used a preheating of the intake gas at 120 °C and n-heptane as reactive additive and Hegner et al. [34] investigated exhaust gas recirculation theoretically. These measures can be easily implemented and investigated experimentally. Therefore, exhaust gas recirculation, preheating, and reactive additives were also investigated in this work.

1.3   Exergoeconomic analysis

As discussed before, it has been known for decades that polygeneration in IC engines is generally feasible. Moreover, first studies demonstrated that the HCCI mode is promising for operation in fuel-rich conditions. However, only if polygeneration in HCCI engines is competitive in terms of both efficiency and costs, it can be considered as a viable solution for reducing greenhouse gas emissions in the short to medium term. Consequently, relying only on kinetic and thermodynamic investigations is questionable, and exergetic and economic evaluations should also be performed.

In this context, Oh et al. compared steam reforming, autothermal reforming, and partial oxidation for producing hydrogen for fuel-cell applications in 2018 theoretically [35]. The partial oxidation was conducted in an reactor and, for comparison, in a fuel-rich operated HCCI engine. In this comparison the engine increased the exergetic efficiency of the overall system by up to 6.0 %-pts, achieving a value of 51.9 %. These results indicate that fuel-rich operated HCCI engines are promising alternatives to conventional reforming processes.

Nevertheless, until the writing of this thesis, there was no thorough analysis considering exergetic efficiency and economics of an HCCI engine polygeneration process. To make meaningful statements about the competitiveness of the polygeneration process using HCCI engines, a separation of the products from the product gas mixture of the engine must also be considered. Therefore, two process flow concepts were developed in this work, including water-gas shift reactors for hydrogen enrichment and two different separation technologies. The separation of hydrogen by a palladium membrane was compared with a standard technology, pressure swing adsorption.

The two process concepts were analyzed by applying the Specific Exergy Costing Method (SPECO) [36], which associates each exergy stream with its specific costs. Although the SPECO approach is the most commonly used, there are several others. For a brief comparison it is referred to the work of Lazzaretto and Tsatsaronis [36].

The authors emphasize that the definition of fuel and product streams, which is important for the following analysis, is unambiguous in the SPECO method compared to the other methods.
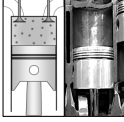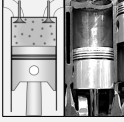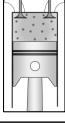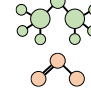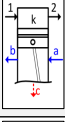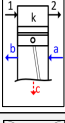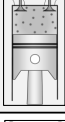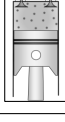
By applying the SPECO approach, each component of a system is analyzed by solving a cost balance based on the costs of the exergy and the component costs; instead of an energy balance. This procedure is called exergoeconomic analysis and is primarily aimed at identifying the components with the highest exergy destruction costs and the highest investments. The analysis also indicates which improvements in terms of efficiency increases or investment cost reductions are promising. It furthermore enables the calculation of the specific costs of the products of the system, for instance electricity, heat, and hydrogen in this work. Exergoeconomic analyses have been applied for a variety of processes in the last decades. Some examples are cogeneration plants [37], combined Brayton/organic rankine cycles [38], solar-geothermal polygeneration systems [39], and fuel cell systems [40].

1.4 Research questions and structure of this work

This thesis is a cumulative thesis, meaning that each chapter represents a published work. At the beginning of each chapter, an introduction is given that sets each publication in the overall context of the thesis. In addition, my own contributions to each publication are highlighted.

As discussed above, no exergetic or exergoeconomic analysis of fuel-rich polygeneration in HCCI engines has been performed to date. Therefore, this thesis aims to answer the following research questions:

1. Are there promising and feasible operating conditions for polygeneration of work, heat, and chemicals?

2. What are the most important underlying kinetic mechanisms of the methane ignition considering additive interactions?

3. What is the resulting exergetic efficiency and how does it compare to conventional processes such as steam reforming and cogeneration?

4. Under what conditions is an overall process concept for the provision of work, heat, and chemicals feasible and favorable, taking into account exergetic efficiency and product costs?

5. What are the main parameters that determine the exergoeconomic results of the overall process?

Chapter		Methods		Fuel	Additive	φ
②	Engine operation with DME		η_{ex}			1.2-2.8
③	Kinetics of DME/ozone interaction		η_{ex} Y_i			1.9
④	Efficiency comparison of DME and ozone		η_{ex} Y_i	+		1.5-2.5
⑤	Exergoeconomics: H$_2$ separation via membrane		η_{ex} €			2.38
⑥	Exergoeconomics: PSA and membrane comparison		η_{ex} €			1.5-2.0
⑦	Biogas conversion for synthesis gas production		η_{ex}			1.0-4.0
⑧	Very fuel-rich operation for ethylene production		η_{ex}	+		1.5-10.0

Legend						
	Engine model		Y_i Kinetics			CH_4
	Engine experiments		η_{ex} Thermodynamics		+	Natural gas
	Process concept		€ Exergoeconomics			CO_2
						DME
						O_3

Figure 1.1: Graphical outline of this thesis.

The first two research questions are addressed in chapters 2, 3, and 4, as presented in figure 1.1. In chapter 2, dimethyl ether (DME) as an additive for fuel-rich combustion of methane is investigated experimentally and theoretically. In chapter 3, the work is expanded towards using ozone as additive and replacing DME partially. To understand the effect of ozone on the ignition kinetics in fuel-rich operation, reaction pathways are analyzed. Chapter 4 bridges the gap between research question two and three: the exergetic efficiency of DME and ozone production are considered and their influence on the overall efficiency is evaluated.

Subsequently, to answer the last two research questions, process concepts were developed and exergoeconomically evaluated. In chapter 5, a first approach with a small-scale engine and a palladium membrane for hydrogen separation is presented. Afterwards, chapter 6 focuses on an improved process concept with a large-scale, industrial-sized engine and a comparison between palladium membrane and pressure swing adsorption (PSA). Moreover, the influence of the input parameters on the exergoeconomic results are discussed, and the specific product costs are compared to conventional processes, including their uncertainty by performing global sensitivity analyses.

In chapters 7 and 8, two alternative approaches are investigated: biogas as fuel and very fuel-rich natural gas mixtures. In chapter 7, biogas is used as fuel and compared to neat methane, to evaluate the feasibility and the exergetic efficiency of the process. In chapter 8, the investigation is expanded to very fuel-rich mixtures of ϕ up to 10 to evaluate the production of higher hydrocarbons such as acetylene, ethylene, and benzene.

Finally, conclusions are drawn for all results presented in this thesis, limitations are discussed, and an outlook for future research is given.

Note

Since I got married in 2020 and my name changed from *Schröder* to *Freund*, the name *Schröder* appears in the chapters that contain my work written before that date.

———

PARTIAL OXIDATION OF FUEL-RICH METHANE/DME MIXTURES IN AN HCCI ENGINE

Introduction to the first paper

The fuel-rich operation of methane in an internal combustion (IC) engine to provide work, heat, and synthesis gas was proven experimentally by Wiemann et al. in 2018 [30]. The authors initially used the spark-ignition (SI) mode and observed misfires if the fuel-air equivalence ratio was increased to 1.6 and higher. Therefore, they changed the combustion mode to HCCI and achieved stable operation. To achieve ignition, n-heptane was successfully utilized as a reactive additive.

In this chapter, dimethyl ether (DME) is firstly used experimentally to achieve ignition of methane in an HCCI engine at fuel rich conditions ($\phi = 1.55$-2.38). DME was chosen, since in contrast to n-heptane, it can be produced from biomass and thus reduce the CO_2 emissions associated with the engine operation. The engine was also modelled using a zero-dimensional single-zone engine model, which was developed in Python to evaluate the product yields and the exergetic efficiency.

The key contributions of this work to the state of the art can be summarized as follows:

– DME was confirmed as a suitable additive for fuel-rich methane ignition.

– In methane/DME mixtures, methane acts as an inert gas until a certain temperature is achieved. Therefore, evaluation of the DME equivalence ratio is crucial for correct ignition timing predictions.

– High synthesis gas selectivities of up to 78 % (H_2) and 79 % (CO) are achieved at $\phi = 2.34$.

– A method is presented to identify stable operation conditions in fuel-rich HCCI experiments.

Author contributions to the first paper

The experiments were conducted by Kai Banke, who also wrote most of the manuscript. Robert Hegner developed the single-zone engine model in Python and initially performed the simulations. My contribution was the recalculation of all simulated results during the revision of the paper and reworking all figures containing simulated data. Furthermore, I investigated the sensitivity of the intake temperature on the outcomes and wrote the according section of the manuscript. Sebastian Kaiser and Burak Atakan were involved in the analysis of the data and the revision of the manuscript. They were also responsible for the supervision of the project.

Table 2.1: Author contributions for chapter 2 following the CRediT author statement methodology [41].

Author	Banke	Hegner	Freund	Atakan	Kaiser
Conceptualization	✓			✓	✓
Methodology	✓	✓	✓		
Software		✓	✓		
Validation	✓	✓	✓		
Formal analysis	✓	✓	✓		
Investigation (simulation)		✓	✓		
Investigation (experiments)	✓				
Resources				✓	✓
Data curation	✓	✓	✓		
Writing - Original draft	✓	✓	✓		
Writing - Review & editing				✓	✓
Visualization	✓	✓	✓		
Supervision				✓	✓
Project administration				✓	✓
Funding acquisition				✓	✓

2.1 Abstract

Polygeneration is the coupling of energy conversion and conversion towards useful chemicals, providing a route towards more flexible and efficient energy systems. In this work, we explore a particular concept of polygeneration using an internal combustion engine as a reactor for partial oxidation to generate synthesis gas in variable combinations with mechanical work and heat. Experiments were performed in a single-cylinder engine operated in homogeneous charge compression ignition (HCCI)

mode on a mixture of methane and air with dimethyl ether (DME) as a reactivity-enhancing additive. For intake temperature from 100 to 190 °C, the range of stable, non-sooting operation with acceptable pressure-rise rates was determined in terms of equivalence ratio and DME mole fraction in the fuel. At 150 °C intake temperature, 8.7 to 9.5 % DME were needed to stabilize operation at equivalence ratios between about 1.3 and 2.7.

Experimental results from fuel-rich conditions with equivalence ratios ranging from 1.65 to 2.34 were compared to simulations with a homogeneous, single-zone engine model. The concept of exergy was used to investigate the thermodynamic performance of the polygeneration engine. The effect of the equivalence ratio on work and heat output, thermal and exergetic efficiency, and selectivity towards useful product species was investigated. In the experiments a work output of up to 160 J ($\phi = 1.65$) per cycle (IMEP = 4.82 bar) and exergetic efficiencies of up to 81.5 % ($\phi = 2.34$) were achieved. The simultaneous generation of synthesis gas had a selectivity of up to 72 % for hydrogen and 79 % for carbon monoxide (both at $\phi = 2.34$).

2.2 Introduction

Fossil fuels are still an essential part of today's energy supply, in particular contributing most of the base load. The limited availability of these resources and efforts to reduce CO_2 emissions encourage the development of flexible and efficient energy conversion schemes. In the case of internal combustion (IC) engines, flexibility means varying the engine load, which is usually associated with decreasing efficiency. Alternatively, the part-load efficiency could be increased by only partially oxidizing the fuel, thus simultaneously generating a reduced amount of work while producing useful chemicals.

Such processes, coupling energy conversion and chemical conversion, are usually called "polygeneration". Common polygeneration processes couple power cycles or another means of power generation with chemical conversion or thermal separation process, e.g., steel or methanol production [42–44]. In contrast, it is also possible to modify a single, integral process – e.g., IC-engine combustion – to obtain variable ratios of mechanical work, process heat, and chemicals. Operating an engine with partial oxidation allows to quickly reduce its work output in favor of generating chemicals that maintain a part of the fuel exergy.

In initial studies on synthesis-gas generation in engines, Karim et al. [45] used Diesel-fuel pilot injection to achieve ignition. They demonstrated syngas (sum of

H_2 and CO) production with dry-gas mole fractions of up to 80 % at $\phi = 2.4$.

Yang et al. [46] operated an HCCI engine at $3.1 < \phi < 9.1$ and achieved syngas mole fractions of 27 %, while Szeszich investigated spark ignition (SI) of CH_4 resulting in up to 90 % syngas [27]. While these experiments demonstrated the feasibility of syngas generation in engines, some relied on highly (up to 90 % O_2-enriched air to prevent misfires. High pressure-rise rates limited the range of operating conditions and none of the studies discussed how the additional oxygen could be provided.

Experiments with air were conducted by McMillian and Lawson, who investigated a fuel-rich natural-gas SI process, but also modeled an HCCI process [28]. With SI, they successfully produced syngas (up to 21 % at $\phi = 1.62$).

In investigations with the more conventional goal of reducing emissions from vehicle engines, it was shown that in SI multi-cylinder engines operating one engine cylinder fuel-rich and transferring the generated syngas to the other, stoichiometrically operated cylinders can improve combustion characteristics [29].

A recent review discusses a broad range of in-cylinder fuel-reforming processes [32].

In previous work, we theoretically investigated HCCI engine operation over a wide range of equivalence ratios ($0.5 < \phi < 10$), supported by experiments in a rapid compression machine (RCM) [47] with 10 mol% DME as a reactivity-enhancing additive. Besides synthesis gas, up to 1 % C_2H_4 was formed at $\phi = 7$. A polygeneration concept was developed based on fuel-rich HCCI combustion, including product-gas treatment [34]. This process provides flexible amounts of power and H_2 by varying the amount of recirculated product (exhaust) gas.

In experiment and simulation, Wiemann et al. compared fuel-rich SI and HCCI operation to fuel-lean combustion [30]. To achieve autoignition of methane, 5 mol% n-heptane was used as additive. An exergetic efficiency of 45 % was achieved at $\phi = 0.72$ and 81 % at $\phi = 2.42$. While SI led to misfires at $\phi > 1.5$, HCCI enabled operation up to $\phi = 2.42$, where soot formation became the limiting factor. Because of the potential for stable and efficient fuel-rich operation, we focus on HCCI in the current work. As a reactive additive, DME is used here, representing a class of fuel compounds that can be derived from biomass [48, 49].

Expanding on our previous work, we determine the limits of stable HCCI operation with a systematic variation of the additive concentration and intake temperature. Within the stable operating range, we evaluate product yields and exergetic efficiencies of the engine process. Experimental results are compared to those from simulations using a single-zone engine model in terms of work and heat output,

thermal and exergetic efficiency, and selectivity towards useful product species.

2.3 Experiment and model

Engine instrumentation and operation

The experiment is similar to that in Ref. [30]. Thus, only a brief summary is given here (Fig. 2.1). A single-cylinder BASF-type octane-number test engine was modified to run on gaseous fuels. The in-cylinder pressure was recorded as a function of the crank angle (°CA). Except for water, which is condensed at 3 °C and removed before analysis, and N_2, the major product-stream species ($H_2, CO, CH_4, CO_2, O_2, C_2H_4$) were detected with an exhaust-gas analyzer (ABB, Type Advance Optima 2020). Soot was monitored with a filter smoke meter (AVL 415S).

Gaseous CH_4 and DME were metered by mass-flow controllers (MFC), electrically heated from 100 to 190 °C, and continuously injected into the intake manifold. The overall equivalence ratio ϕ is calculated from Eq. 2.1 with all volume flows at standard conditions.

$$\phi = \frac{0.21\dot{V}_{air}}{2\dot{V}_{CH_4,in} + 3\dot{V}_{DME,in}} \tag{2.1}$$

The engine was operated at $1.2 < \phi < 2.8$ under the conditions listed in Table 2.2. DME was added to the methane fuel at 5.9–11.2 mol%. Before recording data, the engine was run in SI mode on CH_4 until the coolant reached 100 °C. HCCI was then initiated by adding DME to the mixture. Data recording was started once the measured product-gas composition was stable. For each experiment, the intake flow rates, product-gas mole fractions, temperatures, and 140 cycles of pressure data were recorded. The indicated mean effective pressure (IMEP) and the maximum pressure-rise rate (PRR_{max}) were calculated for each cycle and averaged over all cycles. The coefficient of variation (CoV) is usually calculated as the standard deviation of IMEP divided by its mean over a series of cycles. Here, instead of using IMEP, the difference of IMEP of a single cycle and IMEP of a motored cycle was used. This yields a metric that is more closely correlated with combustion instability. The apparent heat release rate was calculated from the averaged pressure trace without taking into account heat losses. From this, the center of combustion (CA50) was determined, i.e., the crank angle at which the cumulative heat release reaches 50 % of its eventual total.
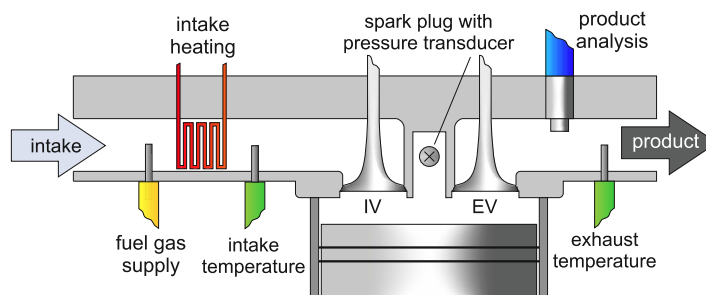
Figure 2.1: Instrumentation and fuel supply of the single-cylinder engine.

Table 2.2: Engine properties and operating conditions.

Engine parameter	Value
Engine type	4-stroke 2-valve single cylinder
Fuel	$CH_4 + CH_3OCH_3$
Displacement	332 cm^3
Bore/stroke	65/100 mm
Connecting rod length	200 mm
Compression ratio	10
Engine speed	600 min^{-1}
Intake temperature	100-190 °C
Intake pressure	1 bar
Coolant temperature	100 °C

Engine model

The in-cylinder processes were simulated with spatially-homogeneous time-dependent chemical kinetics considering the compression and expansion strokes, starting at bottom dead center with closed valves. The reactor model in Cantera within Python [50] was used for modeling with a detailed reaction mechanism from Yasunaga et al. (214 species, 1216 reactions) [51, 52]. For this mechanism, experiments in shock tubes, RCMs, and flow reactors showed good agreement between simulation and experiment in terms of ignition delay time and product gas species ($CH_4, DME, H_2, H_2O, CO_2, CO$) for DME/$CH_4$ mixtures at $\phi = 2$ [53–56]. The engine model developed here, described in more detail in [30], is based on solving the time-dependent differential equations for conservation of species and energy. It includes wall heat transfer and residual-gas content and is comparable to the single-zone model by Caton and Zheng [57]. Engine parameters and intake conditions were taken from the experiment.

Heat transfer was estimated using Woschni's formulae (Eqs. (2.2) and (2.3)) for

14

Table 2.3: Parameters for the heat-transfer estimate according to Woschni [58].

Woschni-parameter	Value
C	127.9
r	0.53
C_1	2.557
C_2	0.4354

the convective heat transfer coefficient α [58] as a function of temperature T and pressure p in the combustion chamber.

$$\alpha = Cd^{-0.2}p^{0.8}w^{0.8}T^{-r} \tag{2.2}$$

The values of the constants used here are listed in Table 2.3. In Eq. (2.2), d is the diameter of the cylinder and w is a corrected velocity accounting for turbulence during combustion, calculated as

$$w = C_1 u + C_2 \frac{V_D T_0}{p_0 V_0}(p - p_d) \tag{2.3}$$

where V_D is the cylinder displacement, T_0, V_0, p_0 are the temperature, volume (in SI base units), and pressure at the beginning of compression, p_d is the motored pressure (both in bar) and u is the mean piston speed. The factor C_2 was adjusted to match the total heat transfer derived from the energy balance of the experiment at $\phi = 1.65$. This set of constants was then used for all other simulations. Even though in general the Woschni model is known to be inaccurate for predicting heat transfer for HCCI modeling [59–61], here, it yielded total heat losses matching the experimentally determined ones, possibly because α does not vary much across our experiments.

The mass of residual gas remaining in the cylinder m_{RG} was estimated as that of the product gas (temperature, pressure, and composition at bottom-dead center of the expansion stroke) filling the clearance volume of the cylinder (i.e., the volume at top-dead center). This mass is then subsequently adiabatically mixed with the experimentally determined fresh-gas mass m_{FG} with the intake temperature T_{int}. This simple "empty-and-fill" model is considered sufficient here since the engine does not have valve overlap and the exhaust valve closes near top-dead center. By this estimate, about 10 % (by mass) of gas from the previous cycle remain in the cylinder and mix with the fresh charge of the next cycle. In other words, multiple cycles were simulated transferring 10 % of the product gas to the next cycle. For each cycle, the initial temperature for the simulation was the adiabatic mixing temperature of fresh charge and residual gas. The product-gas composition, work and heat output, and

exergetic and thermal efficiencies were then averaged over 20 simulated cycles. The total heat transferred to the coolant was calculated by summing over the incremental heat transfer estimated via Woschni's approach at each step of the simulation.

Exergy balance and selectivity

Conventionally, the exhaust gas of ICEs mainly contains the products of complete combustion. The product gas in polygeneration in contrast contains useful species and thus remaining chemical and internal energy that is evaluated by calculating the exergy flows entering and leaving the system. Unlike energy, exergy can be destroyed. The corresponding exergy losses, caused by irreversibilities, were used to evaluate how well the fuel exergy is converted to work or conserved in the product gas. The losses in exergy E_l are calculated based on the Gouy-Stodola theorem ($E_l = T_{sur}S_{irr}$) [62] from the ambient temperature T_{sur} (298 K) and the entropy generation S_{irr} over the engine cycle. The corresponding exergetic efficiency η_{ex} is determined by Eq. (4) under the assumption that exergetically valuable outputs (work, heat, product gas) are used outside the engine and not lost to the environment. The exhaust enthalpy is included among the useful outputs assuming that in the envisioned stationary applications the product gas also provides process heat. The specific chemical exergies of methane $e_{CH_4} = 52.3$ MJ/kg and DME $e_{DME} = 30.9$ MJ/kg were taken from [63].

$$\eta_{ex} = 1 - \frac{E_l}{m_{CH_4}e_{CH_4} + m_{DME}e_{DME}} \tag{2.4}$$

The experimental data were used to calculate the work output, the heat transferred to the cooling water, and the exergetic efficiency using the thermodynamic data available through the Cantera modules together with the first and second laws of thermodynamics, as detailed in [30].

Selectivity is a useful metric to compare chemical conversion in simulation and experiment. However, the present gas analysis cannot determine the fractions of water, nitrogen, and higher hydrocarbons (other than ethylene) in the product gas, thus, the outgoing molar product flow $\dot{n}''$ cannot be calculated. Some assumptions where made to calculate conversions and selectivities. The first assumption is that the additive's conversion is equal to the methane conversion. Combustion quenching near walls and in particular in crevices results in low temperatures that stop both the conversion of methane and DME. This assumption is supported by preliminary gas chromatography measurements in the product gas that in fact show similar methane and DME conversion. These measurements also showed that at $\phi = 1.9$ the

mole fraction of higher hydrocarbons (except for DME and C_2H_4) in the product gas was negligible, which we then assumed to be true for all of the current data evaluation. This may lead to increasing uncertainties for $\phi > 2$, because soot production increases, which also implies increased formation of acetylene, benzene, and other soot precursors.

The remaining unknown mole fractions in the product stream are that of nitrogen, x''_{N_2}, and water, x''_{H_2O}. These were calculated based on the species balance for hydrogen, Eq. (2.5), and condition that all product mole fractions add to unity Eq. (2.6). Only the hydrogen balance is used here because the oxygen measurement has lower accuracy.

$$\dot{n}'(2x'_{CH_4} + 3x'_{DME}) = \dot{n}''(2x''_{CH_4} + 3x''_{DME} + 2x''_{C_2H_4} + x''_{H_2O}) \qquad (2.5)$$

$$1 = \sum_i x''_i = x''_{N_2} + x''_{H_2} + x''_{CH_4} + x''_{C_2H_4} + x''_{CO_2} + x''_{CO} + + x''_{O_2} + x''_{H_2O} + x''_{DME} \quad (2.6)$$

The outgoing molar flow $\dot{n}''$ can be calculated from the known mass flow $\dot{m}$ through the engine and the mean molar mass of the product flow M''_{mean}, which is again a function of the mole fractions x''_i.

$$\dot{n}'' = \frac{\dot{m}}{M''_{mean}} \qquad (2.7)$$

For convenience, this system of equations was solved numerically. Then $\dot{n}''$ is used to determine conversions X_i, yields Y_i, and selectivities S_i as defined in Eqs. (8)–(10) with ν_i being the number of molecules of species i formed by theoretical total conversion of the fuel towards this species and the incoming and outgoing molar flow of species i, $\dot{n}_i'$ and $\dot{n}_i''$, respectively.

$$X_i = \frac{\dot{n}_i' - \dot{n}_i''}{\dot{n}_i'} \qquad (2.8)$$

$$Y_i = \frac{\dot{n}_i''}{\dot{n}_i'(x'_{fuel}\nu_i)} \qquad (2.9)$$

$$S_i = \frac{Y_i}{X_{fuel}} \qquad (2.10)$$

This procedure results in conversions, yields, and selectivities that include the error of the hydrogen measurement.

2.4 Results and discussion

Operating envelope and mixture reactivity

Since HCCI combustion is controlled kinetically, engine operation mainly depends on equivalence ratio, fuel composition, and the temperature-pressure history. With CH_4 as the base fuel, some DME is needed for autoignition, but too much of it may over-advance combustion phasing, leading to excessive pressure-rise rates that potentially damage the engine. For determining DME concentrations for "acceptable" engine operation, two criteria were set: CoV < 5%, and PRR_{max} < 10 bar/°CA. The dependence of the engine operation on the DME mole fraction was evaluated in an experiment with 8.17 standard liters per minute (slm) CH_4. The DME flow was increased stepwise from 0.5 to 1.0 slm in 0.05-slm increments, corresponding to 5.9–11.2 mol% DME in the fuel. This also led to a change of ϕ from 1.66 to 1.84, however, as we will see, ϕ has much less influence on the engine operation than the DME concentration. The results for IMEP, CoV, and PRR_{max} are shown in Fig. 2.2a as a function of DME mole fraction while Fig. 2.2b shows the combustion phasing as CA50 in °CA after top dead center. For negative IMEP, CA50 was not considered meaningful and is suppressed in the plot.

Error bars are calculated from the specification of the MFCs, the pressure sensor, and the air-flow meter. At low DME concentrations, no ignition occurs, resulting in a negative IMEP. Increasing x_{DME} to ∼7 % leads to sporadically firing cycles and high CoV. Further increase in x_{DME} results in a higher number of firing cycles and increasing IMEP. The x_{DME} at the exact operating limits was determined by interpolation. The lower limit (CoV = 5 %) is reached at x_{DME} = 8.6 %. At x_{DME} = 9.1 %, the first data point within the limits for acceptable engine operation was recorded. Increasing x_{DME} even further leads to higher pressure-rise rates, because ignition shifts to earlier crank angles. At about x_{DME} = 9.8 %, the pressure-rise rate exceeds the limit of 10 bar/°CA. As expected, adding more DME advances the combustion phasing, with stable operation concurring with a CA50 around 15 °CA.

For further investigation, this operability scan was abbreviated and performed for different CH_4 flows just until a CoV < 5 % could be established before recording was started. Using higher x_{DME} was not beneficial, because it led to lower IMEP and higher PRR_{max}. This results in the choice of the lowest x_{DME} (in this example 9.1 %) within the operating limits. This scan in the DME mole fraction was performed for methane flows from 6.17 to 11.67 slm in 0.5 slm increments and four intake temperatures (100, 130, 150, and 190 °C, see Fig. 2.3).
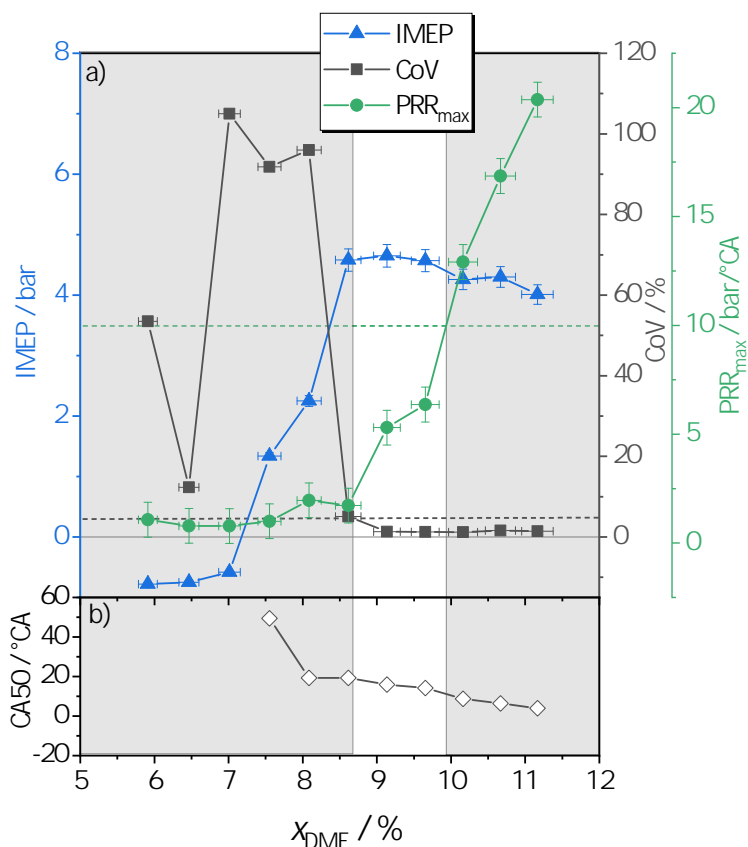
Figure 2.2: a) IMEP, CoV, and PRR_{max}, and b) CA50, all for varying x_{DME} at a constant methane flow of 8.17 slm and an intake temperature of 150 °C. The white region in the graph marks acceptable engine operation, dashed lines mark the limits for acceptable CoV and PRR_{max}.

The lower limit of the investigated equivalence ratios is given by excessive PRR. At this limit, adding sufficient amounts of additive to fulfil the CoV criterion resulted in exceeding the PRR limit. The upper limit is given by excessive soot formation at high equivalence ratios. The required amount of DME is highest for the lowest intake temperature, 100 °C, which is expected because the mixture reactivity is lowest here. At higher temperatures, no systematic correlation between required x_{DME} and intake temperature was found. Considering error bars, for intake temperatures higher than 100 °C and at equivalence ratios around 2, the required DME mole fraction does not significantly depend on temperature. At all temperatures, less DME is needed both at low and at high ϕ. The decrease for low ϕ is steep and results from the increasing sensitivity of the PRR to x_{DME} and increasing energy content closer to stoichiometric conditions. Somewhat counter-intuitive is the decrease of
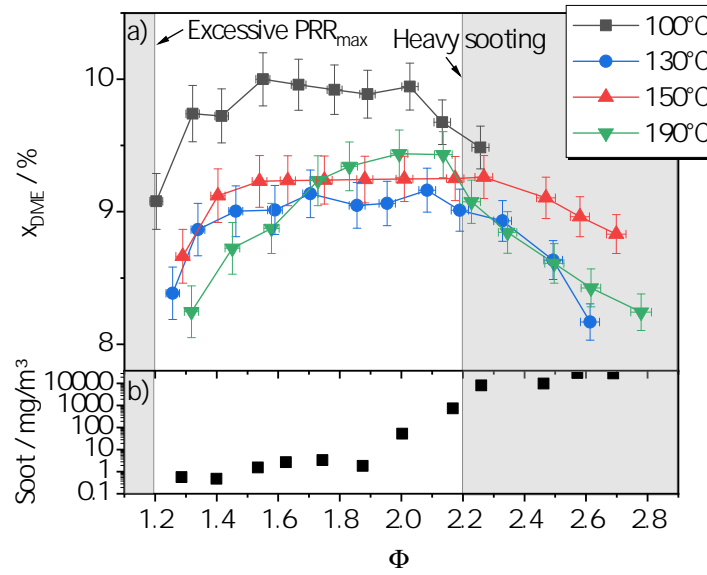
Figure 2.3: a) DME mole fraction x_{DME} required for stable engine operation at different intake temperatures as a function of equivalence ratio ϕ. b) Soot concentration in the product stream for 150 °C intake temperature.

the required x_{DME} for increasing ϕ above 2, discussed in more detail below. Finally, since for an intake temperature of 150 °C the required x_{DME} is nearly constant at $\sim$9.3 % in the range of $\phi = 1.6$–2.3, this range and intake temperature were selected for further analysis. A slightly higher x_{DME} of 9.5 % was chosen to ensure operation within the stability limits.

Fig. 2.4a shows experimental traces of the cylinder pressure for operation at three different equivalence ratios. Dashed lines represent experimental data and solid lines the simulation results. Additionally, the simulated conversion of CH_4 and DME as a function of the crank angle is shown. Fig. 2.4b shows the temperature from the simulation.

The most noticeable feature is the early-shift in combustion phasing with increasing ϕ, in experiment and simulation. One might expect the contrary, because $\phi > 1$ generally suggests lower mixture reactivity. A possible explanation is that the *overall* equivalence ratio is indeed further from $\phi = 1$, but the equivalence ratio ϕ_{DME} based on the additive DME *alone* is closer to stoichiometric.

The simulation results in Fig. 2.4a show that significant CH_4 conversion starts when already about half of the DME is converted. If CH_4 is considered inert at the start of combustion, which is a reasonable approximation compared to DME [64], ϕ_{DME} is very lean for all cases, as the values in the legend of Fig. 2.4a show.
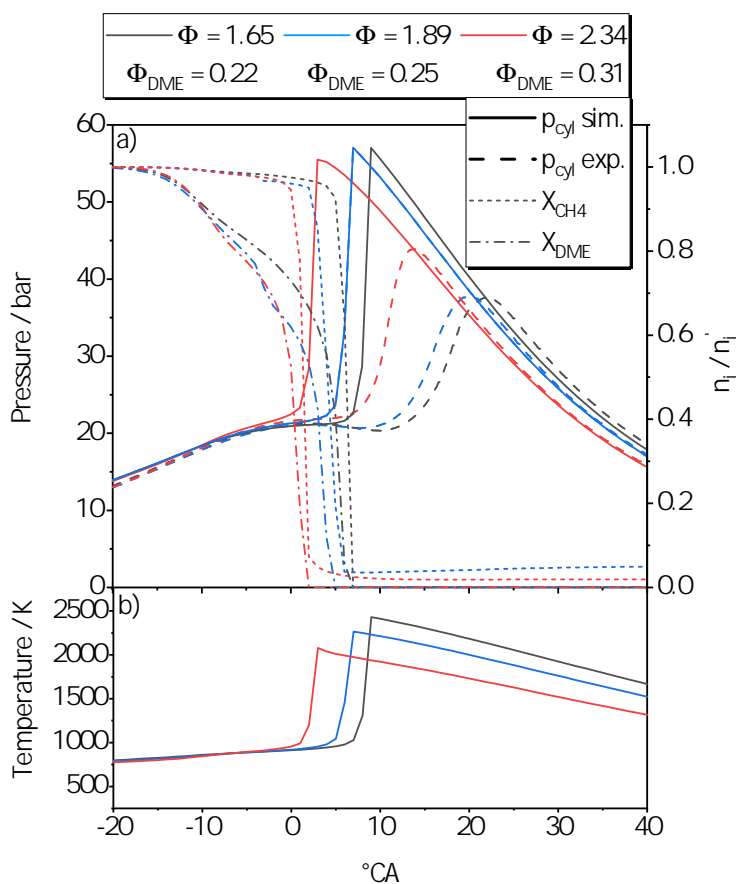
Figure 2.4: a) Pressure traces from experiment and simulation as well as simulated CH_4 and DME conversion. b) Temperature traces from the simulation. All at 150 °C intake temperature, x_{DME} of 9.5 %, and for three equivalence ratios.

Increasing this equivalence ratio enhances reactivity. This explanation is supported by the simulations showing that the DME conversion shifts towards earlier crank angles with increasing ϕ (Fig. 2.4a), suggesting an increased reactivity.

In the experiments, the lower heat-release rate of richer mixtures is compensated by the heat release taking place at smaller cylinder volumes, leading to increased peak pressures. In the simulations, ignition takes place closer to TDC, where the change in volume per degree CA is small and cannot compensate the reduced heat release rate, resulting in decreasing peak pressures for richer mixtures.

As expected, the maximum temperatures (Fig. 2.4b) decrease with increasing equivalence ratio due to lower heat release. At $\phi = 2.34$, the peak temperature is 2050 K, and Fig. 2.3b shows increased soot formation. This is consistent with previous findings that soot formation is especially strong at temperatures between

1500 and 2000 K and equivalence ratios above $\phi = 2$ [65].

Another unexpected result is that the pressure traces obtained from the simulation predict much earlier ignition than the experimental data (in addition to the overly fast combustion that is due to the single-zone model not capturing thermal stratification [66]). This may be due to differences between the initial conditions in experiment and simulation.

In the simulation, the temperature of the fresh charge in the cylinder (to which the residual gas is then added) is assumed to be the same as the intake temperature. The actual temperature in the experiment is likely to be lower due to heat loss to the walls before the intake valve closes, reducing both the fresh-gas and residual product-gas temperatures. Temporally inaccurate modeling of heat transfer may also induce differences in the pressure traces between simulation and experiment. Since HCCI ignition is highly sensitive to temperature, higher temperatures in the simulation would lead to earlier ignition.

To evaluate the impact of this uncertainty, the mixing temperature (the temperature at the start of compression) and the residual gas content were varied in the simulation. As shown in Fig. 2.5, at $\phi = 1.65$, reducing the mixing temperature by $\Delta T = 8$ and 15 K delays ignition by 4° and 11° crank angle, respectively. The pressure traces at these two reduced temperatures roughly bracket the experimental trace. Similar results are found for other equivalence ratios.

At $\phi = 1.65$, increasing the residual gas content in the simulation by 50 % advances the peak pressure by only 2 °CA, while there is no significant change for $\phi = 2.34$. This low sensitivity may be due to the fact that intake and product-gas temperatures are similar, differing only by 141 K and 56 K for $\phi = 1.65$ and 2.34, respectively. From this sensitivity study we conclude that the systematic difference in combustion phasing between experiment and simulation is likely due to inaccuracies in the simulation's starting temperature that are well within the uncertainty of estimating that temperature and could be accounted for by an adjustment of about 10 K.

Increasing the residual gas mass by 50 % in the simulation changes the synthesis gas mole fractions insignificantly, but the CH_4 conversion decreases. For example, at $\phi = 2.34$ the H_2 and CO mole fractions decrease by 2.6 % and 1.7 % respectively while the CH_4 slip increases by 61 %.
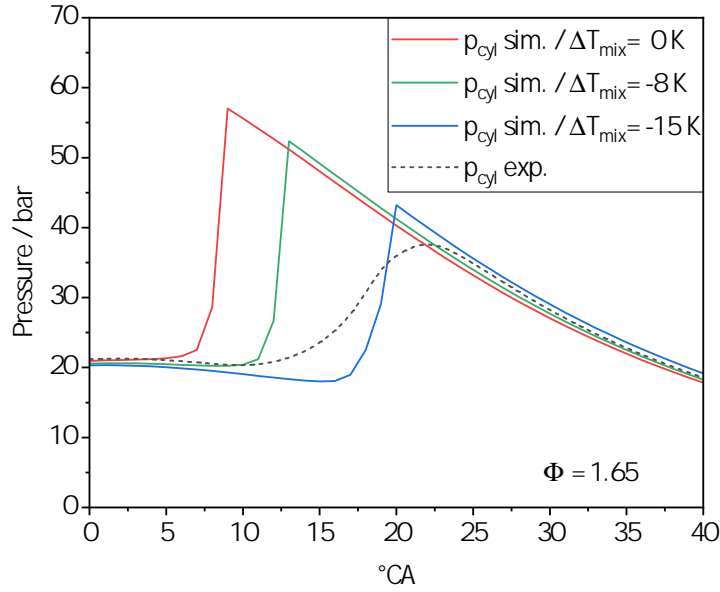
Figure 2.5: Pressure traces from experiment and simulation with a variation of the initial temperature T_{mix} at the start of compression.

Fuel conversion and product-gas composition

Simulated and measured CH_4 conversion is compared in Fig. 2.6. The experimental uncertainties for the conversion and selectivities were calculated from the specifications of the gas analyzer.

The methane conversion decreases with increasing ϕ in both experiment and simulation. This effect can be attributed to the lower maximum temperatures and lower oxygen content at fuel-rich conditions, both impeding fuel conversion. Maximum simulated temperatures at $\phi = 1.65$ are about 2430 K, but at $\phi = 2.34$ only 2080 K. It is a well-known problem that HCCI single-zone models tend to overestimate the fuel conversion [30, 66, 67], in this case by about 9 percent points at $\phi = 1.65$ and increasing with ϕ, because in the engine, the lower temperatures near the cylinder walls and higher temperatures in the core gas lead to reduced fuel conversion in the wall-near regions. Single-zone models however, consist of only one zone of comparably hot gas, where most of the fuel is converted.

We discuss the selectivity in this work since we can qualitatively compare results from experiment and model despite the difference in fuel conversion. The results for the product species $H_2, CO, CO_2,$ and C_2H_4 are shown in Fig. 2.7.

Generally, the selectivity of the potentially valuable species H_2, CO, and C_2H_4 is increasing with increasing ϕ. While the selectivities of CO, CO_2, and C_2H_4
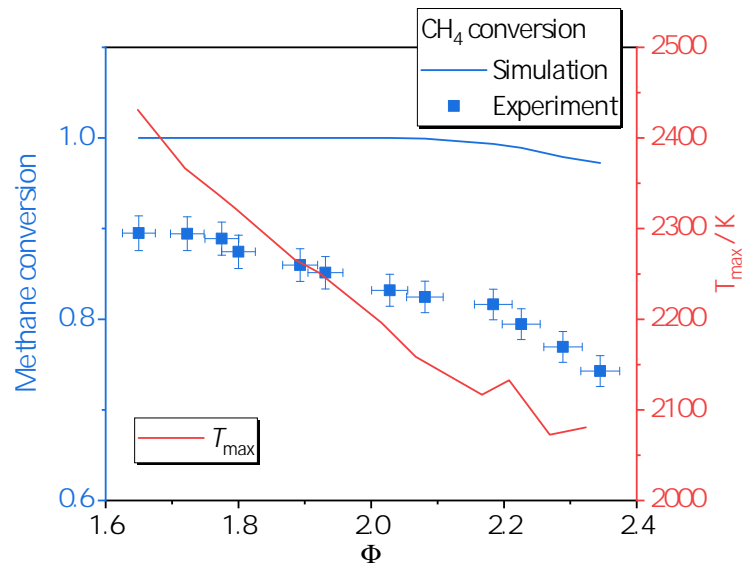
Figure 2.6: Methane conversion and maximum (simulated) temperatures as a function of equivalence ratio. Symbols: experiment, lines: simulation
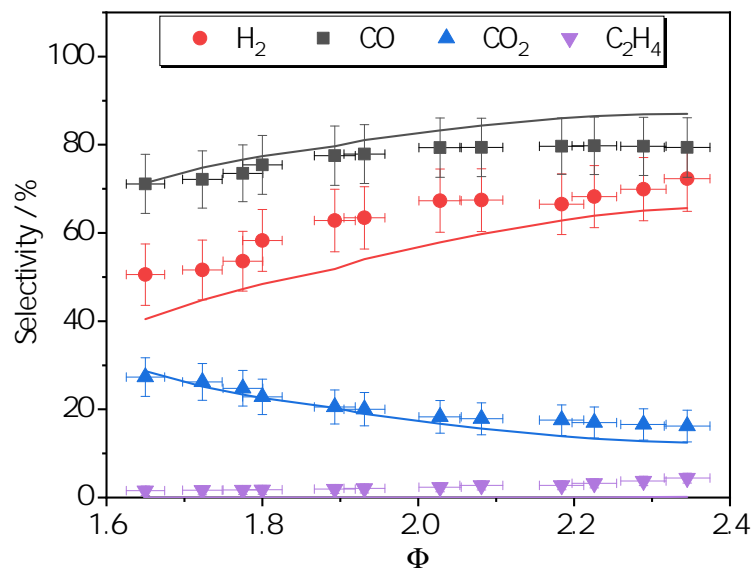
Figure 2.7: Selectivities of product-gas species. Symbols: experiment, lines: simulation

add up to 100 % in the simulation, a sum of 117–122 % was obtained from the measurement. This indicates that the experimentally-obtained carbon balance is inaccurate, probably due to uncertainties in the product-gas analysis and mass-flow controllers. Here, we account for the carbon excess of about 17–22 % by dividing the selectivities of the carbon-containing species by their corresponding sum at each equivalence ratio. Experimentally, as ϕ increases from 1.65 to 2.34, H_2 selectivity increases from 50 to 72 %, CO from 71 to 79 %, and ethylene from 1.5 to 4 %, while the CO_2 selectivity decreases from 27 to 16 %. The decreasing O_2 content and the consequently lower maximum temperature can explain these trends. The formation of H_2O and CO_2 from H_2 and CO at high ϕ is limited by the low O_2 concentration, thus a significant fraction of CO and H_2 is not converted and remains in the product gas. The H/C ratio in the product gas varies between 1.1 and 1.4. Experiment and simulation are in good agreement with a mean deviation of 10 % for CO, H_2, and CO_2, which is within the experimental uncertainty. The C_2H_4 selectivity shows the highest deviation between simulation and experiment, with almost no C_2H_4 formed in the simulation. A possible explanation is that C_2H_4 mostly forms in colder regions of the cylinder, like crevices and boundary layers that are not included in single-zone models. Again, the use of a multi-zone model could improve the agreement between model and experiment with respect to hydrocarbon species [67, 68]. The selectivity seems to be an appropriate means to compare experimental and modeling results with deviating fuel conversion.

Work and heat output

Polygeneration processes are designed to not only provide base chemicals but also work and heat. The latter two outputs are shown in Fig. 2.8 as a function of ϕ. As expected, these outputs decrease with increasing equivalence ratios, ranging between 314 and 245 J per cycle for heat and 160 and 135 J for work. The decrease is a result of the decreasing maximum temperatures with increasing ϕ, which reduces heat transfer to the coolant, but also fuel conversion (see Section 4.2) and reaction enthalpies (less CO_2 and H_2O formed). This consequently reduces the work output of the engine in favor of the generation of valuable product species. Simulation and experiment are in very good agreement for the heat output, while the work output of the engine is slightly over-predicted. The deviation can be explained by the higher fuel conversion and the fact that the gas exchange strokes are not included in the model. Experimental data suggest that the gas exchange strokes reduce the work output by about 11 J.
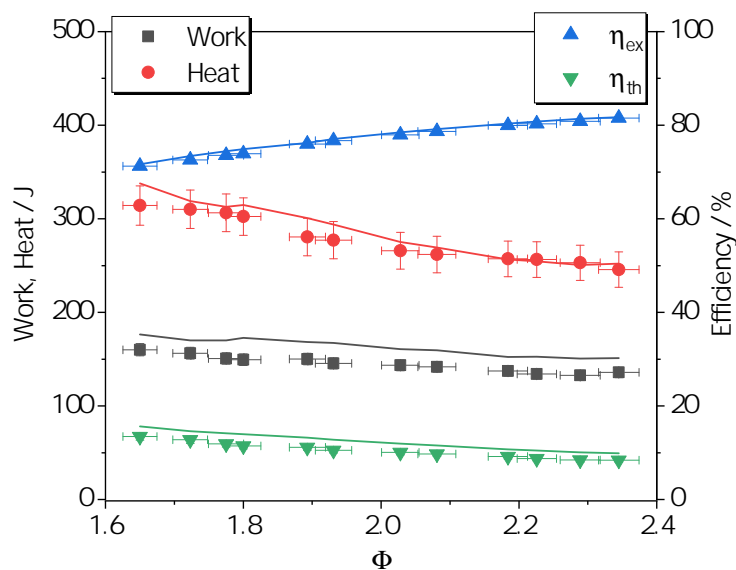
Figure 2.8: Work and heat output per cycle and exergetic and thermal efficiencies. Symbols: experiment, lines: simulation.

Efficiencies

In order to assess polygeneration in the engine on a thermodynamic basis, at least two efficiency metrics are available: thermal and exergetic efficiency. Both are shown in Fig. 2.8. The thermal efficiency is comparably low and decreases from 13 to 8 % in the range of investigated equivalence ratios. However, the thermal efficiency alone is not a suitable parameter to assess polygeneration processes, since the heat output and energy content of the chemical products are neglected. The exergetic efficiency, which includes all three forms of available energy, increases from 71 to 82 % as ϕ increases from 1.65 to 2.34, exceeding those for common syngas-production processes like methane steam reforming, which has an exergetic efficiency of ∼63 % [26]. In addition, the resulting efficiencies are also exceeding those for other polygeneration processes: Polygeneration based on solar collectors, providing electricity, heat, cooling, and desalinated water yield exergetic efficiencies up to 32 % [69]. Other systems combining power cycles with methanol production or desalinization reach efficiencies up to 60 % [39, 44]. For both metrics (thermal and exergetic efficiencies), simulation and experiments are in very good agreement. Compared to our previous work with n-heptane as additive [30], the exergetic efficiency slightly increases with DME, by about 1 percent point. This is consistent with the fact that heat losses with DME as an additive are about 8 % lower than with n-heptane, while the work output is only 3 % higher. This may be due to

differences in combustion phasing with the two additives. Nearly the same mass fractions of both n-heptane and DME are needed for HCCI.

2.5 Conclusions

An IC engine operating in HCCI mode at fuel-rich equivalence ratios with methane/DME as reactants was considered as a device for a polygeneration process that simultaneously produces synthesis gas, work, and heat. Experiments were compared with simulations based on a homogeneous engine model. Work, heat, selectivities, and thermal as well as exergetic efficiencies were evaluated.

A method to experimentally identify stable operating points was introduced. For an intake temperature of 150 °C, the mole fraction of DME that was needed for stable operation was mostly constant at 9.3 % in a range from $\phi = 1.6$ to 2.3, however, significant soot production starts at $\phi = 2$. Below this limit the soot concentration in the product gas was less than 10 mg/m^3 . Within the envelope of stable engine operation increasing the equivalence ratio shifted the combustion phasing towards earlier crank angles. Results from the simulation suggest that this is because during ignition, initially methane is almost inert and the equivalence ratio of DME alone shifts closer to stoichiometric conditions for increasing overall ϕ.

The trends observed in the experiments were well reproduced by the simulations. However, the combustion phasing differs, probably because of the high sensitivity to uncertainty in the experimental temperature at the start of compression. Adjusting the starting temperature by about 10 K brings the simulated phasing in line with the experiments. In the experiment, C_2H_4 is measured with selectivities up to 5 %, while the single-zone model predicts almost no output of that species, likely because in the experiment it is formed at low temperatures in crevices and near the wall. The thermal efficiency, work, and heat output were decreasing with increasing equivalence ratios, while selectivities towards CO and CO_2 as well as the exergetic efficiency were increasing.

The results show that the engine can be used for polygeneration in a flexible manner. When less work (likely to be converted to electricity) is required, the work output can be reduced by 20 % by increasing the equivalence ratio, while the exergetic efficiency increases from 71 to 82 %, exceeding efficiencies of other polygeneration processes. Simultaneously, the fuel is converted to synthesis gas by partial oxidation, with selectivities of up to 72 % for H_2 and 79 % for CO. The resulting H/C ratios range from 1.1 to 1.4 and could be increased to the desired value, which is usually 2, by the water-gas shift reaction [34]. A complete shift from

the production of chemicals to that of power would be possible by operating the engine on a stoichiometric mixture.

In conclusion, polygeneration in internal combustion engines may provide an advantage in terms of exergetic efficiency and flexibility, and DME is a promising additive for methane. Since the amount of DME needed is not negligible, further autoignition-supporting additives should be evaluated. Based on the results presented here, future work will also include the development of a multi-zone model to further improve the simulations, and improvements in the product-gas analysis to close the carbon balance more accurately. Also, we expect an increase of the ethylene yields by increasing the equivalence ratios to even higher values, beyond the upper sooting limit.

2.6 Acknowledgement

—————

KINETICS OF METHANE IGNITION: DME REPLACEMENT BY OZONE

Introduction to the second paper

The previous study on methane/DME combustion in fuel-rich HCCI mode proved on the one hand the suitability of DME as a potentially CO_2-neutral additive, but on the other hand it pointed out an issue: 8.6 % to 9.8 % of the fuel-additive mixture consisted of DME, and therefore a lot of chemical exergy was added to the system by the additive. Moreover, DME is a typical by-product of methanol synthesis, which itself uses synthesis gas as feedstock. Consequently, the engine would be partially fueled with its own product, reducing the efficiency due to multiple additional conversion steps.

Subsequently, a comprehensive comparison between n-heptane, DME, and DEE as ignition promoter was published by Banke et al. in 2023 [70]. Although the three hydrocarbon-additives showed different low-temperature kinetics and operation stability limits, high energy fractions of 15 % to 17 % were needed for DME and DEE, whereas n-heptane was responsible for 23 % to 26 % of the energy input. However, using n-heptane, DME, or DEE as additive made ignition controllable and reduced the intake temperature requirements to a practically feasible level of 150 °C. Therefore, omitting additives for fuel-rich HCCI operation presents a challenge.

To overcome this, an additive is required which is not needed in such large quantities. From fuel-lean HCCI research it has been known since the 2000s that ozone is a suitable hydrocarbon-free alternative additive for HCCI of methane containing fuels [71, 72]. Therefore, we investigated the ignition enhancing properties of ozone in fuel-rich methane mixtures and conducted experiments, in which DME was successively replaced by ozone. Using the single-zone engine model and the elemental

reaction mechanism of Burke [73], the reaction pathways were investigated to understand the benefits of ozone in fuel-rich mixtures. To our knowledge, ozone in fuel-rich HCCI engines has not been studied before.

The key contributions of this work to the state of the art can be summarized as follows:

– Ozone was confirmed as a suitable additive for fuel-rich methane ignition.

– Comparatively to fuel-lean mixtures, ozone is very effective and only needed in small amounts (ppm).

– Ozone decomposes at low temperatures of 200 °C and full decomposition is reached early in the compression stroke, it does therefore not interact directly when methane ignites.

– Ozone decomposition provides O radicals for H abstraction of methane and leads to CH_3OOH formation.

– CH_3OOH remains stable for a short time and then decomposes, releasing OH radicals.

– Several advantages of ozone were found: an early heat release, no increase of the fuel-air mixture's heat capacity, and on-demand, on-site, potentially CO_2-neutral production.

Table 3.1: Author contributions for chapter 3 following the CRediT author statement methodology [41].

Author	Freund	Banke	Atakan	Kaiser
Conceptualization	✓	✓	✓	✓
Methodology	✓	✓		
Software	✓			
Validation	✓	✓		
Formal analysis	✓	✓		
Investigation (simulation)	✓			
Investigation (experiments)		✓		
Resources			✓	✓
Data curation	✓	✓		
Writing - Original draft	✓	✓		
Writing - Review & editing			✓	✓
Visualization	✓			
Supervision			✓	✓
Project administration			✓	✓
Funding acquisition			✓	✓

Author contributions to the second paper

The experiments that lay the basis for this work were carried out by Kai Banke. My contribution was the validation of the engine model and the evaluation of the reaction pathways. Furthermore, I wrote the manuscript, except for the section on experimental setup, which was written by Kai Banke. All co-authors were involved in the review and revision process. Sebastian Kaiser and Burak Atakan were responsible for the supervision of the project.

3.1 Abstract

Fuel-rich combustion of methane in a homogeneous-charge compression-ignition (HCCI) engine can be used as a polygeneration process producing work, heat, and useful chemicals like syngas. Due to the inertness of methane, additives such as dimethyl ether (DME) are needed to achieve ignition at moderate inlet temperatures and to control combustion phasing. Because significant concentrations of DME are then needed, a considerable part of the fuel energy comes from DME. An alternative ignition promotor known from fuel-lean HCCI is ozone (O_3).

Here, a combined experimental and modelling study on the ignition of fuel-rich partial oxidation of methane/air mixtures at $\phi = 1.9$ with ozone and DME as additives in an HCCI engine is conducted. Experimental results show that ozone is a suitable additive for fuel-rich HCCI, with only 75 ppm ozone reducing the fuel-fraction of DME needed from 11.0 % to 5.3 %. Since ozone does not survive until the end of the compression stroke, the reaction paths are analyzed in a single-zone model.

The simulation shows that different ignition precursors or buffer molecules are formed, depending on the additives. If only DME is added, hydrogen peroxide (H_2O_2) and formaldehyde (CH_2O) are the most important intermediates, leading to OH formation and ignition around top dead center (TDC). With ozone addition, methyl hydroperoxide (CH_3OOH) becomes very important earlier in the compression stroke under these fuel-rich conditions. It is then later converted to CH_2O and H_2O_2.

Thus, ozone is a very effective additive not only for fuel-lean, but also for fuel-rich combustion. However, the mechanism differs between both regimes. Because less of the expensive additives are needed, ozone could help improving the economics of a polygeneration process with fuel-rich operated HCCI engines.

3.2 Introduction

Flexibility in energy conversion is a task of growing importance. A possible way to achieve more flexibility combined with high efficiency is the use of so-called polygeneration processes. These concepts combine the production of mechanical power (or electricity), heat, and useful chemicals in one single process. An example is the oxidation of methane in a stationary internal combustion engine (ICE). For power production only, the engine would typically be run lean to stoichiometric. However, in times of electric energy excess the power output could be reduced by operating the engine fuel-rich (as part of a chemical plant), partially oxidizing the fuel and producing syngas (H_2 + CO) or hydrocarbons like ethylene.

This concept was first investigated by Szeszich [27] who produced syngas by partial oxidation of methane/oxygen mixtures in a heavy-duty spark ignition engine. Ignition and flame speed in the fuel-rich regime limit stable ICE operation. Several approaches dealt with this problem [28, 45, 74–77]. Karim et al. used a dual-fuel concept with diesel pilot injection and oxygen enrichment. They found stable operation for syngas production at equivalence ratios up to $\phi = 2.4$ depending on the level of oxygen enrichment [45]. McMillian and Lawson investigated the partial oxidation of natural gas in a spark ignition (SI) engine. Equivalence ratios between $\phi = 1.3$ and 1.6 at a compression ratio of $r_c = 13.3$ yielded product gas with up to 11 % H_2. A slightly different approach using SI of methane with preheating up to 480 °C and the addition of hydrogen and ethane was investigated by Lim et al. [75] at equivalence ratios from $\phi = 1.8$ to 2.8 and $r_c = 13.8$.

In our own previous work [30] we showed that with homogeneous-charge compression-ignition (HCCI) the partial oxidation of methane in an ICE can reach exergetic efficiencies of 81.5 %. This is 18.5 %-points higher than methane steam reforming [26]. Since methane is relatively difficult to ignite, more reactive additives like n-heptane [30] or dimethyl ether (DME) [78] were used to achieve and control ignition at moderate compression ratios and intake temperatures. However, it was found that for these experimental conditions a relatively high fraction of the fuel energy (about 15–20 %) was then provided by the valuable additives. This runs counter the idea of using methane, i.e., natural gas, as an inexpensive and easily available base fuel. In fact, DME is typically produced from syngas via methanol. Thus, on a systems level, adding DME to the reactants would lower the overall yield.

This then motivates the search for an ignition promoter that could substitute more expensive ones like n-heptane, DME, or other reactive hydrocarbons while still providing some control over combustion phasing. Nitrogen oxide (NO) or on-site

produced ozone could be a possible solution. In lean HCCI combustion, following the pioneering work of Flynn [79], several researchers investigated ozone as an ignition-promoting additive [71, 80–87]. Work at the University of Orleans (France) investigated various aspects of ozone addition in lean HCCI combustion. It was found that at $\phi = 0.3$ only 50 ppm of ozone in n-heptane shifted the combustion phasing by 10 °CA [88]. Enhanced reactivity was also found for ozone addition to other fuels, for example isooctane [84] and several alcohols [85]. NO is a suitable additive as well, but less effective [89]. Dubreuil et al. [90] showed that 100 ppm NO promote the ignition of n-heptane and isooctane in lean HCCI by only 2 °CA. Contino et al. [91] achieved a shift of 15 °CA for isooctane, but needed 500 ppm NO for that. Given these encouraging results in lean HCCI it seemed obvious to ask whether ozone may also promote ignition in fuel-rich methane HCCI. Thus, we conducted experiments with a range of ozone fractions in fuel-rich methane/DME/air mixtures at $\phi = 1.9$ and investigated the ignition kinetics with a single-zone engine model to understand the effect of ozone on auto-ignition. Some DME was still needed because the experiments were performed at the rather low compression ratio of 10 [78].

It is well known from literature on the oxidation in fuel-lean mixtures that ozone decomposes already at temperatures below 300 °C to O_2 and O radicals. That means that in an engine's compression stroke, ozone itself probably does not survive long enough to still be present when the auto-ignition temperatures of methane are reached. Masurier et al. [89] showed that typical intermediate species in fuel-lean methane/propane/air mixtures are formaldehyde (CH_2O), hydrogen peroxide (H_2O_2), hydroperoxyl radicals (HO_2), and hydroxyl radicals (OH), and that those species are formed earlier when 10 ppm of ozone were added. Basevich et al. [92] investigated the auto-ignition of fuel-lean methane/air mixtures and the occurrence of a blue-luminescent preflame zone in which partial oxidation takes place before ignition. According to their work methyl hydroperoxide (CH_3OOH) and H_2O_2 are formed simultaneously. Subsequently they decompose and yield OH that accelerates the oxidation. In a plug-flow reactor, Kaczmarek et al. [93] showed that the reaction of methane with OH radicals is the most important one for methane consumption in fuel-rich mixtures ($\phi = 2$–20). They also demonstrated that for methane/air mixtures at $\phi = 8$ OH is formed along different paths depending on temperature: below 800 K this occurs mainly by the decomposition of CH_3OOH, while above 800 K H_2O_2 is the main precursor. Wang et al. [94] simulated the reforming of an isooctane/n-heptane mixture in an HCCI engine at $\phi = 1.4$. They found that CH_3OOH, H_2O_2, and 1-hydroperoxyl propionaldehyde ($C_3H_6O_3$) were formed at

temperatures below 740 K and therefore regarded them as important intermediates in low-temperature reactions. Adding these species individually in their engine model, they found that each shortens the ignition delay time.

To summarize the relevant previous work, it is established that ozone strongly accelerates lean HCCI auto-ignition, but there appears to be a number of important intermediate species in the oxidation of alkanes that are directly or indirectly influenced by the interaction of ozone with the various fuels. The objective of this work is to establish if ozone is an effective ignition promoter also in fuel-rich HCCI of methane, and – since we found that this is the case – to understand the ignition kinetics and the importance of different intermediate species.

3.3 Methods

Experiment

The experiments are performed in a four-stroke single-cylinder octane-number test engine modified to also operate with gaseous fuels. The experimental arrangement is basically that used in our previous work [78]. In addition, here, ozone is produced via corona discharge in two different ozone generators (Innotec OGuA 5000 for fractions up to 250 ppm, Ozone Solutions TG-40 for up to 1700 ppm). The generators are fed with 2 slm pure oxygen and 7.6 slm N_2 are fed to the engine's intake to keep the O_2/N_2 ratio of air. The intake air pressure is controlled to 1 bar with the flow measured by a mass flow meter, while the other gases are metered by mass flow controllers and ad-mixed to the air flow upstream of the preheater. There, the mixture is preheated to 150 °C before entering the intake. The cylinder pressure traces for each operating point were recorded and then averaged over 140 consecutive cycles. Table 3.2 shows the engine properties and operation conditions and Fig. 3.1 illustrates the instrumentation.

Simulation

The model consists of a zero-dimensional single-zone reactor representing the reaction volume inside the cylinder including one inlet and one outlet valve for gas exchange. The engine is simulated in Python using the library Cantera [50] for describing the thermodynamics and reaction kinetics. We chose the engine parameters according to those of the engine experiments as shown in Table 3.2 with the piston movement given by the piston velocity equation of Heywood [95]. The crank angle convention in this paper assigns 0 °CA to compression TDC, i.e., crank angles before

Table 3.2: Engine properties and operating conditions.

Description	Symbol	Value	Unit
Rotational speed	rpm	595	1/min
Compression ratio	r_c	10	
Bore	d	65	mm
Stroke	s	100	mm
Displacement	D	332	cm³
Fuel/air equivalence ratio	ϕ	1.9	
Intake temperature	T_{in}	150	°C
Intake pressure	p_{in}	1	bar
Coolant temperature	T_c	100	°C
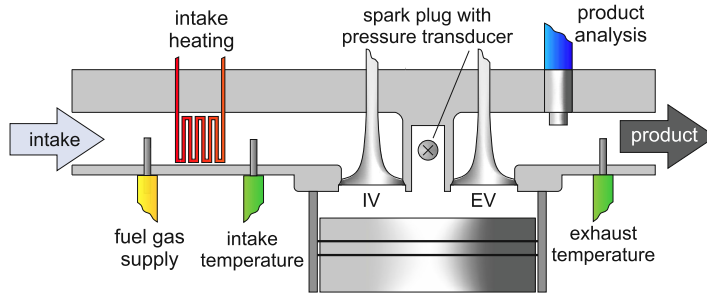
Figure 3.1: Schematic of the instrumentation (see also [78]).

compression TDC are negative.

For the thermodynamics and reaction kinetics two reaction mechanisms are combined: the mechanism of Burke et al. [73] that includes 116 species and 710 reactions for methane/DME mixtures is expanded with the ozone mechanism of Zhao et al. [96]. Although the latter is validated for ambient pressure and our simulation shows ozone decomposition at below 7 bar, we think that the reaction paths for decomposition do not differ qualitatively. After decomposition, the O-radical kinetics covered by the Burke mechanism are more important, and Zhao et al. [96] and Halter et al. [97] showed that direct interactions of O_3 + DME or O_3 + CH_4 are then insignificant.

For each pre-determined step of 0.2 °CA, with the reactor volume changing due to the piston movement, Cantera solves the species and energy conservation equations. For each step, as many integrator timesteps are taken as needed for convergence. With smaller step size, the results do not change significantly. The heat transfer through the walls is modeled by the Woschni correlation [58] as in our previous work [78]. The gas-exchange strokes are now included, and this leads to additional
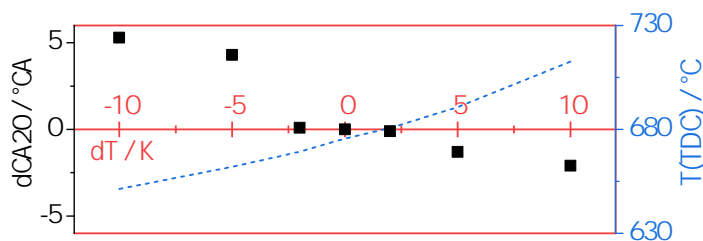
Figure 3.2: Change of CA20 (dCA20) and temperature at top dead center (TDC) as a function of the change in initial temperature (dT), illustrating the sensitivity of the combustion phasing on the initial temperature.

heat transfer through the walls during gas-exchange. The Woschni parameters were adjusted to reflect this. The residual gas leads to small changes in the simulation results for each cycle. In stable operating conditions the results converge within three cycles. For the analysis we simulate 10 cycles after convergence and average the results.

Since the aim of this work is to investigate ignition, the start of combustion in the experiment should be matched by the simulation. Here, CA20 (the crank angle at which 20 % of the heat release has taken place) was chosen as a metric for ignition timing. Eq. (3.1) defines the heat release rate (HRR) in the engine simulation, which is then accumulated and peak-normalized to calculate CA20.

$$HRR(t) = V(t)RT(t) \sum_i \left(\frac{dh_{f,i}^0}{RT(t)} \dot{\omega}_i \right) \qquad (3.1)$$

The HRR depends on the volume V and temperature T of the mixture, the ideal gas constant R, and the net production rates of each species $\dot{\omega}_i$ and their corresponding standard enthalpies of formation $dh_{f,i}^0$. The simulation is adjusted to match the experiment in two steps. First, we adjust the compression ratio to 10.35, which is within the experimental uncertainty, such that the motored pressure trace from the simulation matches the experimental one. Then, for a methane/DME/ozone mixture at $\phi = 1.9$ with 5.3 mol% DME and 75 ppm ozone we adjust the Woschni parameters and the initial temperature at the inlet such that CA20 matches that in the experiment. Fig. 3.2 shows the sensitivity of the simulation's CA20 and temperature at TDC on the initial temperature.

Temperature changes of ± 10 K result in CA20 changes of -2.1 and $+5.3$ °CA, while the temperature at TDC changes by $+37$ K and -24 K, respectively. In the experiment, the in-cylinder temperature after intake valve closing cannot be measured and the simulation cannot accurately account for the temperature change
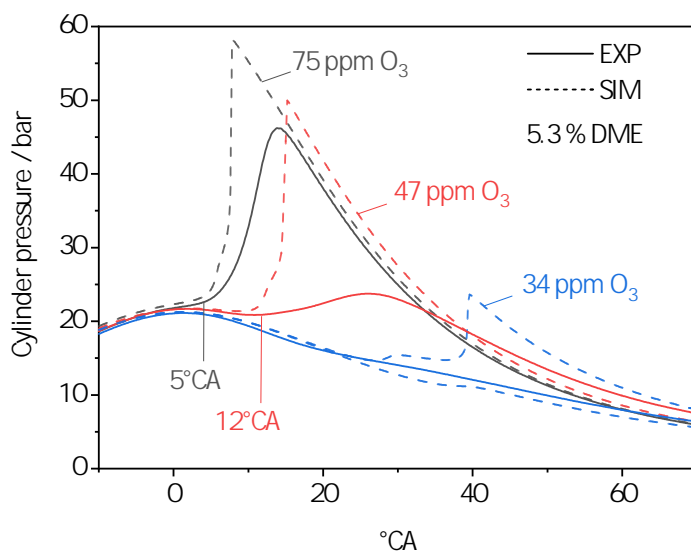
Figure 3.3: Cylinder pressure as a function of crank angle for a constant DME mole fraction of 5.3 % (in methane/DME) and ozone mole fractions of 75, 47, and 37 ppm (in methane/DME/air). Solid lines: experiments, dashed lines: simulation. Labels mark CA20 (except for unstable operation with 34 ppm).

during the intake stroke, so there is a small uncertainty in the initial temperature. Reflecting this uncertainty, we thus adjusted the main parameters affecting the TDC temperature to match CA20 in experiment and simulation.

3.4   Results and discussion

Effect of ozone on the combustion phasing

Our experiments showed that the product-gas composition does not significantly change when the additive is replaced. Therefore, we focus here on reaction-path analysis to understand the effect of ozone on combustion phasing. Fig. 3.3 compares the cylinder pressure traces in experiment and simulation for three different ozone fractions (34, 47, 75 ppm) in the intake mixture at a DME fraction of 5.3 % of the fuel and $\phi = 1.9$.

In the simulation, the Woschni parameters and the intake temperature had been adjusted to match experimental and simulated CA20 for 75 ppm ozone to within 1 °CA. For 47 ppm, only a slight increase in the intake temperature (by 2 K) was sufficient to match the experimental CA20. We conclude that the simulation predicts the net effect of ozone addition on combustion phasing sufficiently well. With 34 ppm ozone, combustion becomes unstable in both experiment and simulation; in the

experiment the coefficient of variation of the indicated mean effective pressure is 73 %. The averaged experimental pressure trace shown in Fig. 3.3 contains many misfires, while for the simulation two different cycles are shown, also demonstrating the strong cycle-to-cycle variations influenced by the residual gas from each previous cycle.

The more ozone is added, the earlier ignition occurs, resulting in higher maximum cylinder pressure in both experiment and simulation. The simulation results show higher maximum pressures at earlier crank angles and much higher pressure rise rates, typical for single-zone models [90, 98, 99]. A single-zone model is used here because the goal of the simulation is to qualitatively investigate the chemical pathways during compression and early ignition, rather than accurately predicting the pressure trace during the main part of fuel conversion. This approach is common in chemistry investigations, like Schönborn et al. [100] or Amjad et al. [101]. Our previous work showed that using a single-zone model results in slight overprediction of the engine's work output, but has no significant influence on the product-gas composition [78]. The main result here is that in both experiment and simulation small amounts of ozone influence the ignition also for fuel-rich HCCI, as already known for lean HCCI [71, 79–88]. The combustion can thus be controlled by adjusting the ozone content.

The efficacy of DME substitution by ozone was quantified systematically at $\phi = 1.9$. DME was substituted by ozone while keeping CA50 at about 15 °CA. Without ozone, 11 % DME in methane were needed for stable ignition. The DME content of the fuel needed for stable operation in experiment and simulation was systematically reduced by ozone addition. The results are shown in Fig. 3.4.

The trends in experiment and simulation agree well: small amounts of ozone substitute large amounts of DME, but the effect exponentially decreases with increasing O_3 fraction. The simulation predicts a stronger effect of ozone addition so that more DME may be substituted by less ozone than in the experiment while holding the combustion phasing constant. This deviation may be explained by the over-prediction of DME oxidation when ozone kinetics are included in the Burke mechanism [73]. Our research group is developing a reaction mechanism specifically designed for fuel-rich conditions [102]. Preliminary results with this mechanism including ozone kinetics indicate that the same reaction-paths are important as with the Burke mechanism, but with about three times more ozone needed, which would match the experimental results better. The fuel energy (lower heating value) provided by DME to the overall fuel energy (CH_4 + DME) is 17 % for the case with 11 % DME without O_3. By adding just 64 ppm O_3, the energy contribution of DME
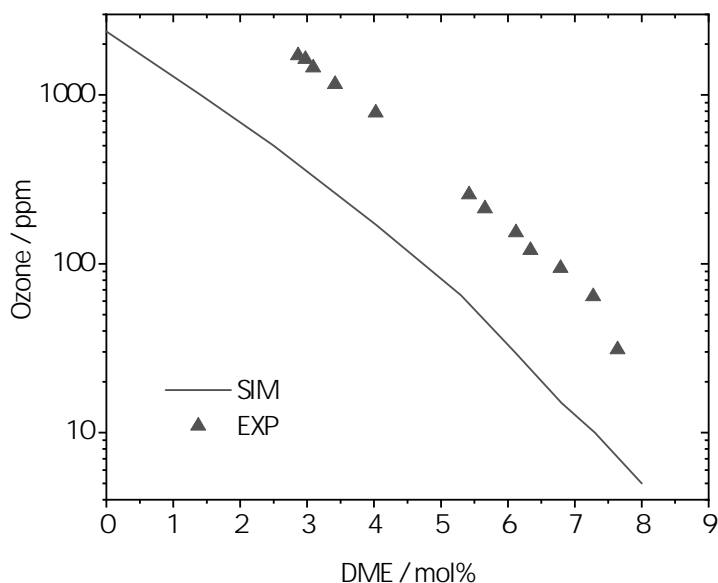
Figure 3.4: Ozone mole fraction in ppm (of methane/DME/air mixture) as a function of DME mole fraction (in mol% of methane/DME mixture) needed for a constant CA50 in simulation and experiment.

is reduced to 12 %, while the ozone generator needs less than 1 % of the overall fuel energy.

Buffer intermediates and reaction-path analysis

To understand the mechanism of this DME substitution by ozone, we first investigate the mole fractions of the major intermediates before ignition. Then reaction-path analyses at certain important crank angles are carried out to gain further mechanistic insight. We start with pure ozone addition to methane, which was not studied experimentally, because at the compression ratio of the current study ($r_c = 10$) the necessary ozone concentrations exceeded the capacity of our ozone generator. Then, further cases both with only DME addition and with both additives will be compared.

Fig. 3.5 shows the mole fractions for 2380 ppm O_3 as the sole additive (corresponding to the simulated 0 % DME case in Fig. 3.4).

Significant decomposition of ozone into oxygen molecules and oxygen radicals starts at −100 °CA and a temperature of 220 °C. At −60 °CA around 30 % of the initial ozone amount is consumed. At this time the formation of reactive intermediates begins, but larger amounts are not present. At −40 °CA ozone is completely

39
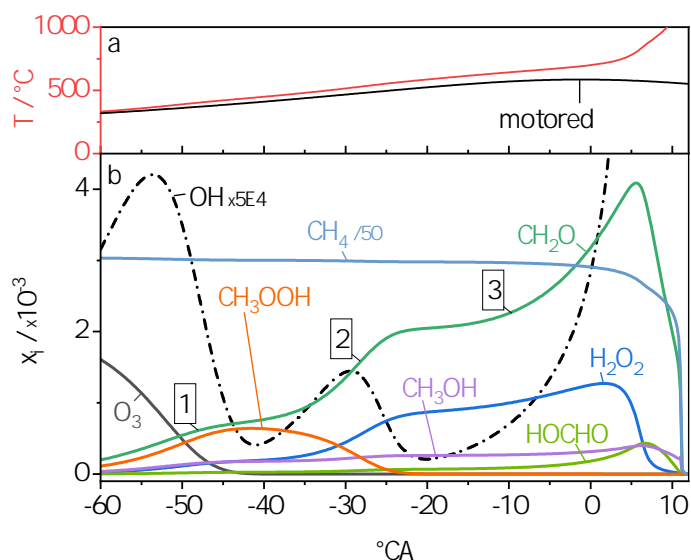
Figure 3.5: (a) Temperature and (b) mole fractions of the most important interme-diates, OH radicals and methane as a function of crank angle (for 2380 ppm ozone as the sole additive).

decomposed. Thus, it is not a reactant at ignition. The mole fractions of the intermediates O and OH at that crank angle are negligibly small. The effect of ozone on ignition must therefore be an indirect effect of the oxygen radicals gen-erated from ozone decomposition. The main intermediate species that are formed and subsequently consumed again between the start of the ozone decomposition and the ignition of the mixture are in decreasing order of their maximum mole fractions: formaldehyde (CH_2O), hydrogen peroxide (H_2O_2), methyl hydroperoxide (CH_3OOH), formic acid (HOCHO), and methanol (CH_3OH). CH_3OOH is the only intermediate species that is formed in larger quantities and does not remain in the mixture until ignition. The CH_2O and H_2O_2 mole fractions increase in three distinct steps until the temperature is high enough for ignition (about 1050 K in this case). The three steps are at -50 °CA, -30 °CA, and -11 °CA as labeled in Fig. 3.5. Reaction-path analyses were carried out for these crank angles. They are illustrated in Fig. 3.6.
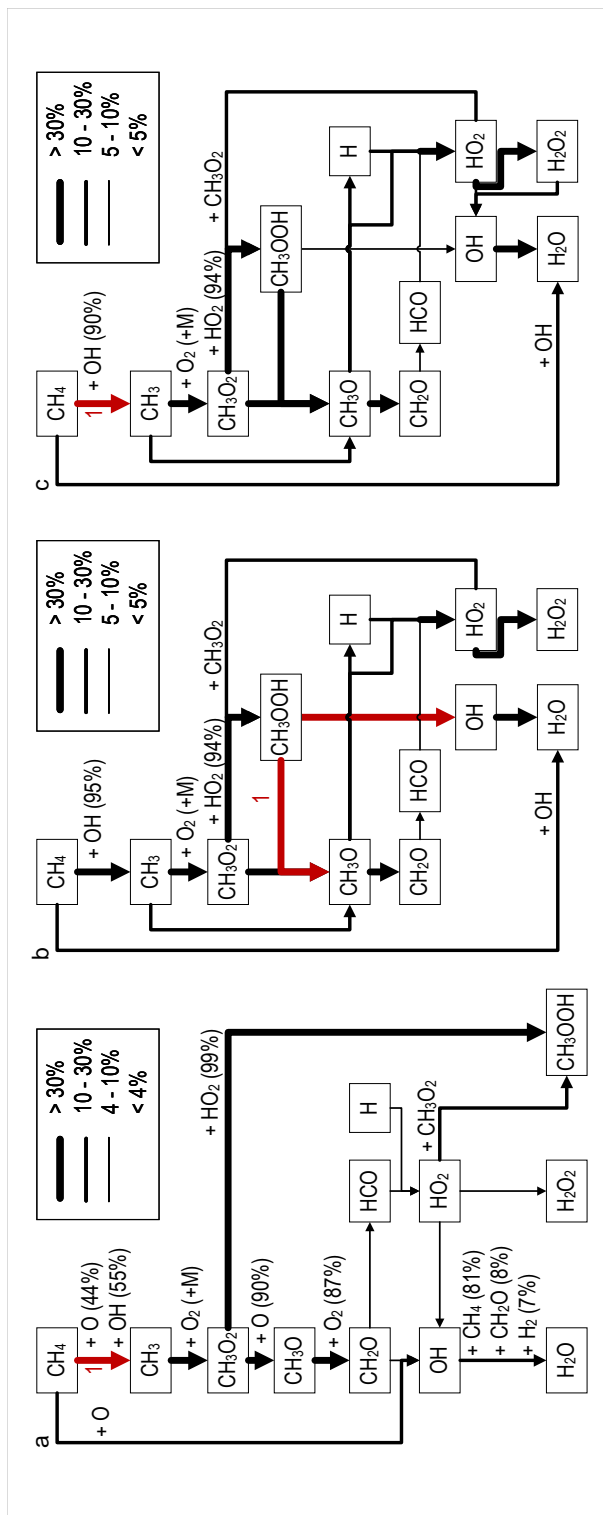
Figure 3.6: Reaction paths for the most important species containing H atoms. Red arrows (marked with 1) represent the highest mole flows (kmol/m³/s). The mole flows are divided by the highest mole flow (indicated by 1) and the ratio is represented by the line thickness. (a) step 1 (−50 °CA, $T = 390$ °C, $p = 5.1$ bar); (b) step 2 (−30 °CA, $T = 515$ °C, $p = 10.3$ bar); (c) step 3 (−11 °CA, $T = 643$ °C, $p = 19.4$ bar).

Step 1: ozone decomposition. Fig. 3.6a illustrates the most important reaction pathways for H atoms at -50 °CA. Oxygen radicals abstract hydrogen from methane, forming CH_3 and OH radicals. CH_3 and its oxidation products undergo several reactions with molecular and atomic oxygen, which end in the formation of CH_2O, HO_2, and CH_3OOH. CH_2O and CH_3OOH do not react further in this temperature range, and HO_2 forms H_2O_2, then CH_3OOH, and then OH radicals. The OH radicals also abstract hydrogen from methane, yielding water.

These reactions take place as long as ozone is present and provides oxygen radicals. This explains the first strong increase in CH_2O, H_2O_2, and CH_3OOH concentrations. As the concentration of ozone in the mixture is low, methane conversion and temperature increase due to exothermal reactions are both very low at this time.

Step 2: methyl hydroperoxide decomposition. Fig. 3.6b shows the most important reaction pathways for H atoms at -30 °CA and thus the importance of the CH_3OOH decomposition. Due to ongoing compression and the heat release of the reaction, the temperature of the mixture is increasing. At approximately 440 °C and -40 °CA a threshold is reached at which CH_3OOH decomposes to CH_3O and OH radicals.

Consistent with the findings of Kaczmarek et al. [93] this is the main source for OH radicals under such conditions. Molecular oxygen reacts with CH_3O and forms HO_2 (and then H_2O_2) and CH_2O. Additionally, OH radicals abstract hydrogen from methane and this also leads to the formation of CH_2O and H_2O_2 via CH_3OOH.

The latter is therefore a key species for the ongoing conversion of methane and the formation of CH_2O and H_2O_2. The increase of CH_2O and H_2O_2 formation is thus higher if CH_3OOH is present, which explains the second step in the species profiles.

Step 3: reaction of formaldehyde and hydrogen peroxide. The most important reaction pathways for H atoms at -11 °CA are shown in Fig. 3.6c. The conversion of H_2O_2 starts earlier than the conversion of CH_2O, as can be seen in Fig. 3.5. With the additional OH radicals the hydrogen abstraction from methane, similarly to step 2, is accelerated further, leading to more CH_3OOH that decomposes as well. The additional CH_3 radicals increase the conversion of CH_2O via HO_2 to H_2O_2 and thereby yield further OH radicals.

With increasing temperature, CH_2O is increasingly converted with H radicals to HCO and H_2, or with OH radicals to H_2O and HCO. HCO increases the formation of H_2O_2 via HO_2 and then of OH radicals as well. At 5 °CA a temperature of 780 °C is reached and H_2O_2 decomposes to OH radicals. This finally leads to conditions in which the OH concentration is high enough to convert a considerable amount of

methane whereby the temperature quickly rises, and ignition occurs.

The ozone decomposition indirectly accelerates the formation of OH radicals and thus increases the temperature during the late compression stroke. The effectiveness as an additive for ignition depends on a chain of buffer molecules, CH_3OOH, CH_2O, and H_2O_2, all with different thermal stability.

In the simulation, also other "virtual additives" were tested: If instead of ozone the intermediate species CH_2O, H_2O_2, and CH_3OOH are added separately with initial mole fractions according to their maximum mole fractions before ignition in the case with 2380 ppm ozone, ignition does not occur. The reason is that although CH_3OOH decomposes and OH radicals are present, the temperature increase in the first step (ozone decomposition and CH_3OOH formation) is missing. The temperature necessary for the decomposition of CH_3OOH is reached much later, at -12 °CA instead of -40 °CA, and this leads to a temperature at TDC that is about 100 K lower – too low for ignition.

When more (1775 ppm) CH_3OOH is used, the same CA20 as for the case with 2380 ppm ozone is observed and the pressure and temperature traces are nearly identical, showing the great importance of CH_3OOH as a buffer molecule or precursor for ignition in the partial oxidation of methane/air/ozone mixtures. Additional CH_2O or H_2O_2 are not necessary in this case; these intermediates are formed from CH_3OOH as described above.

Fig. 3.7 shows the mole fractions as a function of crank angle after TDC for two cases, (a) 12.2 mol% DME and (b) the experimentally investigated mixture of 5.3 mol% DME and 75 ppm ozone.

In case (a) with 12.2 % DME as the only additive the maximum mole fractions of CH_2O and H_2O_2 are much higher than with ozone as the only additive, and their formation is delayed. About 59 % of the initial DME is still present at TDC in case (a). With DME as the only additive, the role of CH_3OOH is minor, because it is not a product of the low-temperature DME chemistry. Now mainly CH_2O (and H_2O_2 from CH_2O) and OH radicals are formed. Additionally, DME decomposes at higher temperatures than ozone. A second effect hindering an earlier ignition with DME is the higher molar heat capacity. With 12.2 mol% of DME in the methane/DME mixture the molar heat capacity increases by 4.4 % over neat methane, which reduces the temperature increase during compression and hinders ignition.

If small fractions of ozone, e.g. 75 ppm, are added to the DME as is shown as case (b), CH_3OOH is formed at earlier crank angles; also formaldehyde is formed earlier. Again, the CH_3OOH decomposition leads to H_2O_2 formation and both provide the OH radicals needed for ignition. This is not enough ozone to convert
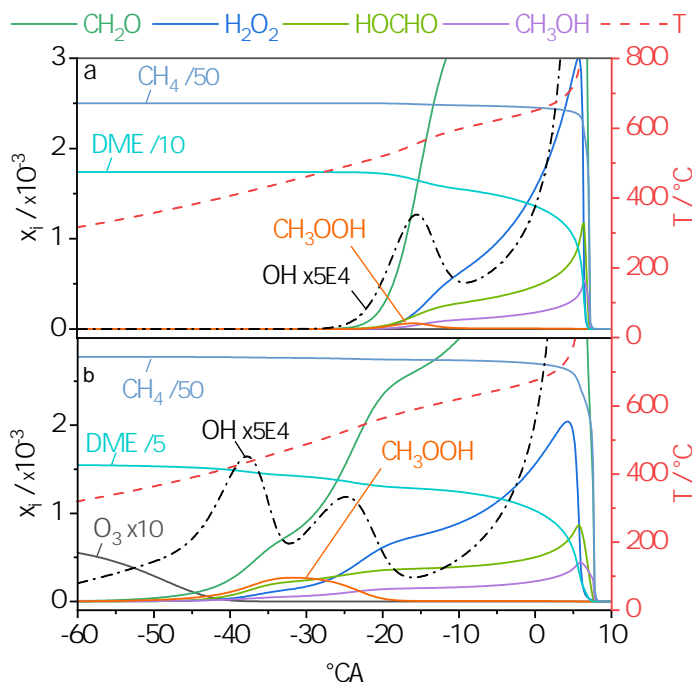
Figure 3.7: Mole fractions and temperature as a function of crank angle. (a) 12.2 mol% DME, (b) the experimentally investigated mixture of 5.3 mol% DME and 75 ppm ozone.

DME completely, but a multi-step reaction appears again.

3.5 Conclusions

Internal combustion engines can be operated fuel-rich for the "polygeneration" of work, heat and base chemicals, but for homogeneous compression ignition of methane, reactive additives may be needed. While our previous work used DME as an ignition promoter, it is an expensive additive that could be a product of syngas production rather than an input. We showed that as in fuel-lean HCCI [71, 80–89], also in fuel-rich HCCI ozone is an effective ignition-promoting additive. This was shown experimentally for the first time here for methane/DME fuel mixtures. At a compression ratio of 10 with moderate intake heating, it could not totally replace DME, but reduce the needed DME fraction considerably. Thus, the energy provided by DME to the fuel mixture can be reduced considerably as well.

Zero-dimensional modelling with detailed kinetics provided insight to the mechanism of ignition promotion. From the general kinetics of ozone decomposition, it was clear that ozone does not survive the compression process. A more detailed

analysis showed that reactions of the decomposition products of ozone with methane lead to the formation of two buffer molecules early in the compression stroke. Under the fuel-rich conditions explored here, these are CH_3OOH and CH_2O. In particular the former is a key intermediate. It is converted prior to ignition into H_2O_2 and more CH_2O, which are also the main intermediates from ozone in fuel-lean HCCI. Without such buffer molecules that survive to relatively high temperatures and then form reactive radicals, ozone would not affect the ignition process.

The simulation systematically underestimated how much ozone is needed to substitute a given amount of DME, since the DME oxidation is over-predicted [96]. Preliminary work with a mechanism developed specifically for fuel-rich conditions [102] indicate that this discrepancy can be strongly reduced, but further validation is needed. Experimentally, in future work, higher compression ratios will be investigated to further reduce the fraction of additives needed for ignition. It may be feasible to use ozone as the sole additive.

3.6 Declaration of Competing Interest

The authors declare that they have no known competing financial interests or personal relationships that could have appeared to influence the work reported in this paper.

3.7 Acknowledgements

KINETIC AND EXERGETIC ANALYSIS OF NATURAL GAS CONVERSION: COMPARISON BETWEEN OZONE AND DME

Introduction to the third paper

In the previous chapter, it was shown that ozone is preferred over DME for ignition of fuel-rich methane in HCCI engines: smaller quantities of ozone are required and can be produced on-site, while DME is usually a by-product of methanol synthesis and requires synthesis gas as an educt. This raises the question of how the two additives compare in terms of engine efficiency.

Since pure methane is rarely used as an educt in practice, natural gas, a mixture of 90 % methane, 9 % ethane, and 1 % propane, was chosen for this investigation. Furthermore, a multi-zone model was developed and used to account for the inhomogeneities in the cylinder and evaluate their influence on the product selectivity and exergetic efficiency. Therefore, the previous work was extended by multi-zone model calculations and an ozone generator model with data taken from a manufacturer.

The key contributions of this work to the state of the art can be summarized as follows:

– The exergetic efficiency of commercially available ozone generators is about 5.5 % and thus very poor.

– Ozone contributes only 0.2 % to the fuel-air mixture's exergy, whereas DME contributes 21 %.

– Selectivities of synthesis gas, H_2O, and CO_2 do not depend on natural gas composition or inhomogeneities in the cylinder.

– Exergetic efficiency is strongly dependend on the additive: ozone production reduces it by 3.3 %-pts. and DME production by 17.0 %-pts.

– The highest exergetic efficiency including ozone production, modelled with the multi-zone model, is 88.7 % at $\phi = 2.5$.

Author contributions to the third paper

My contribution was the conceptualization, the process concept modeling, simulation, and analysis of the data. I also wrote the first draft of the manuscript. The extension of the single-zone model by multi-zone model functionality was conducted by Christoph Horn during his master thesis in 2020, which I supervised. In his thesis, he validated the multi-zone model using experimental data for methane/DME mixtures at $\phi = 1.9$ provided by Kai Banke. Christoph Horn and Burak Atakan were engaged in the review and reworking of the manuscript and Burak Atakan was responsible for the supervision of the project.

Table 4.1: Author contributions for chapter 4 following the CRediT author statement methodology [41].

Author	Freund	Horn	Atakan
Conceptualization	✓		✓
Methodology	✓	✓	
Software	✓	✓	
Validation	✓	✓	
Formal analysis	✓	✓	
Investigation	✓	✓	
Resources			✓
Data curation	✓	✓	
Writing - Original draft	✓		
Writing - Review & editing	✓	✓	✓
Visualization	✓		
Supervision			✓
Project administration			✓
Funding acquisition			✓

4.1 Abstract

Fuel-rich operated HCCI engines are suitable for the polygeneration of work, heat, and base chemicals like synthesis gas (CO and H_2). Under favorable conditions, these engines are exergetically more efficient than separate steam reformer and cogeneration gas engines. However, to achieve ignition, reactive fuel additives

like dimethyl ether or ozone must be supplied, which have some, probably negative and not yet quantified, impacts on the exergetic efficiency.

Therefore, the aim of this work is to compute and evaluate the effect of DME and ozone on the exergy input and exergetic efficiency of fuel-rich operated HCCI engines, which convert natural gas at equivalence ratios of 1.5 to 2.5.

Results of a single-zone-model (SZM) and a multi-zone model (MZM) are compared to analyze the influence of inhomogeneities in the cylinder on the system's exergetic efficiency. Natural gas as fuel is compared with previous neat methane results.

The single-zone model results show that natural gas is much more reactive than methane. Ethane and propane convert partially in the compression stroke and lead to ethene, propene, and OH radicals. However, the ethane and propane conversions do not favor but slightly reduce the formation of methyl hydroperoxide, which is an important buffer molecule for fuel-rich methane ignition. But in addition, further buffer molecules like ethene or ethyl hydroperoxide are intermediately formed. The product selectivities are neither influenced by the natural gas composition, nor by the chosen additive.

Compared to ozone, the DME molar and mass fractions needed for ignition are up to 11 times higher, and its exergy contribution to the total mixture is even 95 times higher. Therefore, the system's exergetic efficiency is much higher when ozone is chosen as additive: reasonable values of up to 82.8 % are possible, compared to 67.7 % with DME. The multi-zone model results show that the efficiency is strongly dependent on the fuel conversion and thus unconverted fuel should be recycled within the polygeneration system to maintain high efficiencies. Comparing the total exergetic efficiency, ozone is a favorable additive for fuel-rich operated HCCI polygeneration.

4.2 Introduction

Fossil resource usage can be reduced by more efficient and flexible energy and chemical compound conversion technologies. A promising approach is the polygeneration of work, heat, and synthesis gas in fuel-rich operated internal combustion (IC) engines which is a mid-term alternative to separate cogeneration gas engines and steam reforming processes.

Several works in the 2000s and 2010s showed that partial oxidation of methane or natural gas is feasible in spark-ignition (SI), compression ignition (CI), and homogeneous charge compression ignition (HCCI) engines. Each ignition type has its

own challenges for stable operation, though.

CI engines typically need an additional fuel injection, e.g. diesel or n-heptane, leading to stratification within the cylinder. Karim et al. [45] investigated the partial oxidation of methane with highly oxygenated air in a dual-fuel CI engine experimentally in 2008 for equivalence ratios of 2.0 to 3.5 and found that this process is feasible and yields up to 80 % synthesis gas in the dry exhaust gas. However, a diesel injection was still needed for ignition and combustion control.

Ignition in SI engines is dependent on the flame speed and thus limited to lower equivalence ratios. However, Lim et al. [75] modified a CI engine to perform spark ignition and achieved stable operation of methane/air-mixtures for equivalence ratios up to 2. For ignition, high intake temperatures of up to 450 °C were needed and the spark ignition timing was adjusted between 45 and 30° crank angle (°CA) before top dead center. This operation range could be extended by adding 5 % hydrogen and 10 % ethane to the fuel mixture – to represent natural gas. Then, a stable operation at an equivalence ratio (ϕ) of up to 2.8 was possible.

A very high flexibility can be achieved with HCCI engines, which are kinetically controlled and thus do not depend on fuel injection timing or flame speed. Our previous experimental work has shown that polygeneration with methane fueled HCCI engines is feasible and exergetic efficiencies of up to 81.5 % are achieved [30, 78]. However, methane containing fuels (such as biogas or natural gas) represent a challenge for achieving HCCI due to their inertness leading to high octane-numbers and relatively high specific heat capacities. Ignition can be promoted with reactive additives such as ethers [78] or higher alkanes [93]. In our previous work we found that high additive mass fractions of up to 28 % in the fuel mixture are needed when dimethyl ether (DME) [47, 78], diethyl ether (DEE), or n-heptane [30] are used.

The production of these additives leads to additional, yet partially unknown, exergy losses, and the added DME is typically produced from synthesis gas, and thus, is a product of the polygeneration system. Therefore, from a holistic viewpoint, alternatives are preferable. Ozone may be a much more suitable additive, since it is produced on demand via corona discharge [103] using surrounding air and much smaller amounts are needed to ignite methane (typically, less than 5000 ppm). Keum et al. [104] investigated the effect of ozone as an ignition promoter under stoichiometric conditions in 2018 and found that 100 ppm ozone provide a significant promotion effect in HCCI engines, whereas SI engines benefit from an increased flame speed only from an addition of 3000 to 6000 ppm. Sayyosouk et al. [87] modelled a zero-dimensional HCCI engine fueled with iso-octane at lean conditions ($\phi = 0.3$) and found that even 4 ppm ozone promote ignition effectively.

These results encouraged us to investigate the effect of ozone in fuel-rich operated HCCI engines [105]. There, the influence of ozone on the kinetics of methane in fuel-rich HCCI engines has been investigated in comparison to DME [105]. We have found that ozone is a much more effective additive than DME. Ozone decomposes very early in the compression stroke, does not noticeably increase the heat capacity of the mixture, and it leads to the formation of methyl hydroperoxide (CH_3OOH), which leads to OH radical formation near the end of the compression stroke via formaldehyde (CH_2O) and hydrogen peroxide (H_2O_2) formation. For a practical application, the HCCI engine is likely fueled with natural gas instead of neat methane. Therefore, in the present work the kinetic investigation is extended towards natural gas.

As discussed before, Lim et al. found that the addition of hydrogen and ethane extended the operation stability of fuel rich operated SI engines from $\phi = 2$ to $\phi = 2.8$. Duan et al. [106] compared neat methane with natural gas experimentally in a fuel lean operated HCCI engine. With 2.88 % ethane and 0.41 % propane in the natural gas mixture, the in-cylinder pressure increased by up to 4 bar, compared to neat methane. Although the combustion phasing (CA50) was shifted slightly towards earlier crank angles, this effect was not significant. Kaczmarek et al. [107] measured ignition delay times of natural gas/DME/air mixtures in a shock tube at fuel rich mixtures ($\phi = 2, 10$) and concluded that under those conditions, natural gas is much more reactive compared to methane due to its ethane and propane contents (which were set to 9 % and 1 %, respectively). As the natural gas composition may vary during the operation of a fuel-rich HCCI engine, the evaluation of the effect of ozone on the ignition is analyzed here and compared to the operation with neat methane.

Additionally, a comparison between ozone and DME, based on exergy methods, is carried out here. This comparison includes a comparative modelling study on the influence of DME and ozone on the engine's exergy input and their influences on the exergetic efficiency of the polygeneration system. The exergetic efficiency of the ozone generator is calculated with a Python model and the exergetic efficiency of the DME production is taken from the work of Zhang et al. [108]. Zhang et al. conducted a profound exergy analysis on the steam gasification of biomass and determined an exergetic efficiency of 43.5 %.

This paper aims to answer the question, whether ozone is an exergetically favorable additive compared to DME, representative for other oxygenated hydrocarbons, when natural gas fueled HCCI engine are operated at equivalence ratios of 1.5 to 2.5. Our previous work [105] showed that trends are well reproduced with a single

zone model, while the fuel conversion is overestimated for fuel-rich conditions. Thus, a comparison with a multi-zone model is included here, and the importance of the colder zones on the outcome is analyzed.

4.3 Methodology

The engine model is written in Python and the thermodynamics and reaction kinetics are computed by using the module Cantera [50]. A four-stroke single-zone model (SZM) and recently a two-stroke multi-zone model (MZM) were developed. The multi-zone model contains seven zones (numbered as subscript i) with interzonal heat and mass transfer and a non-reactive crevice zone of 1.5 vol % of the dead volume. The heat transfer between the zones $\dot{q}_{i-1 \to 1}$ Eq. (4.1) is modelled as heat conduction according to the approach of Komninos et al. [61], which was developed for HCCI engines [109].

$$\dot{q}_{i-1 \to 1} = -k_{tot}\frac{\partial T}{\partial r_n} \cong -k_{tot}\frac{T_i - T_{i-1}}{(t_i + t_{i-1})/2} \tag{4.1}$$

The temperature gradient $\frac{\partial T}{\partial r_n}$ between two zones is discretized to a temperature difference, whereas $-k_{tot}$, T_i, and t_i are denoted as the total thermal conductivity, the zone temperature, and the zone thickness, respectively. The total thermal conductivity consists of a laminar and a turbulent part, which are calculated by estimating laminar and turbulent Prandtl numbers and gas mixture viscosities. Kominos et al. adapted this approach from Yang and Martin [110] and described it in more detail in [61, 109].

To assure a uniform pressure within all zones, each zone is connected to its adjacent zones within Cantera as valves, allowing a pressure difference dependent mass flow from one zone to another. The crevice zone and the outermost zone also transfer heat and mass to their adjacent zones, but also to the cylinder wall as a global heat transfer. The gas mixture in each zone of the single-zone and the multi-zone model is homogeneous and the piston movement induces volume changes.

For each timestep, the energy and species conservation equations are solved. For the single-zone model, the global heat transfer coefficient is calculated with the semi-empirical Woschni correlation [58] and the coefficents are taken from our recent work [105]. For the multi-zone model, a slightly modified version of the Woschni equation was used, according to Chang et al. [60], who measured the in-cylinder heat fluxes in an HCCI engine experimentally.

Our multi-zone model was then validated against our own measurements with methane/DME mixtures at $\phi = 1.9$ from [105] by using a zone distribution which led

to a good agreement between the simulated fuel conversion, work, and heat output and the experimental data.

At TDC, the core zone and the crevice zone are set at 30 % and 1.5 % of the dead volume, respectively. The remaining volume is distributed between the five other zones so that the volume decreases from the inner to the outermost zone. The bore d and the height of the dead volume h_{TDC} of the cylinder are thus divided into the thickness of the outer zones t_i and the thickness of the core zone $t_{core,x}$ Eq. (4.2) and $t_{core,y}$, respectively Eq. (4.3).

$$d = 2 \sum (t_i + 2t_{core,x}) \tag{4.2}$$

$$h_{TDC} = 2 \sum (t_i + 2t_{core,y}) \tag{4.3}$$

The core zone thickness in direction of the piston movement $t_{core,y}$ is given by the cylinder height at top dead center h_{TDC} and the sum of the thickness of the outer zones Eq. (4.4). The thickness $t_{core,x}$ corresponds to the half diameter of the core zone and is kept constant.

$$t_{core,y} = \frac{h_{TDC} - 2 \sum t_i}{2} \tag{4.4}$$

The thickness t_i of each outer zone is calculated according to Eq. (4.5).

$$t_i = LR^{N-(i+1)} \tag{4.5}$$

Here, $N = 7$ is the number of zones, R is set to 0.45 and L is solved within the model to assure that Eq. (4.3) is fulfilled. The zone volumes change with height changes due to the piston movement. The resulting volume distribution is visualized in Fig. 1.

It was also proven that the MZM reproduced the methane conversion found experimentally in our previous work [105] within ± 1.9 %.

A representative natural gas is the fuel in this work, and it consist of 90 % methane (CH_4), 9 % ethane (C_2H_6), and 1 % propane (C_3H_8). To compute the chemical kinetics of DME (CH_3OCH_3) and ozone (O_3), the Burke mechanism [73] for C1-C3 species is extended by the Zhao sub-mechanism [96] for ozone kinetics.

Table 4.2 presents the investigated engine properties and operation parameters. The equivalence ratio is varied between 1.5 and 2.5 and all other conditions remain constant. For the calculation of the equivalence ratio the additives are considered, and the amount of air is adjusted accordingly.
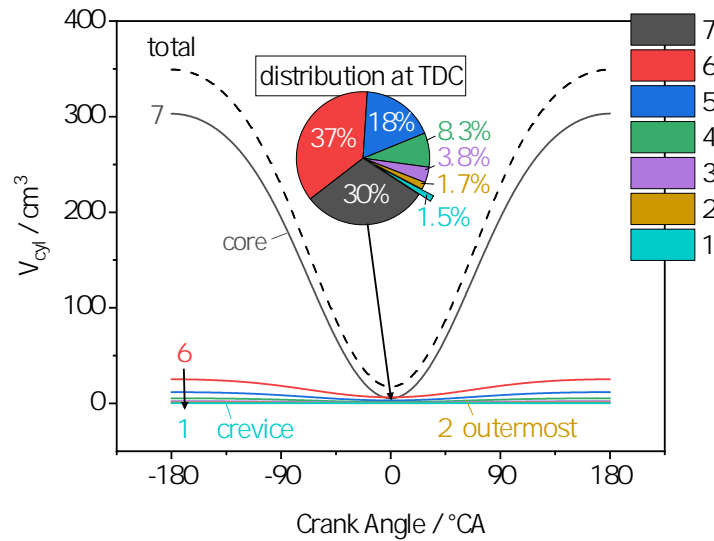
Figure 4.1: Volumes of the seven zones of the multi-zone model as a function of crank angle and volume distribution at TDC (pie chart). At TDC, the core zone accounts for 30 % of the dead volume, whereas the crevice zone accounts for 1.5 %.

Table 4.2: Engine properties and operating conditions.

Description	Symbol	Value	Unit
Rotational speed	rpm	1500	1/min
Compression ratio	r_c	20	
Bore	d	65	mm
Stroke	s	100	mm
Number of cylinders	N_Z	4	
Displacement	D	1.327	dm³
Equivalence ratio	ϕ	1.5-2.5	
Intake temperature	T_{in}	50	°C
Intake pressure	pin	1	bar
Coolant temperature	T_c	100	°C
Thermal conductivity wall	λ_w	53	W/m²/K
Convection coefficient coolant	α_c	3000	W/m²/K

The fuel conversion X_i, product yields Y_i, and product selectivities S_i are evaluated to assess the influence of the additive choice on the chemical output of the polygeneration system. In the corresponding definitions Eqs. (4.6), (4.9), and (4.10), the stoichiometric coefficient, the entering molar flows, and the exiting molar flows are denoted as ν_i, $\dot{n}_i'$, and $\dot{n}_i''$, respectively. The total fuel conversion X_t in Eq. (4.8) considers the conversion of all fuel and additive species, weighted according to their entering mole fractions x_i Eq. (4.7) in the fuel-additive mixture.

$$X_i = 1 - \left(\frac{\dot{n}_i''}{\dot{n}_i'} \right) \tag{4.6}$$

$$x_t' = \sum \left(\frac{\dot{n}_i'}{\sum \dot{n}_i'} \right) = \sum x_i' \tag{4.7}$$

$$X_t = \sum \left(x_i' X_i \right) \tag{4.8}$$

$$Y_i = \frac{\dot{n}_i'' - \dot{n}_i'}{\dot{n}_i' x_t' \nu_i} \tag{4.9}$$

$$S_i = \frac{Y_i}{X_t} \tag{4.10}$$

To evaluate the influence of the additive production on the exergetic efficiency, the HCCI engine is embedded in a system which also includes the additive production: the ozone generator and a black box model of the DME production process. Figure 4.2 displays a flow diagram of those three systems *add*, *eng*, and *sys*, their interconnections, and their corresponding exergy flows.

The exergetic efficiency ε_{add} of the DME production process ε_{DME} is estimated as 43.5 % according to Zhang et al. [108] and the exergetic efficiency of the ozone generator ε_{ozone} is calculated within the Python model Eq. (4.11).

$$\varepsilon_{add} = \left. \frac{\dot{E}_{add}}{\dot{E}_{in,add}} \right|_{add=DME,ozone} \tag{4.11}$$

The ozone generator is supplied with air and power and provides a mixture of air and ozone. The power supply, the incoming air mass flow, and the ozone concentration in the output gas are taken from the data sheets of the Fujian Newland Entech Company [111] to calculate the exergy flows $\dot{E}$.

To compare the exergy-share of DME and ozone, the exergy input ratio r_{ex} is defined as the ratio of the exergy flow of the additive to the total exergy flow of the engine input Eq. (4.12).
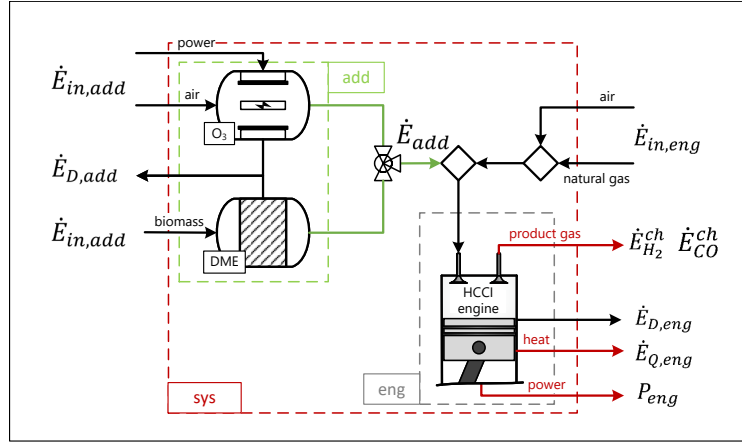
Figure 4.2: Process flow diagram of the system *sys*, divided into two subsystems *add* and *eng*. The HCCI engine is supplied with either ozone or DME as additive.

$$r_{ex} = \frac{\dot{E}_{add}}{\dot{E}_{in,eng} + \dot{E}_{add}} \tag{4.12}$$

Furthermore, the exergetic efficiency of the HCCI engine ε_{eng}^A and of the overall system ε_{sys}^A are defined according to Eqs. (4.13) and (4.14).

$$\varepsilon_{eng}^A = 1 - \frac{\dot{E}_{D,eng}}{\dot{E}_{in,eng} + \dot{E}_{add}} \tag{4.13}$$

$$\varepsilon_{sys}^A = 1 - \frac{\dot{E}_{D,eng} + \dot{E}_{D,add}}{\dot{E}_{in,eng} + \frac{\dot{E}_{add}}{\varepsilon_{add}}} \tag{4.14}$$

The exergy destruction $\dot{E}_D$ in the HCCI engine is estimated with the Gouy-Stodola theorem Eq. (4.15), the irreversible entropy production rate ($\dot{S}_{irr,eng}$) is calculated using the second law of thermodynamics.

$$\dot{E}_{D,eng} = T_{env}\dot{S}_{irr,eng} \tag{4.15}$$

Without full fuel conversion, the aforementioned efficiencies must be evaluated critically, since, as an extreme, the evaluated efficiency would be 100 %, if no conversion takes place, which is not aimed. To assess the conversion to the wanted products only, a second definition for the exergetic efficiency is introduced for *eng* Eq. (4.16) and for *sys* Eq. (4.17), denoted with the superscript B.

$$\varepsilon_{eng}^B = \frac{\dot{E}_{H_2}^{ch} + \dot{E}_{CO}^{ch} + P_{eng} + \dot{E}_{Q,eng}}{\dot{E}_{in,eng} + \dot{E}_{add}} \tag{4.16}$$

56

$$\varepsilon_{sys}^{B} = \frac{\dot{E}_{H_2}^{ch} + \dot{E}_{CO}^{ch} + P_{eng} + \dot{E}_{Q,eng}}{\dot{E}_{in,eng} + \frac{\dot{E}_{add}}{\varepsilon_{add}}} \tag{4.17}$$

Here, only useful exergy stream outputs are considered: the chemical exergy flow of synthesis gas $\dot{E}_{H_2}^{ch}$ and $\dot{E}_{H_2}^{ch}$, the power output P_{eng}, and the exergy flow of the heat transferred to the cooling water $\dot{E}_{Q,eng}$. Species that are not converted towards synthesis gas are thus neglected. Both definitions have advantages and disadvantages, since the second definition now neglects the possibility to re-use the unconverted educts in a following cycle. As a compromise, both will be shown.

4.4   Results and discussion

First, the necessary amounts of ozone and DME for a stable combustion phasing of 7.4 ±0.2 °CA after top dead center (°CA aTDC), using the SZM, are evaluated and compared. An ignition shortly after reaching top dead center is most favorable, the sensitivity of the combustion phasing on the exact amount of additive was investigated systematically by varying the additive amounts by ±20 % at $\phi = 1.9$. The reference case for ozone represents the amount of ozone that was needed in the work of Schröder et al. [105] to substitute DME completely by ozone.

Second, these amounts are reduced or increased when reducing or increasing ϕ, respectively, and the equivalence ratio dependent product selectivities and exergetic efficiencies are discussed. All single-zone model results shown in this chapter are an average of four consecutive engine cycles. The multi-zone model results are taken from the fourth cycle.

Figure 4.3 illustrates the pressure traces for the DME and the ozone case at $\phi = 1.9$. The relatively high compression ratio of 20 leads to maximum pressures of 53 bar and 59 bar before, and 174 bar and 167 bar after ignition, for DME and ozone, respectively. A similar CA50 is obtained with about 11 times less ozone compared to DME in the total mixture. In contrast to DME, ozone does not increase the molar heat capacity of the mixture and supplies radicals at lower temperatures and thus earlier crank angles. Because of the lower heat capacity, the temperature and pressure increase during the compression stroke is higher and less additive is needed. Figure 4.3 also indicates that small amounts of ozone shift the combustion phasing noticeably stronger, although the relative increase is stronger for DME: to shift the combustion phasing by one crank angle degree (considering the black cases as reference), additional 1.3 % or rather 283 ppm DME must be added, whereas 2.5 % or 50 ppm additional ozone is needed.
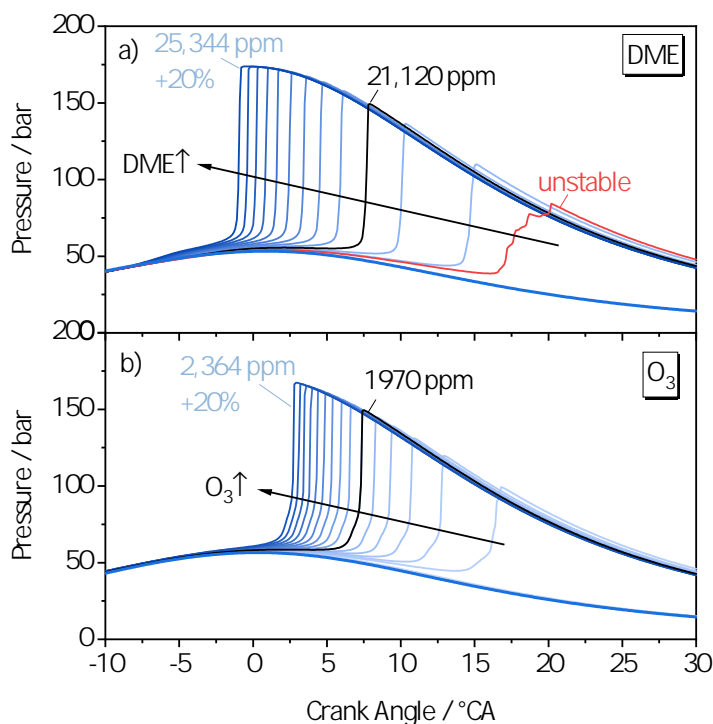
Figure 4.3: Averaged pressure traces (SZM, four consecutive cycles) as a function of crank angle and additive amount in the total mixture for a) DME and b) ozone at $\phi = 1.9$. The reference additive amount (black line) is varied by ± 20 % (blue lines). For DME, an unstable ignition is found for the second lowest DME amount (red line).

For DME, a small combustion phasing range is found, in which the ignition is unstable and only every second cycle ignites after intermediate species, such as formaldehyde and hydrogen peroxide, from the previous cycle are accumulated, which will be discussed later in this chapter. This effect is seen for the condition where the DME amount of the reference case is reduced by 4.5 % or 950 ppm, marked in red in Fig. 4.3a. A pressure increase is noticeable, but the combustion phasing is very late, and the averaged pressure trace is not smooth, because every cycle differs.

The kinetic effects of ozone and DME on fuel-rich HCCI engine operated with neat methane was analyzed in our previous work [105]. We found that ozone decomposes very early and is completely converted at -40 °CA. Its decomposition yields atomic and molecular oxygen, the atoms react with methane, initiating the conversion. Furthermore, a buffer molecule was found to be important, previously: methyl hydroperoxid (CH_3OOH). This relatively unstable molecule is formed for a
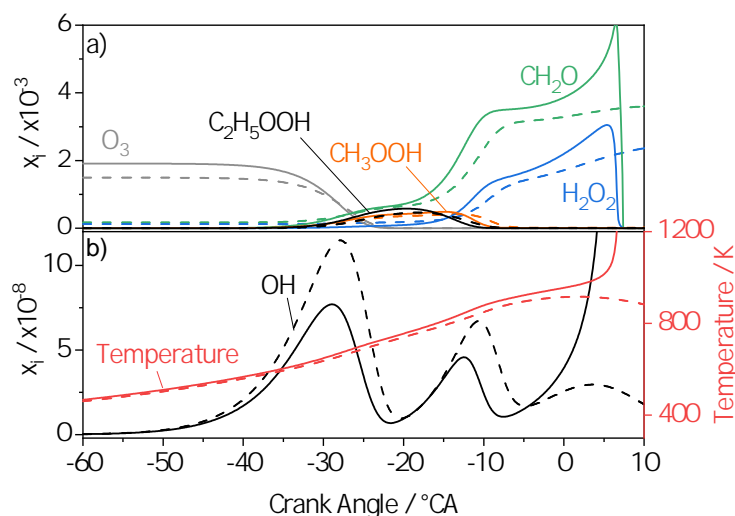
Figure 4.4: Intermediate species mole fractions and in-cylinder temperature as a function of crank angle at $\phi = 1.9$ (SZM). Solid lines: 1970 ppm ozone cause ignition; dashed lines: 1570 ppm ozone ($-20\ \%$) is insufficient for ignition. a) Illustrates ozone and the most important intermediate species, b) shows the in-cylinder temperature and OH radical formation.

brief period and increases the OH radical concentration later, due to decomposition at higher temperatures after further compression. Thus, it promotes the conversion of methane and the formation of formaldehyde (CH_2O) and hydrogen peroxide (H_2O_2), which are crucial precursors for methane ignition.

On the basis of these findings, the following section deals with the influence of the additional ethane and propane in natural gas mixtures on the intermediate species and the interaction with ozone. In this work, the engine is operated at higher rotational speed ($+905$ 1/min), higher compression ratio ($+10$) and lower intake temperature (-100 °C) compared to [105] in order to investigate conditions for the subsequent exergetic analysis, which are nearer to nowadays' engine parameters. This leads to a higher cylinder charge and shorter residence times.

In Fig. 4.4 two operating conditions are compared: the ozone reference case with 1970 ppm ozone in the total mixture (black line in Fig. 4.4b) and the ozone mixture with 1570 ppm ozone (-20 %, dashed lines), the latter condition does not ignite (flat line in Fig. 4.4b).

Due to the 2.5 times shorter residence time and the lower intake temperature compared to the work of Schröder et al. [105], ozone is barely decomposed at -40 °CA. However, the higher compression ratio leads to a steeper temperature increase and thus ozone decomposition starts shortly after -40 °CA and is complete
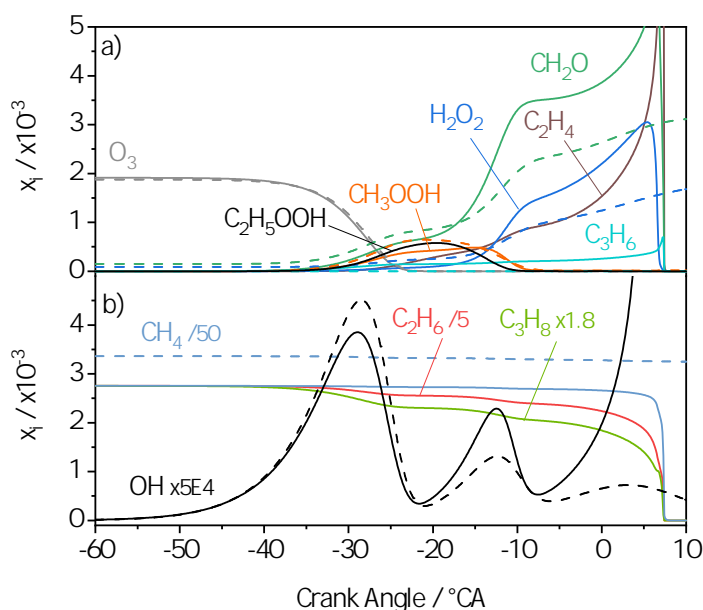
Figure 4.5: Intermediate species mole fractions as a function of crank angle at $\phi = 1.9$ (SZM). Solid lines: natural gas; dashed lines: methane. a) Illustrates ozone and the most important intermediate species, b) shows the fuel conversion and OH radical formation.

at -25 °CA. This applies for both cases and thus both ozone amounts. As a result, CH_3OOH, CH_2O and H_2O_2 are formed as described for the methane case before, but also ethyl hydroperoxide (C_2H_5OOH). If the ozone amount is too low (dashed lines), CH_2O and H_2O_2 are accumulated in each cycle, the OH formation is increased, and the formation of CH_3OOH is comparable. OH radicals are formed in this first step by H-abstraction from the natural gas components, which react with oxygen atoms from the ozone decomposition. The OH radicals are then mainly reacting with the natural gas constituents, leading to a peak. Nevertheless, the second OH peak, which results from CH_3OOH decomposition to CH_3O and OH, is shifted by 2 °CA, because the temperature increases slightly slower. This leads to the effect that the expansion after reaching top dead center quenches the reactions and prevents the ignition of the mixture, illustrated by low OH radical amounts and no CH_2O or H_2O_2 conversion. However, the OH radical mole fraction is slightly higher in the non-igniting case, since CH_2O and H_2O_2 are accumulated, which lead to additional OH radical formation. Nevertheless, this effect is not sufficient for achieving ignition.

In Fig. 4.5, the case with 1970 ppm ozone which leads to ignition for natural gas, is compared to a methane case with the same ozone amount.

It is seen that the natural gas mixture starts to ignite, while methane is not

converted yet. In the methane case the CH_3OOH formation shows a distinctive maximum at -22 °CA, whereas in the natural gas case, the formation is reduced at that point, and the maximum is found later at -14.4 °CA. In addition, ethene and propene are formed from twostep H abstractions from ethane and propane by OH radicals and ethyl hydroperoxide, as well as ethene and propene are formed as further buffer molecules. Kaczmarek et al. [107] showed that ethene and propene are typical intermediate species for the fuel-rich combustion of natural gas and that ethane and propane do not influence the CH_3OOH formation. This leads to a lower CH_3OOH mole fraction compared to the methane case, but due to the exothermal H-abstraction of ethane and propane, which leads to an intermediate C_2H_5OOH formation, the in-cylinder temperature and OH radical concentration are high enough for ignition. The initial ethane and propane mole fractions in the mixture correspond to 14,180 ppm and 1,580 ppm, respectively. If neat methane is to be ignited instead, these additives have to be replaced by only 640 ppm ozone, which emphasizes the effectiveness of ozone as an ignition promoter. The product yields are not affected by combustion phasing and are thus not further discussed here.

In the subsequent section, the necessary ozone and DME amounts for the equivalence ratio range of 1.5 to 2.5, to achieve ignition at CA50 = 6.5 $\pm$0.6 °CA, and the influence on the exergetic efficiencies are discussed. Figure 4.6a shows the necessary mole and mass fractions of DME and ozone as a function of equivalence ratio. Figure 4.6b illustrates the resulting exergy contribution of the additive to the exergy entering the engine r_{ex} and the efficiency of the additive production ε_{add}.

With increasing equivalence ratio, the additive mole and mass fractions needed for ignition increase for both additives. However, the DME-related gradients are larger: 1.0 mol%/ϕ for DME and only 0.065 mol%/ϕ for ozone. Up to 2.7 mol% and 4.5 mass% of DME in the total mixture are needed. This is about 9.9 to 11.6 times more compared to the ozone case, increasing with ϕ. The difference of the exergy ratios r_{ex} are even higher, as Fig. 4.6b illustrates. DME contributes 21 % to the exergy input, whereas ozone is only accountable for a negligible contribution of 0.2 %. On the contrary, the calculated exergetic efficiency of the ozone generator is poor with a rather constant value of 5.5 %. At $\phi = 2.5$, for instance, 4.28 kW of electrical energy must be supplied to generate an ozone mass flow of 0.26 kg/h. The multi-zone model predicts similar figures for the DME case, for which it was validated. On the contrary, when the additive is switched from DME to ozone, much higher ozone amounts or higher intake temperatures are needed compared to the single-zone model. In Fig. 4.6, the multi-zone model results with ozone are
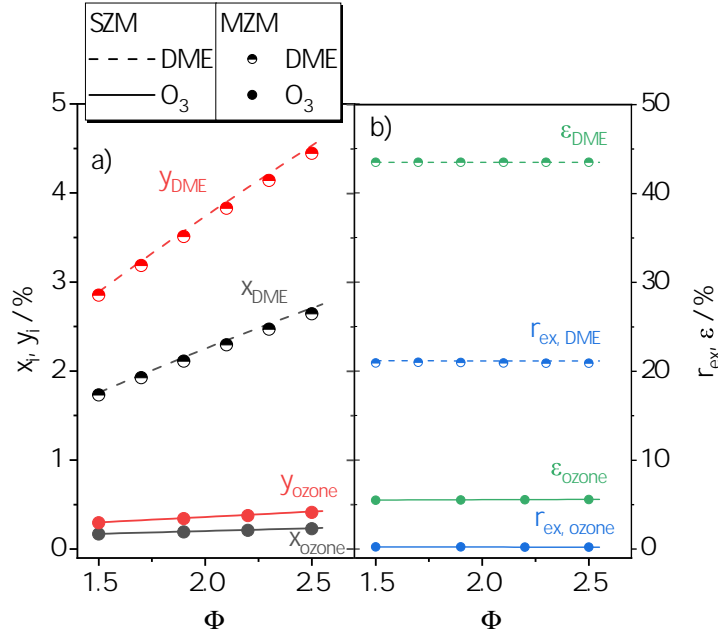
Figure 4.6: a) Intake additive mole fractions x_i in black and mass fractions y_i in red, and b) intake exergy ratio r_{ex} and exergetic efficiency of the additive production ε_{add} as a function of equivalence ratio at CA50 = 6.5 ±0.6 °CA (solid lines: ozone, dashed lines: DME; filled symbols: ozone multi-zone model with $T_{in} = 100$ °C (+50 °C), semi-filled symbols: DME multi-zone model).

obtained with an intake temperature of 100 °C, which is 50 °C higher than in the SZM case; this leads to an ignition with the same amount of ozone as in the single-zone model. Although ozone decomposes early in the compression stroke, it needs about 38 °CA for full decomposition in the core zone ($\phi = 1.9$, $T_{in} = 50$ °C). This leads to a relatively late CH_3OOH formation and decomposition compared to the single-zone model. In the single-zone model, as shown in Fig. 4.4a and Fig. 4.5a, CH_3OOH is completely converted at −8 °CA. By contrast, in the multi-zone model, CH_3OOH is converted in the four innermost zones until +2 °CA, and no ignition is achieved. With an increased intake temperature of 100 °C, CH_3OOH is converted again at −8 °CA, comparable to the single-zone model, and the mixture ignites. This is illustrated in Fig. 4.7.

In contrast to ozone, DME converts late in the compression stroke and in the core zone: it is converted nearly twice as fast, which makes DME less sensitive on the heat and mass transfer from the core zone to its adjacent zones. This shows that due the complexity of the heat and mass transfer within the multi-zone model, this model must be validated against ozone measurements explicitly and investigated
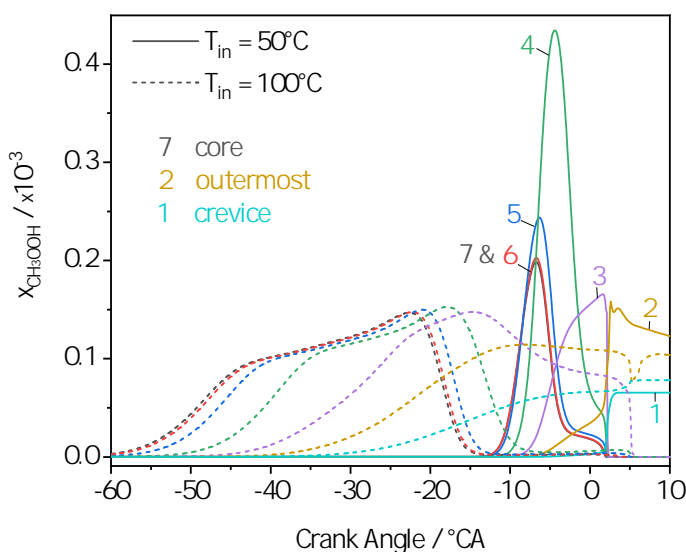
Figure 4.7: Methyl hydroperoxide (CH$_3$OOH) mole fraction as a function of crank angle for all seven zones of the multi-zone model ($\phi = 1.9$). Solid lines: intake temperature of 50 °C, no ignition. Dashed lines: intake temperature of 100 °C, ignition.

further in future work.

However, as seen from Fig. 4.8, the system's resulting exergetic efficiency decrease is minor compared to the DME case. In the figure, a comparison of the single-zone and multi-zone model is also included.

The exergetic efficiency of the HCCI engine (*eng*) reaches a value of 87.5 %, regardless of which additive is used. Figure 4.8a also indicates that when the conversion is not considered in the efficiency definition, there is no distinctive difference between the SZM and MZM results. If the whole system is regarded, including the production efficiency of the additive, and not only the engine, further differences are recognized. The strong efficiency reduction by the DME production by up to 17.3 percentage points at $\phi = 2.5$ (Fig. 4.8b, blue arrow) is remarkable, whereas the ozone production with the quite inefficient generator only leads to a reduction by 2.7 percentage points.

When the efficiency is defined only with the intended products, as done in definition *B*, Fig. 4.8b results from it. The efficiencies of ozone and DME still reach high values of 86.1 % and 86.3 %, respectively, but at lower equivalence ratios. At higher equivalence ratios, methane remains in the product gases, leading to a drop. The maximum efficiency for DME addition is slightly shifted to higher equivalence
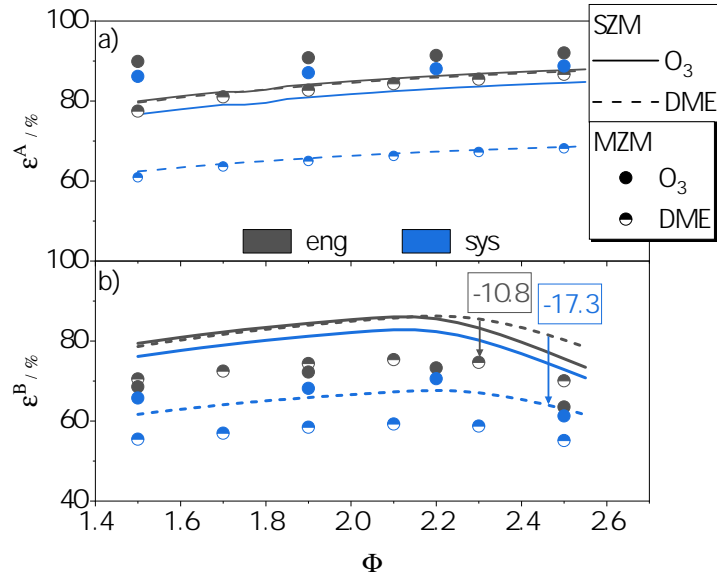
Figure 4.8: Exergetic efficiency of the HCCI engine (*eng*, grey) and the entire system (*sys*, blue) as a function of equivalence ratio ϕ at CA50 = 6.5 ±0.6 °CA (solid lines: ozone, dashed lines: DME; filled symbols: ozone multi-zone model with $T_{in} = 100$ °C (+50 °C), semi-filled symbols: DME multi-zone model). Top: definition A, bottom: definition B.

ratios compared to ozone addition: 2.2 compared to 2.15 in the ozone case.

The efficiency reduction, when the efficiency of additive production is considered (*sys*), is noticeable as well. In the DME case, the maximum efficiency decreases by 18.6 percentage points to 67.7 %. With ozone there is a smaller reduction by 3.3 percentage points to 82.8 %.

At $\phi = 2.2$ the conversion starts decreasing with decreasing amount of oxygen and thus the efficiency decreases as well. At $\phi = 2.3$, the efficiency of the HCCI engine (*eng*) calculated with the multi-zone model is up to 10.8 percentage points lower than those predicted by the single zone model (Fig. 4.8b, grey arrow). This is mainly an effect of the reduced conversion due to colder regions in the cylinder, e.g. crevice zones and zones adjoining the cylinder walls. With reduced conversion, the efficiency decreases since less chemical exergy of the fuel is converted to work, heat, and synthesis gas.

In Fig. 4.9, the conversions predicted by the single-zone model and multi-zone model are compared.

In the single-zone model, propane and DME are always completely converted, whereas the ethane conversion decreases slightly at equivalence ratios above 2.2. The
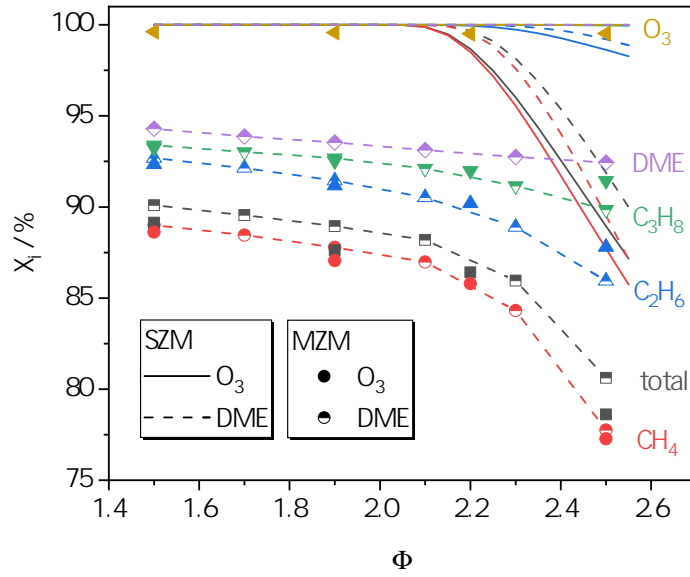
Figure 4.9: Fuel and DME conversions as a function of equivalence ratio at CA50 = 6.5 ±0.6 °CA (solid lines: ozone, dashed lines: DME, filled symbols: ozone multi-zone model with T_{in} = 100 °C (+50 °C), semi-filled symbols: DME multi-zone model).

methane conversion is the lowest, so that the total conversion is 90.0 % for DME and 87.2 % for ozone at $\phi = 2.5$. The natural gas/DME mixture is more reactive at TDC, since DME is not fully converted until ignition occurs. This leads to a slightly higher overall fuel conversion compared to ozone and thus higher exergetic efficiencies at higher equivalence ratios, as seen in Fig. 4.8b.

The results of the multi-zone model shall be compared further to the single-zone model. The multi-zone model predicts up to 12 percentage points smaller total conversions; values of 80.6 % to 90.1 % are estimated and thus the efficiencies are reduced. DME is converted by 94.3 % to 92.4 %, decreasing with ϕ – mainly because of the unreactive crevice zone, which, for example at $\phi = 1.9$, contains 3.5 % to 9 % of the total cylinder mass during combustion. This mass stems from mass transfers from outer, cooler zones when the inner zones ignite and induce a pressure increase. On the contrary, ozone is always converted completely, as emphasized before. The MZM calculations with ozone provide no additional insights since the outcome does not differ significantly from the single zone model results and are not further discussed in the following.

The efficiency reduction for DME addition at $\phi = 2.5$ is illustrated in more detail in Fig. 4.10, where the exergy stream outputs for the SZM and MZM are compared.
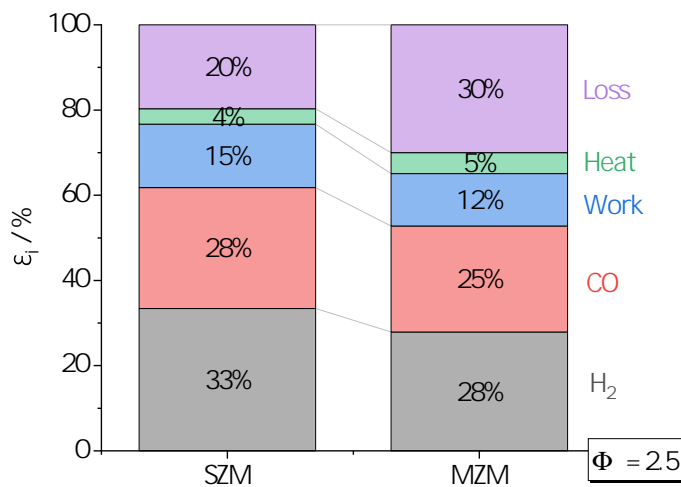
Figure 4.10: Segmentation of the system's exergy stream outputs; comparison of the single zone model on the left and the multi-zone model on the right at $\phi = 2.5$ in the DME case.

The lower conversion in the MZM leads correspondingly to lower heat, work, and synthesis gas exergy streams in the system output. Nevertheless, the changes are quite uniform for the different useful outputs.

To determine promising operating conditions, it is also imperative to evaluate the equivalence ratio dependent product selectivities and compare them for both additives. In Fig. 4.11, the equivalence ratio dependence of the selectivities of CO, CO_2, H_2, H_2O, C_2H_2 and C_2H_4 are shown, again from both models. The main finding is that the predicted selectivities mainly depend on the equivalence ratio but only to a minor extent on the additive or the model used.

The acetylene (C_2H_2) and ethene (C_2H_4) selectivities reach 1.4 % and 2.6 % at the maximum investigated equivalence ratio of 2.5. Higher selectivites are expected at equivalence ratios of 5 and higher [112], but since synthesis gas is the target chemical here, these regions are not further examined. The synthesis gas selectivites increase with increasing equivalence ratio and reach a maximum at the equivalence ratio, where the highest efficiencies were found. Again, the maximum selectivities in the DME case are shifted slightly to higher equivalence ratios, compared to ozone. The maximum achievable selectivities of CO and H_2 are 88.4 % and 66.5 %, respectively. The MZM predicts slightly smaller synthesis gas selectivities and instead a small increase of the water selectivity. In comparison with methane, the natural gas selectivities do not differ noticeably for any investigated
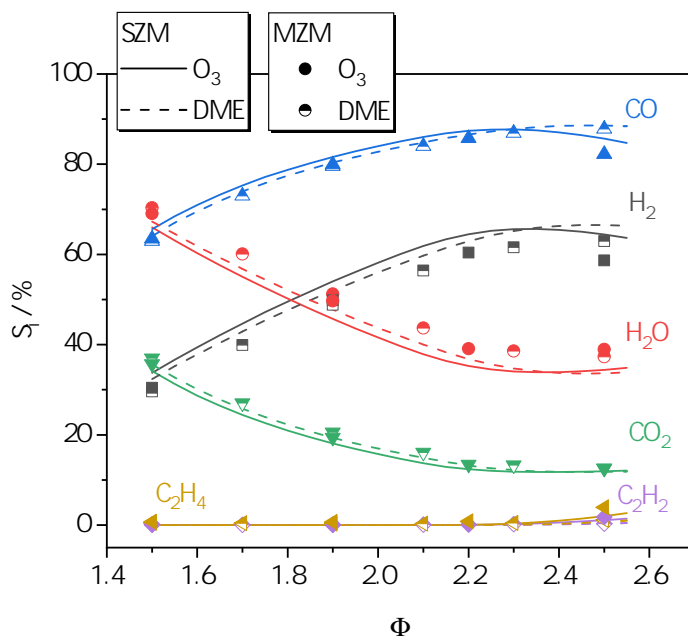
Figure 4.11: Selectivities of the most important product gas species as a function of equivalence ratio ϕ at CA50 = 6.5 ±0.6 °CA (solid lines: ozone, dashed lines: DME, filled symbols: ozone multi-zone model with T_{in} = 100 °C (+50 °C), semi-filled symbols: DME multi-zone model).

case. In practice, the natural gas composition does thus not influence the outcome of the process and must not be considered, when at least 90 % of the natural gas consists of methane. However, for combustion control it is surely important to consider natural gas composition changes, since ignition is sensitive on this composition. Therefore, for combustion control, the additive mass flow must be adjusted on the same time-scale as the natural gas composition varies.

Finally, the decision about the most favorable additive for polygeneration in fuel-rich HCCI engines is not based on the product gas composition, but on the effort in producing the additive and its fuel conversion enhancement properties.

4.5 Conclusions

Fuel-rich HCCI engines for polygeneration of work, heat, and synthesis gas can be operated with natural gas with the help of additives such as ozone or DME.

In this work, the influence of ozone on natural gas ignition and the exergy input of DME and ozone were investigated theoretically, and the influence of the additive production on the exergetic efficiency was evaluated.

The single-zone model results showed that natural gas is much more reactive than methane. Ethane and propane convert partially in the compression stroke and lead to ethene, propene, and OH radicals. However, the ethane and propane conversions do not favor, but slightly reduce the formation of methyl hydroperoxide, which is an important buffer molecule for fuel-rich methane ignition. Instead, ethyl hydroperoxide is intermediately formed as a second buffer molecule. If the same ignition timing shall be achieved with neat methane, ethane and propane can be substituted by only 640 ppm additional ozone, which emphasizes the efficiency of the ozone decomposition.

Compared to ozone, the necessary DME molar and mass fractions are up to 11 times higher, and its exergy contribution to the total mixture is even 95 times higher: DME contributes 21 % to the exergy input of the engine, whereas 1700 ppm ozone only contribute 0.2 %.

The exergetic efficiency of the ozone generator was determined and reached small values of 5.5 %, but since ozone is used in small quantities the system's efficiency declines by only 3.3 percentage points and reasonable values of 82.8 % are possible. The DME production reduces the system's efficiency by unfavorable 17 percentage points. The multi-zone model results show that the efficiency is strongly dependent on the fuel conversion and thus non-converted fuel should be recycled within the polygeneration system to maintain high efficiencies – especially at very fuel rich conditions.

The single-zone model predicted the product selectivities accurately and provided helpful species profiles for kinetic analyses. Additionally, if the exergetic efficiency is calculated with the Gouy-Stodola theorem, the resulting exergetic efficiencies only differed about 1 percentage point from the ones calculated with the multi-zone model. If the fuel conversion and the exergetic efficiency considering the conversion must be predicted accurately, the multi-zone model is much more suitable. The fuel conversion calculated by the multi-zone model matched our experimental values by ± 1.9 % and the exergetic efficiency was found to be 10.8 percentage points lower in the DME case. Since the multi-zone model has not been validated against ozone experiments so far, these results were obtained with a 50 °C higher intake temperature. Therefore, those conditions will be used for validation of the multi-zone model against natural gas/ozone experiments in a future work.

To conclude, ozone is a more favorable additive compared to DME – not only based on the necessary mass flows but on exergetic efficiency as well. These results encourage profound investigations of ozone kinetics for fuel-rich combustion technologies that require reactive fuel additives.

4.6 Acknowledgments

EXERGOECONOMIC ANALYSIS OF AN HCCI ENGINE POLYGENERATION PROCESS

Introduction to the fourth paper

As it was shown in the previous chapters, the efficiency of the engine only is not sufficient for evaluating the polygeneration process; at least the additive production must be considered as well.

To compare the polygeneration with conventional processes like cogeneration and steam reforming, the HCCI engine should provide the chemical products at a demanded purity. Therefore, the exhaust gas must be further treated and the chemicals separated. This reduces the exergetic efficiency further and a more appropriate comparison with conventional processes is possible.

Additionally, high exergetic efficiency is not the only argument for favoring novel systems over conventional processes; profitability and product costs are at least equally important. Therefore, thermodynamic and economic analyses are often combined to evaluate processes using thermoeconomic approaches, e.g. Ghaebi et al. [113]. If exergy-based methods are used the term exergoeconomics is more appropriate. The method of exergoeconomics originates back to the year 1949 and the historical development was instructively described by Tsatsaronis in 1996 [114].

As discussed before, exergy-based methods are more meaningful for the evaluation of the polygeneration process, since energy-based methods would omit most of the exergy stored in the chemicals.

Consequently, in this chapter, a process concept was developed which provides work, heat, steam, and purified hydrogen. This process was then evaluated by applying exergoeconomic methods. All cost data input used in this chapter dates back to the year 2018; no time-value corrections had been made by the time this

thesis was written.

The key contributions of this work to the state of the art can be summarized as follows:

- For the first time, an exergoeconomic method was applied for fuel-rich operated engine processes.

- The most crucial input parameters that influence the hydrogen costs are interest rate, lifetime, operating hours, but also membrane and engine investment costs and fuel costs.

- Exhaust gas recirculation should be avoided or reduced to a minimum.

- An high exergetic efficiency of 65 % is achieved, which is comparable to steam reforming, and 17 %-pts. better than cogeneration of power and heat in conventional engines.

- Hydrogen costs are found at a range of 3.2-4.0 €/kg (at low EGR ratios).

- An economic evaluation should always be paired with a sensitivity analysis.

- A global sensitivity analysis is an easy to use and very helpful method for the cost analysis of processes.

In the original publication [115], the feed and retentate pressures of the palladium membrane were incorrectly reported and calculated as absolute pressures instead of hydrogen partial pressures. However, the main findings and conclusions did not change. This chapter presents a corrected version of the publication and a documentation of the corrections can be found in the electronic supplementary of this thesis.

Author contributions to the fourth paper

This work resulted from a collaboration with our dear friend Prof. Ali Güngör, who visited us in Duisburg for two months in 2018. Together, we carried out the first exergoeconomic work on the proposed polygeneration system.

The process concept results, including the single-zone engine model, were initially provided by Robert Hegner. On the basis of this data, Burak Atakan and me developed a Python script which solves the process concept exergoeconomically, and validated it together with Ali Güngör.

My further contribution was the data analysis, visualization, and the writing of the original manuscript. Ali Güngör and Burak Atakan were also engaged in reviewing the manuscript and Burak Atakan was the supervisor of this project.

Table 5.1: Author contributions for chapter 5 following the CRediT author statement methodology [41].

Author	Freund	Hegner	Güngör	Atakan
Conceptualization	✓	✓	✓	✓
Methodology	✓	✓	✓	✓
Software	✓	✓	✓	✓
Validation	✓		✓	
Formal analysis	✓		✓	
Investigation	✓		✓	
Resources				✓
Data curation	✓	✓		
Writing - Original draft	✓			
Writing - Review & editing	✓		✓	✓
Visualization	✓			
Supervision				✓
Project administration				✓
Funding acquisition				✓

5.1 Abstract

A polygeneration system producing hydrogen, electricity, process steam, and heating water is modeled and studied by conducting an exergoeconomic analysis. This system includes a homogeneous charge compression ignition (HCCI) engine burning a rich methane-air mixture, a water-gas shift reactor (WGSR) and a palladium membrane for hydrogen separation. Different cost-apportioning methods were considered in the present work in order to assess their suitability for the studied system. Furthermore, a global sensitivity analysis was used to identify the relevant system parameters as well as to quantify the influence that the input data uncertainty causes on the costs of the system products. It is shown that these costs are sensitive to the investment costs of only few system components and that the highest exergy destruction rates and costs occur in the engine. With the predicted cost of hydrogen ranging from 3.23 to 4.05 €/kg at EGR ratios of up to 25 %, the studied process is promising.

5.2 Introduction

High efforts are made nowadays to reduce the emissions of carbon dioxide and the consumption of fossil fuels. Internal combustion (IC) engines operated as decentralized cogeneration of heat and power (CHP) plants play an important role for achieving these objectives and are therefore widely used. IC engines are favorable since they are technically mature, require reasonable installation space, and have low investment and operation costs [116, 117]. Nevertheless, the improvement of such CHP plants in terms of exergetic efficiency is more and more reaching its limit. Therefore, an integration of separate processes to a polygeneration system that provides energy and chemical products could lead to a significant improvement with reasonable efforts in research and development [118]. The polygeneration system investigated in this work provides power, heat, and hydrogen by operating an IC engine in HCCI mode under fuel-rich conditions. We use methane as the fuel as it is the main part of natural gas and biogas which are fuels that may later be used in industrial applications. The fuel is partially oxidized in the HCCI engine and this results in high amounts of carbon monoxide and hydrogen in the exhaust gas which can be subsequently separated and used in downstream processes. Hydrogen is an important product since it is one of the main chemicals for the chemical industry and the majority of hydrogen used is currently produced by the steam reforming of natural gas [119].

In a previous work [34], a fuel-rich operated test HCCI engine for polygeneration of work, heat and hydrogen was investigated by means of an exergy analysis. It was found that the exergetic efficiency of such a system reaches values of up to 80 %. The polygeneration is therefore favorable compared to separate production as the overall exergetic efficiency of an engine for lean conditions in CHP operation is below 48 % for a medium-scale engine (903 kW power output) [23] and below 40 % for a large-scale engine (5.76 MW power output) [24]. The exergetic efficiency of steam methane reforming (SMR) to provide carbon monoxide and hydrogen does not exceed 63 % [26]. In addition to the theoretical work, it was shown experimentally that such a polygeneration process using HCCI engines is feasible and that it is exergetically favorable [30, 78]. This was accomplished using methane as a fuel, which requires high temperatures or alternatively the employment of some additives in order to ignite it through a compression. Syngas was produced in such engines with additional output of power and heat.

In this work we expand the investigation of the proposed process concept by Hegner et al. [34] towards an exergoeconomic analysis since not only the efficiency

74

of a novel energy system is crucial to evaluate but the economics as well. This kind of analysis helps to determine the cases in which an improvement of the exergetic efficiency is economically reasonable and whether non-exergy-related parameters, e.g. investment costs, are limiting. Therefore, this work aimed at determining the costs of the system products and comparing them with those of conventional systems. Literature reports applications to the study of combined-cycle power plants [120, 121], steam power plants [122], CHP plants [123] or geothermal plants [124], with the purpose of identifying components with the highest costs of exergy destruction and assessing the cost of power production.

To our knowledge, an exergoeconomic analysis of a fuel-rich operated HCCI engine for polygeneration has not been conducted before. In this first application we follow the standard exergoeconomic approach as described by Bejan, Tsatsaronis, and Moran [125]. There are different approaches using auxiliary equations to solve the cost balances in exergoeconomic analyses. Therefore, we investigate the methodology itself to identify the suitability of different methods when applied to polygeneration systems using engines. After finding a suitable method, we will identify the system components that should be improved in order to reduce the costs associated to exergy destruction. Due to the uncertainty in the costs and further used model parameters we carry out a global sensitivity analysis of these values on the estimated hydrogen costs and present the results. This also helps us to identify the most important parameters for process improvements.

5.3   Process concept

The polygeneration system is modeled in Python using the library Cantera to describe the thermodynamics and kinetics [50]. The system consists of an HCCI engine (IV) operated with neat methane as fuel, a water–gas shift reactor (WGSR; VIII), a palladium membrane for hydrogen separation (H2M; IX), several shell and tube heat exchangers (HE; V, X, XII, XIV, XVII), and hydrogen compressors (H2C; XI, XIII) to produce four different product streams: hydrogen, power, heating water, and process steam. Fig. 5.1 shows the flow diagram of the process.

To auto-ignite neat, relatively inert methane as fuel in the engine the temperature level must be increased at the engine entrance 3 as previously shown by Hegner and Atakan [34] and Wiemann et al. [30]. This also increases the radical concentrations after compression so that autoignition takes place after compression. We use a combination of two measures for this purpose: a preheater (II) heats the air–fuel mixture 1 using the exergy from the exhaust gas 18, and an external exhaust gas re-

75
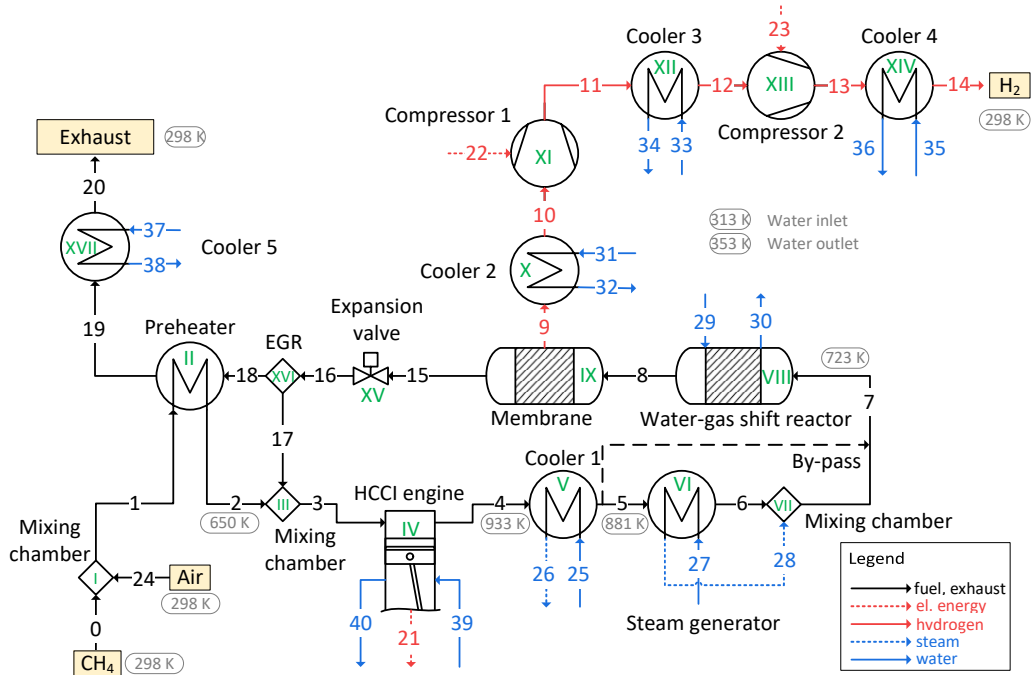
Figure 5.1: Process flow diagram of the polygeneration process.

circulation (EGR) increases the initial temperature. The EGR ratio x_{EGR} is defined as the molar ratio of recirculated exhaust gas n_{EG} to the total amount of mixed gas (fresh gas n_{FG} and exhaust gas n_{EG}) flowing into the engine (5.1).

$$x_{EGR} = \frac{n_{EG}}{n_{FG} + n_{EG}} \tag{5.1}$$

An expansion valve (XV) decreases the pressure of the exhaust gas to the pressure of the air fuel mixture before mixing both flows. We model one cylinder of the HCCI engine, which is part of a four-cylinder four-stroke engine, as a single zone reactor including the compression and combustion stroke but without gas exchange. Table 5.2 shows the engine's parameters.

We choose these parameters according to typical parameters of automotive engines [34]. The high rotational speed of 3000 1/min achieves high power and hydrogen outputs, thus lower specific product costs and lower heat losses. A detailed description of the engine model can be found in the previous work of Hegner et al. [34, 47].

Table 5.2: HCCI engine parameters used for the calculations.

Description	Symbol	Value	Unit
Rotational speed	rpm	3000	1/min
Compression ratio	r_c	16.5	
Bore	d	79.5	mm
Stroke	s	80.5	mm
Number of cylinders	N_Z	4	
Displacement	D	1.598	dm³
Fuel-air equivalence ratio	ϕ	2.38	
Mechanical power output[1]	P	18.54	kW

[1] The maximum mechanical power output for the lowest investigated $x_{EGR} = 0.05$.

Heat exchanger V (Cooler 1) and heat exchanger VI (Steam generator) produce steam and the high-pressure steam from Cooler 1 ($p = 50$ bar) is used as a system output and therefore as a product. The steam from the steam generator is used internally to provide the necessary amount of water vapor for the water–gas shift reaction. At EGR ratios above 40 % the steam generator VI and the mixing chamber VII are bypassed due to the higher concentrations of water vapor in the exhaust gas. We use a water–gas shift reaction (5.2) to increase the amount of hydrogen in the exhaust gas and to prevent CO molecules from inhibiting the permeation of hydrogen molecules. The latter is an important issue with palladium membranes [126]. The exothermal reaction proceeds at a constant temperature of 723 K. The produced heat increases the temperature of the heating water.

$$CO + H_2O \longleftrightarrow CO_2 + H_2 \tag{5.2}$$
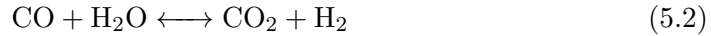
For the hydrogen separation we assume that the hydrogen membrane IX is designed for an effectiveness of 0.9, meaning that 90 % of the hydrogen initially in the feed gas stream 8 (which is the exhaust gas) permeates through the membrane [127].

We utilize the permeation law (5.3) from the work of Spallina et al. [128] to describe the mole flow of hydrogen through the membrane and we use the membrane parameters from experimental studies of Fernandez et al. [129–131] who investigate Pd-Ag alloy membranes, see Table 5.3.

$$\dot{n}_{H_2} = \frac{P_0}{t_m} \exp\left(\frac{-E_a}{RT}\right) A_m \left(p_{H2,ret}^{0.74} - p_{H2,perm}^{0.74}\right) \tag{5.3}$$

Table 5.3: Permeation law parameters used for membrane area calculation for cost estimation [129]. Membrane area and partial pressures are given for $x_{EGR} = 0.05$.

Description	Symbol	Value	Unit
Permeability	P_0	$1 \cdot 10^{-8}$	mol/s/m/Pa$^{0.74}$
Membrane thickness	d_m	$5.00 \cdot 10^{-6}$	m
Activation energy	E_a	$5.81 \cdot 10^3$	J/mol
Universal gas constant	R	8.314	J/mol/K
Reaction temperature	T	723	K
Membrane exponent	n	0.74	-
Membrane area	A_m	1.24	m^2
H$_2$ partial pressure retentate	$p_{H_2,ret}$	6.89	kPa
H$_2$ partial pressure permeate	$p_{H_2,perm}$	3.3	kPa

We utilize the permeation law to calculate the membrane area A_m which we need for the cost estimation. The system and its components do not contain the calculation of pressure drops. By performing the sensitivity analysis, we show in the discussion section that this is justified in terms of the influence on the prices. For further information on the system and its components see Tables 5.12, 5.13, and the previous work of Hegner et al. [34].

5.4 Methodology

The main principle of exergoeconomic analyses is defining the costs of an exergy flow i as the product of the specific exergy costs c_i and the total exergy flow $\dot{E}_i$ according to (5.4) using the **S**pecific **E**xergy **Co**sting approach (SPECO) [36].

$$\dot{C}_i = c_i \dot{E}_i \tag{5.4}$$

According to SPECO the exergy flows entering and exiting a component must be defined as fuel, product, or exergy loss. The fuel is defined as a stream whose exergy is decreased by flowing through the device. The exergy of a product is thus increased by flowing through a device. If an exergy stream exiting the component is not used it is defined as exergy loss (which is in this work the exhaust gas exiting the system into the environment). To calculate the specific exergy costs of the products cost balances (5.5) for each component k are carried out that lead to a system of linear equations [125, 132].

$$\sum \dot{C}_{F,i} + \dot{Z}_k = \sum \dot{C}_{P,i} + \dot{C}_{L,k} \tag{5.5}$$

In this equation $\dot{C}_{F,i}$, and $\dot{C}_{P,i}$, are the cost rates associated with the fuel and product, respectively and $\dot{C}_{L,k}$, is the cost rate of the exergy loss flow. The cost rates associated with the total device costs $\dot{Z}_k$ of component k are defined as the sum of the total capital investment (CI) costs $\dot{Z}_k^{CI}$ and the total operating and maintenance (OM) costs $\dot{Z}_k^{OM}$ allocated to the time units [123]. For these costs we consider the time value of money and the salvage value (SV) of the devices, see (5.6), (5.7), and (5.8).

$$\dot{Z}_k = \dot{Z}_k^{CI} + \dot{Z}_k^{OM} = (Z_k^{CI}(1 - \Omega \cdot PVF)CRF)\tau^{-1} + \dot{Z}_k^{CI}\varphi \tag{5.6}$$

$$CRF = \frac{i(1+i)^L}{(i+1)^L - 1} \tag{5.7}$$

$$PVF = \frac{1}{(1+i)^L} \tag{5.8}$$

In this calculation CRF denotes the capital recovery factor and PVF denotes the present value factor. The component cost rates depend on the interest rate i, the operating hours per year τ, the lifetime T, the salvage value factor Ω at the end of the lifetime, and the operating and maintenance costs factor φ.

We establish the device investment costs Z_k^{CI} by using the purchased equipment costs method (5.9) from Turton et al. and Bejan et al. for known device costs, also known as the sixth-tenth rule [125, 133], and the Chemical Engineering Plant Cost Index (CEPCI) to take inflation into account (5.10) [133–135].

$$Z_k^{CI} = Z_{ref}^{CI} \cdot \left(\frac{B_k}{B_{ref}}\right)^N \tag{5.9}$$

$$Z_{2018}^{CI} = Z_{ref}^{CI} \cdot \frac{Cost\ index\ 2018}{Cost\ index\ reference\ year} \tag{5.10}$$

The estimated component costs Z_k^{CI}, the basis costs Z_{ref}^{CI}, the components' basis properties B_{ref}, the cost exponents N, and the cost indexes can be found in the appendix in Tables 5.14, 5.15, and Fig. 5.11. Subsequently, as a worst-case scenario, we use the maximum device costs of all EGR ratios for the calculations. Table 5.4 shows the financial parameters for the exergoeconomic analysis including the uncertainty range that we use for the sensitivity analysis.

For devices with n exiting flows $n - 1$ auxiliary relations are required to solve the cost balances [124].

There are many different approaches in the literature, but it is not clear which of them is well suited for such a polygeneration system. We consider three different

Table 5.4: Financial parameters used for the calculations.

Description	Symbol	Value	Unit	Uncertainty	Min.	Max.
Lifetime	L	15	a	±30 %	10.5	19.5
Operating hours	τ	7920	h/a	±30 %	5544	8760
Interest rate	i	0.10	-	±30 %	0.07	0.13
SV-factor	Ω	0.05	-	±30 %	0.035	0.065
OM-factor	φ	0.03	-	±30 %	0.021	0.039
Air exergy costs	c_{air}	0.00	€/MWh	±30 %	0.00	0.00
CH_4 exergy costs	c_{CH_4}	17.90	€/MWh	±30 %	12.53	23.27
Electricity costs	c_{el}	42.00	€/MWh	±30 %	29.40	54.60

methods for defining those auxiliary equations for the important components of the investigated polygeneration system: the Fuel and Product Principle (FP) [36], the Extraction Method (Extr), and the Equality Method (Eq) [136].

For components with more than two product streams and mainly chemical conversion, i.e. HCCI engine and WGSR, the apportionment of the specific exergy costs plays a significant role. For example, for the WGSR the exergy flow of the exhaust stream is reduced during the process while the exergy flow of the heating water is increased. This suggests that the heating water should be its main product.

On the contrary, the reactor's main purpose is to increase the hydrogen concentration in the exhaust gas and the chemical exergy represents a major part of the total exergy. Therefore, the costs can be charged equally on both the heating water and the exhausted gas (FP/Eq) or only on the exhaust gas (Extr). The same considerations hold for the HCCI engine. Table 5.5 presents the equations corresponding to the three investigated approaches.

Table 5.5: Methodology for the exergoeconomic analysis.

Component	Engine	WGSR	HE	H2C	MIX	H2M
Schematic						
Cost rates fuel	$\dot{C}_1$	$\dot{C}_1$	$\dot{C}_1 - \dot{C}_2$	$\dot{C}_c$	$\dot{C}_1 + \dot{C}_2$	$\dot{C}_1 - \dot{C}_2$
Cost rates product	$\dot{C}_b - \dot{C}_a + \dot{C}_c + \dot{C}_2$	$\dot{C}_b - \dot{C}_a + \dot{C}_2$	$\dot{C}_b - \dot{C}_a$	$\dot{C}_2 - \dot{C}_1$	$\dot{C}_3$	$\dot{C}_3$
Product streams	3	2	1	1	1	1
Auxiliary equations	2	1	1	0	0	0
F/P principle	$\frac{\dot{C}_b - \dot{C}_a}{E_b - E_a} = \frac{\dot{C}_c}{E_c} = \frac{\dot{C}_2}{E_2}$	$\frac{\dot{C}_b - \dot{C}_a}{E_b - E_a} = \frac{\dot{C}_2}{E_2}$	$c_2 = c_1$			
Extraction method	$c_c = c_b = c_1$	$c_b = c_1$	$c_2 = c_1$			
Equality method	$c_c = c_b = c_2$	$c_2 = c_b$	$c_2 = c_1$			
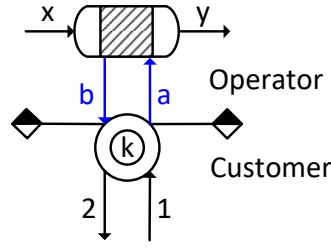
Figure 5.2: Process flow diagram of a subsystem showing the coupling of the operator's component (reactor) and the customers component (consumer device).

The specific exergy cost of (cooling) water flowing into the system c_a is set to zero. We do that because an external customer shall pay for all component costs incurred by the operator of the polygeneration system to provide the product (here: heating water). Fig. 5.2 illustrates exemplarily a subsystem with a cooled reactor on the operator's side and a consumer on the customer's side and eq. (5.11) shows the cost balance of the customer's device k.

$$\dot{C}_2 = \dot{C}_1 + \dot{C}_b - \cancelto{0}{\dot{C}_a} + \dot{Z}_k \qquad (5.11)$$

If $\dot{C}_a$ is zero, this will lead to the highest costs for the customer's product which is the heated stream 2. This is a worst-case scenario for the costs of the heating water and therefore used in this analysis. By setting the costs of the inflowing water to zero the Equality Method is identical to the Fuel and Product Principle and neglected in the following investigation.

We vary the evaluation methods of the engine and the water–gas shift reactor for the method comparison. In addition, we apportion the exergy-loss cost rate $\dot{C}_{20}$ to all products weighted by their relative exergy flow according to Eq. (5.12) because the exhaust gas is not used further but is released into the environment [125].

$$\dot{C}_{P,i} = \dot{C}_{P,i} + \dot{C}_L \frac{\dot{E}_{P,i}}{\sum \dot{E}_{P,i}} \qquad (5.12)$$

To distinguish the different method combinations, we introduce an abbreviated nomenclature. The first method stands for the WGSR and the second one for the HCCI engine leading to the following four combinations: FP-FP, FP-Extr, Extr-FP, Extr-Extr. Then, we compare the evaluated production costs to the mean reference production costs shown in Table 5.6. We calculate the steam costs by only taking

Table 5.6: Reference production costs for the products of the polygeneration system.

Product	Min.	Mean	Max.	Unit	Ref. systems	Ref.
Electricity	38.0	69.0	100.0	€/MWh	Power plants[3]	[137]
Hydrogen	1.47	2.43	3.90	€/kg	SMR[2]	[119]
Steam	14.40	-	-	€/t	Steam boiler[1]	
Heating water	0.956	1.368	1.780	€/t	District heating	[138]

[1] Calculated for high pressure steam $p = 50$ bar, $T_{Feed} = 10$ °C with a boiler efficiency of $\eta_B = 0.95$ considering fuel costs only.

[2] Small and large scale SMR providing hydrogen mass flows from 72 kg/h to 9,000 kg/h.

[3] Coal power plants, as well as gas and steam power plants in Germany (2018).

the fuel costs c_{CH_4} into account as the boiler costs depend on the application. This leads to minimal steam production costs which we use for the comparison.

The cost balance Eq. (5.5) does not consider exergy destruction even though this is very important when correlating exergy flows with cost flows. Therefore, we calculate the cost rates of exergy destruction $\dot{C}_{D,k}$, following [125] (p. 426) with the assumption that the exergy destruction $\dot{E}_{D,k}$, is independent of the specific fuel costs $c_{F,k}$ (5.13).

$$\dot{C}_{D,k} = c_{F,k}\dot{E}_{D,k} \qquad (5.13)$$

We calculate the exergoeconomic factor f_k (5.14) for each component k. This figure helps us to distinguish between the causes of the specific product costs [125, 132]. If the value is low, the cost increase is mainly caused by exergy-loss-related costs and therefore the exergetic efficiency of the device should be improved even if it increases the device costs. On the contrary, the device costs should be lowered if the factor has a high value, even at some expense of the exergetic efficiency. Furthermore, we use the relative cost difference r_k (5.15) that is helpful to determine the components in which the product costs increase strongly. These components should thus be optimized on an exergetic or economic basis [125].

$$f_k = \frac{\dot{Z}_k}{\dot{Z}_k + c_{F,k}(\dot{E}_{D,k} + \dot{E}_{L,k})} \qquad (5.14)$$

$$r_k = \frac{c_{P,k} - c_{F,k}}{c_{F,k}} \qquad (5.15)$$

We calculate the exergetic efficiency ε_k (5.16) of each component k to provide further information on where crucial exergy destructions in the polygeneration system occur [125, 139]. To compare the exergetic efficiency of this process concept to conventional processes we consider the system's exergetic efficiency ε_{sys} (5.17).

$$\varepsilon_k = \frac{\left(\sum \dot{E}_{i,k}\right)_P}{\left(\sum \dot{E}_{i,k}\right)_F} = 1 - \frac{\sum(\dot{E}_{D,k} + \dot{E}_{L,k})}{\left(\sum \dot{E}_{i,k}\right)_F} \tag{5.16}$$

$$\varepsilon_{sys} = \frac{\sum \dot{E}_{i,out}}{\sum \dot{E}_{i,in}} = 1 - \frac{\sum(\dot{E}_{D,k} + \dot{E}_{L,k})}{\sum \dot{E}_{i,in}} \tag{5.17}$$

In addition to the calculations with constant financial parameters we carry out a global sensitivity analysis using the Sobol method [140] as implemented in $SALib$ [141]. A global sensitivity analysis is a variance-based method to identify to what extent the input parameters of a system influence the output parameters [142]. The Sobol method utilizes the Monte Carlo method: A defined number of samples with values with a defined uncertainty range for each input parameter are randomly selected and used for the calculation of the output parameters. The variance of the model's output when a single input parameter is fixed $V_{X_i}(E_{X_{\sim i}}(Y|X_i))$ is then compared to the variance of the model's output $V(Y)$. The first order sensitivity index S_i (5.18) is defined as the ratio of these two values as described in [140].

$$S_i = \frac{V_{X_i}(E_{X_{\sim i}}(Y|X_i))}{V(Y)} \tag{5.18}$$

The advantage over local sensitivity analysis, which is derivative-based, is that it remains reliable even for non-linear models, but they are computationally more expensive [140]. The sensitivity analysis helps to determine the influence of the uncertainty in model parameters, like device costs, fuel costs, and financial parameters on the final product costs. In this work we calculate and analyze the first order sensitivity coefficients S_1 and the total sensitivity coefficients S_T. We vary all cost parameters within ± 30 % which is the expected accuracy of economic values for studies [134]. We choose a base sample of 1024 with 25 parameters. According to Saltelli's extension of Sobol's method this leads to 27,648 model runs for each EGR ratio.

5.5 Results and discussion

First, we compare the calculated production costs with the four methods for a typical EGR ratio of 0.05. The production costs from the different auxiliary
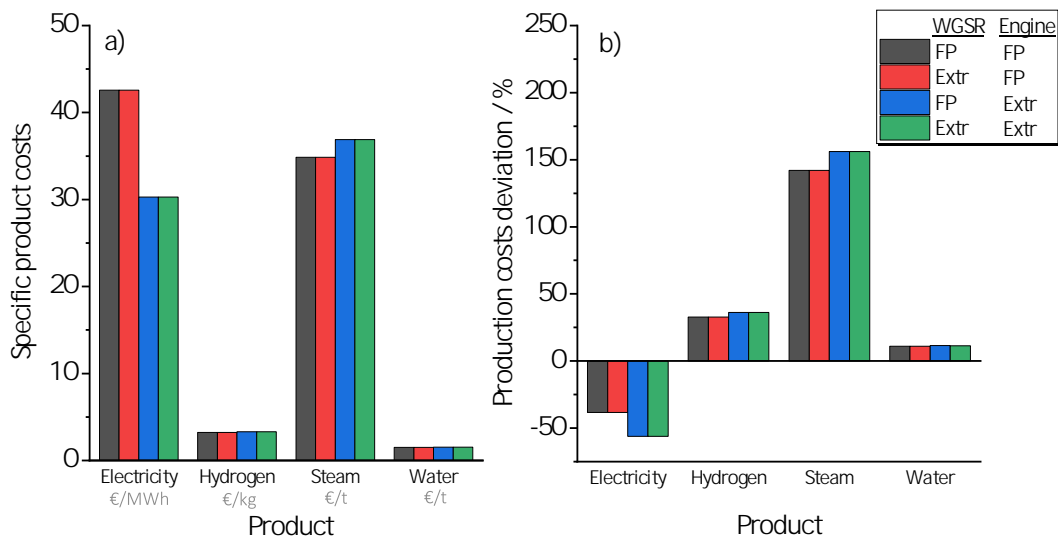
Figure 5.3: Production costs comparison for different auxiliary equation methods (EGR ratio = 0.05; FP = Fuel/Product Principle; Extr = Extraction Method; in the colored legend the first value shows the applied method for the WGSR and the second value shows the applied method for the HCCI engine). a) illustrates the specific product costs and b) illustrates the deviation from the mean reference production costs shown in Table 5.6.

equation methods stay below the mean reference costs for electricity but exceed the mean hydrogen costs, the mean heating water costs, and the minimal steam costs as shown in Fig. 5.3. The minimal steam costs are exceeded since the same fuel costs, but no boiler costs are considered for the steam production comparison. At first sight, some points are recognizable: The differences between all four methods seem to be minor for each product except the electricity. The change of the method for the evaluation of the HCCI engine changes the electricity costs significantly. The engine's method is thus more important than the reactor's method. If the Extraction Method is used for the WGSR, the decrease in heating water costs is below 0.16 % and the increase in hydrogen costs is below 0.01 %. Thus, there is no significant dependency on the method.

In contrast to the WGSR, the choice of the HCCI engine method affects the costs for electricity, hydrogen, and steam substantially: if the Extraction Method (Extr) is used and all costs are charged on the exhaust gas containing the hydrogen, the electricity costs deviation decreases by 17.81 %-points. This happens at the expense of the steam and hydrogen costs; they increase by 13.99 %-points and 3.36 %-points, respectively. For the heating water costs there are no noticeable dependencies. In
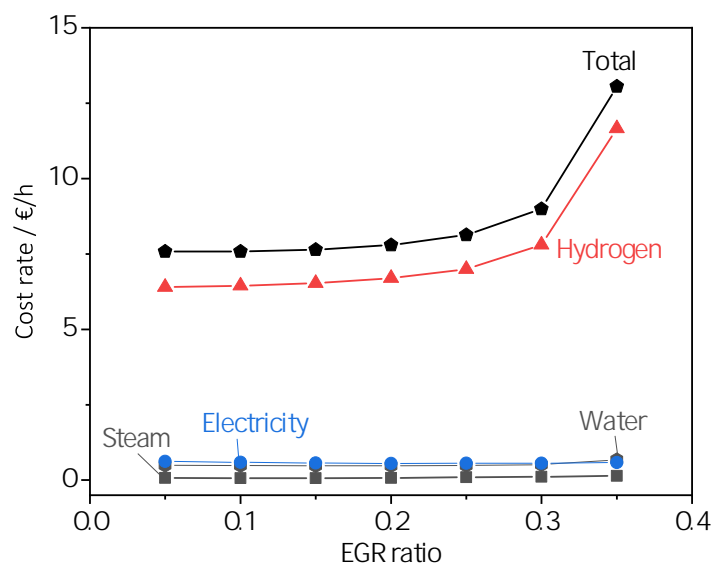
Figure 5.4: Cost rates of the system's products as a function of external exhaust gas recirculation ratio.

general, the electricity costs are lower than the reference costs while all other product costs are higher for both methods. The deviation of the hydrogen and steam costs can be reduced when the Fuel and Product Principle is used for the HCCI engine. If the polygeneration system benefits from scale-up effects, which we will investigate in the future, this would lead to competitive product costs at lower scales. Therefore, we use the Fuel and Product Principle for the engine and, for the sake of consistency, for all components including the WGSR throughout the remaining part of the paper. Thus, all three useful outputs of the engine are charged with the costs.

Fig. 5.4 shows the cost rates of the products using the Fuel and Product Principle for the investigated process concept as a function of the EGR ratio for the given constant financial parameters of Table 5.4. In general, the cost rates increase with increasing EGR ratio since, on the one hand the exergy flows decrease by recirculating exhaust gas (having a lower specific exergy than the fuel–air mixture) as illustrated in Fig. 5.5 and, one the other hand the hydrogen mole fractions decrease, which leads to strongly increasing membrane area and thus investment costs. At EGR ratios of 0.4 and higher, the hydrogen partial pressure on the permeate side of the membrane is lower than on the retentate side and thus no hydrogen can be separated. Therefore, EGR ratios of 0.4 and higher are neglected in the following analysis.

The hydrogen costs are responsible for 84.4 % up to 89.3 % of the total costs
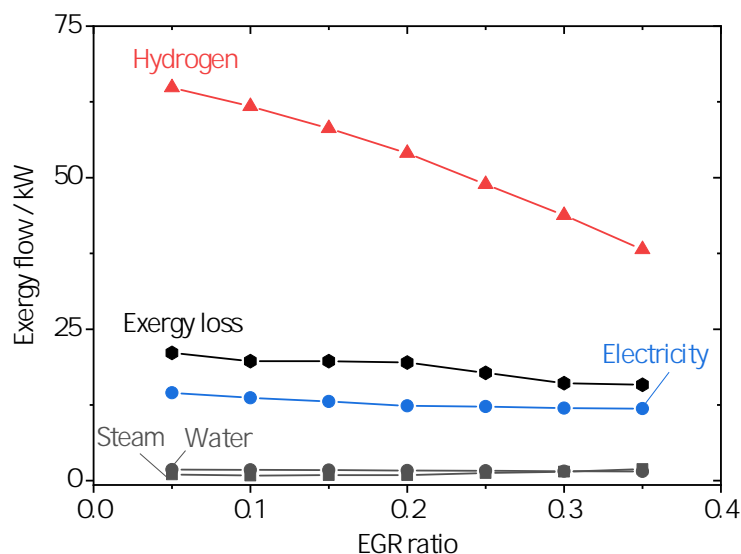
Figure 5.5: Exergy flows of the system's products and exergy losses as a function of external exhaust gas recirculation ratio.

increasing with the EGR ratio while those of electricity, steam, and water are comparatively low (with maximum values of 8.1 %, 1.1 %, and 6.5 %, respectively).

The cost rates do not indicate whether the production costs of the products are competitive compared to the reference costs shown in Table 5.6. Therefore, they are converted to specific product costs by dividing the cost rates by the associated exergy flows for electricity or mass flows for the other product streams, respectively. Fig. 5.6 compares those specific product costs as a function of the EGR ratio.

The specific product costs strongly increase with increasing EGR ratio as the exergy flows decrease and the total component costs increase. The costs for hydrogen, electricity, and heating water rise from 3.23 €/kg to 10.00 €/kg, 42.57 €/MWh to 49.12 €/MWh and 1.52 €/t to 2.52 €/t, respectively. The specific steam costs decrease at low EGR ratios because the mole fraction of water vapor increases with increasing EGR ratio and thus the steam generator must produce gradually less steam. This leads to an increasing heat flow through Cooler 1 to ensure the desired reaction temperature of 723 K for the water–gas shift reaction. At higher EGR ratios the component costs overlay this effect. At low EGR ratios the production costs of hydrogen, electricity, and heating water are competitive and reasonable although the mean reference costs of the hydrogen production are exceeded. The maximum reference value for hydrogen (3.9 €/kg) is exceeded at EGR ratios higher than 0.2 while the costs of heating water and electricity are still competitive. It follows that
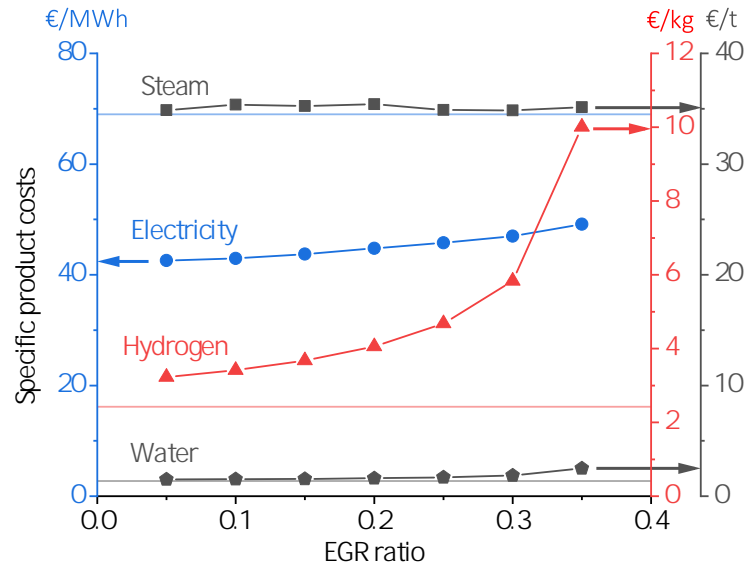
Figure 5.6: Specific production costs of the system's products as a function of external exhaust gas recirculation ratio. First axis, blue circles: electricity costs in €/MWh; second axis, red triangles: hydrogen costs in €/kg; third axis, grey squares and pentagons: steam and water costs in €/t. Horizontal lines illustrate the mean reference costs taken from Table 5.6.

high EGR ratios should be avoided or only used for short periods per year. The financial parameters limit the flexibility of the polygeneration system in part, but this does not seem to be severe because EGR ratios approaching 1 can never be rational, due to the large dilution.

We perform a global sensitivity analysis for different EGR ratios and vary the economic parameters shown in Table 5.4 by ±30 % as listed in Table 5.14. Fig. 5.7 shows two histograms that give an impression of the calculated hydrogen costs and total costs from the statistically varying uncertainty of the parameters, resulting from 27,648 calculations.

Due to the non-linearity of the model the calculated hydrogen costs and total costs, resulting from the fix values from Table 5.4, deviate from the mean values by −9.66 % and −9.41 %, respectively. The product costs may therefore be slightly higher if the actual economic parameters differ from the parameters chosen in this work.

Fig. 5.8 shows the results of the sensitivity analysis for parameters with first order sensitivities S_1 above 0.01 as a function of the EGR ratio. In general, the dependency on the EGR ratio is minor. Also, the first order sensitivity coefficients do not deviate strongly from the total sensitivity coefficient which are also plot-
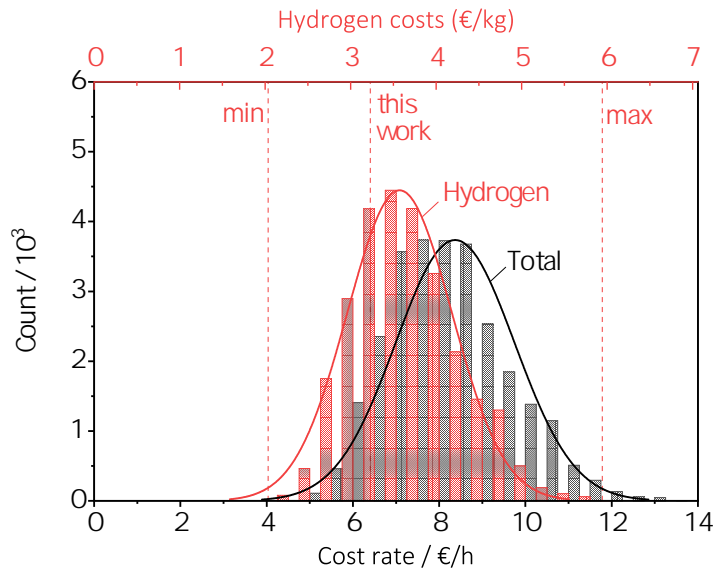
Figure 5.7: Histograms of the hydrogen and total cost rates resulting from statistically varying the uncertain parameters by ± 30 %; the parameters are shown in Table 5.14 (EGR ratio = 0.05).
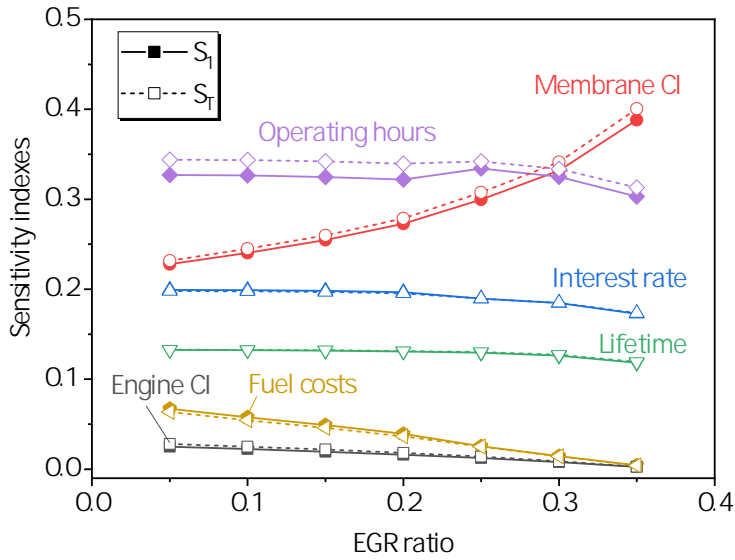
Figure 5.8: First order and total order sensitivity indexes as a function of EGR ratio for first order sensitivity indexes larger than 0.001 (solid lines: first order; dashed lines: total order).
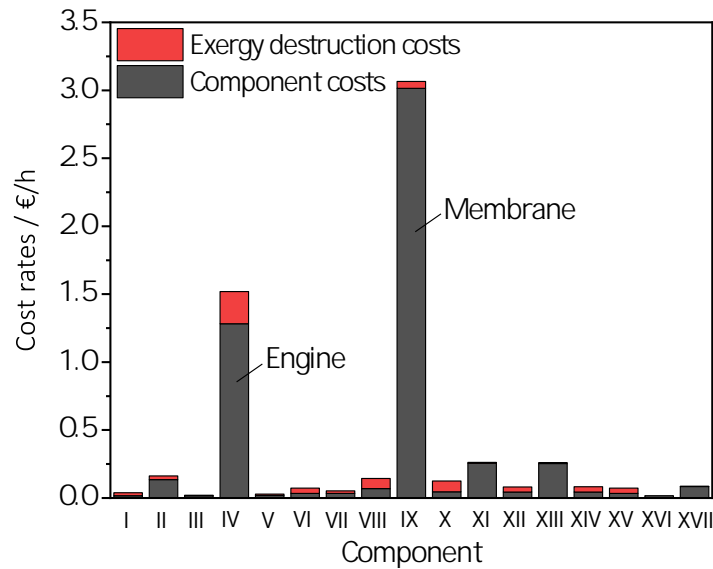
Figure 5.9: Component costs (grey) and exergy destruction costs (red) of the components.

ted. Thus, the main effects are direct effects. Six parameters have non-negligible sensitivities: the interest rate, the lifetime, the operating hours, the fuel costs, and the device costs of the engine and the hydrogen membrane. The membrane has the highest investment costs of all devices. The compressor work is not among the sensitive parameters which also holds for the sum of both compressors. Thus, some pressure drop in the devices should not influence the costs considerably.

Except for the fuel costs and the H2M capital investment, the sensitivities of these parameters do not depend significantly on the EGR ratio. The dependency on the fuel costs decreases since the exergy flow of the fuel decreases with increasing EGR ratio. On the contrary, the first order sensitivity index for the H2M capital investment increases by 70.3 %. If only the sensitivities were considered it could be reasoned that the hydrogen and engine investment costs should be reduced to reduce the product costs. A reduction in investment costs could lead to a reduction in efficiency as well, which could eventually be more crucial for the product costs. Therefore, the evaluation of the characteristic numbers of the exergoeconomic analysis is important to decide whether it is more reasonable to increase the efficiency of the components or to decrease the investment costs.

Table 5.7: Exergoeconomic analysis for EGR ratio = 0.05, ordered by relative exergy destruction $y_{D,k} > 3\%$ ($\dot{E}_{D,k}$: exergy destruction rate; $y_{D,k}$: relative exergy destruction; $\dot{C}_{D,k}$: cost rate of exergy destruction; $\dot{Z}_k$: cost rate of component costs; ε_k: exergetic efficiency; f_k: exergoeconomic factor; r_k: relative cost difference). Complete Table 5.16 can be found in the appendix.

No.	Component	$\dot{E}_{D,k}$ (W)	$y_{D,k}$ (%)	$\dot{C}_{D,k}$ (€/h)	$\dot{Z}_k$ (€/h)	ε_k (%)	f_k (%)	r_k (%)
IV	HCCI engine	11,665.6	51.0	0.236	1.283	62.0	84.5	64.7[1]
VIII	WGS reactor	2,146.9	9.4	0.074	0.069	14.6	48.0	4.4[1]
IX	Hydrogen membrane	1,447.5	6.3	0.052	3.014	97.8	98.3	132.9[1]
I	Mixing chamber fuel	1,252.3	5.5	0.022	0.017	99.0	42.6	1.7[1]
VI	Steam generator	1,215.0	5.3	0.040	0.033	58.7	44.9	127.3[2]
XV	Expansion valve	1,085.3	4.7	0.039	0.033	96.0	45.9	0.0[1]
X	Cooler 2	945.4	4.1	0.08	0.045	26.0	36.4	401.1[3]
II	Preheater	756.5	3.3	0.027	13.5	80.0	83.2	9.3[1]

[1] Hydrogen
[2] Steam
[3] Heating water

At an EGR ratio of 0.05 the exergetic efficiency of the polygeneration system is high with a value of 65.2 % but it may be possible to improve it further. Thus, we regard the exergy destruction in the process for the devices with the highest exergy destruction and their costs. Table 5.7 shows that the engine and the WGSR cause the highest exergy destruction rates with about 51.0 % relative exergy destruction in the engine and 9.4 % in the reactor. Thus, these components produce the highest exergy destruction costs as well.

We compare the total costs of different components in Fig. 5.9. It shows the sum of the component costs (grey) and the exergy destruction costs (red). A decrease of the engine costs, either by reducing the irreversibility or the investment costs, and a decrease of the membrane costs would have the highest effect on product costs reductions. The influence of the costs of all other components on the products' cost rates are minor.

The hydrogen cost increase from the membrane and the HCCI engine is mainly caused by their high investment costs and not by their exergy destruction rates as the exergoeconomic factors f_k have high values of 98.3 % and 84.5 %. Due to their high cost rates these components increase the hydrogen costs the most. This is seen from their relative cost differences of 64.7 % for the engine and 132.9 % for the membrane, respectively. In contrast, the expansion valve causes a relatively high exergy destruction but because of its low investment costs it does not significantly affect the product costs. All other components influencing the hydrogen costs have relative cost differences below 9.3 %. As engines are well approved in terms of thermal efficiency, reliability, and production costs, a larger leverage for lowering the hydrogen production costs should be a replacement or improvement of the hydrogen membrane, e.g. reducing the investment costs. This can even be accompanied with a lower exergetic efficiency of the separation process, since the membranes' exergoeconomic factor is close to 1. To achieve lower hydrogen costs than the mean reference costs of 2.43 €/kg for SMR the membrane's investment costs must be decreased by 54 % at an EGR ratio of 0.05. The minimal reference costs of 1.47 €/kg cannot be reached by solely reducing the membrane's investment costs. Since the minimal reference costs for an SMR process lead to a 4540 times higher hydrogen mass flow rate, scale-up effects for all components may play a significant role. The exergetic efficiencies range from 26 % to 80 % in the heat exchangers and reach values of 14.6 % for the WGS-reactor, and 62.0 % for the engine. Therefore, the exergetic efficiency of the WGS-reactor has the highest potential for improvements.

Finally, the system's exergetic efficiency should be compared to those of conventional processes as mentioned in the introduction: an engine CHP plant (48 %) and
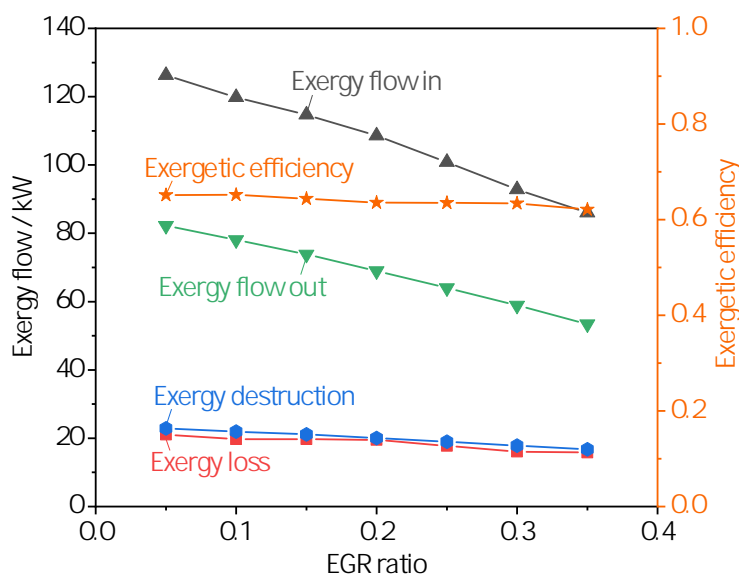
Figure 5.10: Exergy flows (left scale) and exergetic efficiency of the system (right scale) as a function of external exhaust gas recirculation ratio.

steam methane reforming (63 %). Fig. 5.10 illustrates the inflowing and outflowing exergy flows of the system, the exergy destruction, and the exergetic efficiency as a function of EGR ratio. The exergetic efficiency of the system decreases slightly with increasing EGR ratio having a maximum value of 65.2 % and a minimum value of 62.1 % at EGR ratios of 0.05 and 0.35, respectively. Consequently, higher EGR ratios are not favorable, even if the membrane would be operable under these conditions.

Therefore, the system's exergetic efficiency surpasses engines for cogeneration by 17 %-points but it is comparable to the efficiency of steam methane reforming processes. Since a facility using steam methane reforming usually has the need for electricity and process heat, e.g. in the chemical industry, a conventional reforming process could be substituted by this polygeneration process and replace a part of the external electricity supply as well as heat generation, e.g. by boilers, and increase the system's overall exergetic efficiency.

5.6 Conclusions

We investigate a process concept using a fuel-rich operated HCCI engine for providing work, heat, steam, and hydrogen by conducting an exergoeconomic analysis including a comparison of the Extraction method, the Equality method, and the Fuel and Product Principle.

Main results

For such polygeneration systems the SPECO method using the Fuel and Product Principle is the most suitable method, because it leads to the lowest hydrogen, water and steam costs. This increases the electricity costs, which stay below the reference costs. To reduce the product costs – especially the hydrogen costs – of the investigated HCCI polygeneration system the investment costs of the hydrogen membrane should be reduced or substituted by a different, cheaper hydrogen separation technology, e.g. pressure swing adsorption. If this reduces the exergetic efficiency of the hydrogen separation, it should not influence the hydrogen costs significantly, since the membrane's exergoeconomic factor is high (98.3 %).

Hydrogen costs and exergetic efficiency

The hydrogen costs per kg for the given financial parameters have a reasonable range of 3.23–4.05 €/kg for EGR ratios below 25 % compared to about 1.47 to 3.90 €/kg when using steam methane reforming. From the sensitivity analysis we find that the costs depend only on a few parameters and that the resulting variance is smaller than the variance or uncertainty of the parameters. The overall exergetic efficiency is about 65 %. This is 17 %-points higher compared to an engine CHP plant and it is comparable to the efficiency of steam methane reforming.

Necessary improvements

We show that the proposed polygeneration system is promising and several improvements should be made in the future to reduce the overall costs: e.g. finding a cheaper separation technology for hydrogen or scaling-up of the engine.

Limitations

There are as well some limitations due to the model's level of detail. For instance, the gas exchange in the cylinder is not modeled and therefore the heat transfer during these strokes is neglected. The single zone model does not represent the reaction kinetics in colder parts of the cylinder, e.g. crevices and cylinder walls. This reduces the chemical conversion. We do not consider pressure losses in some of the components as well as the post-treatment of the exhaust gas.

Outlook

The model's limitations may be overcome by increasing the level of detail of the process concept model and including a multi-zone model in the future. Furthermore, we will compare these results to an exergoeconomic analysis of alternative, separate processes for energy conversion and hydrogen production. We also plan to extend this analysis towards further chemical products.

5.7 Funding

5.8 Declaration of Competing Interest

The authors declare that they have no known competing financial interests or personal relationships that could have appeared to influence the work reported in this paper.

5.9 Acknowledgments

5.10 Nomenclature

Table 5.8: Abbreviations.

Abbreviation	Description
CEPCI	Chemical Engineering Plant Cost Index
CHP	Cogeneration of heat and power
CI	Capital investment
CRF	Capital recovery factor
EGR	Exhaust gas recirculation
Eq	Equality Method
Extr	Extraction Method
FP	Fuel and Product Principle
H2C	Hydrogen compressor
H2M	Hydrogen membrane
HCCI	Homogeneous charge compression ignition
HE	Heat exchanger
MIX	Mixing chamber
OM	Operating and maintenance
PVF	Present value factor
SMR	Steam methane reforming
SV	Salvage value
WGSR	Water-gas shift reactor

Table 5.9: Symbols.

Symbol	Unit	Description
$\dot{C}$	€/s	Cost rate associated with exergy flows
$\dot{E}$	W	Exergy flow
$\dot{E}_a$	J/mol	Activation energy
P_0	$mol/(smPa^{0.74})$	Permeability
$\dot{Z}$	€/s	Cost rate associated with device costs
$\dot{n}$	mol/s	Mole flow
A	m^2	Area
B		Device property (e.g. Area, Power)
D	m^3	Displacement

L	years	Lifetime
N		Cost exponent
N_Z		Number of cylinders
P	W	Power
R	J/mol/K	Universal gas constant
S		Sensitivity index
T	K	Temperature
V		Variance
X		Arbitrary input value (sensitivity index definition)
Y		Arbitrary output value (sensitivity index definition)
Z_k	€	Device costs
c	€/J	Specific exergy costs
d	m	Bore
f_k		Exergoeconomic factor
n_{FG}	mol	Molar amount of fresh gas
n_{EG}	mol	Molar amount of exhaust gas
p	Pa	Pressure
r_c		Compression ration
r_k		Relative cost difference
rpm		Rotational speed
n		Membrane exponent
s		Stroke
d_m		Thickness membrane
x		Mole fraction
y		Share of exergy destruction

Table 5.10: Greek symbols.

Symbol	Unit	Description
ϕ		Operating and maintenance factor
Ω		Salvage value factor
ε		Exergetic efficiency
η		Energetic efficiency
τ	h	Operating hours
Φ		Fuel-air equivalence ratio

Table 5.11: Subscripts

Abbreviation	Description
1	First order (sensitivity index)
B	Boiler
CH_4	Methane
D	Destruction
F	Fuel
$Feed$	Feed of hydrogen membrane
$H_2, perm$	Permeate hydrogen membrane
H_2, ret	Retentate hydrogen membrane
L	Loss
P	Product
T	Total order (sensitivity index)
$a, b, c, 1, 2, 3$	Indexes of flows or components
air	Ambient air
el	Electricity
i	Index of flows
in	In
k	Index of component
out	Out
ref	Reference data
sys	System (whole process concept)

5.11 Appendix

Table 5.12: State Data for an EGR ratio of 0.05.

No.	p	T	$\dot{m}$	$\dot{E}^{ph}$	$\dot{E}^{ch}$	$\dot{E}^{t}$	$\dot{C}$
	(bar)	(°C)	(kg/h)	(kW)	(kW)	(kW)	(€/h)
0	1.013	25.00	8.70	0.00	126.11	126.11	2.26
1	1.013	25.00	71.32	0.00	124.85	124.85	2.27
2	1.013	376.85	71.32	3.03	124.85	127.88	2.55
3	1.013	380.32	75.33	3.23	125.84	129.07	2.61
4	1.774	665.11	75.33	10.43	87.94	98.37	3.28
5	1.774	601.01	75.33	9.06	87.94	97.00	3.23
6	1.774	449.85	75.33	6.12	87.94	94.06	3.13
7	1.774	449.85	81.02	6.75	88.45	95.21	3.30
8	1.774	449.85	81.02	6.89	85.80	92.69	3.35
9	0.033	449.85	1.98	-1.03	64.86	63.83	5.37
10	0.033	49.85	1.98	-2.31	64.86	62.55	5.27
11	0.182	301.80	1.98	-0.52	64.86	64.35	5.59
12	0.182	49.85	1.98	-1.16	64.86	63.71	5.53
13	1.013	304.27	1.98	0.66	64.86	65.52	5.86
14	1.013	49.85	1.98	0.01	64.86	64.87	5.80
15	1.774	449.85	79.04	5.22	22.19	27.42	0.99
16	1.013	449.85	79.04	4.14	22.19	26.33	0.95
17	1.013	449.85	4.01	0.21	1.13	1.34	0.05
18	1.013	449.85	75.03	3.93	21.07	25.00	0.90
19	1.013	90.85	75.03	0.15	21.07	21.21	0.77
20	1.013	49.85	75.03	0.02	21.07	21.09	0.76
21	-	-	-	18.54	0.00	18.54	0.62
22	-	-	-	2.01	0.00	2.01	0.07
23	-	-	-	2.03	0.00	2.03	0.07
24	1.013	25.00	62.62	0.00	0.00	0.00	0.00
25	1.013	39.85	2.12	0.00	0.00	0.00	0.00
26	50.000	79.85	2.12	1.05	0.00	1.05	0.06
27	1.013	39.85	5.69	0.00	0.00	0.00	0.00
28	1.774	449.85	5.69	1.73	0.00	1.73	0.13
29	1.013	39.85	76.02	0.03	0.00	0.03	0.00
30	1.013	79.85	76.02	0.40	0.00	0.40	0.01

31	1.013	39.85	68.83	0.03	0.00	0.03	0.00
32	1.013	79.85	68.83	0.36	0.00	0.36	0.15
33	1.013	39.85	43.34	0.02	0.00	0.02	0.00
34	1.013	79.85	43.34	0.23	0.00	0.23	0.10
35	1.013	39.85	43.76	0.02	0.00	0.02	0.00
36	1.013	79.85	43.76	0.23	0.00	0.23	0.10
37	1.013	39.85	20.38	0.01	0.00	0.01	0.00
38	1.013	79.85	20.38	0.11	0.00	0.11	0.09
39	1.013	25.00	72.01	0.03	0.00	0.03	0.00
40	1.013	89.85	72.01	0.52	0.00	0.52	0.02

Table 5.13: Mole fractions for an EGR ratio of 0.05.

No.	CH_4	O_2	H_2	CO	CO_2	H_2O	N_2
0	1.00	0.00	0.00	0.00	0.00	0.00	0.00
1	0.20	0.17	0.00	0.00	0.00	0.00	0.63
2	0.20	0.17	0.00	0.00	0.00	0.00	0.63
3	0.19	0.16	0.00	0.00	0.01	0.01	0.63
4	0.00	0.00	0.22	0.15	0.02	0.10	0.52
5	0.00	0.00	0.22	0.15	0.02	0.10	0.52
6	0.00	0.00	0.22	0.15	0.02	0.10	0.52
7	0.00	0.00	0.20	0.13	0.02	0.18	0.48
8	0.00	0.00	0.29	0.05	0.10	0.09	0.48
9	0.00	0.00	1.00	0.00	0.00	0.00	0.00
10	0.00	0.00	1.00	0.00	0.00	0.00	0.00
11	0.00	0.00	1.00	0.00	0.00	0.00	0.00
12	0.00	0.00	1.00	0.00	0.00	0.00	0.00
13	0.00	0.00	1.00	0.00	0.00	0.00	0.00
14	0.00	0.00	1.00	0.00	0.00	0.00	0.00
15	0.00	0.00	0.04	0.06	0.14	0.12	0.64
16	0.00	0.00	0.04	0.06	0.14	0.12	0.64
17	0.00	0.00	0.04	0.06	0.14	0.12	0.64
18	0.00	0.00	0.04	0.06	0.14	0.12	0.64
19	0.00	0.00	0.04	0.06	0.14	0.12	0.64
20	0.00	0.00	0.04	0.06	0.14	0.12	0.64

Table 5.14: Capital investment costs of the components.

No.	Component	$Z^{CI\ 1}$ (€)	Cost factor [2]	Z^{CI} (€)	Uncertainty [3]	Min. (€)	Max. (€)
I	Mixing chamber fuel	500.00	2	1,000.00	±30 %	700.00	1,300.00
II	Preheater	4,054.44	2	8,108.87	±30 %	5,676.21	10,541.53
III	Mixing chamber EGR.	500.00	2	1,000.00	±30 %	700.00	1,300.00
IV	HCCI engine	45,457.15	1.695	77,046.01	±30 %	53,932.21	100,159.81
V	Cooler 1	553.57	2	1,107.14	±30 %	775.00	1,439.28
VI	Steam generator	989.44	2	1,978.88	±30 %	1,385.22	2,572.54
VII	Mixing chamber steam	1,000.00	2	2,000.00	±30 %	1,400.00	2,600.00
VIII	Water-gas shoft reactor	2,060.98	2	4,121.96	±30 %	2,885.37	5,358.55
IX	Membrane	90,494.02	2	180,988.04	±30 %	126,691.63	235,284.46
X	Cooler 2	1,354.09	2	2,708.19	±30 %	1,895.73	3,520.65
XI	Compressor 1	7,681.89	2	15,363.78	±30 %	10,754.65	19,972.92
XII	Cooler 3	1,316.38	2	2,632.77	±30 %	1,842.94	3,422.60
XIII	Compressor 2	7,616.57	2	15,233.14	±30 %	10,663.20	19,803.08
XIV	Cooler 4	1,317.89	2	2,635.78	±30 %	1,845.04	3,426.51
XV	Expansion valve	1,000.00	2	2,000.00	±30 %	1,400.00	2,600.00
XVI	EGR	500.00	2	1,000.00	±30 %	700.00	1,300.00
XVII	Cooler 5	2,561.60	2	5,123.20	±30 %	3,586.24	6,660.16

[1] Purchased equipment cost from literature for the component only, without installation and peripherals. These are added by multiplying this value with a cost factor.

[2] Assumption: purchased equipment = 50 % of fixed capital investment [134] p. 240.

[3] Expected accuracy of economic values for studies [134] p. 237.

Table 5.15: Cost estimation.

Component	Z_{ref}^{CI}	Year of Z_{ref}^{CI}	Z_{2018}^{CI}	B_{ref}	N	Ref.
Heat exchanger	17,400.00 €	2002	26,009.17 €	100.00 m^2	0.60	[134]
Steam generator	26,100.00 €	2002	39,013.76 €	100.00 m^2	0.60	[134, 143]
Hydrogen membrane	2,040,000.00 €	2016	2,226,921.54 €	257.30 m^2	0.60	[128]
Water-gas shift reactor	9,540,000.00 €	2007	10,737,220.97 €	1,246,060,000.00 kW	0.67	[128]
H2 compressor	1,200.00 €	1987	2,191.48 €	746.00 W	0.82	[128]
HCCI engine	45,023.97 €	2011	45,457.15 €	18,544.50 W	0.54	[144]

[1] Stainless steel, 6 bar maximum pressure.
[2] Stainless steel, 50 bar maximum pressure.

Table 5.16: Exergoeconomic analysis for EGR ratio = 0.05, ordered by relative exergy destruction $y_{D,k} > 3\%$ ($\dot{E}_{D,k}$: exergy destruction rate; $y_{D,k}$: relative exergy destruction; $\dot{C}_{D,k}$: cost rate of exergy destruction; $\dot{Z}_k$: cost rate of component costs; ε_k: exergetic efficiency;c: exergoeconomic factor; r_k: relative cost difference).

No.	Component	$\dot{E}_{D,k}$ (W)	$y_{D,k}$ (%)	$\dot{C}_{D,k}$ (€/h)	$\dot{Z}_k$ (€/h)	ε_k (%)	f_k (%)	r_k (%)
I	Mixing chamber fuel	1,252.3	5.5	0.022	0.017	99.0	42.6	1.7
II	Preheater	756.5	3.3	0.027	0.135	80.0	83.2	9.3
III	Mixing chamber EGR	142.6	0.6	0.003	0.017	99.9	85.4	1.6
IV	HCCI engine	11,655.5	51.0	0.236	1.283	62.0	84.5	64.7
V	Cooler 1	317.0	1.4	0.011	0.018	76.9	63.6	82.6
VI	Steam generator	1,215.0	5.3	0.040	0.033	58.7	44.9	127.3
VII	Mixing chamber steam	585.1	2.6	0.019	0.033	99.4	63.1	4.0
VIII	Water-gas shift reactor	2,146.9	9.4	0.074	0.069	14.6	48.0	4.4
IX	Membrane	1,447.5	6.3	0.052	3.014	97.8	98.3	132.9
X	Cooler 2	945.4	4.1	0.08	0.045	26.0	36.2	401.1
XI	Compressor 1	218.6	1.0	0.007	0.256	89.1	97.2	3.2
XII	Cooler 3	430.5	1.9	0.037	0.044	32.7	54.0	402.4
XIII	Compressor 2	219.8	1.0	0.007	0.254	89.2	97.2	2.9
XIV	Cooler 4	438.0	1.9	0.039	0.044	32.6	52.9	395.8
XV	Expansion valve	1085.3	4.7	0.039	0.033	96.0	45.9	0.0
XVI	EGR	0.0	0.0	0	0.017	100.0	100.0	0.0
XVII	Cooler 5	25.6	0.1	0.001	0.085	79.4	98.9	2218.4

Figure 5.11: Engineering Plant Cost Index (CEPCI) for the years 1987–2018 [134, 135, 145].

_____

EXERGOECONOMIC ANALYSIS AND COMPARISON BETWEEN PRESSURE SWING ADSORPTION AND MEMBRANE

_____

_____

Introduction to the fifth paper

The exergoeconomic analysis of the polygeneration concept discussed in the previous chapter indicated that the palladium membrane may not be the most suitable solution for separating hydrogen from gas mixtures originating from fuel-rich operated HCCI engines. The investment costs of the membrane are high and the partial pressure of hydrogen in the feed is relatively low compared to typical membrane applications, due to the nitrogen dilution.

Therefore, in this chapter, the palladium membrane is compared with the most commonly used hydrogen separation process: the pressure swing adsorption (PSA). PSA processes are dynamic processes in which impurities of a gas mixture are adsorbed under high pressure on adsorbents such as zeolite or activated carbon and a purified target gas leaves the adsorption column [146–148].

In this work, we are interested in only a few values which are important for the comparison of membrane and PSA, namely hydrogen recovery, hydrogen purity, and investment costs. Therefore, a black box model of the PSA process was developed based on experimental data from literature, using a random forest regression algorithm implemented in the machine learning module *scikit-learn* available in Python.

Afterwards, two process concepts were developed for hydrogen, work, heating water, and steam production; comparable to the process discussed in the previous chapter. Furthermore, an ozone generator as discussed in chapter four was used to

evaluate the economics of additive addition. The main differences are:

– Instead of fixed process parameters a parameter study on the most important process parameters is performed and analyzed by conducting a global sensitivity analysis.

– The engine is scaled up from lab size to a typical industrial size.

– Two water-gas shift reactors are used instead of one: high-temperature and low-temperature reactions are combined to increase the hydrogen yield, which is typically done in conventional steam reforming processes.

– The additive ozone is used instead of exhaust gas recirculation (EGR), since EGR was too expensive and also dilutes the mixture, making hydrogen separation more difficult and inefficient.

To reduce the computational time of the parameter study on the process parameters, a linear regression algorithm was used to create a black box model of the engine, trained with data generated by the previously validated single-zone engine model. In this chapter, the two processes with membrane separation and PSA separation are compared in three steps:

1. Sensitivity analysis for process parameters with constant economic input parameters.

2. Exergoeconomic analysis at best process parameters, with constant economic input parameters.

3. Sensitivity analysis for economic input parameters, with fixed process parameters.

The key contributions of this work to the state of the art can be summarized as follows:

– The most suitable engine operating parameters were found at an equivalence ratio of 2, an intake temperature of 200 °C, a rotational speed of 1500 1/min, and a compression ratio of 22, which were the upper limits in this study.

– The PSA process yielded a higher efficiency and lower costs.

– An efficiency of up to 68.3 % was achieved.

– The electricity and hydrogen costs range from 44.2 €/MWh to 97.6 €/MWh and 2.7 €/kg to 7.2 €/kg, respectively.

– Although being lower scale than conventional power plants, electricity production by the polygeneration system is competitive.

– Hydrogen costs are comparable to electrolysis, although the engine process is small scale. Nevertheless, conventional steam reforming outperforms every other technology with prices from 1 €/kg to 3 €/kg.

– CO_2 costs crucially increase electricity and hydrogen costs.

Table 6.1: Author contributions for chapter 6 following the CRediT author statement methodology [41].

Author	Freund	Güngör	Atakan
Conceptualization	✓	✓	
Methodology	✓	✓	
Software	✓		
Validation	✓	✓	
Formal analysis	✓		
Investigation	✓		
Resources			✓
Data curation	✓		
Writing - Original draft	✓		
Writing - Review & editing		✓	✓
Visualization	✓		
Supervision			✓
Project administration			✓
Funding acquisition			✓

Author contributions to the fifth paper

In 2021, we again had the opportunity to host Ali Güngör in Duisburg and further develop our process concept and work on the exergoeconomic analysis. In constant exchange with Ali Güngör I modified the original process concept and added the ozone generator, the second water-gas shift reactor, as well as rearranged the water and steam streams to reduce the exergy destruction and losses of the system. Afterwards, I developed the black box models of the PSA and the single-zone engine model and performed the global sensitivity analyses.

Together with Ali Güngör and Burak Atakan, we discussed the outcomes and constantly improved the process concept as well as the model. I evaluated the data

and wrote the first draft of the manuscript, which was afterwards revised by Ali Güngör and Burak Atakan. Burak Atakan was also responsible for the funding acquisition and the supervision of the project.

6.1 Abstract

Hydrogen is one of the most important base chemicals and discussed as a future energy carrier for power and heat generation, as well as energy storage. Producing hydrogen at low costs and low CO_2 emissions is thus of increasing importance. This study addresses the thermodynamics and economics of hydrogen, power, and heat generation by partial oxidation of methane in fuel-rich operated homogeneous charge compression ignition (HCCI) engines. Therefore, a Python model of two different process concepts with different hydrogen separation technologies was developed and analyzed: pressure swing adsorption (PSA) and palladium membrane separation. The operating conditions of the engine and the separation were evaluated by conducting a global sensitivity analysis. The most suitable engine operating parameters were found at an equivalence ratio of 2, an intake temperature of 200 °C, a rotational speed of 1500 1/min, and a compression ratio of 22. In direct comparison, PSA consistently yielded better results than the palladium membrane, and low feed pressures were favorable. Subsequently, the uncertainty of economic input values was investigated and the power and hydrogen costs evaluated. In the PSA case, the electricity and hydrogen costs were found in a range of 44.2 €/MWh to 97.6 €/MWh and 2.7 €/kg to 7.2 €/kg, respectively, with an overall exergetic efficiency of 68.3 %. Therefore, the proposed polygeneration system provides electricity at competitive costs and hydrogen at costs similar to a small-scale steam reforming plant at comparable efficiencies. Further scaling up of the engine could provide hydrogen at the cost of large-scale steam reforming, making the proposed concept a promising alternative.

6.2 Introduction

Hydrogen is discussed as a future energy carrier for transportation, heat generation, and energy storage [149]. Moreover, it is an important feed stock for chemical industry. Therefore, efficient hydrogen production with low CO_2 emissions is gaining importance. A possible solution is the use of conventional internal combustion engines and modifying them for fuel-rich HCCI operation. If the engine is fueled with natural gas or biogas, it provides power, heat, and synthesis gas simultaneously with high exergetic efficiencies of more than 80 % [34], which is at least 17 points

higher than conventional steam reforming of natural gas [26]. The concept of a larger cooperative approach for this polygeneration is summarized in [112]. HCCI engines can be used as bridging technology for the production of synthesis gas and substitute conventional processes like steam reforming while increasing efficiency and flexibility. Using engines is promising because they are cheap, technically mature, robust, and can swiftly change their operating conditions. The application possibilities are manifold: if electricity is cheap, e.g. when high amounts of wind and solar power are available, the HCCI engine could produce chemicals at high equivalence ratios, e.g. 2, which can then be used or stored. Otherwise, at high electricity costs, the equivalence ratio could be reduced to produce more electricity on-site. With increasing installed capacities of renewable energy systems, the ability of the engine to react quickly to fluctuations could help to accelerate building of renewable energy systems and stabilize the power grid in the future. Furthermore, industrial off-gases could be used and converted chemically instead of being burned. For instance, Rudolph et al. [150] showed that the partial oxidation of industrial ammonia containing off-gases seems feasible. The advantage of using the HCCI mode compared to spark ignition (SI) at high equivalence ratios is that due to the low flame speeds at such conditions, SI often leads to misfires as discussed in [112].

In the short term, HCCI engines fuelled with biogas or natural gas could help increase the amount of hydrogen available while reducing CO_2 emissions. HCCI engines could be combined with water-gas shift reactors to increase the hydrogen yield, which is typically done in synthesis gas producing facilities which rely on steam reforming. After separation of the hydrogen from the product gas, neat hydrogen can be used for fuel cells, chemical energy storage, or as base chemical for chemical industry. However, important questions arise:

– Which separation technology should be used, considering costs and thermodynamic efficiency?

– What is the cost of hydrogen produced and is it competitive with steam reforming of natural gas or water electrolysis?

– What is the overall exergetic efficiency of polygeneration in HCCI engines when separation is included?

There are several technologies for hydrogen separation from gaseous mixtures, as summarized by Mao et al. [151]: cryogenic separation, polymer membrane separation, palladium membrane separation, metal hydride separation, solid polymer electrolyte cells, pressure swing adsorption, and catalytic purification. Mao et al.

pointed out that among these processes, pressure swing adsorption and cryogenic separation are the main methods used in industrial applications. However, due to their high energy requirements for compression or cooling, respectively, membranes have been investigated intensively in the last decades, as an alternative. Two separation technologies seem to be specifically suitable for separating hydrogen from the product gas of HCCI engines: pressure swing adsorption and palladium membrane separation.

In the pressure swing adsorption process, the impurities of the feed gas mixture are adsorbed on a homogeneous or layered bed, often containing active carbon and/or zeolites at moderate or high pressures from 5 to 34 bar [152]. The purified hydrogen is partially used to purge the adsorbent at low pressure. Therefore, the main energy requirement is the compression of the feed gas mixture to the desired adsorption pressure. Conveniently, the compressor power could be provided by the HCCI engine.

Since hydrogen purification is a widely investigated topic, there are several experimental and theoretical works about hydrogen purification via PSA, e.g. [153–155]. However, the investigated hydrogen mole fractions in the feed of the PSA are typically high, with values between 0.38 and 0.89. Since the HCCI engine uses air as oxidizer, the product gas and thus the hydrogen is highly diluted. Similar feed gas conditions for the PSA process were investigated by Yu et al. [156] who proposed a polygeneration process pilot design in which biogas is reformed and used in a commercially available fuel cell to produce work, heat, and an anode off-gas containing H_2, H_2O, CO_2, and CO. The hydrogen mole fraction was increased in a water-gas shift reactor from 0.112 to 0.163 and to separate the hydrogen from the mixture, they proposed a two bed PSA process containing active carbon, zeolite, and silica gel. They concluded that PSA is feasible for this process, which provides 154 kW power together with 2.58 kg hydrogen per hour.

Metallic membranes for hydrogen separation gain in importance; especially palladium membranes due to their high selectivity for hydrogen diffusion. Such membranes can be operated with a high-pressure feed or low pressure permeate to achieve a suitable hydrogen partial pressure difference. Therefore, the main energy requirement is, comparable to the PSA process, the compression of the feed gas mixture and/or the permeate gas. As a disadvantage, unsaturated hydrocarbons, as ethylene, and CO impurities in the feed reduce the permeability [151] and should thus be avoided. One example for an experimental work on palladium membranes is the work of Fernandez et al. who developed thin palladium-silver supported membranes and determined important properties like permeability, hydrogen selectivity,

and hydrogen purity [129, 130].

Based on the data by Fernandez et al., we previously modelled the coupling of a small-scale engine with a high temperature water gas-shift reactor and a palladium membrane for hydrogen purification and separation from the engine's product gas [115]. The objective was to determine the hydrogen costs and to identify the most important components or economic factors that contribute to the overall costs and the costs of inefficiencies. Therefore, an exergoeconomic analysis was performed: a combination of exergy analysis and economic analysis [115]. The hydrogen costs were predicted between 3.23 €/kg and 3.99 €/kg and the overall exergetic efficiency was 66 %. The exergoeconomic analysis revealed that the hydrogen costs mainly depend on the high costs of the membrane. However, this was only performed for a small-scale engine and fixed operating conditions, which may not be optimal. Furthermore, the membrane was designed for low pressure on the permeate side. It was later found that there was a mistake in the calculation of the pressure difference, which did not change the overall outcome but required an even lower hydrogen pressure at the permeate side of 3.3 kPa. Consequently, a high pressure on the feed side is assumed to be favorable and thus should be investigated.

Since methane and small alkanes are relatively inert and not easily ignited in HCCI mode, either different additives can enhance the reactivity, like n-heptane [93], DME [78, 102, 107], and ozone [105], or higher temperatures of the fuel-air mixture can be selected. We selected the latter two and investigated the effect of ozone as a reactive additive by producing it with an ozone generator. The advantages were discussed in detail in our previous work [157]. We found that the exergetic efficiency of ozone generation is relatively low with about 5 %, but since the alternative additives like dimethyl ether (DME) [78] must be used in higher amounts, the overall efficiency with ozone was 15.1 points higher than for DME. However, the influence on the costs remained unclear. Consequently, the present work aims to answer the following questions:

- What are the best operating parameters for the engine in terms of low costs and high efficiency?

- Are the hydrogen costs competitive to conventional processes if an industrial scale engine is used?

- How do PSA and membrane separation perform in comparison?

Therefore, a process model in Python was developed. With this model an exergoeconomic analysis was performed several times with varying process and economic

Table 6.2: Engine properties and operating conditions.

Description	Symbol	Value	Unit
Rotational speed	rpm	600-1500	1/min
Compression ratio	r_c	18-22	
Bore	d	190.0	mm
Stroke	s	220.0	mm
Number of cylinders	N_Z	20	
Displacement	D	124.75	dm³
Fuel-air equivalence ratio	ϕ	1.5-2.0	
Intake temperature	T_{in}	50-200	°C
Intake pressure	p_{in}	1	bar
Coolant temperature	T_C	100	°C
Thermal conductivity wall	λ_w	53	W/m/K
Convection coefficient coolant	α_c	3000	W/m²/K
Woschni coefficients	C	127.9	-
	C_1	2.16	-
	C_2	0.051	m/s/K
	r	0.535	-

parameters and the results were used for a global sensitivity analysis. This work is divided into four parts: in the second section, the engine model, PSA model, and the process concepts are described and the fundamentals of the exergoeconomic analysis and the global sensitivity analysis are explained. Afterwards, the results are presented and discussed and finally conclusions are drawn.

6.3 Methodology

Engine model

The engine is modelled in Python as a homogeneous single-zone engine. The thermodynamics and reaction kinetics are calculated with the module *Cantera* [50]. Four strokes, including intake and exhaust stroke, were modelled to get more accurate results for the work and heat output. The inner convective heat transfer coefficient, which determines the heat flow through the cylinder wall and cylinder head, was modelled by the semi-empirical equation by Woschni [58]. The Woschni coefficients were previously validated for our small-scale test engine and are shown in Table 6.2, together with the engine properties and operating conditions.

The geometry is taken from a typical cogeneration gas engine with 20 cylinders, a displacement of 124.8 liters and an electrical power output of 3.35 MW at con-

ventional, lean conditions. The compression ratio is typically 11 but increased here to values of 18-22, as typically used in Diesel engines, to reduce the inlet temperature to 50-200 °C and the amount of ozone to achieve ignition in HCCI mode. The equivalence ratio investigated in this work ranges from 1.5 to 2.0 and the rotational speed is varied from 600 to 1500 1/min.

The engine conditions used in this study have been proven in previous experiments. For instance, Banke et al. [78] operated the engine at equivalence ratios of 1.2 to 2.2 successfully, with inlet temperatures of 100 °C to 190 °C and pressure rise rates and coefficient of variations within reasonable limits and our engine model was validated with this engine data. Wiemann et al. [30] and Atakan et al. [112] also showed recently that SI mode is possible for fuel-rich operation, but at equivalence ratios of 1.5 and higher, and with air as oxidizer, misfires occur. Therefore, HCCI mode is chosen here.

Since the purpose of this study is to determine favorable operating conditions, continuous output of the engine model with changing input parameters at low computation time is required. Therefore, a surrogate model using machine learning algorithms was developed, which was fed with 128 simulation results within the operating condition ranges given in Table 6.2. The machine learning algorithms are taken from *scikit-learn* [158]. A linear regression model was used, since a linear behavior between two data points was assumed to be sufficient and a sample testing yielded plausible results.

Pressure swing adsorption machine learning model

The pressure swing adsorption process was modelled with a random forest regression machine learning algorithm from *scikit-learn* [159], trained and tested with 90 data sets from seven works. The methodology is described in detail in our previous work [152]. Fig. 6.1 illustrates the input and output parameters of the machine learning model.

The algorithm was trained with data on adsorption pressure p_{ads}, hydrogen purity P_{H_2}, number of adsorption beds N_c, hydrogen mole fraction in the feed x_{H_2}, active carbon to zeolite ratio AC/Z, purge to feed ratio P/F, and adsorption time t_{ads}. By using this data, the model predicts the according hydrogen recovery R_{H_2}, which is defined as the ratio of hydrogen mole flow in the product stream to the hydrogen mole flow of the feed and thus illustrates the effectiveness of the PSA process. In this work, the chosen train size is 0.8; meaning 80 % of the data is used for training and 20 % for testing the model.
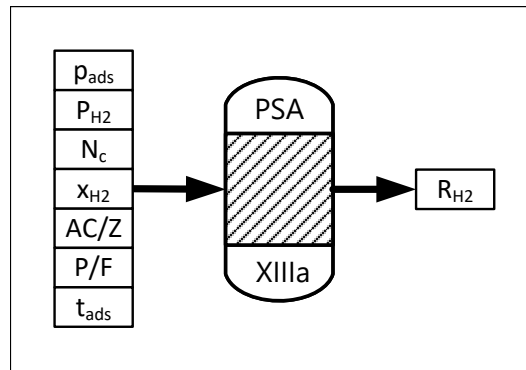
Figure 6.1: The input and output parameters of the machine learning model of the PSA.

Process concepts

The following process concepts are designed to simultaneously provide power, hydrogen, heating water, and steam. Those processes could replace conventional steam reforming in several applications where hydrogen is needed [160]:

– Metallurgical and steel industry

– Petrochemical and refining industry

– Glass and float glass manufacturing

– Chemical and pharmaceutical industry

– Production of hydrogen peroxide (H_2O_2)

– Food industry

– Electronics industry

– Production of technical gases

Therefore, the generated power can be used to reduce the purchase of electricity from the power grid for the overall facility and a surplus could be sold. The heating water could be used for heating nearby offices. Another advantage compared to conventional reforming is that the required high temperature thermal energy for driving the endothermal reforming process is produced directly within the process. Typically, the aforementioned facilities have further heat demands at higher temperature levels and thus the steam produced in the proposed polygeneration concepts should be used internally, e.g. for preheating. Furthermore, surplus hydrogen could

be supplied to fuel cell vehicles.

Pressure swing adsorption. The process concept model with PSA for hydrogen separation consists of 15 components and 48 fluid or energy streams and is illustrated in Fig. 6.2; PSA-specific streams are indicated by 'a'. Components are denoted with Roman numerals, whereas the streams are conventionally numbered. Firstly, methane and air are mixed (N) and an air/ozone mixture is generated from air with the use of electrical power (24). The methane/air mixture is preheated by exhaust gas (IV) and subsequently mixed with the air/ozone mixture (II) so that the desired fuel-air equivalence ratio is achieved. Due to the expansion of the cylinder volume and the resulting low pressure in the cylinder, this mixture is sucked into the engine (III). The engine also includes a generator to convert mechanical work to electrical energy, as cost data from cogeneration plants are used in the economic evaluation, as described in the appendix.

The engine produces electrical power (23), heating water (29), and a synthesis gas containing product gas (7). After preheating the fuel/air mixture, the product gas is cooled to 300 °C (V), which produces steam at 290 °C and 6 bar. Subsequently, it is mixed with parts of the steam (VI) to match the conditions for a water-gas shift reaction, eq. (6.1), in the high temperature reactor (VII). This increases the hydrogen mole fraction for the sake of decreasing CO and increasing CO_2 mole fractions. A steam to carbon ratio of 1.3 is fixed.

$$CO + H_2O \longleftrightarrow CO_2 + H_2 \tag{6.1}$$
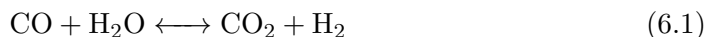
As preparation for a low temperature water-gas shift reaction (IX), which increases the hydrogen mole fraction further, the product gas is cooled to 200 °C (VIII). Since the separation of hydrogen in a pressure swing adsorption process requires feed conditions at high pressures and temperatures near to ambient conditions, the product gas must be treated further. First, it is cooled to 35 °C (X) and water is condensed. Secondly, it is compressed to the desired adsorption pressure (XI) which varies between 2 and 20 bar. All compressors in the model have a fixed isentropic efficiency of 80 %. Due to the temperature increase by compression, the product gas is cooled again (XII), so that it enters the pressure swing adsorption (XIIIa) at adsorption pressure and 25 °C. The off-gas of the pressure swing adsorption is exhausted (17a), whereas the purified hydrogen (18a) is compressed to 50 bar (XIV) and finally cooled (XV).

Only steam and water flows at moderate temperatures can be used for other processes as heat source. Here, all exiting steam and water flows are assumed to
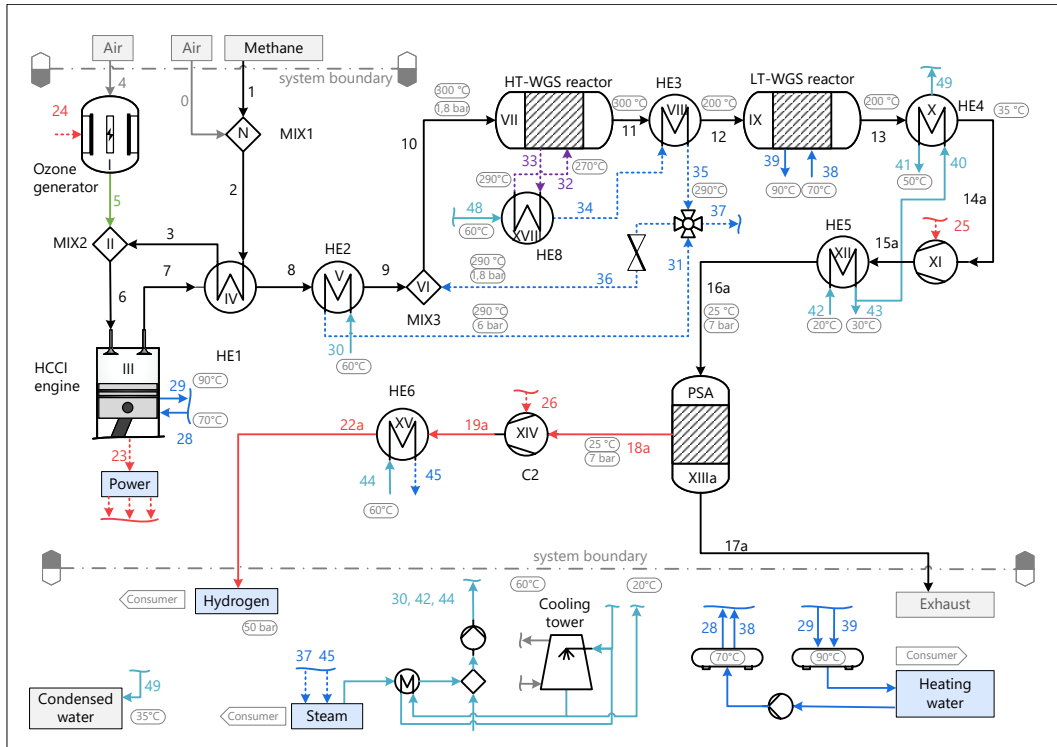
Figure 6.2: Process flow diagram of the polygeneration system with pressure swing adsorption for hydrogen purification. (Flows are numbered conventionally, components as roman numerals. MIX: mixing device, HE: heat exchanger, C: compressor, HT/LT: high/low-temperature, WGS: water gas shift reactor, PSA: pressure swing adsorption. Flows indicated by 'a' are PSA-specific.)

be products of the system, although states 41, 43, and 49 exit at low temperatures and could thus be regarded as exergy loss flows. However, their contribution to the total exergy flow and cost was found to be less than 1 %, so there is no significant impact on the outcome of the process.

Palladium hydrogen membrane. The process concept model with a palladium membrane for hydrogen separation is basically the same as the one with the pressure swing adsorption described before. The main difference is the higher feed pressure, and a permeate pressure of 1 atm, which demands two compression steps after separation to achieve the desired product pressure of 50 bar. The schematic is shown in Fig. 6.3; changes to Fig. 6.2 are made visible by the addition 'b'.

In this study, the membrane's hydrogen recovery and purity are taken from the literature. The molar flow of hydrogen through the membrane is calculated with the

Figure 6.3: Process flow diagram of the polygeneration system with palladium membrane for hydrogen purification. (Flows are numbered conventionally, components as roman numerals. MIX: mixing device, HE: heat exchanger, C: compressor, HT/LT: high/low-temperature, WGS: water gas shift reactor, H2M: palladium membrane for hydrogen separation. Flows indicated by 'b' are membrane-specific).

permeation law (6.2) which was used to determine the necessary membrane area A_m, which is the most important parameter for calculating the membrane's investment costs.

$$\dot{n}_{H_2} = \frac{P_0}{d_m} exp \left(\frac{-E_a}{R_u T} \right) A_m (p^n_{r,H_2} - p^n_{p,H_2}) \qquad (6.2)$$

The permeation law and the parameters for the membrane are taken from Fernandez et al., Medrano et al., and Spallina et al. [128–131] and are given in Table 6.3.

The pressure exponent n is 0.5 for ideal membranes, meaning Sievert's Law can be applied and the hydrogen flux through the membrane is proportional to the difference of the square roots of the hydrogen partial pressure on both sides of the membrane [161]. However, Alraeesi et al. [161] pointed out that in experiments this is rarely found. Therefore, they performed experiments and determined a pressure

Table 6.3: Permeation law parameters for the palladium membrane.

Description	Symbol	Value	Unit
Permeability	P_0	$1 \cdot 10^{-8}$	mol/s/m/Pa^n
Membrane thickness	d_m	$5.00 \cdot 10^{-6}$	m
Activation energy	E_a	$5.81 \cdot 10^{3}$	J/mol
Universal gas constant	R_u	8.314	J/mol/K
Reaction temperature	T	*varies*	K
Membrane area	A_m	*varies*	m^2
Partial pressure, retentate	p_{r,H_2}^{n}	*varies*	Pa
Partial pressure, permeate	p_{p,H_2}^{n}	*varies*	Pa
Pressure exponent	n	0.5-0.98	-

exponent of 1.0 for their setup, which results in a much higher hydrogen flux compared to the ideal case. Moreover, they compared six different experimental works which reported exponent values between 0.5 and 1.41. In this work, we investigate the influence of the exponent on the necessary membrane area and thus investment costs in a range of 0.5 (ideal behavior) to 0.98, so that the mean value is 0.74; which is the behavior of the membrane of Fernandez et al. [129, 130] and Medrano et al. [131], see Table 2.

Exergoeconomic analysis

The main idea of an exergoeconomic analysis is to define specific exergy costs ci in €/J for each exergy stream $\dot{E}_i$ (6.3) according to the **S**pecific **E**xergy **Co**sting method (SPECO) [36]. The resulting cost rates $\dot{C}_i$ are then used for cost balances (6.4), which are set up for each component of the system.

$$\dot{C}_i = c_i \dot{E}_i \tag{6.3}$$

$$\sum \dot{C}_{F,i} + \dot{Z}_k = \sum \dot{C}_{P,i} + \dot{C}_{L,k} \tag{6.4}$$

The costs balance also contains the total cost rate of the components $\dot{Z}_k$, which is defined in the appendix. $\dot{C}_{F,i}$ and $\dot{C}_{P,i}$ denote the cost rates of the fuel and product of a component. The fuel is defined as the exergy stream which provides exergy, whereas the product stream receives it. In each component, cost rates for exergy losses $\dot{C}_{L,k}$ and exergy destruction $\dot{C}_{D,k}$ may occur. The first is defined as the cost rate of an exergy stream leaving the cost balance boundaries without further purpose, e.g. exhausting residual gas to the environment. The latter is defined

as a cost rate of exergy destruction caused by irreversibility and therefore entropy production. The cost rate of exergy destruction $\dot{C}_{D,k}$ is calculated by multiplying the exergy destruction rate $\dot{E}_{D,k}$ with the mean specific exergy costs of the fuel streams $\dot{c}_{F,k}$ (6.5).

$$\dot{C}_{D,k} = c_{F,k}\dot{E}_{D,k} \tag{6.5}$$

Together, the cost balances build a linear equation system which can be solved analytically or numerically. However, the product and fuel streams must be defined first and if a component has more than one output, auxiliary equations are required which provide relations between the multiple outputs. Table 6.4 summarizes the fuel and product definitions and the auxiliary equations for each component k.

One of the most important characteristic numbers for exergoeconomic evaluation is the sum of component costs and costs of exergy destruction. This number can be calculated for each component and thus gives information about the most important components which contribute to the systems' costs; and to what extent costs are caused by inefficiencies. If these values are totaled for all components, as shown in equation (6.6), the total cost rate of the overall system can be determined. This value is used in this work to find promising operating conditions, by finding conditions with low total cost rates.

$$\dot{Z}^t + \dot{C}_D^t = \sum \dot{Z}_k + c_f^t \sum \dot{E}_{D,k} \tag{6.6}$$

After determining reasonable process conditions, the components can be evaluated with several exergoeconomic figures, namely the exergoeconomic factor f_k (6.7) and the relative cost difference r_k 6.8).

$$f_k = \frac{\dot{Z}_k}{\dot{Z}_k + c_{F,k}(\dot{E}_{D,k} + \dot{E}_{L,k})} \tag{6.7}$$
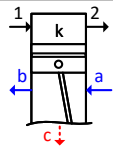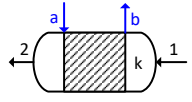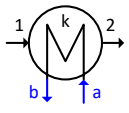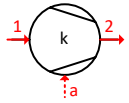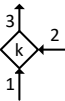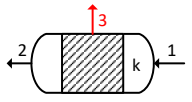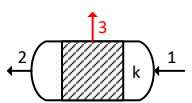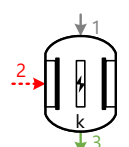
$$r_k = \frac{c_{P,k} - c_{F,k}}{c_{F,k}} \tag{6.8}$$

Additionally, the exergetic efficiency of each component ε_k and of the total system ε_{sys} are evaluated according to equations (6.9) and (6.10).

$$\varepsilon_k = \frac{\left(\sum \dot{E}_{i,k}\right)_P}{\left(\sum \dot{E}_{i,k}\right)_F} = 1 - \frac{\sum(\dot{E}_{D,k} + \dot{E}_{L,k})}{\left(\sum \dot{E}_{i,k}\right)_F} \tag{6.9}$$

$$\varepsilon_{sys} = \frac{\sum \dot{E}_{i,out}}{\sum \dot{E}_{i,in}} = 1 - \frac{\sum(\dot{E}_{D,k} + \dot{E}_{L,k})}{\sum \dot{E}_{i,in}} \tag{6.10}$$

Table 6.4: Definition of fuel and product and auxiliary equations for setting up the cost balances (ENG: HCCI engine, HT/LT: high/low-temperature, WGS: water gas shift reactor, HE: heat exchanger, C: compressor, MIX: mixing device, H2M: palladium membrane, PSA: pressure swing adsorption, O3G: ozone generator).

Component	Schematic	Fuel	Product	Auxiliary equation
ENG		$\dot{C}_1$	$\dot{C}_b - \dot{C}_a + \dot{C}_c + \dot{C}_2$	$\frac{\dot{C}_b - \dot{C}_a}{\dot{E}_b - \dot{E}_a} = \frac{\dot{C}_c}{\dot{E}_c} = \frac{\dot{C}_2}{\dot{E}_2}$
HT/LT-WGSR		$\dot{C}_1$	$\dot{C}_b - \dot{C}_a + \dot{C}_2$	$\frac{\dot{C}_b - \dot{C}_a}{\dot{E}_b - \dot{E}_a} = \frac{\dot{C}_2}{\dot{E}_2}$
HE1-HE8		$\dot{C}_1 - \dot{C}_2$	$\dot{C}_b - \dot{C}_a$	$\frac{\dot{C}_2}{\dot{E}_2} = \frac{\dot{C}_1}{\dot{E}_1}$
C1-C3		$\dot{C}_c$	$\dot{C}_2 - \dot{C}_1$	
MIX1-MIX3		$\dot{C}_1 + \dot{C}_2$	$\dot{C}_3$	
H2M		$\dot{C}_1 - \dot{C}_2$	$\dot{C}_3$	$\frac{\dot{C}_2}{\dot{E}_2} = \frac{\dot{C}_1}{\dot{E}_1}$
PSA		$\dot{C}_1 - \dot{C}_2$	$\dot{C}_3$	$\frac{\dot{C}_2}{\dot{E}_2} = \frac{\dot{C}_1}{\dot{E}_1}$
O3G		$\dot{C}_1 + \dot{C}_2$	$\dot{C}_3$	

Sensitivity analysis

To determine process conditions that result in low overall system costs, the process parameters were varied and the results analyzed. Therefore, we performed a global sensitivity analysis with the help of the Python module *SALib* [141], which uses the Sobol method as described by Saltelli et al. [140]. According to the Monte Carlo method, 2^8 samples within a defined uncertainty range of the input parameters were created and used to solve the process model. For the second analysis, in which only economic parameters are varied, 2^{10} samples are used. Afterwards, the first order sensitivity index S_i was evaluated for each input i (11). It is defined as the ratio of the reduction of the variance of the model's output if one input parameter is fixed $V_{X_i}(E_{X_{\sim i}}(Y|X_i))$ and the overall variance of the model's output $V(Y)$.

$$S_i = \frac{V_{X_i}(E_{X_{\sim i}}(Y|X_i))}{V(Y)} \tag{6.11}$$

The first order sensitivity index is a value in the range zero to one. If it is near to one, the variance reduction by fixing input i is nearly as high as the overall variance of the model's output. Thus, a high S_i value means that the output of the model depends strongly on this input. Sensitivity indices of higher orders also exist but are not evaluated here. Instead, the total sensitivity index $S_{T,i}$, which summarizes all higher order indices, is compared to S_i.

The global sensitivity analysis helps to identify the most important process parameters for the product and overall system costs. Moreover, preferable parameter sets can be identified, comparable to a parameter study but with a randomized approach. The chosen process parameters and their uncertainty ranges are shown in Table 6.5.

Table 6.5: Process condition parameters for the first sensitivity analysis.

Component	Description	Symbol	Value	Unit	Uncertainty range	Min	Max
Engine	Equivalence ratio	Φ	1.75	-	±15.5 %	1.5	2
Engine	Intake temperature	T_{in}	125	°C	±60 %	50	200
Engine	Rotational speed	rpm	1050	1/min	±42.8 %	600	1500
Engine	Compression ratio	r_c	20	-	±10 %	18	22
PSA	Hydrogen purity	P_{H_2}	98.999	%	±1.01 %	98	99.999
PSA	Adsorption pressure	p_{ads}	11.5	bar	±74 %	3	20
PSA	Adsorption time	t_{ads}	700	s	±70 %	210	1190
PSA	Purge to feed ratio	P/F	0.2	-	±50 %	0.1	0.3
PSA	Number of adsorption beds	N_c	4	-	±0 %	4	4
PSA	Active carbon to zeolite ratio	AC/Z	7/3	-	±0 %	7/3	7/3
Membrane	Permeate pressure	p_p	1	bar	±0 %	1	1
Membrane	Feed pressure	p_f	25	bar	±20 %	20	30
Membrane	Hydrogen purity	P_{H_2}	99.999	%	±0 %	99.999	99.999
Membrane	Hydrogen recovery	R_{H_2}	60	%	±16.5 %	50	70
Membrane	Exponent	n	0.74	-	±32.43 %	0.5	0.98

The engine parameters equivalence ratio, intake temperature, rotational speed, and compression ratio were varied in ranges that showed stable operation and significant synthesis gas output. It must be noted that at equivalence ratios of 2 and above, soot formation increased significantly in previous experimental investigations, which should be avoided [78].

Two of the PSA parameters were chosen to be fixed: the number of adsorption columns N_c and the ratio of active carbon to zeolite AC/Z. The adsorption bed number strongly influences the investment costs of the PSA process, since with an increasing number of beds, more housing and adsorbent material is required. However, no cost function for N_c was available, so it was chosen to be a fixed four-bed PSA process. For the same reason a typical layered bed containing 70 % active carbon and 30 % zeolite was assumed. The other PSA parameters hydrogen purity P_{H_2}, adsorption pressure p_{ads}, adsorption time t_{ads}, and purge to feed ratio P/F, do not define the design but the operation of the PSA process and are therefore varied in this work.

The hydrogen purity was chosen in the range of 98.0 % and 99.999 %, which covers a wide range of applications according to the ISO standard 14687. The ISO standard is divided into different grades, depending on the application, as discussed by Yanez et al. [154]. For instance, grade A defines the hydrogen purity of conventional combustion engines and sets the minimal purity to 98.0 %. With increasing grade, the purity increases. The grade D purity is set to 99.97 % and required for PEM fuel cells [151]. According to Omoniyi et al. [162], this is also the required purity for injection of hydrogen into the natural gas network, although grade A is sufficient for combustion applications.

However, small changes of the hydrogen purity can have a significant influence on the combustion in internal combustion engines. Gurbuz investigated two hydrogen gases with different purities in 2020 [163]: 99.995 % and 99.998 %. Both purities are "industrial standard". The higher purity improved the IMEP, the thermal efficiency, and the specific fuel consumption in the range of 1.9 % to 2.4 %.

By performing the first sensitivity analysis, promising process parameters shall be found and fixed. Subsequently, the influence of the uncertainty of the economic parameters is evaluated according to Table 6.6. The uncertainty is typically in a range of ±30 % if taken from literature. This includes the capital investment costs of the components, as well as fuel costs and the economic parameters lifetime, operating hours, interest rate, salvage value, and operation and maintenance costs.

Table 6.6: Economic parameters for the second sensitivity analysis.

Description	Symbol	Value	Unit	Uncertainty range	Min	Max
Lifetime	L	15	a	±30 %	10.5	19.5
Operating hours	τ	7920	h/a	−30 %, +10.6 %	5,544	8,760
Interest rate	i	0.10	-	±30 %	0.07	0.13
Salvage value factor	Ω	0.05	-	±30 %	0.035	0.065
Operation and maintenance factor	φ	0.03	-	±30 %	0.021	0.039
Specific water exergy costs	c_{water}	56.01	€/GJ	±30 %	39.21	72.81
Specific fuel exergy costs	c_{NG}	30.30[1]	€/MWh	±30 %	21.21	39.39
Capital investment of component k	Z_k^{CI}	*varies*	€	±30 %	*varies*	*varies*

[1] Average natural gas price for non-household consumers in the EU in 2021, see appendix Fig. 6.15.

6.4 Results and discussion

Process conditions

In this section, the results of the sensitivity analysis of the process parameters are presented, which are the parameters summarized in Table 6.5. The evaluation of the total sensitivity indices showed no significant differences to the first order indices, hence interdependencies between the investigated input parameters are minor and not discussed further. Fig. 6.4 and Fig. 6.5 illustrate the first order sensitivity indices of the process parameters on important outcomes of the model, for the PSA and the membrane case. In the figures, each output is defined by a differently colored bar and Fig. 6.4 illustrates the influence of the input parameters on the totals system costs per kg fuel, the system's exergetic efficiency, the PSA's hydrogen recovery, and the specific hydrogen costs. Arrows under the bar indicate the dependency of the output value if the input value increases, e.g. a decreasing arrow for the equivalence ratio under the first bar, which corresponds to the specific system costs, means that these costs decrease as the equivalence ratio increases.

Moreover, the size of the bar and thus the sensitivity index imply, how significant this behavior is, compared to the other input values. Afterwards, it is discussed for each input value, whether the value should be increased or decreased to improve the polygeneration system operating conditions. If there was a conflicting goal, e.g. for reducing costs and increasing efficiency, it was decided in favor of the parameter with the higher sensitivity index.

System costs per kg fuel (red bars). The total system costs per kg fuel depend mainly on the engine's fresh gas equivalence ratio, the rotational speed, and compression ratio. In the PSA case, the adsorption pressure is also important, whereas for the membrane the exponent in equation (6.2) is the second important parameter. The rotational speed is the most important parameter since the engine investment costs do not differ with increasing rotational speed and thus the specific costs are reduced per output. A higher equivalence ratio is beneficial since it leads to more synthesis gas output and thus more valuable products at constant engine costs. This is supported by the specific hydrogen costs being strongly reduced by increasing equivalence ratio (yellow bar). Therefore, a high equivalence ratio, intake temperature, rotational speed, compression ratio should be chosen for reducing the overall costs.
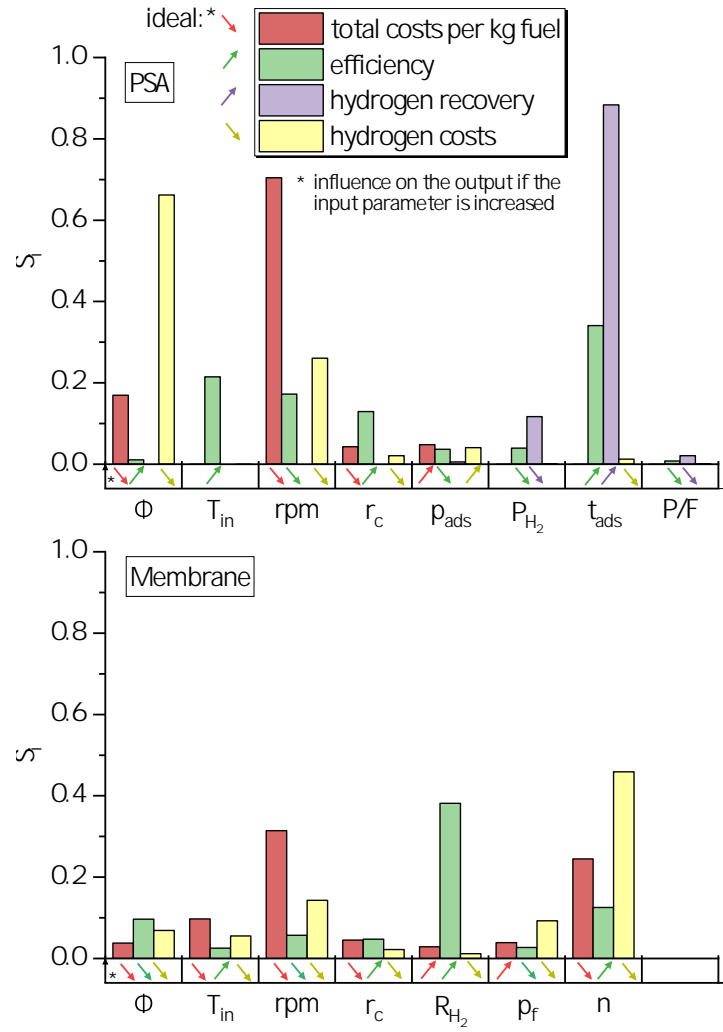
Figure 6.4: First order sensitivity indices of the process parameters for PSA (top) and membrane separation (bottom).

System efficiency (green bars). The exergetic efficiency of the system depends in both cases mainly on the hydrogen recovery from the product gas of the engine. In the PSA case the efficiency is influenced by the demanded hydrogen purity, the adsorption time, and the purge to feed ratio; those parameters influence the hydrogen recovery directly. To increase the recovery and thus the efficiency, a low purity, a high adsorption time, and a low purge to feed ratio are favorable. In the membrane case, the hydrogen recovery strongly influences the efficiency. The hydrogen recovery of the membrane is determined by the pressure difference, geometry, thickness, and the other parameters of the permeation law as described in equation (6.2). Increasing the pressure further to values above 30 bar leads to net power input into the system, which is undesirable. Increasing the area of the membrane further leads to strongly increasing investment costs. The hydrogen recovery can thus only be reasonably improved if the permeability can be increased, or the thickness of the membrane can be decreased without running into mechanical stability issues. It must be noted that the chosen membrane is already relatively thin. However, improving the design of palladium membranes is not the scope of this work and is done extensively by other researchers, as described in the introduction.

Besides the hydrogen recovery, also the engine operating parameters influence the efficiency, but the effect is minor. A high efficiency is favored at high intake temperatures and high compression ratios, whereas the rotational speed should be low. However, the effect of the rotational speed on the total costs is much higher, thus higher rotational speed seems favorable. An increasing intake temperature strongly reduces the amount of ozone needed for ignition and reduces the investment costs of the ozone generator.

The exergetic efficiency of the engine typically increases with increasing equivalence ratio, as described by Wiemann et al. [30]. However, the exergetic efficiency of the overall process does not follow this trend. In the PSA case, the efficiency slightly increases but the increase is rather negligible. In the membrane case, the equivalence ratio is clearly reduced: from a mean value of 53.8 % at $\Phi = 1.5$ to 51.0 % at $\Phi = 2.0$. There are two explanations for this behavior: first, the hydrogen recovery in the membrane case is significantly lower and secondly, the effort for compression increases with increasing equivalence ratio since the feed mass flow increases. This leads to a larger effort in the membrane case.

To conclude, high system efficiency is achieved with engine parameters at which the system costs are low, but one should pay attention to the hydrogen recovery since it is the crucial parameter for efficiency.
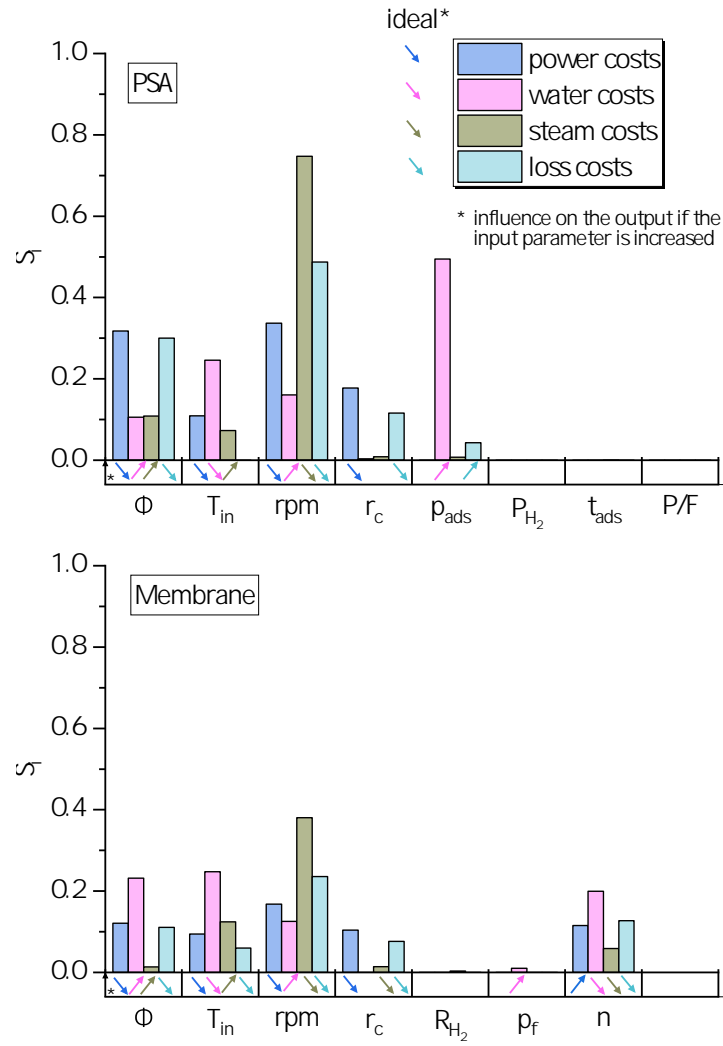
Figure 6.5: First order sensitivity indices of the process parameters on the other products of polygeneration for PSA separation (top) and membrane separation (bottom).

Specific hydrogen costs (yellow bars). The specific hydrogen costs are mainly determined by the equivalence ratio and the rotational speed. Higher equivalence ratios and higher rotational speeds yield higher hydrogen molar flows and thus reduce the costs per kg of hydrogen. It must be noted that, contrary to the hydrogen recovery, the PSA parameters do not strongly influence the hydrogen costs because the investment costs of the PSA are independent of those parameters.

In comparison, one membrane property determines the hydrogen costs: the exponent of the pressure difference. As discussed before, this is an experimentally determined factor with values between 0.5 and 1.41, see Alraeesi and Gardner [161]. A high exponent favors the hydrogen flux and thus strongly decreases the necessary membrane area for a desired hydrogen flux through the membrane. However, it cannot be influenced easily and therefore, an ideal membrane behavior with an exponent of 0.5 is considered for the following investigations. For achieving low hydrogen costs, the same conclusion can be drawn as for the total system costs.

Other specific product costs. Fig. 6.5 illustrates the influence of the input parameters on the specific power, water, steam, and exhaust or exergy loss costs. In general, only engine parameters influence these cost. The only exception is the adsorption pressure of the PSA, which mainly determines the water costs. A greater pressurization of the feed flow increases the investment costs of the compressor and the intercoolers; thus, the specific water costs also increase. The effect is greater in the PSA case, because the hydrogen recovery and thus the hydrogen molar flow in the product flow depends on the adsorption pressure, whereas the membrane's recovery value is fixed.

The specific power and exergy loss costs show the same behavior as the total system costs and the hydrogen costs: high equivalence ratio, intake temperature, rotational speed, and compression ratio decrease the costs. On the contrary, the specific water and steam costs increase with increasing equivalence ratio, but the reduction of the power and exergy loss costs are more important.

Table 6.7 provides an overview of the proposed measures to reduce system costs or increase efficiency. It can be concluded that high equivalence ratio, intake temperature, rotational speed, and compression ratio are favorable to decrease the system costs and specific product costs and to increase the system's exergetic efficiency.

Table 6.8 gives an overview of the parameters chosen for the following exergoeconomic analysis.

Table 6.7: Overview of the influence of the input parameters on the system costs and efficiency. Symbols indicate reasonable actions on the input parameters to reduce the costs or to increase the efficiency of the system: ▲ = increase input parameter, ⊖ = negligible effect, ▼ = decrease input parameter, ⊗ = not applicable.

Description	Symbol	Reduce costs		Increase efficiency	
		PSA	H2M	PSA	H2M
Equivalence ratio	ϕ	▲	▲	▲	▼
Intake temperature	T_{in}	▲	▲	▲	▲
Ozone total mole fraction	x_{O_3}	▼	▼	▼	▼
Rotational speed	rpm	▲	▲	▼	▼
Compression ratio	r_c	▲	▲	▲	▲
Hydrogen purity	P_{H_2}	⊖	⊗	▼	⊗
Hydrogen recovery	R_{H_2}	⊗	▼	⊗	▲
Adsorption/feed pressure	p_{ads}/p_f	▼	▼	▼	▼
Adsorption time	t_{ads}	⊖	⊗	▲	⊗
Purge to feed ratio	P/F	⊖	⊗	⊖	⊗
Exponent	n	⊗	▲	⊗	▲

Table 6.8: Chosen parameter sets for the following exergoeconomic analysis.

Description	Symbol	PSA	H2M	Unit	Comment
Equivalence ratio	ϕ	2.0	2.0	-	Highest value
Intake temperature	T_{in}	200.0	200.0	°C	Highest value
Ozone total mole fraction	x_{O_3}	10	10	ppm	Lowest value
Rotational speed	rpm	1,500.0	1,500.0	1/min	Highest value
Compression ratio	r_c	22.0	22.0	-	Highest value
Hydrogen purity	P_{H_2}	99.97	99.999	%	ISO 14687 grade C or better
Hydrogen recovery	R_{H_2}	73.3	70.0	%	Calculated/ highest value
Adsorption/feed pressure	p_{ads}/p_f	3.0	20.0	bar	Lowest value
Product/permeate pressure	p_p	3.0	20	bar	Lowest value
Adsorption time	t_{ads}	700.0	-	s	Mean value of experimental data
Purge to feed ratio	P/F	0.100	-	-	Low value
Number of adsorption beds	N_c	4	4	-	Typical value
Active carbon to zeolite ratio	AC/Z	7/3	7/3	-	Typical value
Exponent	n	-	0.5	-	Typical value of ideal membranes

Exergoeconomic analysis

In this section, the exergoeconomic results are discussed and illustrated for each component. The investment costs Z^{CI} of the components strongly influence the product costs and are therefore discussed at first. Afterwards, the exergetic efficiencies of the components are evaluated and the total cost rates of each component are compared. Fig. 6.6 shows the investment costs for each component for the PSA and the membrane case.

The PSA and the palladium membrane are the most expensive components (XIII) with investment costs of 4.87 million Euros (M€) and 4.24 M€, respectively. Hence, the PSA is 13.0 % more expensive than the membrane. The second largest investment of 2.87 M€ must be made for the HCCI engine, followed by the WGS-reactors (1.12 M€ and 1.13 M€). In the membrane case, the costs of compressor XI are also significant because the feed pressure is much higher compared to the PSA case; 20 bar instead of 3 bar. Furthermore, compressor XVI and heat exchanger XVII add costs in membrane case and account for 3.8 % of the total investment costs. This results in 0.67 M€ lower total system costs for the PSA case, which costs 12.55 M€ compared to 13.22 M€ in the membrane case.
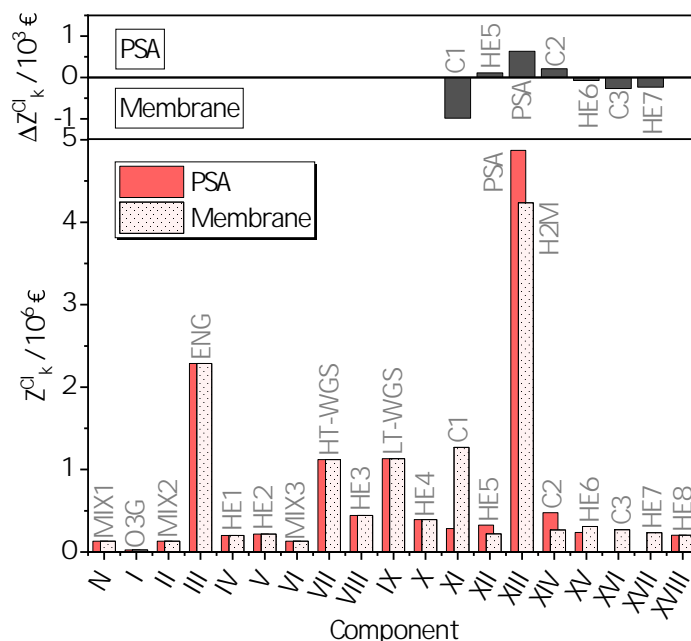
Figure 6.6: Investment costs of the process components for the PSA case (red bars) and the membrane case (bars filled with dots). The upper diagram shows the differences between the PSA and the membrane values.
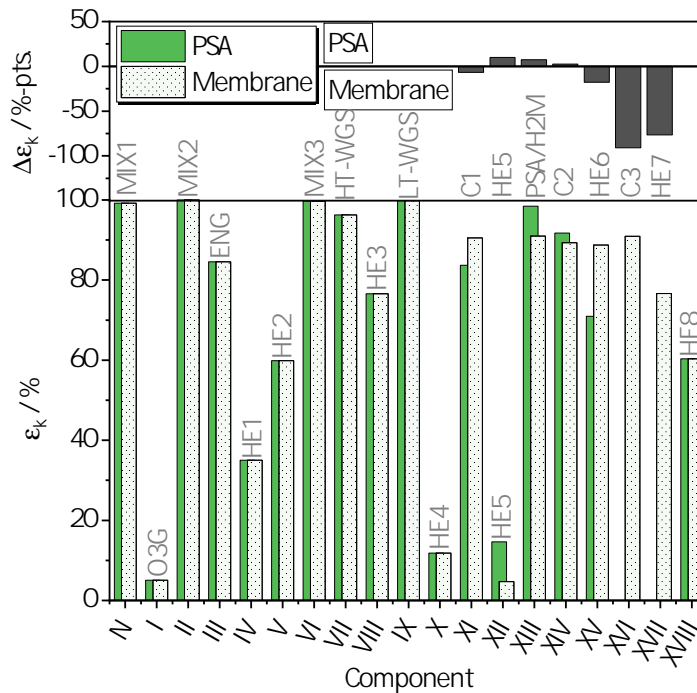
Figure 6.7: Exergetic efficiencies of the process components for the PSA case (green bars) and the membrane case (bars filled with dots). The upper diagram shows the differences between the PSA and the membrane values.

The exergetic efficiency of the components is shown in Fig. 6.7. In general, the mixing efficiencies are close to 100 % and the WGS reactors have also high efficiencies of 96.3 % and 99.8 %. The engine's efficiency is 84.6 %, which is about eight points higher than for the conditions found by Wiemann et al. [30]. The efficiency in this study is greater, mainly because the compression ratio is 2.2 times higher. In the engine, exergy is destroyed due to the conversion of parts of the fuel's chemical exergy to thermal exergy, which is exergetically unfavorable at the given reaction entropy.

The compressor efficiencies are around 90.0 % in the membrane case. In the PSA case the efficiencies of compressors XI and XV are lower, with 83.7 % and 71.0 %, respectively, because with increasing pressure ratio the specific entropy change does not increase as strongly as the specific enthalpy change and thus efficiency increases.

The exergetic efficiency of the ozone generator is very poor and only reaches 5.1 %, as also found in our previous work [157]. Therefore, a high intake temperature is favorable, since it reduces the amount of ozone needed and thus reduces inefficiencies and investment costs for the ozone generator. As the parameter study

in the previous section showed, this is beneficial and leads to lower system costs and higher overall efficiencies; although the efficiency of the preheater IV, which increases the intake temperature, is only 35 %.

The lowest efficiencies were found for the heat exchangers which reduce the temperature of the exhaust gas near to ambient temperature; heat exchanger X and XII. However, these coolers are mandatory to achieve a high pressure at the feed of the PSA and the membrane, therefore this exergy destruction cannot be avoided.

The efficiency of the PSA is high with 98.5 %, whereas the efficiency of the membrane is slightly lower with 91.0 %, but still good. The overall system efficiency of the PSA process is 68.3 %, due to a high predicted hydrogen recovery of 86.3 %. The membrane process performs significantly poorer with a value of 56.8 % and a fixed recovery of 70.0 %. Another reason is that a higher effort for compression and cooling is necessary in the membrane case, because the pressure of the permeated hydrogen is far from the desired output pressure of 50 bar and the feed pressure must be higher compared to PSA case. Therefore, the PSA seems to be favorable economically and exergetically.

The exergoeconomic calculation eventually gives the sum of investment and operating and maintenance cost rates and cost rates of exergy destruction for each component, illustrated in Fig. 6.8.

A similar conclusion as from Fig. 6.6 can be drawn: the highest costs are caused by the separation, the engine, and the WGS reactors. The exergoeconomic factors of these components are above 75 %, except for the engine which has a value of 59.0 %. Thus, investment costs dominate the total costs for all important components. Details are given in Fig. 16 in the appendix. It must be noted that the slightly lower exergetic efficiency of the membrane compared to the PSA leads to a higher exergy destruction cost rate, so that the total cost rates of PSA and membrane nearly equal with values of 83.7 €/h and 84.4 €/h. The engine reaches a total cost rate of 64.5 €/h due to a high fraction of exergy destruction cost rate of 41.0 %. Table 6.9 gives an overview of the resulting exergy flows, specific costs, and cost rates for each product.

The off-gas after the separation of hydrogen contains a mixture of mainly N_2, CO_2 and H_2O, but also about 0.5 % CO and 5 % H_2 remain. In practice, also unconverted hydrocarbons are expected. Therefore, CO_2 and CO reduction and H_2 utilization should be considered. To reduce the CO_2 emissions, carbon capture and storage might be reasonable and the exhaust gas or the separated CO_2 could be mixed with fresh fuel and combusted in a second fuel-rich operated engine. According to our recent, yet unpublished theoretical study on biogas [164], a CH_4/CO_2

133
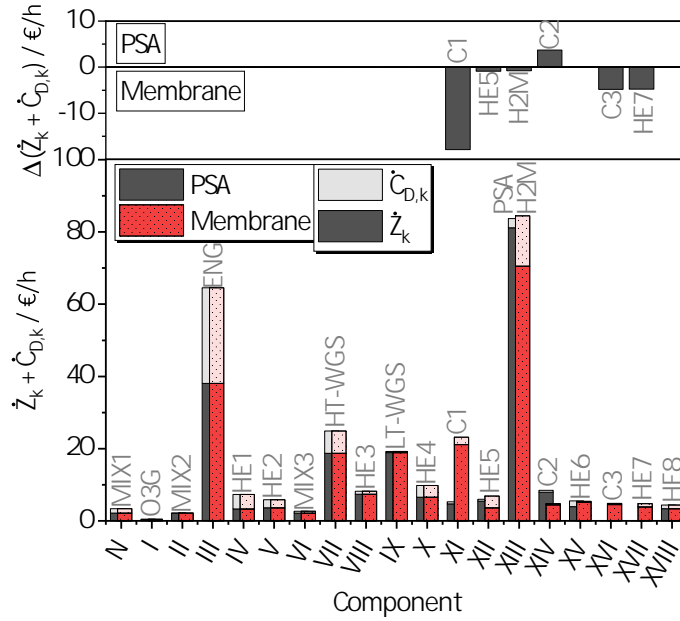
Figure 6.8: Total cost rates of the process components for the PSA case (grey) and the membrane case (red bars filled with dots). The dark bars denote the cost rates associated with investment and operating costs, and the light bars denote the cost associated with exergy destruction. The upper diagram shows the differences between the PSA and the membrane values.

Table 6.9: Exergoeconomic outcome for the products, losses, and input streams of the polygeneration system (PSA case).

Product	$\dot{m}(kg/h)$	$\dot{E}(kW)$	$\dot{C}$ (€/h)	c (€/GJ)
Hydrogen	75.7	2,564.90	256.8	27.8
Electricity	-	621.9	29.7	13.2
Steam	567.8	148.8	33.1	61.7
Heating water	723	46.5	18.1	111.3
Exhaust	3,399.50	517.7	34.1	18.3
Fuel	359.3	5,187.50	157.2	8.4
Air	3,076.80	1.7	0	0

mixture, strong CO_2 reductions are possible. Or, instead of increasing the hydrogen amount in the water-gas shift reactors, both CO and H_2 could be separated as products to reduce CO_2 emissions. Therefore, a second separation step for CO would be required, which we have not investigated yet.

In each case, the remaining synthesis gas could be recycled and fed back to engine, comparable to conventional steam reforming plants [165]. However, our previous work [115], in which we implemented external exhaust gas recirculation, indicated that this is contradictory for an efficient and competitive process if too large recirculation ratios are used, since it dilutes the hydrogen in the product gas and thus increases product costs and complicates the separation in membrane or PSA processes. In the lab, the engine's product gas is mixed with air and combusted before releasing it to the atmosphere. This way, the remaining hydrocarbons and CO can be converted, and harmful emissions are strongly reduced. Moreover, the unburned hydrocarbons and soot formation in the engine could accumulate in the subsequent components, e.g. in the heat exchangers. As long as the engine was run under reasonable conditions, we did not encounter this issue due to the smaller timeframe of the experiments [70, 78]. Since we cannot estimate the issue quantitatively, we have taken it into account indirectly via setting the lifetime of the entire plant to 15 years. In cogeneration gas engine plants, the engine is overhauled after 10 to 15 years, but the other components typically last longer. In this study, it is thus assumed to replace the overall system after 15 years. However, building a prototype plant might be required to assess the significance of this issue.

Influence of the economic parameter uncertainties on the product cost distribution

In this section, the influence of the uncertainty of the economic parameters on the product costs is evaluated. Eventually, the hydrogen costs per kg and the electricity costs per MWh are evaluated and compared to conventional processes. In Fig. 6.9 the most important economic input parameters on the total system costs and the cost rates of the products are visualized by showing the first order sensitivity indices as colored bars.

In general, interest rate, lifetime, and operating hours dominate the total costs and have a significant influence on all other costs. The highest sensitivity index of 0.42 was found for the operating hours, which strongly determine the total costs. However, because interest rate, lifetime, and operating hours cannot be addressed by process design, they are not further discussed in the following analysis. The power
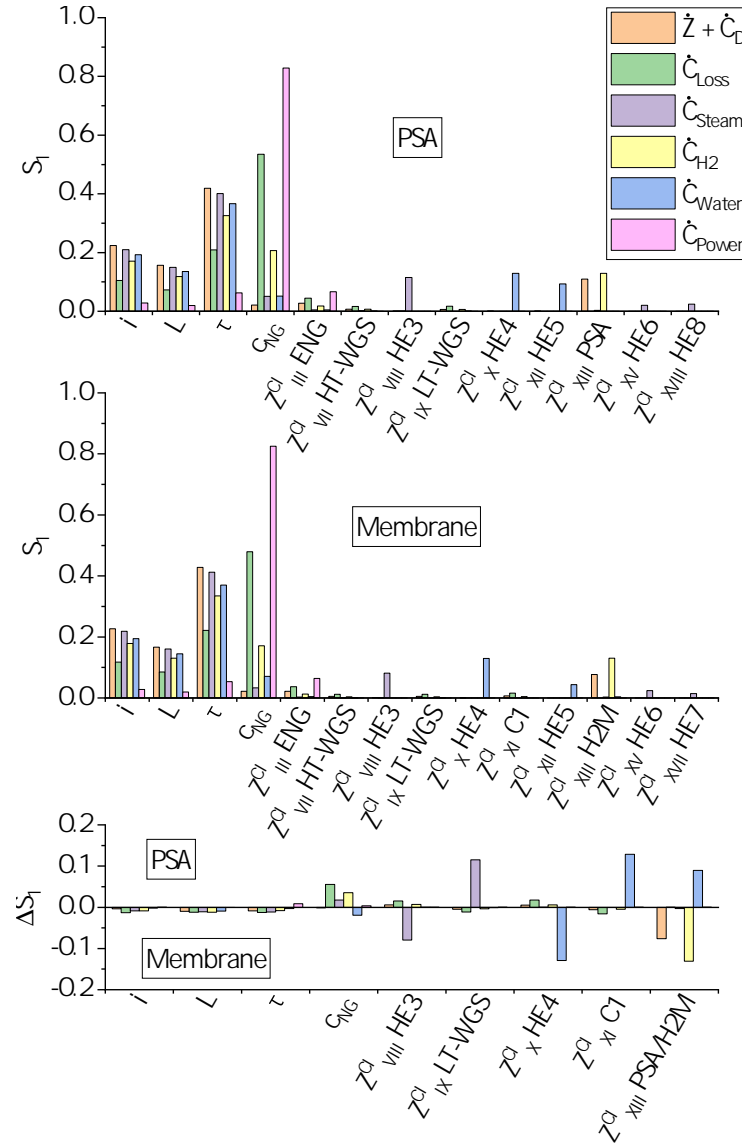
Figure 6.9: First order sensitivity indices of the most important economic input parameters on the total cost rate and the cost rates of the products (see legend). Top: PSA case, middle: membrane case, bottom: difference of PSA and membrane results.

costs are mainly dependent on the fuel costs, the index value is 0.83 and the highest in this comparison. Here, the engine's investment costs are also slightly relevant, which is expected since this is the only component in which the power is generated. Furthermore, the fuel costs dominate the exergy loss costs, since the cost rate of the fuel incrementally increases by passing the components and this eventually results in a higher cost rate of the exhausted residual gas.

The hydrogen costs are equally determined by fuel costs and investment costs of the separation technology (XIII), which emphasizes that an engine, having relatively low investment costs, is an economically reasonable choice for producing hydrogen.

Besides interest rate, lifetime, operating hours, and fuel costs, all other important input parameters are investment costs only. The exergy loss costs depend slightly on engine and WGSR investment costs, and in the membrane case also on compressor XI investment costs. Since these are the components with the highest investment costs, this effect is comprehensible. The PSA and membrane costs do not influence the exergy loss costs, because their costs are completely apportioned to the hydrogen flow. Furthermore, the steam costs depend on steam generator investment costs VIII, XV, and XVIII and the heating water costs are determined by the investment costs of heat exchangers X and XII, which are the ones with the lowest efficiencies. Fig. 6.10 shows the electricity cost distributions in €/MWh for the PSA and membrane case, calculated from the Monte Carlo distributed parameters, as given in Table 6.6. The distribution is a result of 38,912 calculations, performed for the sensitivity analysis. These costs are compared by conventional electricity production costs from renewable and fossil sources, taken from a study of the Fraunhofer Institute performed for Germany in 2018 [137]. For the latter only the x-axis is relevant. It must be noted that the capacities of the different energy systems differ strongly: for instance, the combined cycle gas turbine plants (CCGT), gas plants, and coal plants provide electricity in the range of hundreds of MW, whereas photovoltaics (PV) and wind operate in the kW range to small MW range. The HCCI engine provides 835 kW in this comparison.

Since the costs of exergy loss are apportioned on the products that can be sold, the electricity costs for the membrane case are higher compared to the PSA. The electricity costs range from 44.2 €/MWh to 97.6 €/MWh in the PSA case and from 47.4 €/MWh to 120.5 €/MWh in the membrane case. The mean values are 67.2 €/MWh and 82.3 €/MWh, respectively. Without variation of the input parameters, the electricity costs are likely slightly underestimated. In the PSA case, the electricity costs show intersections with the costs of coal power plants, onshore wind power, and photovoltaics. In the membrane case, the electricity production costs
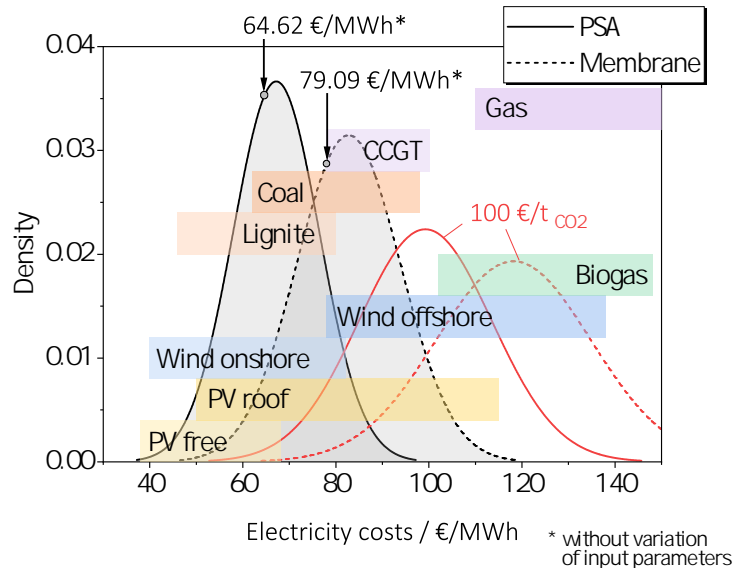
Figure 6.10: Distribution of the electricity production costs by the polygeneration system with PSA (solid line) and membrane (dashed line) as separation technology, calculated from the Monte Carlo distributed initial parameters, as given in Table 5. Red distribution curves result if CO_2 costs of 100 €/t are considered. For the bars, only the vertical width is important.

are higher than onshore wind power and lignite power plants, but still competitive to combined-cycle gas turbine power plants. With both separation technologies, the electricity production by the engine is cheaper compared to offshore wind power, and more importantly much cheaper than power plants using natural gas. Therefore, the PSA process provides competitive electricity costs or is even lower-priced than conventional processes. The membrane process yields also competitive electricity costs, but the PSA process is favorable.

It must be noted that CO_2 costs of up to 94 €/t_{CO_2} are discussed for the European Union [166]. These would incur when methane from fossil sources would be used. In Fig. 6.10, the influence of CO_2 costs of 100 €/t, calculated as explained in the appendix, eq. (6.20) and Fig. 6.16, is also illustrated as red distribution curves. Due to the CO_2 costs, the electricity costs increase strongly; their mean values increase by 47.6 % and 41.9 % to 99.2 €/MWh and 116.8 €/MWh for PSA and membrane, respectively. Consequently, PV, onshore wind, and coal power plants provide electricity at lower costs than the proposed PSA process, but it must be noted that the non-renewable energy systems used for this comparison do not consider CO_2 costs.

Besides the electricity costs, competitive hydrogen costs are crucial for the poly-
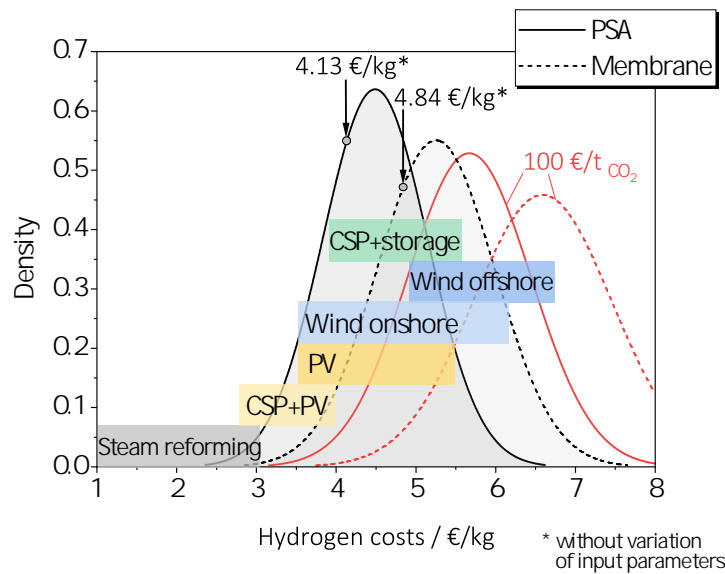
Figure 6.11: Distribution of the hydrogen production costs by the polygeneration system with PSA (solid line) and membrane (dashed line) as separation technology. Red distribution curves result if CO_2 costs of 100 €/t are considered, as would be the case for methane from natural gas and not from biogenic sources. For the bars, only the vertical width is important.

generation system since most of the chemical exergy of the fuel is converted to the chemical exergy of hydrogen. The resulting hydrogen costs for the PSA case and the membrane case are shown in Fig. 6.11 and compared to conventional steam reforming and electrolysis, the latter powered by different renewable electricity sources. The reference values are taken from a study conducted in 2020 for Germany [167]. For the calculation of the hydrogen production costs by electrolysis, the following assumptions were made by the authors: an efficiency of 70 %, investment costs of 1000 €/kW, an interest rate of 5 %, operating and maintenance costs of 3.3 % of the investment costs, and a lifetime of 20 years. In this comparison, the lifetime of the polygeneration system is 5 years shorter, and the interest rate 5 %-pts. higher.

Again, if the membrane is chosen as separation technology, the product costs are higher. The hydrogen costs vary from 3.2 €/kg to 8.0 €/kg, compared to the PSA case with a range of 2.7 €/kg to 7.2 €/kg. The mean hydrogen production costs are determined as 4.5 €/kg and 5.3 €/kg for PSA and membrane, respectively, without CO_2 costs. In both cases the costs are underestimated if the input parameters are not varied. In the membrane case the mean value of the distribution deviates by 10.4 % from the static value of 4.8 €/kg. With a real membrane and a pressure exponent of 0.74, the costs would decrease to 4.3 €/kg and thus be competitive to

139

the PSA case.

With CO_2 costs of 100 €/t the mean hydrogen costs increase by 26.7 % and 19.7 % to 5.7 €/kg and 6.6 €/kg, respectively. Hydrogen produced by conventional steam reforming of natural gas is much cheaper, with production costs of 1.0 to 3.0 €/kg. One reason for the cheaper steam reforming could be the economy of scales: although the engine size is rather large-scale for cogeneration plants, it provides only 52 kg/h hydrogen, which results in an output of 87.3 kg/h after WGS reaction and separation via PSA with a recovery of 86.3 %. In 2017, Keipi et al. [119] defined a 72 kg/h hydrogen producing steam reforming plant as small-scale and an output of 9,000 kg/h as large-scale. The hydrogen production costs were determined as 4.61 €/kg and 1.74 €/kg for small- and large-scale, respectively. Compared with those values, the polygeneration process with PSA in this study performs well with 4.5 €/kg and is therefore comparable to a small-scale steam reforming plant.

The hydrogen production costs by electrolysis range from 2.8 €/kg to 7.0 €/kg, depending on the electricity source. Comparable to the electricity costs, PV and onshore wind energy are the cheapest here as well, followed by concentrated solar power (CSP) and offshore wind energy. The polygeneration process studied here therefore yields competitive results to electrolysis and to small-scale steam reforming. With increasing CO_2 costs in the future, it will be of increasing importance to use fuels from biogenic sources for the proposed process, in order to be competitive in the long-term.

6.5 Conclusions

A polygeneration process model for hydrogen, power, and heat production was developed and an exergoeconomic analysis was performed with a fuel-rich piston engine as central unit. Methane was the fuel and ozone the additive. Reasonable operating conditions were evaluated, and a pressure swing adsorption process was compared with a palladium membrane for hydrogen separation and purification. The most suitable engine operating parameters were found at an equivalence ratio of 2, intake temperature of 200 °C, rotational speed of 1500 1/min, and a compression ratio of 22. In direct comparison, the PSA membrane consistently yielded better results than the palladium membrane, and the lower feed pressure was an advantage. The overall efficiency was 68.3 % in the PSA case and 20.2 % or 11.5 points higher. Therefore, the proposed polygeneration system has a similar efficiency to steam reforming but yields more valuable products.

The total system costs were also lower with 12.55 M€ compared to 13.22 M€,

although the membrane was slightly cheaper than the PSA. Consequently, the resulting electricity and hydrogen costs were also lower in the PSA case and were found in a range of 44.2 €/MWh to 97.6 €/MWh and 2.7 €/kg to 7.2 €/kg. The electricity costs are competitive with photovoltaics, onshore wind energy, and coal power plants, whereas the hydrogen costs are more expensive than conventional large-scale steam reforming processes. However, the hydrogen costs are comparable to small-scale steam reforming and electrolysis powered by different renewable electricity sources.

To conclude, the proposed polygeneration of hydrogen, power, and heat is thermodynamically favorable and economically reasonable. A scale-up of the engine to much higher displacement volumes seems promising for reducing the hydrogen costs even more and to achieve higher hydrogen output so that conventional large-scale steam reforming could be substituted in the future. An experimental investigation of the combination of a fuel-rich operated HCCI engine and a pressure swing adsorption process would be interesting to validate the findings of this study. It would also help to identify possible long-time stability issues due to unconverted fuel within the system components.

The economic findings will also vary with the methane source. If methane comes from fossil fuels, costs for CO_2 will increase the costs for the polygeneration output, while with biogas, the process will remain CO_2-neutral and competitive in the long-term. This study demonstrated the importance of analyzing the influence of process and economic parameter distributions on the cost distribution, as demonstrated here.

6.6 Acknowledgments

6.7 Nomenclature

Table 6.10: Abbreviations.

Abbreviation	Description
C	Compressor
CCGT	Combined cycle gas turbine
CEPCI	Chemical Engineering Plant Cost Index
CHP	Cogeneration of heat and power
CRF	Capital recovery factor
CSP	Concentrated solar power
DME	Dimethyl ether
ENG	Engine
H2M	Palladium membrane for hydrogen seperation
HCCI	Homogeneous charge compression ignition
HE	Heat exchanger
HT	High temperature
ISO	International Organization for Standardization
IMEP	Indicated mean effective pressure (engine)
LHV	Lower heating value
LT	Low temperature
MIX	Mixing chamber
O3G	Ozone generator
OM	Operating and maintenance
PSA	Pressure swing adsorption
PVF	Present value factor
WGS	Water-gas shift
WGSR	Water-gas shift reactor

Table 6.11: Symbols.

Symbol	Unit	Description
A_m	m^2	Membrane area
AC/Z	-	Active carbon to zeolite ratio (PSA)
B	-	Device property (e.g. Area, Power)
$\dot{C}$	€/s	Cost rate associated with exergy flows
D	dm^3	Displacement volume
$\dot{E}$	W	Exergy flow
E_a	J/mol	Activation energy
L	years	Lifetime

N	-	Cost exponent
N_c	-	Number of adsorption columns (PSA)
N_z	-	Number of cylinders (engine)
P	W	Power
P_0	$\text{mol/s/m/}Pa^n$	Permeability
P_{H_2}	-	Hydrogen purity
P/F	-	Purge to feed ratio (PSA)
R_u	J/mol/K	Universal gas constant
R_{H_2}	-	Hydrogen recovery
S_i	-	First order sensitivity index
$S_{T,i}$	-	Total order sensitivity index
T	K	Temperature
T_{in}	°C	Intake temperature (engine)
T_c	°C	Coolant temperature (engine)
V	-	Variance
X	-	Arbitrary input value (sensitivity index definition)
Y	-	Arbitrary output value (sensitivity index definition)
Z	€	Device costs
$\dot{Z}$	€/s	Cost rate associated with device costs
c	€/J	Specific exergy costs
d	mm	Bore (engine)
d_m	m	Thickness (membrane)
f	-	Exergoeconomic factor
f_i	-	Installation factor
f_m	-	Material factor
f_i	-	Location factor
f_{curr}	€/\$	Currency factor
n	-	Pressure exponent (membrane)
$\dot{n}$	mol/s	Mole flow
p	bar	Pressure
p_{ads}	bar	Adsorption pressure (PSA)
p_f	bar	Feed pressure (membrane)
p_{in}	bar	Intake pressure (engine)
p_p	bar	Permeate pressure (membrane)
p_{p,H_2}	Pa	Partial pressure of hydrogen in permeate (membrane)
$p_{r,}$	bar	Retentate pressure (membrane)
p_{r,H_2}	Pa	Partial pressure of hydrogen in retentate (membrane)

r	-	Relative cost difference
r_c	-	Compression ratio (engine)
rpm	1/min	Rotational speed (engine)
s	m	Stroke (engine)
t_{ads}	s	Adsorption time (PSA)
x	-	Mole fraction
y	-	Share of exergy destruction

Table 6.12: Greek symbols.

Symbol	Unit	Description
φ	-	Operating and maintenance factor
Ω	-	Salvage value factor
ε	-	Exergetic efficiency
τ	h	Operating hours
ϕ	-	Fuel-air equivalence ratio

Table 6.13: Subscripts.

Symbol	Description
D	Destruction
F	Fuel
L	Loss
P	Product
$a, b, c, 1, 2, 3$	Indices of flows or components
i	Index of flows
in	In
k	Index of component
out	Out
ref	Reference data
sys	System (whole process concept)

Table 6.14: Superscripts.

Symbol	Description
CI	Capital investment
OM	Operating and maintenance
t	Total
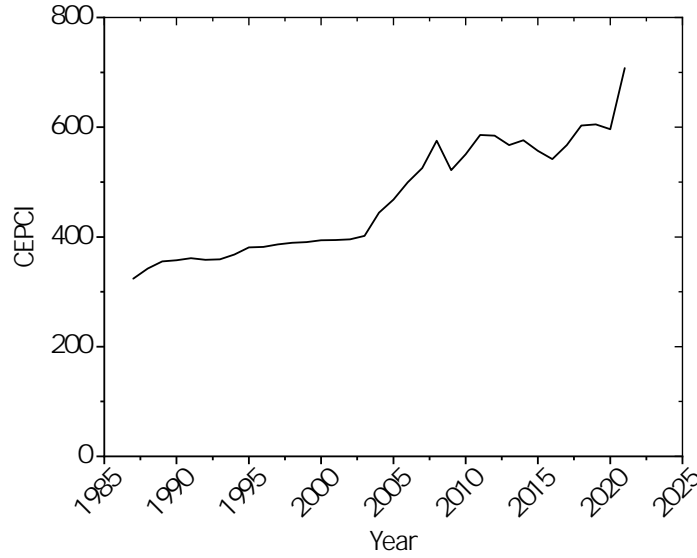
Figure 6.12: Chemical Engineering Plant Cost Index (CEPCI) for the years 1987–2021 [168].

6.8 Appendix

The cost rate $\dot{Z}_k$ of each component k is determined by calculating the investment costs and operating and maintenance costs per time unit, by considering the time value of money and the salvage value of the components [123]. The assigned values in this study are given in Table 6.6.

$$\dot{Z}_k = \dot{Z}_k^{CI} + \dot{Z}_k^{OM} = (Z_k^{CI}(1 - \Omega \cdot PVF)CRF)\tau^{-1} + \dot{Z}_k^{CI}\varphi \qquad (6.12)$$

$$CRF = \frac{i(1+i)^L}{(i+1)^L - 1} \qquad (6.13)$$

$$PVF = \frac{1}{(1+i)^L} \qquad (6.14)$$

The current investment costs of each component are calculated with the chemical engineering plant cost index (CEPCI) and (6.15).

$$Z_k^{CI} = Z_k^{'CI} \cdot \frac{CEPCI_{2021}}{CEPCI_{ref}} \qquad (6.15)$$

The investment costs are scaled by calculating the ratio of a component-specific value B_k, e.g. area for heat exchangers, and the reference value from literature B_{ref} according to the six-tenth rule [125, 133].

145

$$Z_k'^{CI} = a + Z_{ref}^{CI} \cdot \left(\frac{B_k}{B_{ref}} \right)^N \cdot f_i \cdot f_m \cdot f_l \cdot f_{curr} \qquad (6.16)$$

Eq. (6.16) is equal to (6.17) and sometimes more convenient for importing cost data, see Table 6.14.

$$Z_k'^{CI} = (a + b \cdot B_k^N) \cdot f_i \cdot f_m \cdot f_l \cdot f_{curr} \qquad (6.17)$$

$$b = \frac{Z_{ref}^{CI}}{B_{ref}^N} \qquad (6.18)$$

The engine's investment costs are calculated according to a fitted exponential function [144].

$$Z_{Engine}^{CI} = 9,332.6 \cdot P_{Engine}^{0.5389} \cdot 1.695 \qquad (6.19)$$

Since the power output P_{Engine} in partial oxidation mode is reduced, the output power per displacement volume ratio is taken from 24 commercially available cogeneration gas engine plants to calculate the power output the HCCI engine in this study would yield if operated in fuel-lean SI mode.

Table 6.15: Capital investment costs of the components.

Name	Compressor	CHP natural gas engine	Floating head heat exchanger	Static mixer	Ozone generator	WGS reactor	Palladium membrane	PSA large scale
a	0	0	32,000.00	570	0	0	0	0
b	1,525.93	9,332.60	70	1,170.00	83,771.03	33,253.49	73,007.91	53,165.23
N	0.82	0.589	1.2	0.4	0.769	0.65	0.6	0.7
Year	1987	2011	2010	2010	2021	2004	2016	2004
f_i	2.5	1.695	3.5	2.5	2.5	1.81	2.5	1.69
f_m	1	1	1.3	1.3	1	1	1	1
f_l	1	1	1.11	1.11	1.11	1.11	1	1.11
f_{curr}	1	1	0.91	0.91	0.91	0.91	1	0.91
Z_{ref}^{CI}	1,200.00	-	-	-	10,068.79	12,200,000.00	2,040,000.00	32,600,000.00
B_{ref}	0.746	-	-	-	0.063515	8,819.00	257.296	9,600.00
Unit	kW	kW	m^2	1/s	kg/h	kmol/h	m^2	kmol/h
Ref.	[128]	[144]	[169]	[169]	[170]	[171]	[128, 130]	[171]
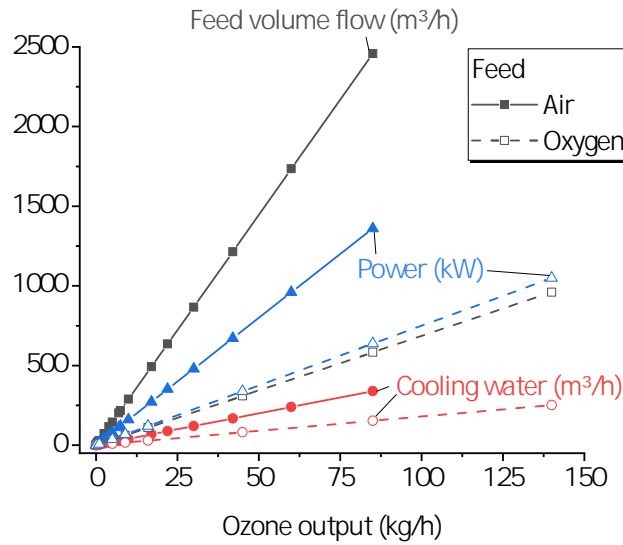
Figure 6.13: Ozone generator characteristics [111].

The ozone generator characteristics are taken from commercially available ozone generators of the Fujian Newland Entech Company [111] and illustrated in Fig. 6.13.

Fig. 6.14 shows the natural gas costs including taxes and levies for the EU and for Germany. The value shown as a green dot for 2021 is considered for this study.

To estimate the influence of increasing CO_2 costs, the natural gas costs are modified according to (6.20). The results are shown in Fig. 6.15 and the maximum natural gas costs (CO_2 costs of 100 €/t are used in this work for comparison).

$$c'_{NG} = c_{NG} + 2.75 \cdot \frac{kg_{CO_2}}{kg_{CH_4}} \cdot c_{CO_2}/LHV \tag{6.20}$$

The base fuel costs are denoted as c_{NG}, and 2.75 kg CO_2 are emitted per kg CH_4 at stoichiometric combustion. This ratio is multiplied by the CO_2 costs c_{CO_2} and divided by the lower heating value of methane (LHV).

Table 6.16: Results of the exergoeconomic analysis with fixed process and economic input parameters; PSA-case, analysis of the streams.

#	p	T	$\dot{m}$	$\dot{E}^{ph}$	$\dot{E}^{ch}$	$\dot{E}^{t}$	c	$\dot{C}$
	(bar)	(°C)	(kg/s)	(kW)	(kW)	(kW)	(€/GJ)	(€/h)
0	1.0	20.0	0.85	0.02	1.64	1.65	0	0
1	1.0	20.0	0.10	0.00	5,187.50	5,187.50	8.4	157.2

2	1.0	20.0	0.95	0.02	5,148.86	5,148.89	8.6	159.4
3	1.0	200.0	0.95	44.75	5,148.86	5,193.61	9	168.8
4	1.0	20.0	0.00	0.00	0	0	0	0
5	1.0	35.0	0.00	0.00	0.06	0.06	2,259.70	0.5
6	1.0	199.9	0.95	44.73	5,148.90	5,193.63	9.2	171.4
7	1.8	605.7	0.95	409.00	3,099.18	3,508.18	13.2	167.3
8	1.8	458.8	0.95	281.26	3,099.18	3,380.44	13.2	161.2
9	1.8	300.0	0.95	165.91	3,099.18	3,265.09	13.2	155.7
10	1.8	299.4	1.00	175.83	3,113.45	3,289.28	14	165.4
11	1.8	300.0	1.00	177.19	2,946.90	3,124.09	16.1	181.6
12	1.8	200.0	1.00	115.92	2,946.90	3,062.82	16.1	178
13	1.8	200.0	1.00	116.07	2,937.23	3,053.29	17.9	196.7
14	1.8	35.0	0.97	59.81	2,936.63	2,996.44	17.9	193
15	3.0	92.4	0.97	121.67	2,936.63	3,058.30	18.3	201.3
16	3.0	25.0	0.97	111.81	2,936.63	3,048.44	18.3	200.6
17	1.0	25.0	0.94	0.06	517.59	517.65	18.3	34.1
18	3.0	25.0	0.02	27.48	2,464.64	2,492.12	27.6	247.7
19	50.0	481.8	0.02	154.77	2,464.64	2,619.41	27.8	262.2
20	-	-	-	-	-	-	-	-
21	-	-	-	-	-	-	-	-
22	50.0	80.0	0.02	100.29	2,464.64	2,564.93	27.8	256.8
23	-	-	-	835.69	0	835.69	13.2	39.9
24	-	-	-	1.14	0	1.14	13.2	0.1
25	-	-	-	73.90	0	73.9	13.2	3.5
26	-	-	-	138.77	0	138.77	13.2	6.6
27	-	-	-	-	-	-	-	-
28	1.0	70.0	3.40	54.42	169.87	224.29	8.6	7
29	1.0	90.0	3.40	102.96	169.87	272.83	9.4	9.3
30	6.0	60.0	0.07	0.82	3.74	4.56	8.6	0.1
31	6.0	290.0	0.07	29.44	44.16	73.6	35	9.3
32	1.0	270.0	2.11	278.70	0	278.7	8.6	8.6
33	1.0	290.0	2.11	320.97	0	320.97	9.6	11.1
34	6.0	158.9	0.08	26.41	4.1	30.51	54.7	6
35	6.0	290.0	0.08	73.33	4.1	77.43	60.9	17
36	1.8	290.0	0.04	31.79	2.15	33.94	60.9	7.4
37	6.0	290.0	0.11	101.76	5.69	107.45	60.9	23.5
38	1.0	70.0	0.25	4.07	12.68	16.75	8.6	0.5

39	1.0	90.0	0.25	7.68	12.68	20.36	10.3	0.8
40	1.0	30.0	0.97	0.67	48.22	48.9	8.6	1.5
41	1.0	50.0	0.97	5.80	48.22	54.02	58.6	11.4
42	1.0	20.0	2.07	0.00	103.51	103.51	8.6	3.2
43	1.0	30.0	2.07	1.44	103.51	104.95	24.6	9.3
44	6.0	60.0	0.04	0.48	2.19	2.67	8.6	0.1
45	6.0	290.0	0.04	39.14	2.19	41.33	63.9	9.5
46	-	-	-	-	-	-	-	-
47	-	-	-	-	-	-	-	-
48	6.0	60.0	0.08	0.90	4.1	5	8.6	0.2

Table 6.17: Results of the exergoeconomic analysis with fixed process and economic input parameters; PSA-case, analysis of the streams (continued).

#	x_{CH_4}	x_{O_2}	x_{N_2}	x_{O_3}	x_{CO_2}	x_{CO}	x_{H_2O}	x_{H_2}
0	0.00	0.21	0.79	0.00	0.00	0.00	0.00	0.00
1	1.00	0.00	0.00	0.00	0.00	0.00	0.00	0.00
2	0.17	0.17	0.65	0.00	0.00	0.00	0.00	0.00
3	0.17	0.17	0.65	0.00	0.00	0.00	0.00	0.00
4	0.00	0.21	0.79	0.00	0.00	0.00	0.00	0.00
5	0.00	0.21	0.78	0.01	0.00	0.00	0.00	0.00
6	0.17	0.17	0.65	0.00	0.00	0.00	0.00	0.00
7	0.00	0.00	0.56	0.00	0.02	0.12	0.12	0.17
8	0.00	0.00	0.56	0.00	0.02	0.12	0.12	0.17
9	0.00	0.00	0.56	0.00	0.02	0.12	0.12	0.17
10	0.00	0.00	0.53	0.00	0.02	0.12	0.17	0.16
11	0.00	0.00	0.55	0.00	0.12	0.02	0.05	0.26
12	0.00	0.00	0.55	0.00	0.12	0.02	0.05	0.26
13	0.00	0.00	0.55	0.00	0.14	0.00	0.04	0.27
14	0.00	0.00	0.57	0.00	0.14	0.00	0.00	0.28
15	0.00	0.00	0.57	0.00	0.14	0.00	0.00	0.28
16	0.00	0.00	0.57	0.00	0.14	0.00	0.00	0.28
17	0.00	0.00	0.76	0.00	0.19	0.01	0.00	0.05
18	0.00	0.00	0.00	0.00	0.00	0.00	0.00	1.00
19	0.00	0.00	0.00	0.00	0.00	0.00	0.00	1.00

20	-	-	-	-	-	-	-	-
21	-	-	-	-	-	-	-	-
22	0.00	0.00	0.00	0.00	0.00	0.00	0.00	1.00
23	0.00	0.00	0.00	0.00	0.00	0.00	0.00	0.00
24	0.00	0.00	0.00	0.00	0.00	0.00	0.00	0.00
25	0.00	0.00	0.00	0.00	0.00	0.00	0.00	0.00
26	0.00	0.00	0.00	0.00	0.00	0.00	0.00	0.00
27	-	-	-	-	-	-	-	-
28	0.00	0.00	0.00	0.00	0.00	0.00	0.00	0.00
29	0.00	0.00	0.00	0.00	0.00	0.00	0.00	0.00
30	0.00	0.00	0.00	0.00	0.00	0.00	1.00	0.00
31	0.00	0.00	0.00	0.00	0.00	0.00	1.00	0.00
32	0.00	0.00	0.00	0.00	0.00	0.00	0.00	0.00
33	0.00	0.00	0.00	0.00	0.00	0.00	0.00	0.00
34	0.00	0.00	0.00	0.00	0.00	0.00	1.00	0.00
35	0.00	0.00	0.00	0.00	0.00	0.00	1.00	0.00
36	0.00	0.00	0.00	0.00	0.00	0.00	1.00	0.00
37	0.00	0.00	0.00	0.00	0.00	0.00	1.00	0.00
38	0.00	0.00	0.00	0.00	0.00	0.00	1.00	0.00
39	0.00	0.00	0.00	0.00	0.00	0.00	1.00	0.00
40	0.00	0.00	0.00	0.00	0.00	0.00	1.00	0.00
41	0.00	0.00	0.00	0.00	0.00	0.00	1.00	0.00
42	0.00	0.00	0.00	0.00	0.00	0.00	1.00	0.00
43	0.00	0.00	0.00	0.00	0.00	0.00	1.00	0.00
44	0.00	0.00	0.00	0.00	0.00	0.00	1.00	0.00
45	0.00	0.00	0.00	0.00	0.00	0.00	1.00	0.00
46	-	-	-	-	-	-	-	-
47	-	-	-	-	-	-	-	-
48	0.00	0.00	0.00	0.00	0.00	0.00	1.00	0.00
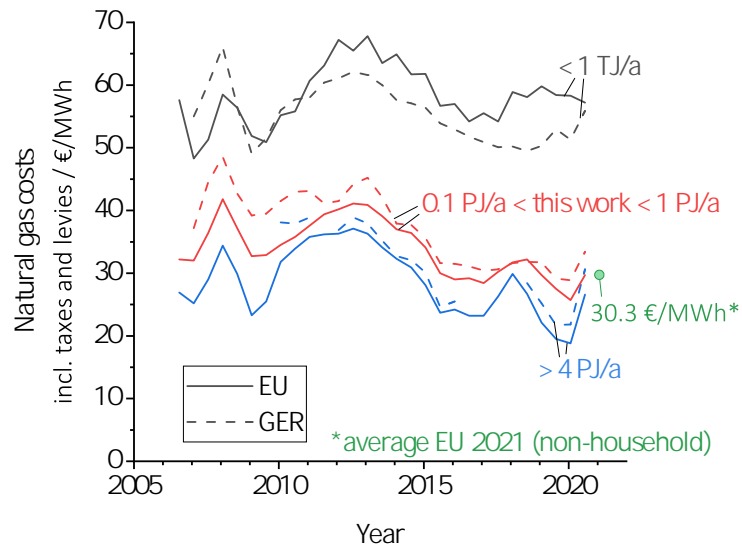
Figure 6.14: Natural gas costs including taxes and levies for the years 2005 to 2021 for three different total energy demands per year. Solid lines averaged values for the EU, dashed lines natural gas costs in Germany [172]. The EU average value for 2021 was taken from [173].
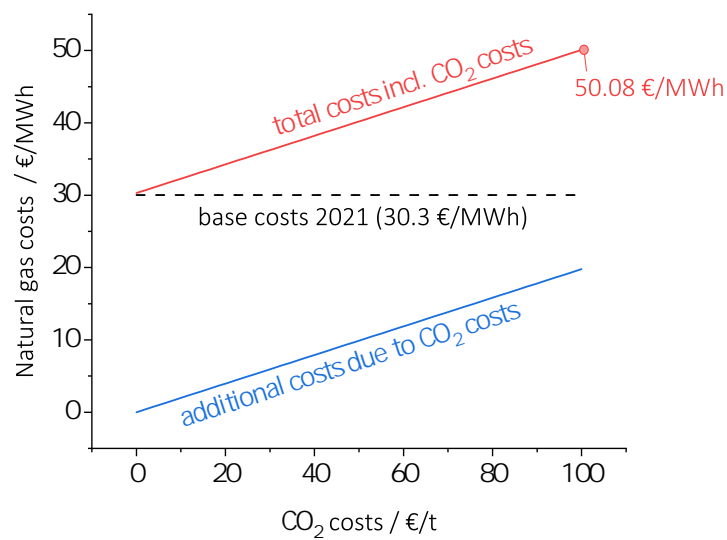
Figure 6.15: Natural gas price as a function of CO_2 costs. Base natural gas price is taken from Fig. 6.15, green dot, and the CO_2 price is varied from 0.0 to 100.0 €/t.

152
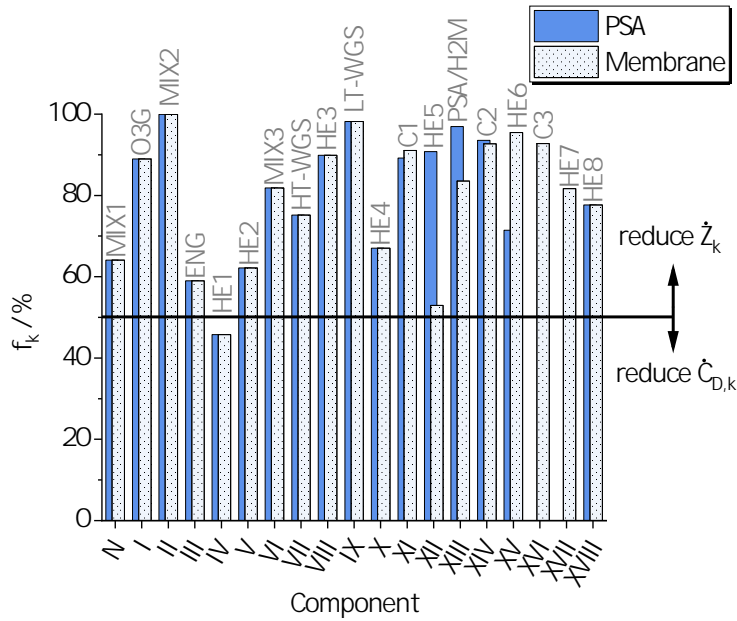
Figure 6.16: Exergoeconomic factor for each component. Above the threshold of 50 %, the investment and operating costs should be reduced, and blow the threshold the costs of exergy destruction should be reduced; hence the efficiency should be increased.
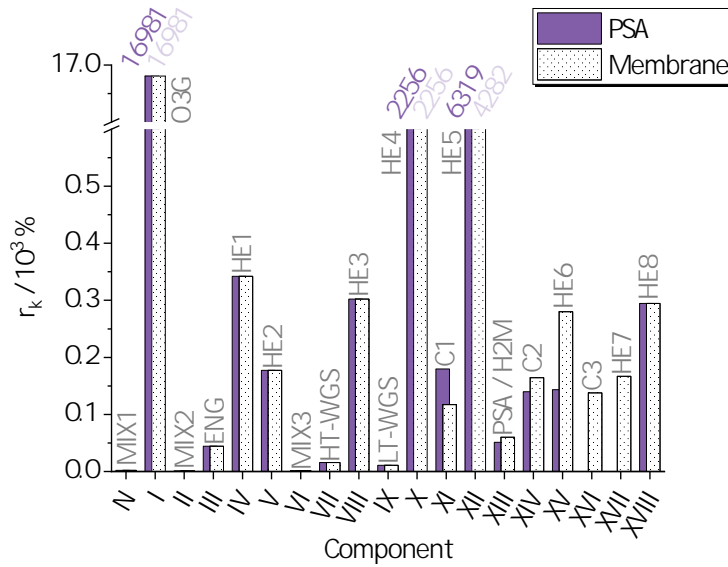
Figure 6.17: Relative cost difference for each component.
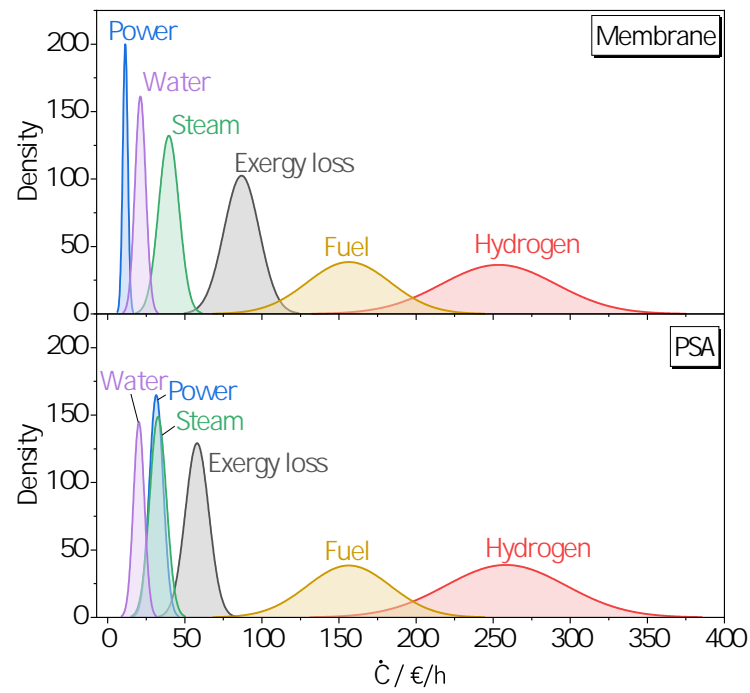
Figure 6.18: Cost rates for each product, calculated from the Monte Carlo distributed input and cost parameters. Hydrogen contributes to a major part of all cost rates and is thus the most valuable product of the system. Due to a higher effort for compression and cooling, the cost rate of exergy loss is much higher for the membrane case which increases all product costs significantly.

BIOGAS CONVERSION IN HCCI ENGINES FOR SYNTHESIS GAS PRODUCTION

This chapter presents a conference contribution referred to as:

D. Schröder und B. Atakan. Theoretische Untersuchung der Umsetzung von Biogasen in HCCI-Motoren zur Erzeugung von Synthesegas. *29. Deutscher Flammentag, Bochum, 17-18 September 2019.*

Introduction to the sixth paper

In the previous chapters, the conditions under which polygeneration in HCCI engines is possible and reasonable were shown. Furthermore, the required equipment to produce pure products such as hydrogen and the resulting product costs were discussed.

For these studies the fuel was pure methane or natural gas. Since CO_2 costs are going to increase [174], it might be reasonable to gradually replace natural gas based applications with low-carbon technologies, as explained in the introduction to this thesis. One option is to replace natural gas with biogenically produced gases; commonly referred to as biogas. The production of biogas has been increasing in recent years, for instance 62.3 billion m³ were produced in 2019 globally, which is about 5 times more than in 2000 and represents an annual growth rate of 9 % [175]. Biogas is also seen as an important part of a circular economy [176]. This raises the question, if such gases, which are typically strongly diluted with CO_2, can be converted in a fuel-rich operated HCCI engine.

In this chapter, a parameter study was performed, in which the single-zone engine model was used to find feasible and efficient operating conditions for different biogas compositions. Since biogas contains different amounts of CO_2, depending on its source, the CO_2 amount is varied from 0 % to 50 %. Moreover, ozone is used as an additive and the ozone amount is varied, as well as the intake temperature and the equivalence ratio (ϕ =1.0-4.0).

The key contributions of this work to the state of the art can be summarized as follows:

– Biogas conversion in fuel-rich HCCI engines is feasible, but higher intake temperatures and ozone amounts are needed compared to neat methane or natural gas.

– The highest synthesis gas output was found at a ϕ range of 2 to 2.25.

– The exergetic efficiency decreases by 9 %-pts with increasing CO_2 content in the biogas, resulting in a nevertheless high value of 78.1 %.

– In a large ϕ range of 1.5 to 4.0, CO_2 is converted to CO, and the process can be considered a CO_2 sink.

Table 7.1: Author contributions for chapter 7 following the CRediT author statement methodology [41].

Author	Freund	Atakan
Conceptualization	✓	✓
Methodology	✓	
Software	✓	
Validation	✓	
Formal analysis	✓	
Investigation	✓	
Resources		✓
Data curation	✓	
Writing - Original draft	✓	
Writing - Review & editing		✓
Visualization	✓	
Supervision		✓
Project administration		✓
Funding acquisition		✓

Author contributions to the sixth paper

I was responsible for the conceptualization, modelling, data analysis and writing of the manuscript. Burak Atakan supported me by reviewing the results, commenting and revising the manuscript, mentoring me, and most importantly, giving me the opportunity to present my results at renowned conferences.

7.1 Abstract

Fuel-rich combustion processes can be used in stationary internal combustion engines to produce base chemicals, such as synthesis gas, from various fuels in addi-

tion to work and heat. Previous studies have shown, model-based and experimentally, that fuel-rich partial oxidation of methane (as a major component of natural gas) is possible in engines with homogeneous charge compression ignition (HCCI). Moreover, hydrogen and carbon monoxide mole fractions of up to 23 % and 15 %, respectively, can be achieved in the exhaust gas, with high exergetic efficiency.

Biogases usually have a relatively low calorific value and are difficult to use in conventional combustion systems without technical modifications. Therefore, the present work theoretically investigates whether biogenically produced gases can be converted in a fuel-rich polygeneration process with an HCCI engine. Different biogas compositions are investigated regarding their ignitability in the HCCI engine. Since the fuel-air mixture is relatively inert, it is preheated by using exhaust gas exergy and ozone is added. Furthermore, the influence of ozone on auto-ignition is investigated. Another challenge is the high amount of inert CO_2 in the biogas of up to 50 %.

Modelling and simulation are performed using Python and the *Cantera* module to calculate the thermodynamics and reaction kinetics of the process. The required inlet temperatures and exhaust gas composition for different biogas compositions for equivalence ratios (ϕ) from 1.0 to 4.0 are investigated. The required inlet temperatures for biogas with 50 % CO_2 increase from 595 K up to 805 K with increasing equivalence ratio.

Furthermore, the CO_2 conversion and the CO mole fraction in the exhaust gas increase with the CO_2 fraction in the biogas, making this process suitable as a CO_2 sink. The mole fractions of H_2 and CO in the exhaust gas reach a maximum of 22.2 % ($\phi = 2.5$) and 14.1 % ($\phi = 2.25$), respectively, with high exergetic efficiencies of 81.1 % and 77.4 %.

To reduce the effort of preheating the fuel-air mixture, the influence of ozone as an additive on the necessary inlet temperature is investigated. If 1000 ppm of ozone is added, the necessary inlet temperature is reduced by up to 100 K, so that an inlet temperature of 570 K is necessary at $\phi = 2$. Therefore, the use of biogases is feasible but requires preheating and reactive additives.

7.2   Introduction

Society today is largely dependent on the use of fossil fuels, e.g. in the transport sector, in the energy and industrial sector or in domestic households. However, the long-term use of fossil energy sources is questionable due to the finite nature of the resources and the strong increase in the anthropogenic generation of greenhouse

gases such as carbon dioxide through combustion processes, which are held responsible for climate change [7]. For these reasons, technologies to reduce CO_2 emissions are becoming increasingly important.

One possible way to achieve this reduction in the energy and industrial sectors is the polygeneration of multiple products at a higher efficiency, compared to the separate conventional technologies [118]. Previous work has already shown experimentally and theoretically that the fuel-rich conversion of methane in HCCI engines can be used for polygeneration: in addition to work and heat, synthesis gas is produced in relevant quantities [30, 78, 105, 157]. In an HCCI engine, a homogeneous fuel-air mixture is compressed until it reaches the required ignition temperature and ignites. The combustion is thus kinetically controlled, making this mode more suitable for fuel-rich partial oxidation in the engine than spark ignition, where flame speed is a limiting factor [30].

The synthesis gas produced by this process is an important feedstock for the chemical industry, for example, for the production of ammonia, methanol, and other higher-value alcohols [177]. Nowadays, synthesis gas is mainly produced by steam reforming of natural gas [119]. The global production of pure hydrogen also uses 96 % fossil fuels and 4 % electrical energy, with natural gas accounting for 48 % of the total feedstock [178].

In this work, an exergetic analysis is performed to evaluate the polygeneration process and compare it with conventional processes. Steam reforming of natural gas is very energy intensive and the maximum achievable exergetic efficiency is 63 % according to the study by Simpson et al. [26]. In comparison with 19 other production methods, such as electrolysis or biomass gasification, steam reforming achieves by far the highest efficiency [179]. In our previous work, it was shown that an HCCI engine used for polygeneration achieves an exergetic efficiency of up to 82 % [78], making it a promising concept for the utilization of natural gas.

In this study, biogenically produced gases with different methane contents were investigated as regenerative fuels for synthesis gas production to determine their suitability for the fuel-rich HCCI combustion process. This is interesting, on the one hand, because fossil CO_2 emissions can be significantly reduced and, on the other hand, because in Germany, for example, 17.2 % of electrical energy was already generated from biogas in 2015 and the biogas supply is therefore sufficiently large.

Biogases are produced as a by-product, sometimes in large quantities, in various processes: landfilling of waste, commercial composting, anaerobic digestion of sewage sludge in wastewater treatment, manure from livestock farming, and food wastes. [180]. Therefore, the use of biogases offers many advantages [33, 181]:

– Local, decentralized generation and use.

– Renewable energy source with low CO_2 emissions.

– Efficient disposal of organic waste.

– Reduction of methane emissions to the environment.

The composition of the biogenically produced gases varies depending on the origin and process, although methane and carbon dioxide always make up the majority of the gas. In small quantities, biogas usually also contains hydrogen, nitrogen, water vapor, ammonia, and traces of hydrogen sulfide and siloxanes [33], although the latter three components must be separated by gas purification processes for various reasons [180]. Hydrogen sulfide is converted to sulfur dioxide and sulfuric acid in combustion processes, and these substances are highly corrosive and harmful to health and the environment. Ammonia is also corrosive and harmful, but to a lesser extent than sulfur compounds. Siloxanes form solids such as silicon dioxide and thus damage moving components. Table 7.2 shows typical biogas compositions.

Table 7.2: Typical components of biogases (in vol%) [33].

Component	Amount
CH_4	50-70
CO_2	25-50
H_2	1-5
N_2	0.3-3.0
H_2O_g	0.3
NH_3	< 1
H_2S	< 1
Siloxane	traces

Therefore, biogases should be pretreated before they can be used for combustion processes. Various technologies are suitable for this purpose [33]:

– Absorption (e.g. wet separator with water as detergent)

– Chemical reagents (e.g. activated carbon)

– Adsorption (e.g. molecular sieves)

– Membrane separation

– Cryogenic distillation

For this study, it is assumed that the impurities in the biogases are negligible or that sufficient treatment has preceded. Thus, pure methane/CO_2 mixtures are investigated with respect to the influence of the CO_2 amount. For detailed information on the gas treatment processes, reference is made to the work of Abatzoglou and Boivin [180].

Biogases are nowadays mostly used for combined heat and power (CHP) in Germany, mainly using spark ignition (SI) engines [182]. In very small proportions, (micro) gas turbines, fuel cells, and gas boilers are also used.

However, biogases can also be used for synthesis gas production in reforming processes. In 2018, Nourbakhsh et al. studied the partial oxidation of biogases (synthetic CH_4/CO_2 mixtures) experimentally and theoretically [183]. They found that synthesis gas production at ambient pressure and temperature, and at an equivalence ratio of 2.5 to 3.0 is most beneficial in terms of methane conversion and synthesis gas yield. Their results are compared with those obtained for the HCCI engine in this study.

A major challenge in using the HCCI combustion process is the necessary high inlet temperature, which is required to achieve ignition of the inert methane by compression. Numerous methods have been investigated in the literature to use such fuels, with stable control of combustion, in fuel-lean HCCI engines. The following methods can be mentioned as excerpts [130]:

– Pilot injection of a more reactive fuel

– Preheating of the mixture

– Exhaust gas recirculation

– Change of fuel composition

– Varying the compression ratio during operation

– Supercharging

– "Fast Thermal Management" - rapid mixing of differently heated air streams

In previous work on polygeneration with pure methane in the fuel-rich HCCI engine, a combination of two methods was used: preheating and the use of reactive fuels as additives such as dimethyl ether [47, 78] and n-heptane [30]. This allowed stable operation at fresh gas temperatures of 100 °C to 190 °C at equivalence ratios of 1.2 to 2.4. With increasing CO_2 content, the properties of the gas deteriorate in terms of flammability and calorific value. Therefore, the question arises whether

biogases are generally suitable for combustion in HCCI engines, especially in fuel-rich operation.

In 2012, Bedoya et al. showed experimentally and theoretically in different works that fuel-lean (ϕ = 0.19-0.5) operation with biogas is possible [184–186]. With a compression ratio of 17 and an inlet pressure of 2 bar, a CH_4/CO_2 mixture of 40/60 could be stably ignited at an inlet temperature of 210 °C. In 2016, Kozarac et al. used n-heptane as an additive and achieved ignition at inlet temperatures ranging from 34 °C to 234 °C, with up to 28 % of the fuel energy delivered from n-heptane (ϕ = 0.33-0.43) [187].

However, the hydrocarbon containing additives provide energy for combustion, are complex and possibly costly to produce. These disadvantages can be avoided if ozone is used as an additive, since it is only required in small quantities (ppm) and can be generated on-site using an ozone generator.

For SI engines, the benefits of ozone have been known since the 1980s [104]. For fuel-lean HCCI engines, its influence on various fuels has been studied, especially in recent years [71, 85, 87, 188]. When ozone is added to the fuel-air mixture, the combustion phasing shifts to earlier crank angles, the inlet temperature is reduced, and combustion can be controlled via the control of the ozone mass flow. Similar positive effects are expected when ozone is used for fuel-rich HCCI engines.

In this work, the influence of the CO_2 content on the usability of biogases for the polygeneration process is investigated and reasonable operating ranges are evaluated. Then, the influence of adding up to 1000 ppm ozone is investigated to evaluate whether ozone is also promising for fuel-rich biogas ignition in HCCI engines.

7.3   Engine model and methodology

The HCCI engine is modeled in Python using the *Cantera* module to calculate thermodynamics and reaction kinetics [50]. The engine model is a zero-dimensional four-stroke single zone model including intake and exhaust valves. Accordingly, a homogeneous distribution of the gas in the cylinder is assumed. The reaction mechanism used is taken from the work of Burke et al. [73] and was extended to include the ozone sub-mechanism of Zhao et al. [96] to represent the decomposition reactions of ozone. For detailed information on the operation of the engine model, the reader is referred to the work of Hegner and Atakan [34]. The engine characteristics and operating conditions are shown in Table 7.3.

A relatively high rotational speed of 3000 1/min is used to achieve high power and product gas mass flows. The cylinder geometry is taken from a typical gas

Table 7.3: Engine properties and operating conditions.

Description	Symbol	Value	Unit
Rotational speed	rpm	3000	1/min
Compression ratio	r_c	18	
Bore	d	130	mm
Stroke	s	142	mm
Number of cylinders	N_Z	12	
Displacement	D	22.62	dm³
Wall thickness	d_w	10	mm
Equivalence ratio	ϕ	1-4	
Coolant temperature	T_c	90	°C
Thermal conductivity wall	λ_w	53	W/m²/K
Convection coefficient coolant	α_c	3000	W/m²/K
Inlet valve opening	-	-180/0	°CA
Outlet valve opening	-	180/360	°CA

engine for cogeneration [189]. The convective heat transfer coefficient of the inner cylinder wall is calculated using Woschni's equation [58] and used to calculate the heat flux $\dot{Q}_{eng}$ through the cylinder wall to the cooling water.

The thermal energy of the exhaust gas is used in two ways. On the one hand, it is used to preheat the fuel-air mixture to the required inlet temperature. On the other hand, the remaining available thermal energy is used as a heat flow $\dot{Q}_{exh}$, as it is common in cogeneration plants. For the calculation of these heat flows, the energy balances of the heat exchangers are implemented in the Python model, and the heat capacities of the fluids are assumed to be constant for simplicity. Finally, the exhaust gas, which in this case is a valuable product gas, leaves the system with a temperature of 30 °C.

In this first parameter study of biogas utilization, the processes required to separate the synthesis gas from the exhaust gas are neglected, since their design depends on the operating point and involves great computational effort. A simplified process concept is shown in Figure 7.1.

The ozone added to the fuel-air mixture is homogeneously distributed and the ozone decomposition starts at -360 °CA (top dead center intake stroke). The heat flows are evaluated exergetically by multiplying them by the Carnot factor, which leads to the calculation of the maximum usable exergy of heat $\dot{E}_Q$ according to equation (7.1).

$$\dot{E}_Q = \dot{Q}_{eng} \left(1 - \frac{T_u}{T_{m,eng}} \right) + \dot{Q}_{exh} \left(1 - \frac{T_u}{T_{m,exh}} \right) \quad (7.1)$$

To calculate the exergetic efficiency η_{ex} (7.2), the chemical exergy flows of the

Figure 7.1: Simplified process concept of the investigated energy system for poly-generation of work, heat, and synthesis gas.

fuel-air mixture, the hydrogen and carbon monoxide contained in the exhaust gas and the mechanical power are determined. Since the fresh gas is aspirated at ambient conditions, its total exergy is equal to its chemical exergy [190].

$$\eta_{ex} = \frac{\dot{W}_{eng} + \dot{E}_Q + \dot{E}_{H_2}^{ch} + \dot{E}_{CO}^{ch}}{\dot{E}_{biogas}^{ch} + \dot{E}_{air}^{ch} + \dot{E}_{O_3}^{ch}} \tag{7.2}$$

To investigate the suitability of the different biogas compositions for the poly-generation process, the equivalence ratio and CO_2/CH_4 ratio were initially varied. The results were examined in terms of required inlet temperature, fuel conversion, work, heat, product gas composition, and exergetic efficiency. Subsequently, at a constant CO_2/CH_4 ratio of 1, an ozone feed of 0 to 1000 ppm was investigated to evaluate the reduction in inlet temperature, as shown in table 7.4.

Table 7.4: Investigated parameters

Description	Symbol	Study 1	Study 2
Equivalence ratio	ϕ	1-4	1-4
CO_2/CH_4 ratio (molar)	x_{CO_2}/x_{CH_4}	0-1	1
Ozone amount (molar)	x_{O_3}	0 ppm	0-1000 ppm

The necessary inlet temperature for ignition of the mixture is defined by pressure

Figure 7.2: Temperature and pressure curve as a function of the crank angle for two different inlet temperatures T_0 (without ozone supply). If the inlet temperature is too low, the mixture will not ignite (red), while in this example ignition is successful at an inlet temperature 2 K higher (black), as can be seen from an strong increase in temperature and pressure.

rise rates of at least 5 bar/°CA. Without ignition, the pressure rise rates in the engine model are always lower than 2 bar/°CA.

Figure 7.2 shows an example of the temperature and pressure curves for two different inlet temperatures to illustrate the difference between an igniting and a non-igniting mixture.

7.4 Results and discussion

First, the inlet temperatures necessary for ignition are calculated and compared with the previous results with pure methane. Here it can be seen that the necessary temperatures increase significantly with increasing equivalence ratio and with increasing CO_2 content in the mixture: from 545 K ($\phi = 1$; 0 % CO_2) up to 805 K ($\phi = 4$; 50 % CO_2), as illustrated in figure 7.3.

Higher inlet temperatures are required with increasing CO_2 content due to the approximately 5 % greater specific molar heat capacity of CO_2 compared to methane, which means that a CO_2-rich mixture heats up less during compression and the pressure also increases less as a result. Temperature and pressure at top dead center are reduced by 5.6 % (-70.5 K) and 5.9 % (-2.3 bar) at $\phi = 2$, for

164
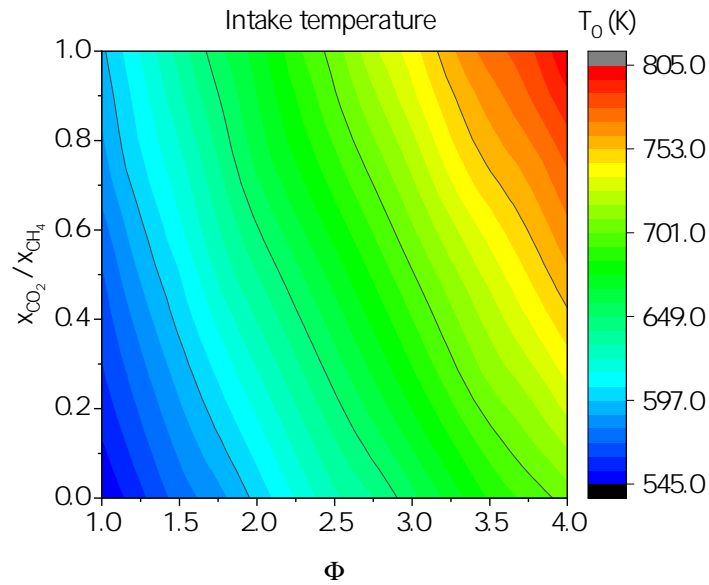
Figure 7.3: Inlet temperatures of the HCCI engine required for ignition of biogas as a function of the CO_2/CH_4 ratio and equivalence ratio.
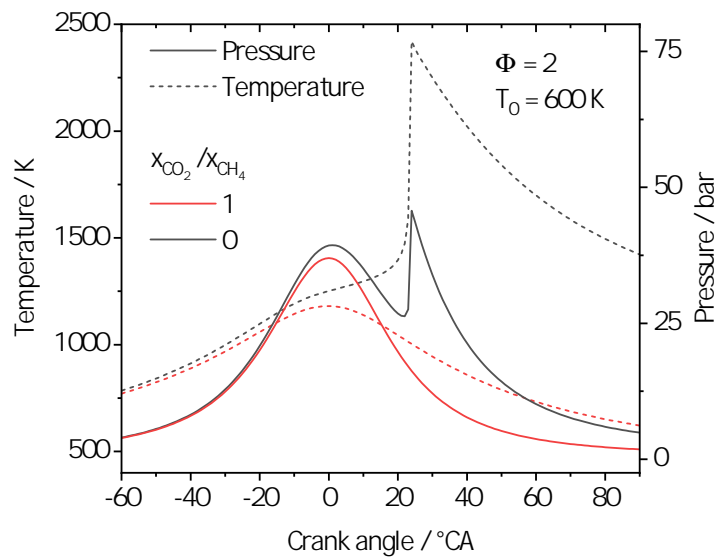
Figure 7.4: Temperature and pressure curve as a function of the the crank angle for two different CO_2/CH_4 ratios.

example, when the CO_2 content increases from 0 % to 50 %, see figure 7.4.

However, methane conversion is not significantly affected by the presence of carbon dioxide. From figure 7.5a, it can be seen that the methane is not fully converted above an equivalence ratio of 2.25 due to the lack of oxygen, and the conversion is reduced to 77 % at $\phi = 4$. Increasing the CO_2 content from 0 % to 50 % reduces the conversion by about 1 to 4 percentage points. While CO_2 is formed during the process at low CO_2 contents and equivalence ratios (black area in Figure 7.5b), more than 50 % of the CO_2 is converted at high CO_2 contents and $\phi = 2.0$-2.5. If the additional CO formed as a result can be used as a product, the process in this range can be operated as a CO_2 sink. At these equivalence ratios, the largest H_2 and CO mole fractions are produced, although this is strongly dependent on the CO_2 content of the biogas, as figures 7.5c and 7.5d show.

It must also be mentioned here that increased soot formation in the engine was observed at equivalence ratios above 2.0 when operating with pure methane [78]. With pure methane as fuel, H_2 and CO mole fractions of 22.2 % and 14.1 % can be achieved at $\phi = 2.5$. The maximum CO mole fraction of 18.2 % is achieved at the maximum CO_2 content of 50 % in biogas and $\phi = 2.25$ in this study. The H_2 mole fraction here is still 9.2 %.

Operation at high equivalence ratios and CO_2 fractions leads to a reduced work output of the engine due to the reduced temperature and pressure rise. For instance, the specific work decreases for pure methane from 15.7 MJ/kg at $\phi = 1$ to 1.3 MJ/kg at $\phi = 4$, as shown in figure 7.5e. For a constant ϕ of 2, the specific work decreases from 5.8 MJ/kg to 0.9 MJ/kg when the CO_2 content increases from 0 % to 50 %. In this case, the lower heating value of the mixture is reduced from 50 MJ/kg to 13.4 MJ/kg. As a result, the conversion of this heating value to work is reduced by 4.9 %-pts.; from 11.6 % to 6.7 %.

Nevertheless, due to the high synthesis gas mole fractions high exergetic efficiencies above 80 % are achieved in almost the entire parameter range from $\phi = 1$-2.25. The maximum efficiency is 87.1 % at $\phi = 2$ with pure methane. With increasing CO_2 content, the efficiency decreases by 9 %-points to 78.1 %. A comparison with the work of Noubarkhsh et al. shows that the maximum mole fractions of 22.2 % (H_2) and 18.1 % (CO) achieved in the engine are 10.1 %-pts. and 5.4 %-pts. lower, respectively, compared to the reactor results. The amounts of synthesis gas produced in the engine can be considered high despite the short residence time and changing temperatures and pressures.

However, the high inlet temperatures and the lack of combustion control are a problem without the use of additives. Therefore, in this parameter study, the
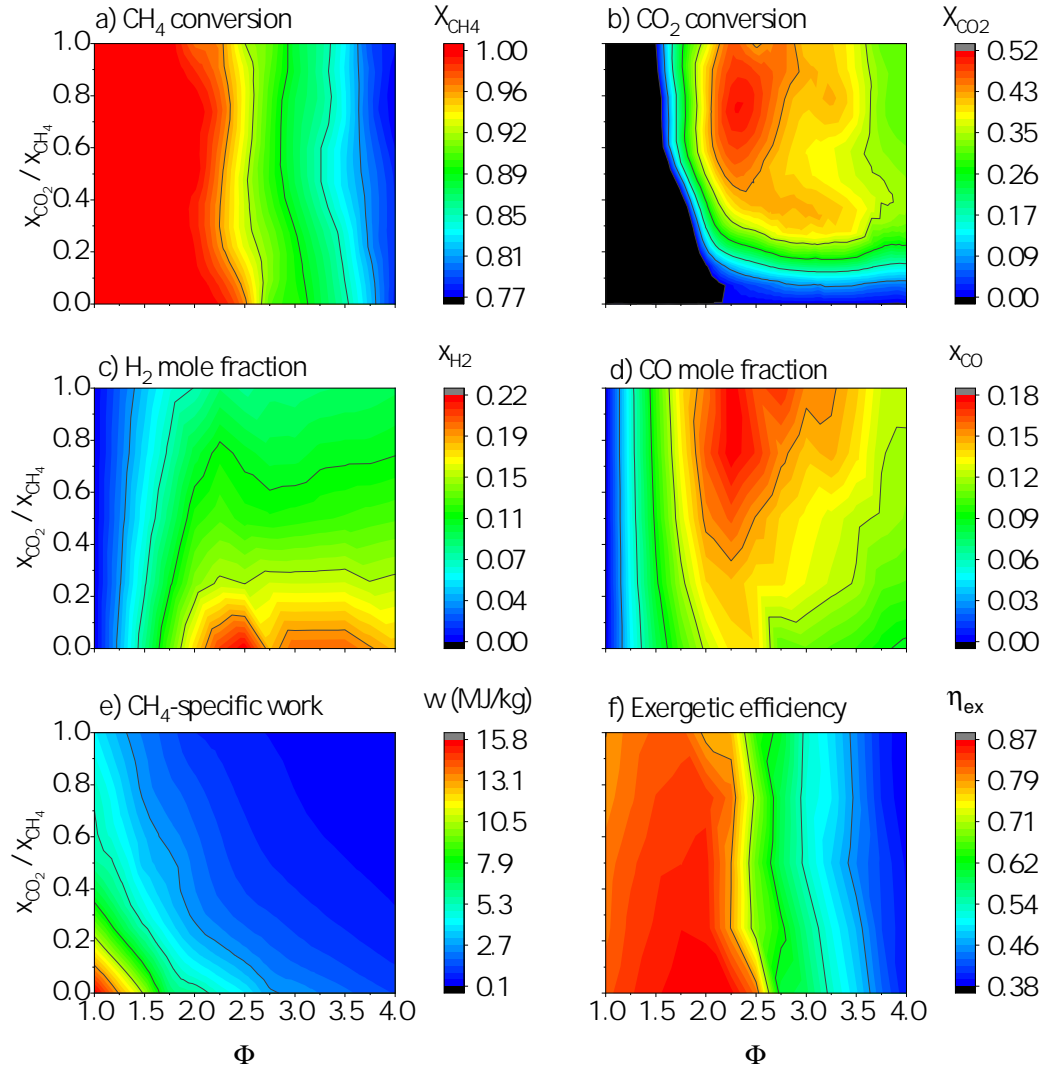
Figure 7.5: Results of the parameter study as a function of CO_2/CH_4 molar ratio and equivalence ratio: a) methane conversion, b) CO_2 conversion, c) specific work produced in MJ/kg d) exergetic efficiency, e) H_2 mole fraction in product gas, f) CO mole fraction in product gas.

167
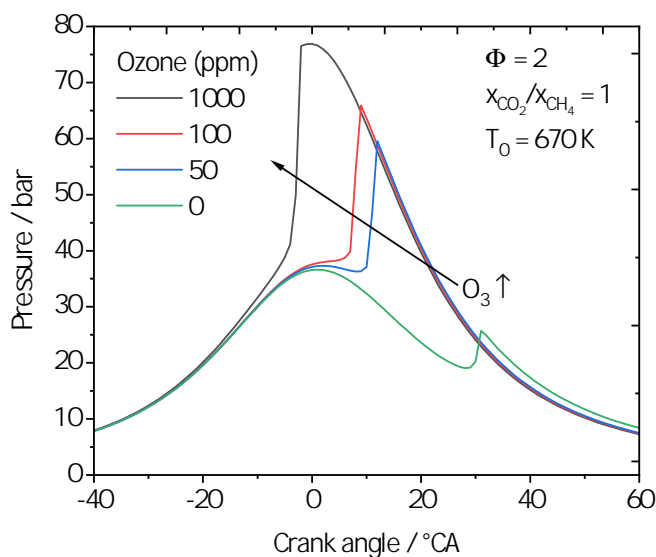
Figure 7.6: The influence of ozone addition on the pressure trace at $\phi = 2$.

influence of 0 to 1000 ppm ozone addition at a constant CO_2/CH_4 ratio of 1 was investigated. Figures 7.6 and 7.7 show the influence of ozone on the pressure profile and methane conversion, respectively, at $\phi = 2$ and a constant inlet temperature of 670 K.

With increasing ozone addition, the combustion phasing is shifted to earlier crank angles, and a low ozone content of 50 to 100 ppm achieves the greatest effect. The ozone decomposes early in the intake and compression stroke. At 1000 ppm ozone addition, small amounts of methane are converted about 100 °CA earlier, mainly to hydrogen peroxide and formaldehyde. This leads to a small additional increase in temperature and pressure and eventually to earlier ignition.

This has a large effect on the inlet temperature required for ignition, but only a small to negligible effect on the product output (work, heat, synthesis gas) or the exergetic efficiency. With increasing ozone amount, ignition occurs at earlier crank angles and, accordingly, work output is increased and heat flux through the cylinder wall is reduced, as shown in figure 7.8. The exergetic efficiency hardly changes in this case.

In return, the inlet temperatures can be reduced from 595 K to 500 K ($\phi = 1$) and 805 K to 740 K ($\phi = 4$), as illustrated in figure 7.9. To achieve these temperature levels, the fuel-air mixture must be preheated, for example by using the thermal energy of the exhaust gas.

168
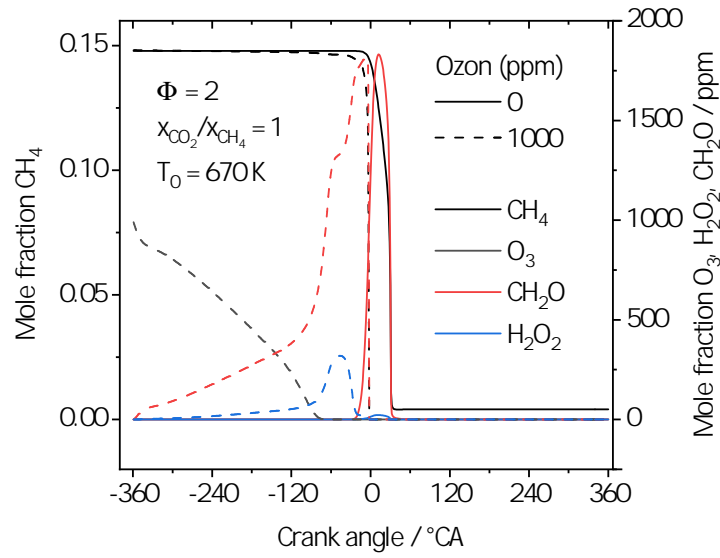
Figure 7.7: The mole fractions of methane, ozone, formaldehyde CH_2O, and hydrogen peroxide H_2O_2 as a function of crank angle for two cases: no ozone added (solid lines) and 1000 ppm ozone (dashed lines) at $\phi = 2$.
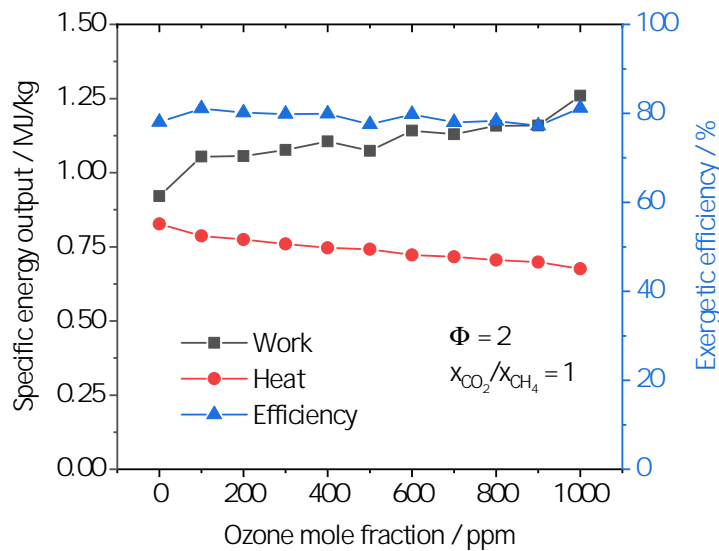
Figure 7.8: Work, heat, and exergetic efficiency as a function of ozone addition.
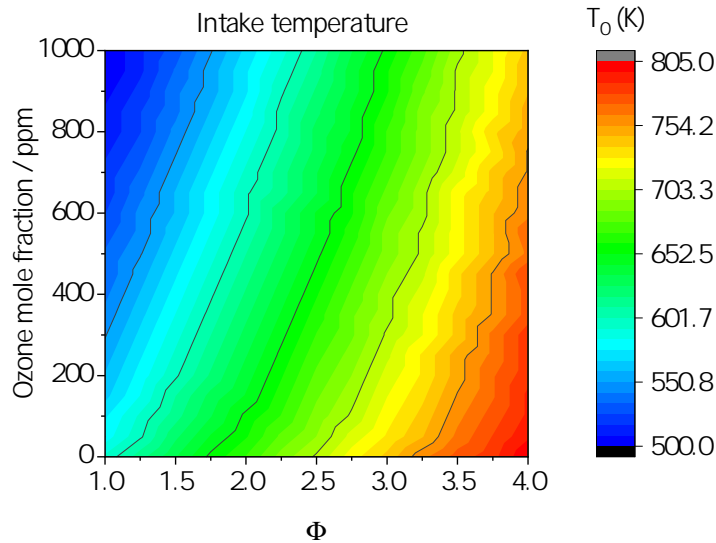
Figure 7.9: The influence of ozone addition on the required inlet temperature T_0 as a function of the equivalence ratio.

7.5 Conclusions

Biogases with high CO_2 contents can be used to produce synthesis gas in fuel-rich HCCI engines with high exergetic efficiencies of over 80 % in some cases. At high CO_2 contents in the biogas, the system can also be regarded as a CO_2 sink, at equivalence ratios of 1.5 and above. Since this leads to a large reduction in the work generated, it will be useful in practice to adjust the operating point to the demand via the equivalence ratio. Therefore, lower equivalence ratios should be selected when the demand for work output is high.

The most promising equivalence ratio range was found at $\phi = 2$-2.25 due to the high amounts of synthesis gas in the product gas and the high exergetic efficiency. The inlet temperatures required for ignition are very high and can be reduced to 570 K ($\phi = 2$) with the addition of 1000 ppm ozone at 50 % CO_2 in the biogas, which still requires a high energetic input to preheat the mixture. However, this could be accomplished by using parts of the thermal energy of the product gas.

If the use of ozone is exergetically and economically favorable must be shown in the future by an investigation of an overall process concept including separation processes for the synthesis gas and consideration of the energy input for ozone generation.

In practice, a combination of preheating and ozone addition will have to be used, especially for high CO_2 contents in the biogas, under the conditions investigated

here. An increase in inlet pressure and compression ratio is conceivable and is worth investigating in the future.

7.6 Acknowledgments

KINETIC AND EXERGETIC ANALYSIS OF ACETYLENE AND ETHYLENE PRODUCTION IN THE HCCI ENGINE

Introduction to the seventh paper

In chapter two, it was observed that the exergetic efficiency increases with the equivalence ratio, illustrated in fig. 2.8. This was explained by a higher conversion of the fuel to mainly synthesis gas, due to the reduced oxidizer availability for the reaction. However, a reasonable operation was limited to a maximum ϕ of 2.0, since soot formation strongly increased at those conditions [78].

Previous studies indicated that there is a high potential of very fuel-rich mixtures with equivalence ratios of six and higher. Atakan et al. [112] showed in 2020 that a significant increase of higher hydrocarbons such as acetylene and ethylene are possible and the findings were supported by shock tube, flow reactor, rapid compression machine, and engine data.

However, to achieve ignition in the HCCI engine at very fuel-rich conditions, diethyl ether (DEE) as a hydrocarbon additive was used, which provides significant exergy to the fuel-air mixture, as discussed in chapter four for DME and by Banke et al. in 2023 [70]. Therefore, the question remained if it is exergetically reasonable to operate the engine at very fuel-rich conditions. Consequently, in this chapter, the single-zone and the multi-zone model were utilized to investigate a wide range of equivalence ratios from 1.5 to 10. At those conditions, ignition timing, ozone amount, product selectivities, and exergetic efficiencies were investigated. The key contributions of this work to the state of the art can be summarized as follows:

– Ozone is a useful additive even in very fuel-rich regimes.

– Late ignition timing and equivalence ratios of 6 are favorable for ethylene production.

– A maximum ethylene selectivity of 45.5 % was found at the maximum equivalence ratio of 10.

– Exergetic efficiencies of up to 95.9 % are then possible, if unconverted fuel is further used.

– Acetylene production is overall negligible.

Author contributions to the seventh paper

Conceptualization, modelling, and data analysis as well as writing the first draft of the manuscript were my tasks. Burak Atakan supported me substantially by improving the quality of the analysis and revising the manuscript. He was also responsible for the acquisition of the funding and the supervision of the project.

Table 8.1: Author contributions for chapter 8 following the CRediT author statement methodology [41].

Author	Freund	Atakan
Conceptualization	✓	
Methodology	✓	
Software	✓	
Validation	✓	
Formal analysis	✓	
Investigation	✓	
Resources		✓
Data curation	✓	
Writing - Original draft	✓	
Writing - Review & editing		✓
Visualization	✓	
Supervision		✓
Project administration		✓
Funding acquisition		✓

8.1 Abstract

The production of synthesis gas, ethylene, and acetylene for the chemical industry is cost and energy intensive. The energy cost can be reduced if these basic chemicals are produced in fuel-rich HCCI engines with simultaneous heat and work production. Previous work has already shown experimentally that synthesis gas

production from methane at equivalence ratios of $\phi = 1.65$ to 2.0 is possible and exergetically advantageous. However, this requires reactive additives, such as ozone.

These studies are extended in this theoretical work to the range up to $\phi = 10$ and the use of natural gas to investigate the applicability of ozone at very fuel-rich conditions for ethylene and acetylene production.

For the analysis, we use single-zone and multi-zone models written in Python, with the *Cantera* module used to calculate the thermodynamics and reaction kinetics. The engine is simulated with a rotational speed of 600 1/min, a compression ratio of 22, an inlet temperature of 150 °C, an inlet pressure of 1 bar, and equivalence ratios of 1.5 to 10.

With increasing ϕ, 250 to 4000 ppm ozone is required for ignition ($\phi = 3\text{-}10$) and exergetic efficiencies of up to 93.4 % are achieved considering ozone production ($\phi = 10$). The selectivity of acetylene is low, reaching a maximum of 5.3 % at $\phi = 8.5$. The selectivity of ethylene, on the other hand, increases with increasing ϕ and reaches a promising value of 45.4 % at $\phi = 10$. At $\phi = 7$, either 2200 ppm ozone or an inlet temperature of 220 °C (+80 °C) are required.

In this comparison, the use of ozone lowers the maximum temperature of a working cycle by up to 71 °C, with the maximum pressure increasing by 15 bar to 94 bar. The selectivity of ethylene increases by about 2 %-pts., reaching a value of 27.4 % at a late ignition timing of 11 °CA. At the same time, 2 %-pts. less benzene is produced. Since benzene is known to be a soot precursor, ozone could thus reduce soot formation at equivalence ratios between 2 and 6 and slightly shift the soot formation limit.

Inhomogeneities in the cylinder are accounted for by simulations with the multi-zone model. Due to the lower temperatures near the cylinder wall, the fuel conversion lower which results in higher selectivities for ethylene and acetylene, but smaller selectivities for hydrogen.

It is found that ozone is a suitable additive in fuel-rich operation, reducing the exergetic efficiency of the system by less than 2 %-pts. and slightly increasing the product yields.

8.2   Introduction

The production of base chemicals for the chemical industry is cost- and energy-intensive, as the required processes are carried out at high temperatures and in several steps. In addition, fossil feedstocks such as crude oil and natural gas are mainly used. This is also the case for the production of synthesis gas, ethylene, and

acetylene.

Synthesis gas, as a mixture of hydrogen (H_2) and carbon monoxide (CO), is nowadays mostly produced by the endothermic steam reforming of natural gas at 750-900 °C [191]. It is an important feedstock for the chemical industry and is used, for instance, for the production of methanol.

Another important feedstock is ethylene (C_2H_4), which is mainly produced by the also endothermic cracking of naphtha at 750-900 °C [192]. Applications range from the production of plastics (including polyethylene, polystyrene, and polyvinyl chloride) to ethylene glycol and ethanol, with demand for ethylene increasing by up to 4.0 % annually according to Rossetti et al. (2019) [193].

Another base chemical, acetylene (C_2H_2), can be produced by the pyrolysis of natural gas or the autothermal reaction of natural gas/oxygen mixtures at more than 1,200 °C [194].

The energy input for the production of these base chemicals can be reduced if natural gas is converted by partial oxidation in reciprocating engines. Instead of the necessary heat input, heat and work can then be dissipated and utilized. Very fuel-rich operated HCCI engines are suitable for this purpose, as previous work has shown.

In 2017, Hegner et al. investigated the partial oxidation of methane in a single-zone engine model, as well as with a rapid compression machine (RCM) at equivalence ratios of 0.5 to 15 [47]. They showed that high amounts of synthesis gas are produced at equivalence ratios of 2 to 3, while low amounts of ethylene and acetylene are produced at equivalence ratios of 6, increasing with ϕ.

In 2019, Banke et al. operated an HCCI engine with a methane/DME/air mixture at $\phi = 1.65$ to 2.34 and obtained high selectivities for H_2 and CO of up to 72 % and 79 %, respectively [78].

Due to the simultaneous output of work, heat, and base chemicals, depending on the equivalence ratio (ϕ), the operation of such an engine can be flexibly adapted to the demand. However, due to the high octane number of methane-containing fuels, either very high inlet temperatures or large amounts of reactive additives such as dimethyl ether, diethyl ether, or n-heptane must be added in this case, as previously shown by Wiemann et al [30] and Banke et al [78]. In this process, the hydrocarbon containing additives contribute up to one fifth of the added exergy, which is undesirable since the additives in turn have to be produced in an energy-intensive way. Moreover, in DME production synthesis gas, a product of the polygeneration, is used as a feedstock.

Ozone represents a possible alternative as an additive, since it is only required

in small quantities and can be produced from ambient air. The benefits of ozone as an additive in SI engines have been known since the 1980s [104]. Moreover, for more than a decade, the positive influence of ozone on combustion and control has been investigated for fuel-lean HCCI engines, since the control of the combustion phasing is a major challenge due to the absence of fuel injection or spark plugs.

In 2005, Yamada et al. [82, 195] studied the combustion of DME in a single-cylinder HCCI engine using methanol and ozone as an additive. The fuel-air mixture was preheated to 400 K, and at an equivalence ratio of $\phi = 0.37$, an addition of 6750 ppm ozone resulted in a shift of the combustion phasing by about 20 °CA.

In 2006, Nishida et al. [71] investigated numerically and experimentally the influence of different ozone additions (600, 700 and 1200 ppm) on the combustion of natural gas in an HCCI engine at $\phi = 0.5$. It was shown that operation is possible with an ozone addition of 600 ppm and the combustion phasing could be further shifted to 30 °CA earlier by an increase of 100 ppm.

Similar results were found by Masurier et al. [89], who studied the combustion of a methane/propane mixture and various methane/hydrogen mixtures at $\phi = 0.4$ and an ozone addition of up to 120 ppm. Even small amounts of ozone (up to 23 ppm) led to a significant increase in pressure and temperature in the cylinder and the combustion phasing shifted toward top dead center. This had a positive effect on the stability of the combustion. Here, the inlet temperature was 495 K. The authors explained this behavior by the decomposition of ozone at already low temperatures to oxygen radicals and oxygen molecules, so that the fuel reacts directly with the oxygen radicals.

Starik et al. [188] also found in 2017 that the energy required to generate ozone in the ozone generator when burning synthesis gas in an HCCI engine is about an order of magnitude smaller than the additional energy released by the more reactive mixture.

Schröder et al. showed in 2020 [105] that larger amounts of DME, which were used by Banke et al. [78] in 2019, can be substituted by small amounts of ozone ($\phi = 1.9$). Based on these results, this work extends the investigated equivalence ratio range to up to $\phi = 10$ to theoretically investigate the applicability of ozone as the sole additive in very fuel-rich conditions and for ethylene and acetylene production.

8.3 Engine model

The HCCI engine is modeled in Python and the thermodynamics and reaction kinetics are calculated using the *Cantera* module [50]. In this work, a zero-dimensional
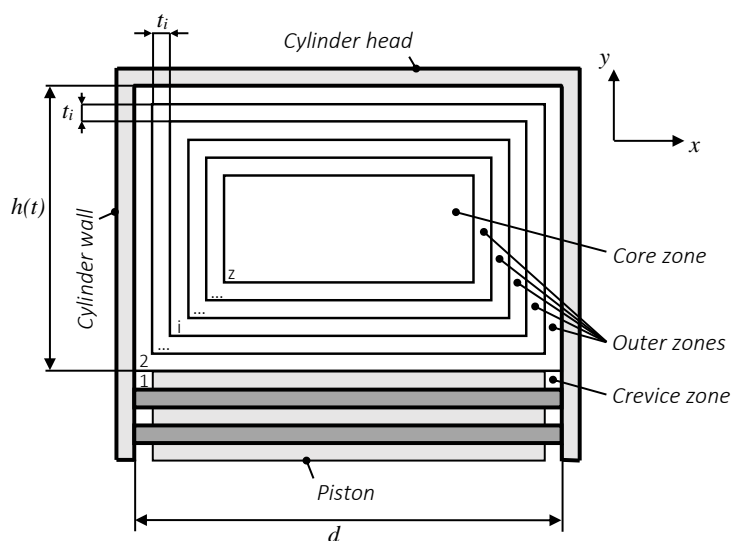
Figure 8.1: Division of the cylinder geometry at top dead center into z zones with a zone thickness t_i. Zone 1: crevice zone, in which no reactions take place, Zone 2: outer zone, which is in contact with the inner wall of the cylinder.

single-zone model (SZM) with four cycles and a multi-zone model (MZM) with two cycles and seven zones are used. A homogeneous distribution of the gas is assumed in each zone.

The multi-zone model was validated using our own measurements with methane/ DME/air mixtures at $\phi = 1.9$ from [78], using a zone distribution that resulted in good agreement between the simulated fuel conversion, mechanical power, and heat flow and the experimental data. At top dead center (TDC), the core zone and the crevice zone are set at 30 % and 1.5 % of the dead volume, respectively. The remaining volume is distributed among the five other zones so that the volume decreases from the inner to the outermost zone. The radial geometry of the zones is fixed and can only be changed in the direction of piston movement by changing the volume of the cylinder in the axial direction. The division of the cylinder into z zones is shown schematically in figure 8.1.

For the global heat transfer of the single zone model, the Woschni equation [58] is used to calculate the internal heat transfer coefficient. The parameters of the Woschni equation were previously validated for the experimental study of methane/DME/ozone/air mixtures [78]. For the multi-zone model, the global heat transfer from the crevice zone and the outer zone to the inner cylinder wall is calculated using the equation of Chang et al. [60]. This is based on the Woschni equation and was adapted based on experimental studies for HCCI engines. Fur-

Table 8.2: Engine properties and operating conditions.

Description	Symbol	Value	Unit
Rotational speed	rpm	600	1/min
Compression ratio	r_c	22	
Bore	d	65	mm
Stroke	s	100	mm
Number of cylinders	Z	4	
Displacement	D	1.327	dm^3
Equivalence ratio	ϕ	1.5-10.0	
Intake temperature	T_{in}	50-300	°C
Intake pressure	p_{in}	1	bar
Coolant temperature	T_c	100	°C
Thermal conductivity wall	λ_w	53	W/m^2/K
Convection coefficient coolant	α_c	3000	W/m^2/K
Inlet valve opening, SZM	-	-180/-135	°CA
Outlet valve opening, SZM	-	150/360	°CA

thermore, heat and mass are transferred between the zones. Heat is transferred by conduction, using the model of Komninos et al. [61]. Mass transfer is modeled by valves which ensure a homogeneous pressure in all zones, with zone volumes changing during the engine cycle.

In this work, a representative natural gas consisting of 90 % methane (CH_4), 9 % ethane (C_2H_6) and 1 % propane (C_3H_8) is used as fuel. To calculate the chemical kinetics of natural gas and ozone (O_3), the reaction mechanism PolyMech 2.0 [107] is used for C1-C3 species and extended by the sub-mechanism of Zhao et al. [96] for ozone kinetics.

For the multi-zone model, the reaction mechanism of Burke et al. [73] is used instead of the PolyMech, since the PolyMech in this version leads to convergence problems in combination with multiple zones and valves in *Cantera*. The engine characteristics and operating conditions are shown in table 8.2.

The engine geometry corresponds to the single-cylinder engine used in the work of Banke et al. [78], although four identical cylinders were simulated for this work. The fuel-air equivalence ratio is investigated in a range from 1.5 to 10. Due to the high equivalence ratios and the associated low ignition capability of the mixture, a high compression ratio of 22 and a low rotational speed of 600 1/min are chosen. The exergetic efficiency ε^A is calculated using equation (8.1).

$$\varepsilon^A = 1 - \frac{\dot{E}_L}{\dot{E}_{in}} \tag{8.1}$$

The exergy loss flow $\dot{E}_L$ is calculated via the Gouy-Stodola theorem and $\dot{E}_{in}$ is

the exergy flow of the fuel/air/ozone mixture at the inlet of the engine. It should be noted here that the lower the fuel conversion, the greater the exergetic efficiency, theoretically reaching a value of one in the limiting case of no conversion. For obtaining an estimate of the influence of the conversion, especially at high equivalence ratios, a second definition is introduced (8.2).

$$\varepsilon^B = \frac{\sum \dot{E}^{ch}_{products} + P + \dot{E}_Q}{\dot{E}_{in}} \tag{8.2}$$

Here, the exergetic efficiency ε^B is calculated with the useful products of the HCCI engine: the mechanical power P, the exergy flow of heat to the cooling water $\dot{E}_Q$, and the chemical exergy flows of the chemical products $\dot{E}^{ch}_{products}$. In this work, the species H_2, CO, C_2H_2, C_2H_4, and C_6H_6 are defined as useful chemical products. Both definitions are used and compared for the evaluation of the polygeneration process.

8.4 Results and discussion

To ignite natural gas at fuel-rich conditions in the HCCI engine either high inlet temperatures and/or the addition of reactive additives, like ozone in this study, is required. This raises the question of the influence of the inlet temperature and the low-temperature kinetics of ozone on the selectivity of the chemical products.

To investigate this, the inlet temperature is varied from 200 °C to 300 °C at a fixed ϕ of 7, using no ozone. For comparison, at an inlet temperature of 150 °C, the ozone addition is varied from 1500 ppm to 3000 ppm, and the results are presented as a function of the combustion phasing (CA50). An equivalence ratio of $\phi = 7$ is suitable for this purpose, since on the one hand high product yields and on the other hand low soot formation can be expected [47].

Subsequently, the selectivities of the chemical products and the exergetic efficiencies of the polygeneration process are investigated and compared as a function of the equivalence ratio from 1.5 to 10.0. For these results, an inlet temperature of 150 °C is chosen and a combustion phasing of 4 °CA (±1) is set with the help of adjusting the ozone amount.

Influence of the ignition timing

Figure 8.2 shows the temperature and pressure curves for $\phi = 7$ and different inlet temperatures and ozone amounts for the single-zone model. The black curves represent the conditions at which the mixture does not ignite. For the comparison
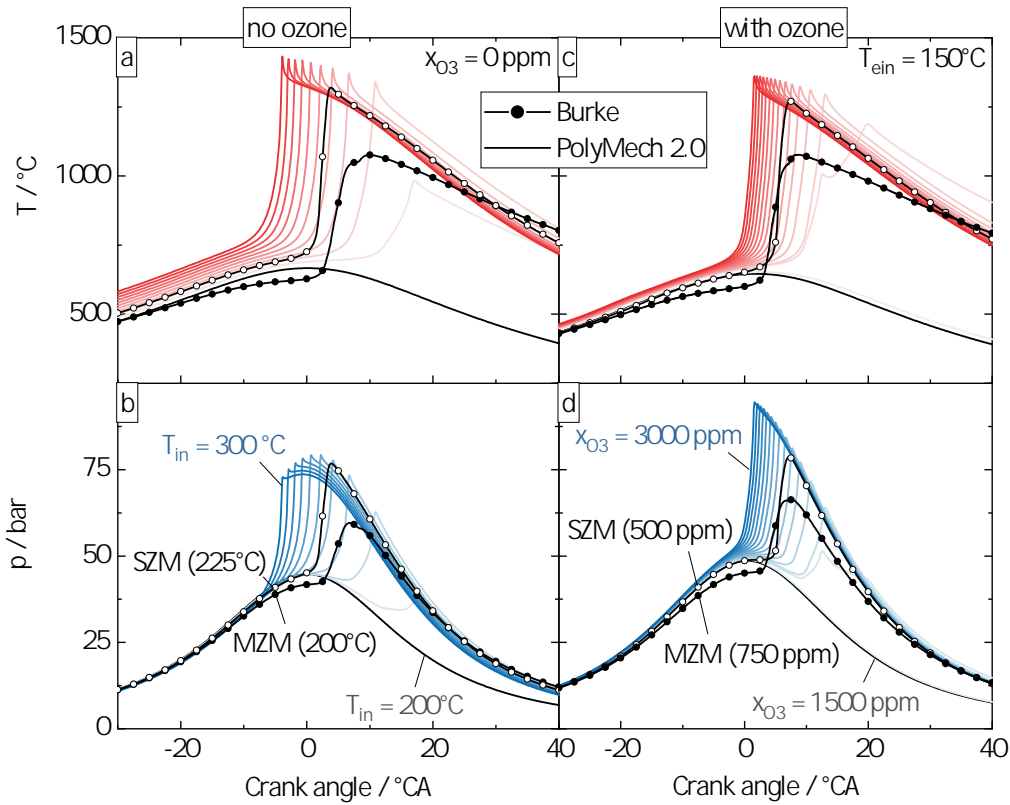
Figure 8.2: (a) and (b): Temperature and pressure curves when inlet temperature is varied from 200 °C to 300 °C with a step size of 10 °C without ozone. (c) and (d): Variation of ozone content from 1500 ppm to 3000 ppm at an inlet temperature of 150 °C. The black curves are conditions where the mixture does not ignite. The gradients are averaged over four cycles. An inlet temperature of 200 °C (a and b) and an ozone fraction of 750 ppm were used for the multi-zone model results (c and d).

between the single-zone model and the multi-zone model, the Burke mechanism for one operating point is also used for the single-zone model. For this comparison, an exemplary result of the single-zone model and the multi-zone model is shown as a line with symbols in each case. The temperature curves of the multi-zone model are mass-weighted values for all seven zones.

In general, if the inlet temperature and the ozone amounts are varied, the combustion phasing can be shifted over a wide range. For the case without ozone, it is shifted between 4.5 and 13.0 °CA. With ozone it is shifted between 0.6 and 11.0 °CA and the maximum temperature of 1433 °C is up to 71 °C higher than in the case with ozone. On the contrary, in the case with ozone, the maximum pressures are
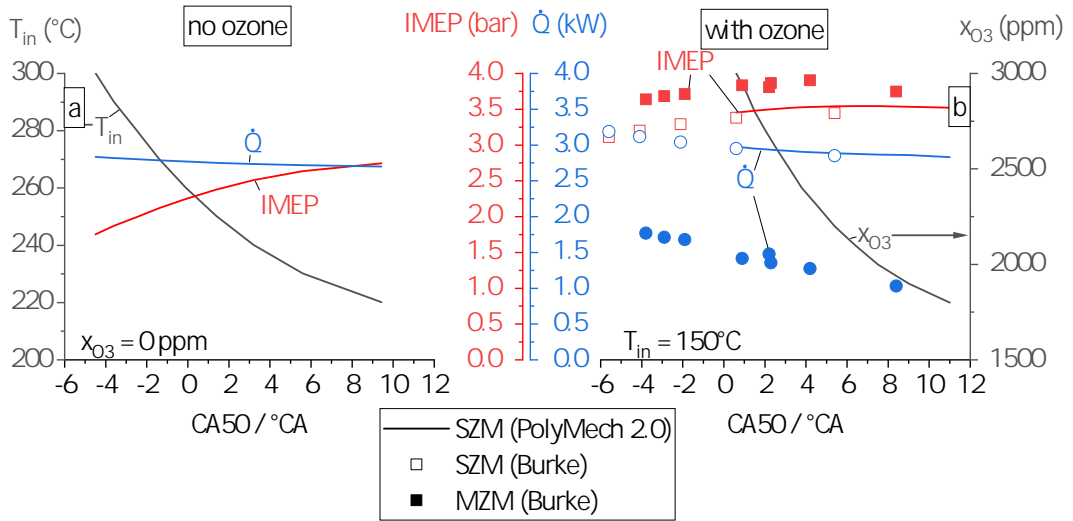
Figure 8.3: Heat flow $\dot{Q}$ and indicated mean pressure (IMEP) as a function of combustion phasing CA50. (a) Variation of inlet temperature from 200 °C to 300 °C, without using ozone. (b) Variation of ozone amount in the mixture from 1500 ppm to 3000 ppm. Symbols represent single-zone and multi-zone model calculations using the Burke mechanism. Operating points without ignition or with unstable ignition are not shown.

significantly higher: values of up to 94 bar instead of 79 bar (-15 bar) are reached.

If the Burke mechanism is used, the single zone model requires about 1700 ppm (77.1 %) less ozone or 20 °C (8.2 %) lower inlet temperatures. This is particularly because the Burke mechanism in combination with the Zhao sub-mechanism overestimates the reactivity of the mixture, as described by Zhao et al. [96].

The overall temperature and pressure profiles calculated with the multi-zone model are slightly lower than with the single-zone model. The maximum temperature at an ozone quantity of 750 ppm reaches a value of 1067 °C and is thus up to 202 °C lower than in the single-zone model. Similarly, the maximum pressure of 66 bar is reduced by 22 bar. In the case without ozone, the result is comparable. The differences between the results of the two models can be explained by the reactions in the multi-zone model which take place at different times in the individual zones and thus heat is transferred over a longer period.

Based on these calculations, figure 8.3 shows the heat flows and mechanical power output of the engine as a function of the combustion phasing.

The influence of the ignition timing on the heat flow is small. With a later ignition timing, less heat is transferred, since the mean temperature difference for

heat transfer is lower with a later ignition. However, the influence of ozone on the heat output is negligible.

A significant difference can be seen in the mechanical power output. For the case without ozone, an IMEP of 1.75 bar is achieved at $T_{in} = 300$ °C and an early combustion phasing of -5.5 °CA. The IMEP is increasing degressively up to 2.75 bar (at 9.4 °CA and $T_{in} = 220$ °C). The case with ozone at a constant inlet temperature of 150 °C does not show such a strong influence of the ignition timing. However, much higher values of 3.45 bar to 3.54 bar are generally achieved, with a weak maximum at about 5 °CA.

The comparison between Burke and PolyMech for the single-zone model yields similar results. Most noticeably, the Burke mechanism shifts the combustion phase to earlier crank angles. In contrast, the multi-zone model predicts higher mean pressures and lower heat flows. This is an indication that the heat transfer model for natural gas/ozone/air mixtures should be validated with experimental data and possibly adjusted. The parameters of the multi-zone model used here were validated with data from methane/DME/air experiments taken from Banke et al. [78].

The strong IMEP influence in the case without ozone is due to the increasing inlet temperature which reduces the mass in the cylinder and therefore also reduces the mechanical power output. Consequently, the use of ozone can lower the inlet temperature and increase the mechanical power output.

In the following, the influence of the combustion phasing on fuel conversion and product selectivity is investigated, to find favorable operation conditions for the HCCI engine. Therefore, the conversion of methane, ethane, and propane for the case without and with ozone is compared in figure 8.4.

The influence of the combustion phasing is moderate and early ignition slightly favors methane conversion due to longer reaction times. With ignition around top dead center, a methane conversion of 40 % is achieved, although with the use of ozone and a lower inlet temperature, the conversion is about 5 %-pts. lower. At a later ignition timing of about 10 °CA, the methane conversion is further reduced to 32 % and 29 %, respectively. In turn, ethane conversion increases slightly to 94 %, while propane conversion remains consistently high at 98 %. The multi-zone model shows the same trends, but with slightly reduced conversions overall due to the cooler zones near the wall.

The reason for the higher ethane conversion at later ignition times is that ethane is formed again in small quantities after ignition. Here, acetylene is converted to ethylene via reactions with hydrogen and methyl radicals, which further reacts with hydrogen atoms to form ethane. Ethane is converted again under these conditions,
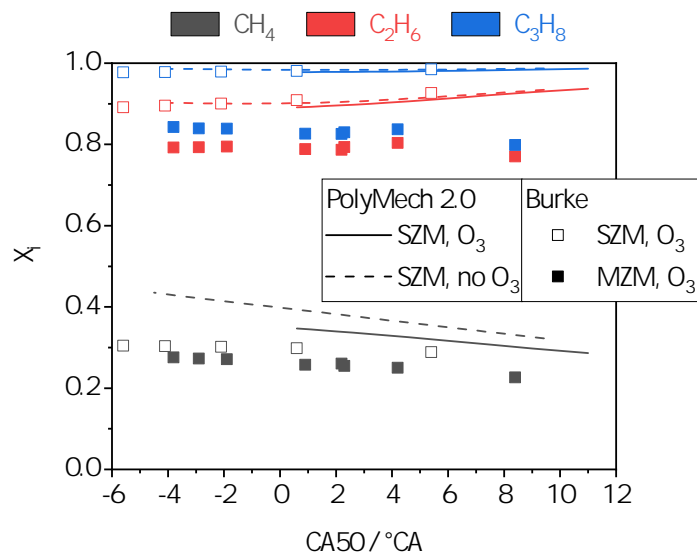
Figure 8.4: Fuel conversion as a function of the combustion phasing (CA50). Symbols represent single-zone and multi-zone model calculations with the Burke mechanism.

but the reaction rate of ethane degradation is lower than that of ethane formation. With later ignition and thus lower temperatures, acetylene and ethylene are converted more slowly and ethane is formed. This also has an influence on the selectivity of acetylene and ethylene. Figure 8.5 illustrates the dependence of the selectivities of the chemical products on the CA50.

It is found that early ignition improves the selectivity of hydrogen; from 35.6 % to 42.9 % in the case with ozone. Without ozone and thus at higher intake temperatures, the selectivity is higher by additional 4 %-pts. Contrarily, the selectivities of carbon monoxide, acetylene, and ethylene are slightly higher when ozone is used. The use of ozone is therefore advantageous for the formation of ethylene and selectivities of 20.3 % (CA50 = 0.6 °CA) to 27.4 % (CA50 = 11 °CA) are achieved.

Therefore, if a large synthesis gas yield with a high hydrogen content is required, ignition should take place at top dead center, while for the production of ethylene the latest possible ignition time is advantageous. However, the slightly reduced fuel conversion must be taken into account. It must also be noted that the selectivity of benzene is reduced at later ignition timings or when ozone is used. Since benzene is a known precursor of soot formation, presumably less soot is produced at those conditions and ozone could potentially shift the soot threshold to lower equivalence ratios.

The trends of the selectivities for CO, CO_2, and H_2O can be reproduced with
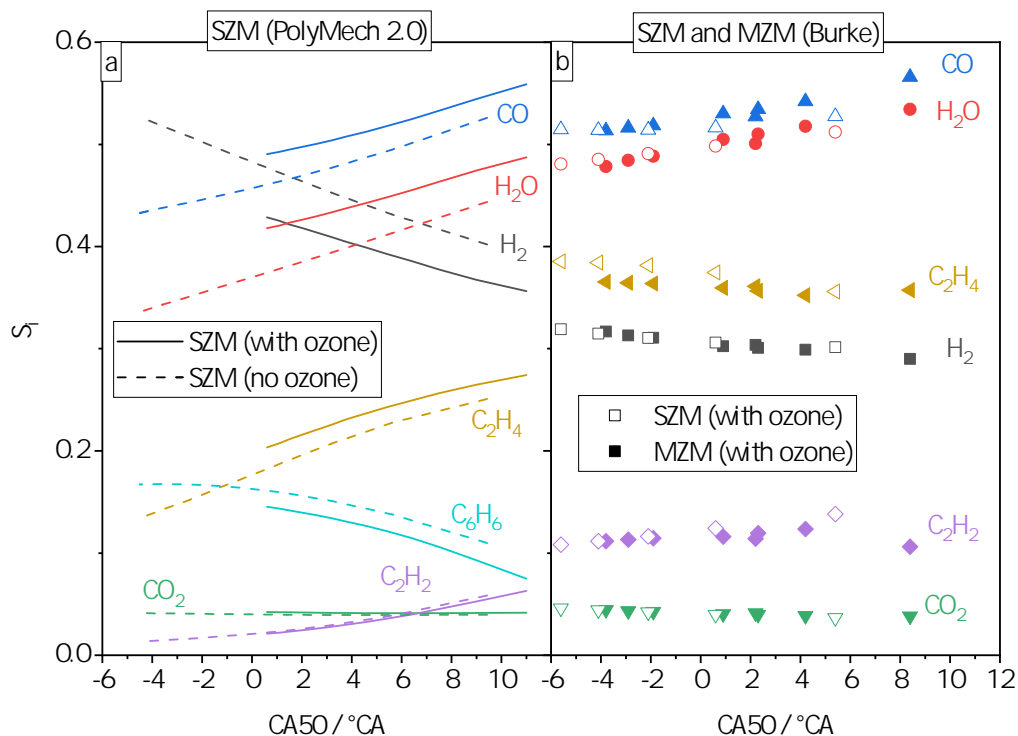
Figure 8.5: Selectivity of the main species in the product gas of the HCCI engine as a function of the combustion phasing (CA50). (a) Calculations with the single-zone model and PolyMech 2.0 for the conditions with and without ozone. (b) Calculations with the single-zone and multi-zone model with the Burke mechanism for the conditions with ozone.

the single-zone and multi-zone models if the Burke mechanism is used. In addition, the selectivities of all species are nearly identical for both engine models. However, it can be seen that the Burke mechanism generally predicts higher acetylene and ethylene selectivities and their dependencies on the CA50 is negligible. It must be noted here that the Burke mechanism, in contrast to the PolyMech, is only validated up to $\phi = 2$.

In the following, the influence of the equivalence ratio on the selectivities of the chemical products and on the exergetic efficiency of the entire process is considered and discussed by using the single-zone model. The CA50 is set to 4 °CA (± 1).

Influence of the equivalence ratio

Dependend on the equivalence ratio, high selectivities of synthesis gas, but also of ethylene, can be achieved, as shown in figure 8.6.
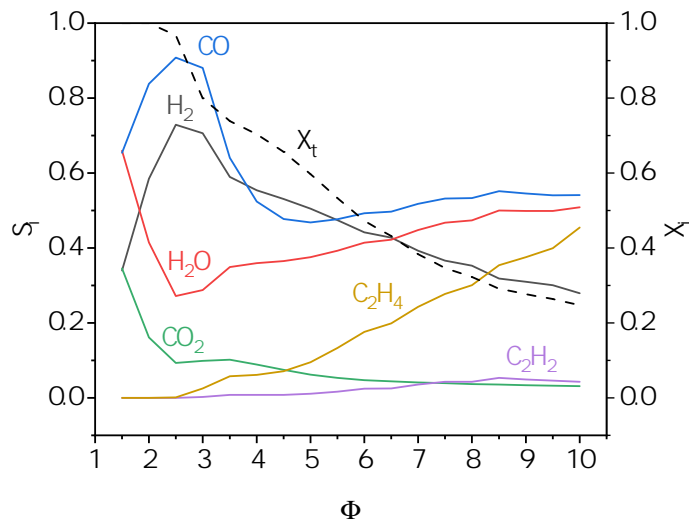
Figure 8.6: Selectivities of the main species in the product gas of the HCCI engine and natural gas conversion as a function of the equivalence ratio.

At an equivalence ratio of 2.5, a maximum selectivity of 90.7 % for CO and 72.9 % for H_2 is achieved. The remaining carbon and hydrogen atoms of the converted natural gas are then completely bound in CO_2 (9.3 %) and H_2O (27.1 %). As the equivalence ratio increases and the maximum temperatures during combustion decrease, the selectivities of the synthesis gas decrease, whereas those of water, acetylene, and ethylene increase. The selectivity of CO passes through a local minimum of 46.8 % at $\phi = 5$. The values for acetylene reach a weak maximum of 5.3 % at $\phi = 8.5$. At $\phi = 10$, the selectivities for CO and H_2 are still 54.1 % and 27.9 %, respectively. In contrast, the selectivity of ethylene increases strongly and reaches a value of 45.4 %.

If the specific chemical exergy of the products is considered, the exergy flows of all products and the exergy losses can be compared as a function of equivalence ratio, as illustrated in figure 8.7. Subsequently, figure 8.8 shows the exergetic efficiency of the polygeneration process and the total fuel conversion for those data points.

The highest absolute values of 10.1 kW and 13.2 kW for the exergy flows of CO and H_2 are found at $\phi = 2.5$. This leads to relative values of 29.2 % and 38.5 %, respectively. As the equivalence ratio increases, the exergy flows for the synthesis gas decrease and the exergy flow for ethylene increases. From $\phi = 7.2$, the exergy flow for ethylene is larger than for H_2 or CO, despite the lower selectivity. At $\phi = 10$, the value for ethylene reaches 8.2 kW, which is similar to that for CO and H_2 at $\phi = 2$. The relative exergy of ethylene reaches 9.4 % here, whereas methane accounts for
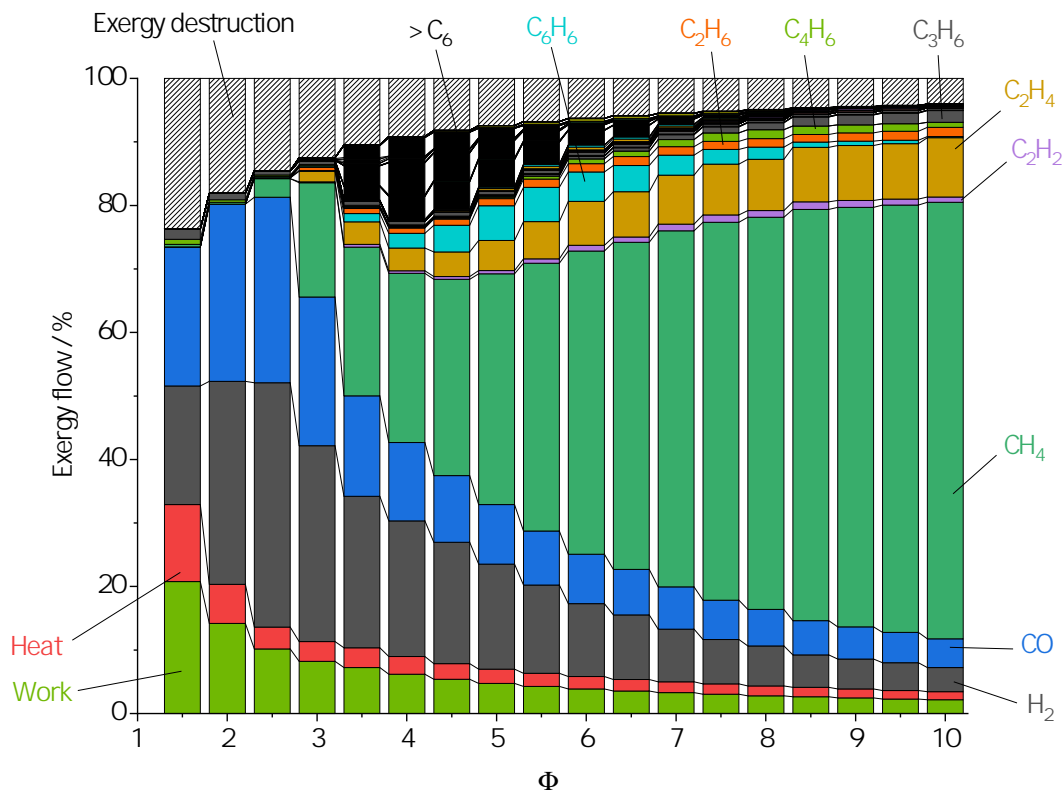
Figure 8.7: Normalized exiting exergy flows of the HCCI engine as a function of the equivalence ratio.

68.7 % due to the low conversion.

In the range from $\phi = 3$-8.5, an increased benzene exergy flow is noticable, with a maximum value of 3.3 kW, or 5.4 %, at $\phi = 5.5$. In addition, species with more than six carbon atoms are increasingly formed (shown in black in figure 8.7). Due to the formation of these long-chain hydrocarbons and the fact that benzene is considered an important precursor of soot formation, soot formation in this region is expected. Experimental work by Hegner et al. [47] and Banke et al. [78] shows for other mixtures that soot is formed between $\phi = 2$ and $\phi = 6$ and therefore supports this assumption.

The power output of the HCCI engine shows a maximum value of 7.0 kW, or 20.8 %, at $\phi = 1.5$, which is the lower limit of the investigated equivalence ratio range. However, from $\phi = 2.5$ and a power of 5.3 kW, the value decreases only weakly; to a minimum value of 2.9 kW and 2.2 % at $\phi = 10.0$. It is thus possible to produce significant mechanical power when the engine is operated at very fuel-rich
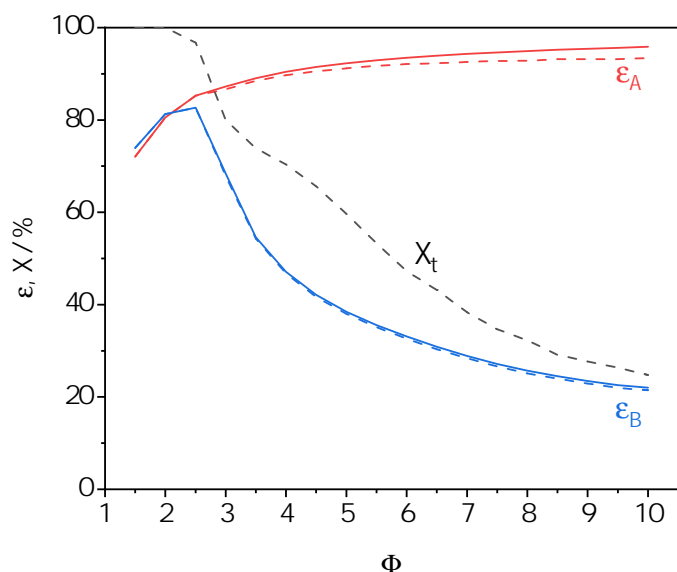
Figure 8.8: Exergetic efficiencies and methane conversion as a function of the equivalence ratio.

conditions. Moreover, exergy flow of at $\phi = 10.0$ is comparable to that of synthesis gas at $\phi = 2.0$.

Based on these results, figure 8.8 illustrates the influence of the equivalence ratio on the exergetic efficiency of the process. With increasing equivalence ratio, the efficiency ε^A (red line) first increases strongly, then degressively. At $\phi = 1.5$, a value of 72.1 % is reached, whereas at the maximum synthesis gas production at $\phi = 2.5$, a significantly higher efficiency of 85.2 % is achieved. The maximum of 95.9 % is obtained at the highest equivalence ratio of 10. The dashed line indicates the total efficiency when ozone production by the ozone generator is taken into account. In this case, the exergetic efficiency is reduced by only about 2 %-pts.

If only the directly usable products are considered for the exergetic efficiency ε^B (blue line), the efficiency is reduced considerably because of the decreasing fuel conversion with increasing equivalence ratio. The methane conversion decreases from 100 % at $\phi = 1.5$ to a low 16.8 % at $\phi = 10$. This reduces the exergetic efficiency to a minimum value of 21.6 % at $\phi = 10$. The influence of ozone production is negligible here.

Consequently, if HCCI engines are used for the simultaneous production of synthesis gas and ethylene it is crucial that unconverted fuel is further utilized to achieve the highest possible efficiencies. This could, for instance, be done in a second HCCI

engine which is operated at a lower equivalence ratio of 1.5 to 2.0.

8.5 Conclusions and outlook

The production of synthesis gas, ethylene, and acetylene by the partial oxidation of natural gas in HCCI engines was studied theoretically, favorable operating points were found, and the exergetic efficiency of the process was evaluated.

Ozone helps to lower the inlet temperature by up to 71 °C. Moreover, the maximum pressure in the cylinder drops by 15 bar to 79 bar at $\phi = 7$. Due to the lower temperature less benzene is produced but also less hydrogen. Instead, more ethylene and carbon monoxide are produced. If the engine is operated close to the soot limit ($\phi = 6$) and high ethylene production is desired, the ignition timing should be set as late as possible.

Synthesis gas production is most promising at $\phi = 2.5$, however, experimental work has shown that soot formation starts at $\phi = 2.0$. Maximum ethylene production can be achieved at the largest equivalence ratio studied here of $\phi = 10$, with a selectivity of 45.5 %, but with moderate methane conversion. Acetylene is produced in only negligible amounts and thus it is not a useful product under the conditions studied here.

The exergetic efficiency of the polygeneration is highest at $\phi = 10$ and reaches a value of 95.9 %. However, if the unconverted fuel and unused species in the product gas are considered exergy loss, the efficiency is only 21.6 % due to the reduced conversion. It is therefore crucial that unconverted fuel is further used. HCCI engines, which are operated at lower equivalence ratios ($\phi = 1.5$ to 2.0), might be suitable for this purpose. An optimal operation of two differently operated, connected HCCI engines should be investigated in the future. Furthermore, an experimental validation of the results presented should be conducted.

8.6 Acknowledgments

_____

CONCLUSIONS AND OUTLOOK

9.1 Conclusions

Kinetic and exergetic analysis for finding suitable operating conditions

In the first part of this thesis the suitablity of HCCI engines for fuel-rich partial oxidation of methane containing fuels is proven. Single-zone and multi-zone model simulations, complemented by experiments perfomed by Kai Banke, showed that polygeneration of work, heat, and synthesis gas is feasible in a wide range of equivalence ratios, namely from 1.2 to 2.8.

Furthermore, reactive additives are easily implemented, enable precise control of the ignition timing, and reduce the requirement of high intake temperatures. DME, DEE, n-heptane, and ozone were found to be suitable additives. Furthermore, the effect of additive choice on product yield is negligible. Therefore, there is no favor for one additive to shift the products into a desired direction. However, ozone was the most effective additive in terms of required amount and thus exergy fraction in the intake gas mixture. For instance, the DME energy fraction was about 21 %, whereas the ozone energy fraction was 0.2 %.

There are three main reasons why ozone is superior to hydrocarbon additives: the fast and complete decomposition at low temperatures and thus early crank angles, a negligible change in the heat capacity of the gas mixture, and the formation of the intermediate methyl hydroperoxide (CH_3OOH), which leads to additional OH radical formation and facilitates ignition. Another advantage of ozone is the possibility of on-demand production from ambient air; in the lab and on-site in an industrial application.

For synthesis gas production equivalence ratios from 1.5 to 2.0 are reasonable and high exergetic efficiencies of up to 82 % were found in the model and the experiment. Compared to the efficiency of steam reforming (63 %) and cogeneration of heat and power (47 %), polygeneration in HCCI engines has the potential to increase flexibility and efficiency of conventional energy and chemical conversion systems.

A direct comparison between DME and ozone showed a strong influence of the additive choice on the exergetic efficiency. In this thesis, data from commercially available devices was used to model the ozone generator and for DME a biomass gasification plant from literature was taken for comparison. The exergetic analysis

revealed a poor efficiency of the ozone generation of 5 %, whereas DME reached 43.5 %. Nevertheless, the low ozone amounts proved to be more important for the overall efficiency. Without taking additive production into account, the efficiency ranged from 80 % to 88 % at equivalence ratios of 1.5 to 2.5. With the ozone generator efficiency considered, the efficiency dropped by 3 %-points to a range of 80 % to 85 %, whereas DME reduced the efficiency strongly to a range of 62 % to 69 %.

With a further increase in the equivalence ratio, exergy destruction decreases, but conversion is also significantly reduced. Consequently, unconverted fuel should always be recycled and, for instance, used for driving a second, fuel-leaner engine. Moreover, the multi-zone model predicted significantly lower conversion than the single-zone model and thus the exergetic efficiency decreases even more, if the unconverted fuel is not recycled. The equivalence ratio range of 2.0 to 6.0 should be avoided due to excessive soot formation, which was detected in the experiment and predicted in the simulation by increasing chemical exergy shares of species with six or more carbon atoms in the product gas.

Exergoeconomic evaluation of simultaneous work, heat, and hydrogen production

The investigated polygeneration process is only reasonable if valuable, neat chemical products with desired purity are provided at competitive costs. Therefore, a major part of this thesis deals with the design of complete process concepts including enrichement and seperation of hydrogen as a chosen target species and evaluating the system with an exergeconomic approach.

Before separation, the water-gas shift reaction increased the hydrogen amount for the sake of CO conversion to CO_2. To separate hydrogen from the engine's exhaust gas mixture, a palladium membrane and a pressure swing adsorption process were compared.

The exergoeconomic analysis revealed that the highest exergy destruction occurs in the HCCI engine due to the entropy production by chemical reactions and by partially converting chemical exergy to exergy of heat, which is significantly less valuable. However, the costs associated with this exergy destruction did not dominate the product costs or the overall costs of the systems. Although the total costs of the engine were the second most important one, the separation costs were always more important and significantly higher.

The global sensitivity analysis revealed a high influence of interest rate, life

time, operating hours, and fuel costs on all product costs, whereas fuel costs were especially important for the electricity costs. The influence of the investment costs of the engine on the product costs is small, which supports the hypothesis that engines are well suited for polygeneration since they are cheap and industrially approved. The investment costs of the PSA and the membrane influenced mainly the specific hydrogen costs. Eventually, pressure swing adsorption is preferable to membranes despite its slightly higher investment costs, since it yielded the highest exergetic efficiency and lowest product costs.

Efficiencies of up to 68 % could be achieved with the PSA, whereas the membrane performed worse with values around 57 %. The main reason lies in the different working principles of both technologies. The pressure swing adsorption requires ambient temperatures and medium to high pressures at the feed, which leads to additional effort for compressing and cooling the engine's product gas mixture. Nevertheless, the product stream, here hydrogen, is produced at the feed pressure, which helps providing hydrogen in tanks at pressures of 50 bar, and the off-gas is released at ambient conditions. The membrane needs even higher pressure differences and favors high feed temperatures, but hydrogen permeates at a low pressure which results in higher efforts for compression and cooling before and after separation; compared to the PSA.

Since PSA is an industrially approved, large-scale technology, it can be concluded that today it is probably the most economic and efficient technology for separating hydrogen from the gaseous products of the HCCI engine.

Finally, the product costs were evaluated and compared to conventional and renewable energy systems, considering the uncertainty of the economic input values by performing a global sensitivity analysis. The model predicted electricity costs of 44.2 €/MWh to 97.6 €/MWh for cost data from 2021 and PSA separation. The process is thus competitive with all major conventional and renewable energy systems that typically provide electricity only, namely onshore wind, photovoltaic, and coal and gas power plants, which provide electricity at a cost range of 37 €/MWh to 150 €/MWh.

With regard to hydrogen costs, the conclusions are not as clear as for electricity. The hydrogen price per kg was found in a range of 2.7 €/kg to 7.2 €/kg. This makes it competitive with electrolysis, which is powered by electricity from renewable energy sources. However, steam reforming is still cheaper with 1.0 to 3.0 €/kg. A further increase of the engine size, which was 124.8 liters in this study, is assumed to decrease the hydrogen productions costs more and benefit from scale-up effects. If this were the case, the engine size would exceed the usual size of a cogeneration gas

engine and therefore require newly developed engines instead of simple modifications of conventional engines.

A view on the broader picture and alternative perspectives

This thesis confirms the economic operation of HCCI engines for polygeneration of work, heat, and hydrogen at equivalence ratios of 1.5 to 2.0. Furthermore, the flexibility of switching between high chemical output or high heat and work output by changing the equivalence ratio to match the demand is a unique and promising feature. In terms of the increasing volatility of energy supply due to renewable energy systems, this is a key advantage over conventional processes, such as steam reforming.

Switching to valuable hydrocarbon products like ethylene by increasing the equivalence ratio to 6 and higher seems feasible and also exergetically reasonable. However, switching from one chemical to another in a single process would require two different separation technologies and thus increase the products costs significantly. It is doubtful that building a polygeneration system which provides work, heat, synthesis gas, and ethylene, by changing the equivalence ratio is economically reasonable to date.

A promising potential for polygeneration was found using biogas with CO_2 fractions of up to 50 % and operable conditions were found. At an equivalence ratio of 2.3, 51 % of the CO_2 could be converted, mainly to CO, and therefore provide a measure for reducing CO_2 emissions and operating the engine almost CO_2-neutral. In return, however, the power output and efficiency were reduced by 42 % and 9 %-points, respectively. The maximum efficiency with 50 % CO_2 content in the biogas was 78.1 %, without product separation.

9.2 Limitations and future perspectives

The engine results presented in this thesis are supported by experiments. Furthermore, detailed reaction mechanisms were used, which were developed specifically for the engine conditions studied. Nevertheless, limitations and compromises remain and are described in the following.

The single-zone and the multi-zone model are validated for one test bench engine only. It is common knowledge that geometry and operating conditions strongly influence the inhomogeneities in the cylinder and thus influence the heat transfer. This results in uncertainties with regard to the temperature distribution, which is significantly influencing the heat transfer and the ignition timing in the cylinder.

Eventually, uncertainties in the required additive amount are expected, especially if the engine geometry or operating conditions differ strongly from our test bench engine. In this case, the results in this thesis are expected to be shifted by absolute values, but the trends and conclusions should remain valid.

The results at high equivalence ratios indicate potential for use in multi-engine applications, where the first engine is operated at high ϕ (7-10) and the second engine at low ϕ (1.0-2.0). Also, multi-compression might be an interesting approach to achieve higher fuel conversion.

In the process concept simulations simplifications had to be made. Membrane and PSA model were black box models without detailed kinetics or adsorption thermodynamics. More insight in the process and higher accuracy could be gained in the future by implementing detailed models. In addition, there is a lack of data in the literature on the performance of palladium membranes at large scales, which should therefore be investigated.

To evaluate the feasibility, efficiency, and economics of simultaneous hydrogen and carbon monoxide or ethylene production, process concepts with detailed PSA models could be applied in the future. Finally, building a pilot plant including product separation is desirable to confirm the results of the investigated process concepts.

9.3   End notes

Many researchers have shown over the past decades that fuel-rich operation in HCCI engines is feasible, but none of them presented a comprehensive investigation of the polygeneration in fuel-rich operated HCCI engines; ranging from chemical kinetics to exergetic evaluation and thermoeconomic assessments by applying exergoeconomic methods. This is the gap this thesis filled.

Furthermore, the results emphasize that economic evaluation should always be accompanied by a sensitivity analysis to evaluate the uncertainties of economic input parameters. In this thesis it was shown that a global sensitivity analysis performed well for investigation of economic input parameters as well as operating parameters of slightly complex chemical engineering systems.

This work was conducted in the framework of the DFG research group FOR1993. Therefore, lots of knowledge could be transferred to and from other sub-projects. For instance, there was a strong interconnection with the engine experiments. Moreover, the engine model and the kinetic evaluation benefited from flow-reactor and shock-tube experiments and the reaction mechanism PolyMech, developed and improved

simultaneously for the engine conditions simulated in this thesis. The FOR1993 approach shows how viable it is that experiments and theoretical work go hand in hand to achieve comprehensive knowledge in a novel research field.

LIST OF PUBLICATIONS AND ASSOCIATED WORKS

This chapter contains a comprehensive list of peer-reviewed publications and conference contributions I worked on during my doctoral studies, followed by the student theses I supervised.

10.1   Peer-reviewed journal articles

K. Banke, R. Hegner, D. Schröder, C. Schulz, B. Atakan, S. A. Kaiser. Power and syngas production from partial oxidation of fuel-rich methane/DME mixtures in an HCCI engine. *Fuel 243 (2019) 97–103.* DOI: 10.1016/j.fuel.2019.01.076 .

D. Schröder, R. Hegner, A. Güngör, B. Atakan. Exergoeconomic analysis of an HCCI engine polygeneration process. *Energy Conversion and Management 203 (2020) 112085.* DOI: 10.1016/j. enconman.2019.112085.

D. Schröder, K. Banke, S. A. Kaiser, B. Atakan. The kinetics of methane ignition in fuel-rich HCCI engines: DME replacement by ozone. *Proceedings of the Combustion Institute (2020).* DOI: 10.1016/j. proci.2020.05.046.

B. Atakan, S. A. Kaiser, J. Herzler, S. Porras, K. Banke, O. Deutschmann, T. Kasper, M. Fikri, R. Schießl, D. Schröder, C. Rudolph, D. Kaczmarek, H. Gossler, S. Drost, V. Bykov, U. Maas, C. Schulz. Flexible energy conversion and storage via high-temperature gas-phase reactions: The piston engine as a polygeneration reactor. *Renewable and Sustainable Energy Reviews 133 (2020).*
DOI: 10.1016/j. rser.2020.110264.

D. Freund, C. Horn, B. Atakan. Fuel-Rich Natural Gas Conversion in HCCI Engines with Ozone and Dimethyl Ether as Ignition Promoters: A Kinetic and Exergetic Analysis. *In: R. King, D. Peitsch (Eds.), Active Flow and Combustion Control 2021, Springer International Publishing, Cham, 2022, pp. 47–65.*
DOI: 10.1007/978-3-030-90727-3 _4.

C. Rudolph, D. Freund, D. Kaczmarek, B. Atakan. Low-calorific ammonia contain-

ing off-gas mixture: Modelling the conversion in HCCI engines. *Combustion and Flame (2022) 112063.* DOI: 10.1016/j. combustflame.2022.112063.

D. Freund, A. Güngör, B. Atakan. Hydrogen production and separation in fuel-rich operated HCCI engine polygeneration systems: exergoeconomic analysis and comparison between pressure swing adsorption and palladium membrane separation. *Applications in Energy and Combustion Science (2022) 100108.*
DOI: 10.1016/j. jaecs.2022.100108.

K. Banke, D. Freund, S. A. Kaiser, B. Atakan. Evaluation of fuel additives for HCCI engines operated on fuel-rich methane/air mixtures: DME, DEE and n-heptane. *Applications in Energy and Combustion Science (2023) 100112.*
DOI: 10.1016/j. jaecs.2023.100112.

10.2   Articles without peer-review

D. Freund and B. Atakan. Surrogate model development for hydrogen separation via pressure swing adsorption processes: selection and evaluation of machine learning algorithms. *engrXiv (2022)* DOI: 10.31224/2372 .

10.3   Conference contributions (oral presentations)

D. Schröder, R. Hegner, A. Güngör, B. Atakan. Exergoeconomic analysis of an engine polygeneration process: methodology, sensitivities, and results. *5th International Conference on Contemporary Problems of Thermal Engineering (CPOTE), Gliwice, PL, 18.09.2018*

D. Schröder, R. Hegner, A. Güngör, B. Atakan. Exergoökonomische Untersuchung eines Prozesses zur Polygeneration mit HCCI Motor: Methodik, Sensitivitätsanalyse und Resultate. *Thermodynamik-Kolloquium 2018, Kassel, D, 26.09.2018*

D. Schröder, R. Hegner, A. Güngör, B. Atakan. Uncertainty of Economic Parameters and their Effects on the Product Costs of an Engine Polygeneration Energy System. *32nd International Conference on Efficiency, Cost, Optimization, Simulation and Environmental Impact of Energy Systems (ECOS), Wroclaw, PL, 23.06.2019*

D. Schröder, B. Atakan. Theoretische Untersuchung der Umsetzung von Biogasen in HCCI-Motoren zur Erzeugung von Synthesegas. *29. Deutscher Flammentag, Bochum, D, 17.09.2019*

D. Schröder, K. Banke, S. A. Kaiser, B. Atakan. The kinetics of methane ignition in fuel-rich HCCI engines: DME replacement by ozone. *38th International Symposium on Combustion, Adelaide, AUS, 27.01.2021*

D. Freund, B. Atakan. Ozon als Zündbeschleuniger für die Produktion von Ethylen und Acetylen im HCCI-Motor: Eine kinetische und exergetische Analyse. *30. Deutscher Flammentag, Hannover, D, 29.09.2021.*

10.4 Conference contributions (poster presentations)

D. Schröder, R. Hegner, A. Güngör, B. Atakan. Exergoeconomic analysis of an engine polygeneration process: methodology, sensitivities, and results. *Joint Meeting: The German and Italian sections of the Combustion Institute, Sorrento, I, 23.05.2018*

D. Schröder, R. Hegner, A. Güngör, B. Atakan. Exergoeconomic analysis of an engine polygeneration process: methodology, sensitivities, and results. *37th International Symposium on Combustion, Dublin, IRL, 29.07.2018*

D. Schröder, B. Atakan. A modeling study of a partial oxidation polygeneration process of fuel-rich ethanol/ozonemixtures in an HCCI engine. *9th European Combustion Meeting (ECM), Lisbon, P, 14.04.2019*

D. Schröder, A. Güngör, B. Atakan. Der Einfluss von Skaleneffekten und der Unsicherheit ökonomischer Parameter auf die Produktkosten eines motorischen Polygeneration-Prozesses. *Thermodynamik-Kolloquium 2019, Duisburg, D, 30.09.2019*

D. Freund, B. Atakan. Ozone and dimethyl ether in fuel rich HCCI engines: An exergetic evaluation. *10th European Combustion Meeting (ECM), 14.04.2021*

10.5 Supervised student theses

Bachelor theses

Neoh, Soon Rick. Partial Oxidation of Natural Gas for HCCI Combustion: The Influence of Additives on the Thermodynamics (2019)

Wouatong, Landry. Partial Oxidation of different Fuel-Additive Mixtures for HCCI Combustion: Investigation of Thermodynamic Limits (2019)

Schäfer, Luca. Untersuchung des Einflusses der Abgasrückführung und von Ozon als Additiv auf die Thermodynamik der partiellen Oxidation von Biogasen in HCCI-Motoren (2019)

Ghayyadah, Nooraldein. The additive contribution to the exergy conversion in HCCI engines for polygeneration (2020)

Öztas, Yusuf. Wasserstoffgewinnung durch Polygeneration im HCCI-Motor: Abtrennung mittels Druckwechseladsorption (2020)

Abu Azab, Mohammed. Modeling of ignition delay times of different fuel/ozone mixtures for fuel-rich operated HCCI engines for polygeneration (2020)

Bezawada, Bhagya Teja. An investigation of the sensitivity of engine thermodynamics predictions on heat transfer correlations (2021)

Ayan, Hilmi Oğuzhan. Fuel-rich operated HCCI engines under varying operating conditions: investigation of the exergy input for separation of base chemicals from the product gas (2021)

Venghaus, Björn. Polygeneration mit Biogas in einem HCCI-Motor: eine exergoökonomische Analyse (2021)

Zhao, Hui. Simultaneous acetylene, ethylene, and synthesis gas production from natural gas: the potential of coupling two fuel-rich operated HCCI engines (2022)

Master theses

Horn, Christoph. Der Einfluss von Inhomogenitäten im HCCI-Motor auf die Synthesegaserzeugung: Modellierung mit einem Mehrzonenmodell (2020)

Vatansever, Kadri. Theoretische Untersuchung der Abtrennung hochverdünnter Wasserstoff-/Kohlenwasserstoffgemische mittels Druckwechseladsorption (2022)

Schmeing, Simon. Solare Reformierung von Biogas: Potentialanalyse mittels Prozesssimulation und techno-ökonomischer Bewertung (2022)

Ghodratizadeh, Arash. Engine reformers for methanol synthesis in wastewater treatment plants: Thermo-economical analysis and modelling (2022)

BIBLIOGRAPHY

[1] Nebojša Nakićenović et al. "Long-term strategies for mitigating global warming". In: *Energy* 18.5 (1993), p. 401. ISSN: 03605442. DOI: 10.1016/0360-5442(93)90019-A.

[2] Akihiro Yamasaki. "An Overview of CO2 Mitigation Options for Global Warming-Emphasizing CO2 Sequestration Options". In: *JOURNAL OF CHEMICAL ENGINEERING OF JAPAN* 36.4 (2003), pp. 361–375. ISSN: 0021-9592. DOI: 10.1252/jcej.36.361.

[3] Joeri Rogelj et al. "Paris Agreement climate proposals need a boost to keep warming well below 2 °C". In: *Nature* 534.7609 (2016), pp. 631–639. DOI: 10.1038/nature18307.

[4] Elizabeth J. Bush and L. DannyD Harvey. "Joint implementation and the ultimate objective of the United Nations Framework Convention on Climate Change". In: *Global Environmental Change* 7.3 (1997), pp. 265–285. ISSN: 09593780. DOI: 10.1016/S0959-3780(97)00012-5.

[5] T. M. L. Wigley. "The Kyoto Protocol: CO 2 CH 4 and climate implications". In: *Geophysical Research Letters* 25.13 (1998), pp. 2285–2288. ISSN: 00948276. DOI: 10.1029/98gl01855.

[6] Charles Gore. "The Post-2015 Moment: Towards Sustainable Development Goals and a New Global Development Paradigm". In: *Journal of International Development* 27.6 (2015), pp. 717–732. ISSN: 09541748. DOI: 10.1002/jid.3109.

[7] Stephane Hallegatte et al. "Mapping the climate change challenge". In: *Nature Climate Change* 6.7 (2016), pp. 663–668. ISSN: 1758-678X. DOI: 10.1038/nclimate3057.

[8] Global Change Data Lab. *Global direct primary energy consumption.* 2022. URL: https://ourworldindata.org/grapher/global-primary-energy.

[9] Global Change Data Lab. *Global CO2 emissions from fossil fuels.* 2020. URL: https://ourworldindata.org/co2-emissions.

[10] World Resources Institute. *Climate Watch Historical GHG Emissions.* Washington, DC: World Resources Institute, 2022. URL: https://www.climatewatchdata.org/data-explorer/historical-emissions.

[11] United Nations Environment Programme. *Emissions Gap Report 2021: The Heat Is On – A World of Climate Promises Not Yet Delivered.* Nairobi, 2021. ISBN: 978-92-807-3890-2.

[12] Institute of Environmental Management and Assessment. *GHG Management & Reporting: Special Report*. 2010. URL: https://www.iema.net/document-download/34686.

[13] Global Change Data Lab. *Share of primary energy from renewable sources*. 2022. URL: https://ourworldindata.org/renewable-energy.

[14] *Global renewables outlook: Energy transformation 2050*. Abu Dhabi: International Renewable Energy Agency, 2020. ISBN: 978-92-9260-238-3.

[15] European Environment Agency. *Efficiency of public conventional thermal power production in Europe*. 2018. URL: https://www.eea.europa.eu/ds_resolveuid/715b039476e64ebaa0f1860f706ad794.

[16] Ibrahim Dincer and Marc A. Rosen. *Exergy Analysis of Heating, Refrigerating and Air Conditioning*. Elsevier, 2015. ISBN: 9780124172036. DOI: 10.1016/C2013-0-06800-4.

[17] C. A. A. F. Leite et al. "Natural gas based cogeneration system proposal to a textile industry: a financial assessment". In: *Energy Efficiency* 14.2 (2021). ISSN: 1570-646X. DOI: 10.1007/s12053-021-09927-2.

[18] International Energy Agency. *Key World Energy Statistics 2021: Final consumption*. 2021. URL: https://www.iea.org/reports/key-world-energy-statistics-2021/final-consumption.

[19] German Energy Agency. *Feedstocks for the chemical industry*. 2019.

[20] ScienceDirect. *Search for keyword "polygeneration"*. 2022. URL: https://www.sciencedirect.com/search?qs=polygeneration.

[21] Ibrahim Dincer and Canan Acar. "A review on clean energy solutions for better sustainability". In: *International Journal of Energy Research* 39.5 (2015), pp. 585–606. ISSN: 0363-907X. DOI: 10.1002/er.3329.

[22] Francesco Calise et al. "Polygeneration". In: *Polygeneration Systems*. Elsevier, 2022, pp. 1–33. ISBN: 9780128206256. DOI: 10.1016/B978-0-12-820625-6.00008-6.

[23] J. M. Sala et al. "Exergetic analysis and thermoeconomic study for a container-housed engine". In: *Applied Thermal Engineering* 26.16 (2006), pp. 1840–1850. ISSN: 13594311. DOI: 10.1016/j.applthermaleng.2006.02.005.

[24] Ugur Yildirim and Afsin Gungor. "An application of exergoeconomic analysis for a CHP system". In: *International Journal of Electrical Power & Energy Systems* 42.1 (2012), pp. 250–256. ISSN: 01420615. DOI: 10.1016/j.ijepes.2012.03.040.

[25] Marie Basin et al. "Hydrogen Production by Steam Reforming". In: *Process Industries 2*. Ed. by Jean–Pierre Dal Pont and Marie Debacq. Wiley, 2020, pp. 31–77. ISBN: 9781119779698. DOI: 10.1002/9781119779698.ch2.

[26]   A. Simpson and A. Lutz. "Exergy analysis of hydrogen production via steam methane reforming". In: *International Journal of Hydrogen Energy* 32.18 (2007), pp. 4811–4820. ISSN: 03603199. DOI: 10.1016/j.ijhydene.2007.08.025.

[27]   L. von Szeszich. "Herstellung von Synthesegas im Otto-Motor bei gleichzeitiger Arbeitsgewinnung". In: *Chemie Ingenieur Technik* 28.3 (1956), pp. 190–195. ISSN: 0009286X. DOI: 10.1002/cite.330280310.

[28]   M. McMillan and S. Lawson. "Experimental and modeling study of hydrogen/syngas production and particulate emissions from a natural gas-fueled partial oxidation engine". In: *International Journal of Hydrogen Energy* 31.7 (2006), pp. 847–860. ISSN: 03603199. DOI: 10.1016/j.ijhydene.2005.08.013.

[29]   Lei Zhu et al. "In-cylinder thermochemical fuel reforming (TFR) in a spark-ignition natural gas engine". In: *Proceedings of the Combustion Institute* 36.3 (2017), pp. 3487–3497. ISSN: 15407489. DOI: 10.1016/j.proci.2016.07.058.

[30]   Sebastian Wiemann et al. "Combined production of power and syngas in an internal combustion engine – Experiments and simulations in SI and HCCI mode". In: *Fuel* 215 (2018), pp. 40–45. ISSN: 00162361. DOI: 10.1016/j.fuel.2017.11.002.

[31]   Jean-Baptiste Masurier et al. "Application of an Ozone Generator to Control the Homogeneous Charge Compression Ignition Combustion Process". In: *SAE Technical Paper Series*. SAE Technical Paper Series. 400 Commonwealth Drive, Warrendale, PA, United States: SAE International, 2015. DOI: 10.4271/2015-24-2456.

[32]   L. Tartakovsky and M. Sheintuch. "Fuel reforming in internal combustion engines". In: *Progress in Energy and Combustion Science* 67 (2018), pp. 88–114. ISSN: 03601285. DOI: 10.1016/j.pecs.2018.02.003.

[33]   M. Feroskhan and Saleel Ismail. "A review on the purification and use of biogas in compression ignition engines". In: *INTERNATIONAL JOURNAL OF AUTOMOTIVE AND MECHANICAL ENGINEERING* 14.3 (2017), pp. 4383–4400. ISSN: 22298649. DOI: 10.15282/ijame.14.3.2017.1.0348.

[34]   Robert Hegner and Burak Atakan. "A polygeneration process concept for HCCI-engines – Modeling product gas purification and exergy losses". In: *International Journal of Hydrogen Energy* 42.2 (2017), pp. 1287–1297. ISSN: 03603199. DOI: 10.1016/j.ijhydene.2016.09.050.

[35]   Sechul Oh and Han Ho Song. "Exergy analysis on non-catalyzed partial oxidation reforming using homogeneous charge compression ignition engine in a solid oxide fuel cell system". In: *International Journal of Hydrogen Energy* 43.5 (2018), pp. 2943–2960. ISSN: 03603199. DOI: 10.1016/j.ijhydene.2017.12.090.

[36] Andrea Lazzaretto and George Tsatsaronis. "SPECO: A systematic and general methodology for calculating efficiencies and costs in thermal systems". In: *Energy* 31.8-9 (2006), pp. 1257–1289. ISSN: 03605442. DOI: 10.1016/j.energy.2005.03.011.

[37] Aysegul Abusoglu and Mehmet Kanoglu. "Exergoeconomic analysis and optimization of combined heat and power production: A review". In: *Renewable and Sustainable Energy Reviews* 13.9 (2009), pp. 2295–2308. ISSN: 13640321. DOI: 10.1016/j.rser.2009.05.004.

[38] Ata D. Akbari and Seyed M.S. Mahmoudi. "Thermoeconomic analysis & optimization of the combined supercritical CO 2 (carbon dioxide) recompression Brayton/organic Rankine cycle". In: *Energy* 78 (2014), pp. 501–512. ISSN: 03605442. DOI: 10.1016/j.energy.2014.10.037.

[39] Francesco Calise et al. "Exergetic and exergoeconomic analysis of a novel hybrid solar–geothermal polygeneration system producing energy and water". In: *Energy Conversion and Management* 115 (2016), pp. 200–220. ISSN: 01968904. DOI: 10.1016/j.enconman.2016.02.029.

[40] S. O. Mert, I. Dincer, and Z. Ozcelik. "Exergoeconomic analysis of a vehicular PEM fuel cell system". In: *Journal of Power Sources* 165.1 (2007), pp. 244–252. ISSN: 03787753. DOI: 10.1016/j.jpowsour.2006.12.002.

[41] Elsevier B. V. *CRediT author statement*. 2022. URL: https://www.elsevier.com/authors/policies-and-guidelines/credit-author-statement.

[42] Gianfranco Chicco and Pierluigi Mancarella. "Distributed multi-generation: A comprehensive view". In: *Renewable and Sustainable Energy Reviews* 13.3 (2009), pp. 535–551. ISSN: 13640321. DOI: 10.1016/j.rser.2007.11.014.

[43] Hamid Ghanbari, Frank Pettersson, and Henrik Saxén. "Optimal operation strategy and gas utilization in a future integrated steel plant". In: *Chemical Engineering Research and Design* 102 (2015), pp. 322–336. ISSN: 02638762. DOI: 10.1016/j.cherd.2015.06.038.

[44] Lin Gao et al. "Proposal of a natural gas-based polygeneration system for power and methanol production". In: *Energy* 33.2 (2008), pp. 206–212. ISSN: 03605442. DOI: 10.1016/j.energy.2007.10.011.

[45] Ghazi A. Karim and I. Wierzba. "The production of hydrogen through the uncatalyzed partial oxidation of methane in an internal combustion engine". In: *International Journal of Hydrogen Energy* 33.8 (2008), pp. 2105–2110. ISSN: 03603199. DOI: 10.1016/j.ijhydene.2008.01.051.

[46] Yoon Cheol Yang, Mun Sup Lim, and Young Nam Chun. "The syngas production by partial oxidation using a homogeneous charge compression ignition engine". In: *Fuel Processing Technology* 90.4 (2009), pp. 553–557. ISSN: 03783820. DOI: 10.1016/j.fuproc.2009.01.002.

[47]   Robert Hegner et al. "Fuel-Rich HCCI Engines as Chemical Reactors for Polygeneration: A Modeling and Experimental Study on Product Species and Thermodynamics". In: *Energy & Fuels* 31.12 (2017), pp. 14079–14088. ISSN: 0887-0624. DOI: `10.1021/acs.energyfuels.7b02150`.

[48]   Abrar Inayat et al. "Parametric Study for Production of Dimethyl Ether (DME) As a Fuel from Palm Wastes". In: *Energy Procedia* 105 (2017), pp. 1242–1249. ISSN: 18766102. DOI: `10.1016/j.egypro.2017.03.431`.

[49]   Zhiqi Wang et al. "Design and operation of a pilot plant for biomass to liquid fuels by integrating gasification, DME synthesis and DME to gasoline". In: *Fuel* 186 (2016), pp. 587–596. ISSN: 00162361. DOI: `10.1016/j.fuel.2016.08.108`.

[50]   David G. Goodwin et al. *Cantera: an object-oriented software toolkit for chemical kinetics, thermodynamics, and transport processes.* 2021. DOI: `10.5281/zenodo.4527812`.

[51]   K. Yasunaga et al. "A multiple shock tube and chemical kinetic modeling study of diethyl ether pyrolysis and oxidation". In: *The journal of physical chemistry. A* 114.34 (2010), pp. 9098–9109. DOI: `10.1021/jp104070a`.

[52]   K. Yasunaga et al. "Detailed chemical kinetic mechanisms of ethyl methyl, methyl tert-butyl and ethyl tert-butyl ethers: The importance of uni-molecular elimination reactions". In: *Combustion and Flame* 158.6 (2011), pp. 1032–1036. ISSN: 00102180. DOI: `10.1016/j.combustflame.2010.10.012`.

[53]   Fikri Sen et al. "Shock-tube and plug-flow reactor study of the oxidation of fuel-rich CH4/O2 mixtures enhanced with additives". In: *Combustion and Flame* 169 (2016), pp. 307–320. ISSN: 00102180. DOI: `10.1016/j.combustflame.2016.03.030`.

[54]   J. Herzler et al. In: *Proceedings of the 7th European Combustion Meeting: March 30–April 2 2015, Budapest, Hungary* (2015).

[55]   J. Herzler et al. "Shock-tube study of the ignition and product formation of fuel-rich CH4/air and CH4/additive/air mixtures at high pressure". In: *Proceedings of the Combustion Institute* 37.4 (2019), pp. 5705–5713. ISSN: 15407489. DOI: `10.1016/j.proci.2018.05.120`.

[56]   D. Nativel et al. "Shock-tube study of methane pyrolysis in the context of energy-storage processes". In: *Proceedings of the Combustion Institute* 37.1 (2019), pp. 197–204. ISSN: 15407489. DOI: `10.1016/j.proci.2018.06.083`.

[57]   Junnian Zheng and Jerald A. Caton. "Use of a single-zone thermodynamic model with detailed chemistry to study a natural gas fueled homogeneous charge compression ignition engine". In: *Energy Conversion and Management* 53.1 (2012), pp. 298–304. ISSN: 01968904. DOI: `10.1016/j.enconman.2011.09.005`.

[58]   G. Woschni. "A Universally Applicable Equation for the Instantaneous Heat Transfer Coefficient in the Internal Combustion Engine". In: *SAE Technical Paper 670931, https://doi.org/10.4271/670931.* DOI: `10.4271/670931`.

[59] H. S. Soyhan et al. "Evaluation of heat transfer correlations for HCCI engine modeling". In: *Applied Thermal Engineering* 29.2-3 (2009), pp. 541–549. ISSN: 13594311. DOI: 10.1016/j.applthermaleng.2008.03.014.

[60] Junseok Chang et al. "New Heat Transfer Correlation for an HCCI Engine Derived from Measurements of Instantaneous Surface Heat Flux". In: *SAE Technical Paper 2004-01-2996, https://doi.org/10.4271/2004-01-2996.* DOI: 10.4271/2004-01-2996.

[61] N. P. Komninos and C. D. Rakopoulos. "Heat transfer in HCCI phenomenological simulation models: A review". In: *Applied Energy* 181 (2016), pp. 179–209. ISSN: 03062619. DOI: 10.1016/j.apenergy.2016.08.061.

[62] Richard E. Sonntag, Claus Borgnakke, and Gordon J. van Wylen. *Fundamentals of thermodynamics*. 6. ed., internat. ed. New York: Wiley, 2003. ISBN: 9780471428831. URL: http://www.loc.gov/catdir/description/wiley036/2002513116.html.

[63] T. J. Kotas. *The Exergy Method of Thermal Plant Analysis*. Elsevier, 1985. ISBN: 9780408013505. DOI: 10.1016/C2013-0-00894-8.

[64] Song-Charng Kong. "A study of natural gas/DME combustion in HCCI engines using CFD with detailed chemical kinetics". In: *Fuel* 86.10-11 (2007), pp. 1483–1489. ISSN: 00162361. DOI: 10.1016/j.fuel.2006.11.015.

[65] H. Kellerer, A. Müller, and H.-J. Bauer. "Soot Formation in a Shock Tube under Elevated Pressure Conditions". In: *Combustion Science and Technology* 113.1 (1996), pp. 67–80. ISSN: 0010-2202. DOI: 10.1080/00102209608935488.

[66] Magnus Sjöberg, John E. Dec, and Nicholas P. Cernansky. "Potential of Thermal Stratification and Combustion Retard for Reducing Pressure-Rise Rates in HCCI Engines, Based on Multi-Zone Modeling and Experiments". In: *SAE Technical Paper Series*. SAE Technical Paper Series. SAE International400 Commonwealth Drive, Warrendale, PA, United States, 2005. DOI: 10.4271/2005-01-0113.

[67] Elaheh Neshat and Rahim Khoshbakhti Saray. "Development of a new multi zone model for prediction of HCCI (homogenous charge compression ignition) engine combustion, performance and emission characteristics". In: *Energy* 73 (2014), pp. 325–339. ISSN: 03605442. DOI: 10.1016/j.energy.2014.06.025.

[68] N. P. Komninos. "Assessing the effect of mass transfer on the formation of HC and CO emissions in HCCI engines, using a multi-zone model". In: *Energy Conversion and Management* 50.5 (2009), pp. 1192–1201. ISSN: 01968904. DOI: 10.1016/j.enconman.2009.01.026.

[69] F. Calise, M. Dentice d'Accadia, and A. Piacentino. "Exergetic and exergoeconomic analysis of a renewable polygeneration system and viability study for small isolated communities". In: *Energy* 92 (2015), pp. 290–307. ISSN: 03605442. DOI: 10.1016/j.energy.2015.03.056.

[70]   Kai Banke et al. "Evaluation of fuel additives for HCCI engines operated on fuel-rich methane/air mixtures: DME, DEE, and n-heptane". In: *Applications in Energy and Combustion Science* (2023), p. 100112. ISSN: 2666352X. DOI: 10.1016/j.jaecs.2023.100112.

[71]   Hiroyuki Nishida and Takeshi Tachibana. "Homogeneous Charge Compression Ignition of Natural Gas/Air Mixture with Ozone Addition". In: *Journal of Propulsion and Power* 22.1 (2006), pp. 151–157. ISSN: 0748-4658. DOI: 10.2514/1.14991.

[72]   J.-B. Masurier et al. "Homogeneous Charge Compression Ignition Combustion of Primary Reference Fuels Influenced by Ozone Addition". In: *Energy & Fuels* 27.9 (2013), pp. 5495–5505. ISSN: 0887-0624. DOI: 10.1021/ef401009x.

[73]   Ultan Burke et al. "An ignition delay and kinetic modeling study of methane, dimethyl ether, and their mixtures at high pressures". In: *Combustion and Flame* 162.2 (2015), pp. 315–330. ISSN: 00102180. DOI: 10.1016/j.combustflame.2014.08.014.

[74]   G. A. Karim and N.P.W. Moore. "Examination of Rich Mixture Operation of a Dual Fuel Engine". In: *SAE Technical Paper Series*. SAE Technical Paper Series. SAE International400 Commonwealth Drive, Warrendale, PA, United States, 1990. DOI: 10.4271/901500.

[75]   Emmanuel G. Lim et al. "The engine reformer: Syngas production in an engine for compact gas-to-liquids synthesis". In: *The Canadian Journal of Chemical Engineering* 94.4 (2016), pp. 623–635. ISSN: 00084034. DOI: 10.1002/cjce.22443.

[76]   Mohamed H. Morsy. "Modeling study on the production of hydrogen/syngas via partial oxidation using a homogeneous charge compression ignition engine fueled with natural gas". In: *International Journal of Hydrogen Energy* 39.2 (2014), pp. 1096–1104. ISSN: 03603199. DOI: 10.1016/j.ijhydene.2013.10.160.

[77]   M. Ghaffarpour, A. Lock, and M. Shojaeefard. "Partial Oxidation of Natural Gas Using Internal Combustion Engines". In: *SAE technical paper 2004-01-0621* (2004).

[78]   K. Banke et al. "Power and syngas production from partial oxidation of fuel-rich methane/DME mixtures in an HCCI engine". In: *Fuel* 243 (2019), pp. 97–103. ISSN: 00162361. DOI: 10.1016/j.fuel.2019.01.076.

[79]   Flynn et al. "Premixed Charge Compression Ignition Engine with Optimal Combustion Control: US Patent". 6,286,482 B1. 11.09.2001.

[80]   Alessandro Schönborn et al. "Ignition control of homogeneous-charge compression ignition (HCCI) combustion through adaptation of the fuel molecular structure by reaction with ozone". In: *Fuel* 89.11 (2010), pp. 3178–3184. ISSN: 00162361. DOI: 10.1016/j.fuel.2010.06.005.

[81]   Wubin Weng et al. "Investigation of formaldehyde enhancement by ozone addition in CH4/air premixed flames". In: *Combustion and Flame* 162.4 (2015), pp. 1284–1293. ISSN: 00102180. DOI: 10.1016/j.combustflame.2014.10.021.

[82]   H. Yamada et al. "Controlling mechanism of ignition enhancing and suppressing additives in premixed compression ignition". In: *International Journal of Engine Research* 6.4 (2005), pp. 331–340. ISSN: 1468-0874. DOI: 10.1243/146808705X30594.

[83]   Ali Mohammadi et al. "Study on Combustion Control in Natural-Gas PCCI Engines with Ozone Addition into Intake Gas". In: *SAE Technical Paper Series*. SAE Technical Paper Series. SAE International400 Commonwealth Drive, Warrendale, PA, United States, 2006. DOI: 10.4271/2006-01-0419.

[84]   Jean-Baptiste Masurier et al. "Investigation of iso-octane combustion in a homogeneous charge compression ignition engine seeded by ozone, nitric oxide and nitrogen dioxide". In: *Proceedings of the Combustion Institute* 35.3 (2015), pp. 3125–3132. ISSN: 15407489. DOI: 10.1016/j.proci.2014.05.060.

[85]   J.-B. Masurier et al. "Ozone applied to the homogeneous charge compression ignition engine to control alcohol fuels combustion". In: *Applied Energy* 160 (2015), pp. 566–580. ISSN: 03062619. DOI: 10.1016/j.apenergy.2015.08.004.

[86]   Francesco Contino et al. "CFD simulations using the TDAC method to model iso-octane combustion for a large range of ozone seeding and temperature conditions in a single cylinder HCCI engine". In: *Fuel* 137 (2014), pp. 179–184. ISSN: 00162361. DOI: 10.1016/j.fuel.2014.07.084.

[87]   S. Sayssouk et al. "Towards control of HCCI combustion by ozone addition: a mathematical approach to estimate combustion parameters". In: *IFAC-PapersOnLine* 49.11 (2016), pp. 361–368. ISSN: 24058963. DOI: 10.1016/j.ifacol.2016.08.054.

[88]   F. Foucher et al. "Influence of ozone on the combustion of n-heptane in a HCCI engine". In: *Proceedings of the Combustion Institute* 34.2 (2013), pp. 3005–3012. ISSN: 15407489. DOI: 10.1016/j.proci.2012.05.042.

[89]   Jean-Baptiste Masurier et al. "Effect of Additives on Combustion Characteristics of a Natural Gas Fueled HCCI Engine". In: *SAE Technical Paper 2014-01-2662*. SAE Technical Paper Series. 400 Commonwealth Drive, Warrendale, PA, United States: SAE International, 2014. DOI: 10.4271/2014-01-2662.

[90]   Anthony Dubreuil et al. "HCCI combustion: Effect of NO in EGR". In: *Proceedings of the Combustion Institute* 31.2 (2007), pp. 2879–2886. ISSN: 15407489. DOI: 10.1016/j.proci.2006.07.168.

[91]   Francesco Contino et al. "Experimental and numerical analysis of nitric oxide effect on the ignition of iso-octane in a single cylinder HCCI engine". In: *Combustion and Flame* 160.8 (2013), pp. 1476–1483. ISSN: 00102180. DOI: 10.1016/j.combustflame.2013.02.028.

[92]   V. Ya. Basevich et al. "Kinetic nature of blue flames in the autoignition of methane". In: *Russian Journal of Physical Chemistry B* 8.3 (2014), pp. 326–331. ISSN: 1990-7931. DOI: 10.1134/S1990793114030026.

[93]   Dennis Kaczmarek, Burak Atakan, and Tina Kasper. "Investigation of the partial oxidation of methane/n-heptane-mixtures and the interaction of methane and n-heptane under ultra-rich conditions". In: *Combustion and Flame* 205 (2019), pp. 345–357. ISSN: 00102180. DOI: 10.1016/j.combustflame.2019.04.005.

[94]   Yang Wang et al. "A Theoretical Investigation of the Combustion of PRF90 under the Flexible Cylinder Engine Mode". In: *SAE Technical Paper 2017-01-1027*. SAE Technical Paper Series. 400 Commonwealth Drive, Warrendale, PA, United States: SAE International, 2017. DOI: 10.4271/2017-01-1027.

[95]   John B. Heywood. *Internal combustion engine fundamentals*. McGraw-Hill series in mechanical engineering. New York: McGraw-Hill, 1988. ISBN: 0-07-028637-x. URL: http://www.loc.gov/catdir/description/mh022/87015251.html.

[96]   Hao Zhao, Xueliang Yang, and Yiguang Ju. "Kinetic studies of ozone assisted low temperature oxidation of dimethyl ether in a flow reactor using molecular-beam mass spectrometry". In: *Combustion and Flame* 173 (2016), pp. 187–194. ISSN: 00102180. DOI: 10.1016/j.combustflame.2016.08.008.

[97]   F. Halter, P. Higelin, and P. Dagaut. "Experimental and Detailed Kinetic Modeling Study of the Effect of Ozone on the Combustion of Methane". In: *Energy & Fuels* 25.7 (2011), pp. 2909–2916. ISSN: 0887-0624. DOI: 10.1021/ef200550m.

[98]   Mohamad Mostafa Namar and Omid Jahanian. "Energy and exergy analysis of a hydrogen-fueled HCCI engine". In: *Journal of Thermal Analysis and Calorimetry* 137.1 (2019), pp. 205–215. ISSN: 1388-6150. DOI: 10.1007/s10973-018-7910-7.

[99]   Magnus Sjöberg and John E. Dec. "An Investigation of the Relationship Between Measured Intake Temperature, BDC Temperature, and Combustion Phasing for Premixed and DI HCCI Engines". In: *SAE Technical Paper Series*. SAE Technical Paper Series. SAE International400 Commonwealth Drive, Warrendale, PA, United States, 2004. DOI: 10.4271/2004-01-1900.

[100]   Alessandro Schönborn et al. "Autoignition Control Using an Additive with Adaptable Chemical Structure. Part 2. Development of a PRF Kinetic Model Including 1,3-Cyclohexadiene Mechanism and Simulations of Ignition Control". In: *Energy & Fuels* 33.12 (2019), pp. 12704–12713. ISSN: 0887-0624. DOI: 10.1021/acs.energyfuels.9b02020.

[101]   A. K. Amjad et al. "Availability analysis of n-heptane and natural gas blends combustion in HCCI engines". In: *Energy* 36.12 (2011), pp. 6900–6909. ISSN: 03605442. DOI: 10.1016/j.energy.2011.09.046.

[102]   S. Porras et al. "An experimental and modeling study on the reactivity of extremely fuel-rich methane/dimethyl ether mixtures". In: *Combustion and Flame* 212 (2020), pp. 107–122. ISSN: 00102180. DOI: 10.1016/j.combustflame.2019.09.036.

[103]   Mohammad Kebriaei, Abolfazl HalvaeiNiasar, and Abbas Ketabi. "A new pulsed power generator topology for corona discharge". In: *2016 7th Power Electronics and Drive Systems Technologies Conference (PEDSTC)*. IEEE, 16.02.2016 - 18.02.2016, pp. 577–581. ISBN: 978-1-5090-0375-4. DOI: 10.1109/PEDSTC.2016.7556924.

[104]   Seunghwan Keum and Tang-Wei Kuo. "Damköhler Number Analysis on the Effect of Ozone on Auto-Ignition and Flame Propagation in Internal Combustion Engines". In: *Volume 1: Large Bore Engines; Fuels; Advanced Combustion*. ASME, Sunday 4 November 2018, V001T03A002. ISBN: 978-0-7918-5198-2. DOI: 10.1115/ICEF2018-9559.

[105]   Dominik Schröder et al. "The kinetics of methane ignition in fuel-rich HCCI engines: DME replacement by ozone". In: *Proceedings of the Combustion Institute* (2020). ISSN: 15407489. DOI: 10.1016/j.proci.2020.05.046.

[106]   Xiongbo Duan et al. "Effects of natural gas composition and compression ratio on the thermodynamic and combustion characteristics of a heavy-duty lean-burn SI engine fueled with liquefied natural gas". In: *Fuel* 254.8 (2019), p. 115733. ISSN: 00162361. DOI: 10.1016/j.fuel.2019.115733.

[107]   D. Kaczmarek et al. "Plug-flow reactor and shock-tube study of the oxidation of very fuel-rich natural gas/DME/O2 mixtures". In: *Combustion and Flame* 225 (2021), pp. 86–103. ISSN: 00102180. DOI: 10.1016/j.combustflame.2020.10.004.

[108]   Xiangping Zhang et al. "Exergy Analysis of the Process for Dimethyl Ether Production through Biomass Steam Gasification". In: *Industrial & Engineering Chemistry Research* 48.24 (2009), pp. 10976–10985. ISSN: 0888-5885. DOI: 10.1021/ie900199e.

[109]   N. P. Komninos, D. T. Hountalas, and D. A. Kouremenos. "Development of a New Multi-Zone Model for the Description of Physical Processes in HCCI Engines". In: *SAE Technical Paper 2004-01-0562, https://doi.org/10.4271/2004-01-0562*. DOI: 10.4271/2004-01-0562.

[110]   J. Yang and J. K. Martin. "Approximate Solution—One-Dimensional Energy Equation for Transient, Compressible, Low Mach Number Turbulent Boundary Layer Flows". In: *Journal of Heat Transfer* 111.3 (1989), pp. 619–624. ISSN: 0022-1481. DOI: 10.1115/1.3250727.

[111]   Fujian Newland Entech Company. *Ozone Portfolio*. 2017. URL: https://
        newlandentecheurope.com/wp-content/uploads/2017/06/Newland-
        EnTech-Europe_Ozone.pdf.

[112]   Burak Atakan et al. "Flexible energy conversion and storage via high-temperature
        gas-phase reactions: The piston engine as a polygeneration reactor". In: *Re-
        newable and Sustainable Energy Reviews* 133 (2020), p. 110264. ISSN: 13640321.
        DOI: 10.1016/j.rser.2020.110264.

[113]   Hadi Ghaebi et al. "Energy, exergy and thermoeconomic analysis of a com-
        bined cooling, heating and power (CCHP) system with gas turbine prime
        mover". In: *International Journal of Energy Research* 35.8 (2011), pp. 697–
        709. ISSN: 0363-907X. DOI: 10.1002/er.1721.

[114]   George Tsatsaronis. "Exergoeconomics: Is it only a new name?" In: *Chemical
        Engineering & Technology* 19.2 (1996), pp. 163–169. DOI: 10.1002/ceat.
        270190210.

[115]   Dominik Schröder et al. "Exergoeconomic analysis of an HCCI engine poly-
        generation process". In: *Energy Conversion and Management* 203 (2020),
        p. 112085. ISSN: 01968904. DOI: 10.1016/j.enconman.2019.112085.

[116]   G. Angrisani, C. Roselli, and M. Sasso. "Distributed microtrigeneration sys-
        tems". In: *Progress in Energy and Combustion Science* 38.4 (2012), pp. 502–
        521. ISSN: 03601285. DOI: 10.1016/j.pecs.2012.02.001.

[117]   Normazlina Mat Isa, Chee Wei Tan, and A.H.M. Yatim. "A comprehensive
        review of cogeneration system in a microgrid: A perspective from architecture
        and operating system". In: *Renewable and Sustainable Energy Reviews* 81
        (2018), pp. 2236–2263. ISSN: 13640321. DOI: 10.1016/j.rser.2017.06.034.

[118]   Luis M. Serra et al. "Polygeneration and efficient use of natural resources". In:
        Energy 34.5 (2009), pp. 575–586. ISSN: 03605442. DOI: 10.1016/j.energy.
        2008.08.013.

[119]   T. Keipi, H. Tolvanen, and J. Konttinen. "Economic analysis of hydrogen
        production by methane thermal decomposition: Comparison to competing
        technologies". In: *Energy Conversion and Management* 159 (2018), pp. 264–
        273. ISSN: 01968904. DOI: 10.1016/j.enconman.2017.12.063.

[120]   Pouria Ahmadi, Ibrahim Dincer, and Marc A. Rosen. "Exergy, exergoeco-
        nomic and environmental analyses and evolutionary algorithm based multi-
        objective optimization of combined cycle power plants". In: *Energy* 36.10
        (2011), pp. 5886–5898. ISSN: 03605442. DOI: 10.1016/j.energy.2011.08.
        034.

[121]   Timo Blumberg et al. "Comparative exergoeconomic evaluation of the lat-
        est generation of combined-cycle power plants". In: *Energy Conversion and
        Management* 153 (2017), pp. 616–626. ISSN: 01968904. DOI: 10.1016/j.
        enconman.2017.10.036.

[122]   Mohammad Ameri, Pouria Ahmadi, and Armita Hamidi. "Energy, exergy and exergoeconomic analysis of a steam power plant: A case study". In: *International Journal of Energy Research* 33.5 (2009), pp. 499–512. DOI: 10.1002/er.1495.

[123]   Ozgur Balli, Haydar Aras, and Arif Hepbasli. "Exergoeconomic analysis of a combined heat and power (CHP) system". In: *International Journal of Energy Research* 32.4 (2008), pp. 273–289. DOI: 10.1002/er.1353.

[124]   Hadi Ganjehsarabi, Ali Güngör, and Ibrahim Dincer. "Exergoeconomic evaluation of a geothermal power plant". In: *International Journal of Exergy* 14.3 (2014), p. 303. ISSN: 1742-8297. DOI: 10.1504/IJEX.2014.061030.

[125]   Adrian Bejan, George Tsatsaronis, and Michael J. Moran. *Thermal design and optimization.* A Wiley-Interscience publication. New York: Wiley, 1996. ISBN: 0-471-58467-3. URL: http://www.loc.gov/catdir/description/wiley032/95012071.html.

[126]   M. A. Murmura and M. Sheintuch. "Permeance inhibition of Pd-based membranes by competitive adsorption of CO: Membrane size effects and first principles predictions". In: *Chemical Engineering Journal* 347 (2018), pp. 301–312. ISSN: 13858947. DOI: 10.1016/j.cej.2018.04.072.

[127]   Raúl Sanz et al. "H2 production via water gas shift in a composite Pd membrane reactor prepared by the pore-plating method". In: *International Journal of Hydrogen Energy* 39.9 (2014), pp. 4739–4748. ISSN: 03603199. DOI: 10.1016/j.ijhydene.2013.12.145.

[128]   V. Spallina et al. "Techno-economic assessment of membrane assisted fluidized bed reactors for pure H 2 production with CO 2 capture". In: *Energy Conversion and Management* 120 (2016), pp. 257–273. ISSN: 01968904. DOI: 10.1016/j.enconman.2016.04.073.

[129]   Ekain Fernandez et al. "Preparation and characterization of metallic supported thin Pd–Ag membranes for hydrogen separation". In: *Chemical Engineering Journal* 305 (2016), pp. 182–190. ISSN: 13858947. DOI: 10.1016/j.cej.2015.09.119.

[130]   Ekain Fernandez et al. "Development of thin Pd–Ag supported membranes for fluidized bed membrane reactors including WGS related gases". In: *International Journal of Hydrogen Energy* 40.8 (2015), pp. 3506–3519. ISSN: 03603199. DOI: 10.1016/j.ijhydene.2014.08.074.

[131]   Jose Antonio Medrano et al. "Pd-based metallic supported membranes: High-temperature stability and fluidized bed reactor testing". In: *International Journal of Hydrogen Energy* 41.20 (2016), pp. 8706–8718. ISSN: 03603199. DOI: 10.1016/j.ijhydene.2015.10.094.

[132]   George Tsatsaronis. "Thermoeconomic analysis and optimization of energy systems". In: *Progress in Energy and Combustion Science* 19.3 (1993), pp. 227–257. ISSN: 03601285. DOI: 10.1016/0360-1285(93)90016-8.

[133]   Richard Turton et al. *Analysis, Synthesis and Design of Chemical Processes, Third Edition.* 3rd. ed. 2009.

[134]   Max Peters, Klaus Timmerhaus, and Ronald West. *Plant Design and Economics for Chemical Engineers.* 2003.

[135]   *Chemical Engineering.* URL: https://www.chemengonline.com/pci.

[136]   Silvio de Oliveira Junior. *Exergy: Production, Cost and Renewability.* Green Energy and Technology. London: Springer, 2013. ISBN: 978-1-4471-4164-8.

[137]   C. Kost et al. *Stromgestehungskosten Erneuerbare Energien: März 2018.* 2018. URL: https://www.ise.fraunhofer.de/content/dam/ise/de/documents/publications/studies/DE2018_ISE_Studie_Stromgestehungskosten_Erneuerbare_Energien.pdf.

[138]   S. Werner. *European District Heating Price Series.* Ed. by Energiforsk AB. 2016.

[139]   W. Stanek, Szargut J., and S. Usón. *Thermodynamics for Sustainable Management of Natural Resources.* Green Energy and Technology. Cham: Springer International Publishing, 2017. ISBN: 978-3-319-48649-9. URL: https://ebookcentral.proquest.com/lib/gbv/detail.action?docID=4866519.

[140]   A. Saltelli, M. Ratto, and T. Andres. *Global Sensitivity Analysis. The Primer.* 2008.

[141]   Will Usher et al. *Salib/Salib: Launch!* 2016. DOI: 10.5281/zenodo.160164.

[142]   J. Morio. "Global and local sensitivity analysis methods for a physical system". In: *European Journal of Physics* 32 (2011), pp. 1577–1583.

[143]   Robin Smith. *Chemical process design and integration.* Chichester, West Sussex: Wiley, 2005. ISBN: 0-471-48680-9. URL: http://www.loc.gov/catdir/description/wiley042/2004014695.html.

[144]   ASUE e.V. *BHKW-Kenndaten 2011: Module, Anbieter, Kosten.* Ed. by ASUE e.V. 2011.

[145]   Richard Turton et al. *Analysis, synthesis, and design of chemical processes.* 4th ed. Prentice Hall international series in the physical and chemical engineering sciences. Upper Saddle River, NJ: Prentice Hall, 2012. ISBN: 978-0-13-261812-0. URL: http://proquest.tech.safaribooksonline.de/9780132618724.

[146]   Amna Abdeljaoued et al. "Simulation and experimental results of a PSA process for production of hydrogen used in fuel cells". In: *Journal of Environmental Chemical Engineering* 6.1 (2018), pp. 338–355. ISSN: 22133437. DOI: 10.1016/j.jece.2017.12.010.

[147]   Francisco A. Da Silva, José A. Silva, and Alírio E. Rodrigues. "A General Package for the Simulation of Cyclic Adsorption Processes". In: *Adsorption* 5.3 (1999), pp. 229–244. ISSN: 0929-5607. DOI: 10.1023/A:1008974908427.

[148] Jaeyoung Yang, Chang-Ha Lee, and Jay-Woo Chang. "Separation of Hydrogen Mixtures by a Two-Bed Pressure Swing Adsorption Process Using Zeolite 5A". In: *Industrial & Engineering Chemistry Research* 36.7 (1997), pp. 2789–2798. ISSN: 0888-5885. DOI: 10.1021/ie960728h.

[149] J. O. Abe et al. "Hydrogen energy, economy and storage: Review and recommendation". In: *International Journal of Hydrogen Energy* 44.29 (2019), pp. 15072–15086. ISSN: 03603199. DOI: 10.1016/j.ijhydene.2019.04.068.

[150] Charlotte Rudolph et al. "Low-calorific ammonia containing off-gas mixture: Modelling the conversion in HCCI engines". In: *Combustion and Flame* (2022), p. 112063. ISSN: 00102180. DOI: 10.1016/j.combustflame.2022.112063.

[151] Donglai Mao et al. "Metal organic frameworks for hydrogen purification". In: *International Journal of Hydrogen Energy* 46.45 (2021), pp. 23380–23405. ISSN: 03603199. DOI: 10.1016/j.ijhydene.2020.12.181.

[152] Dominik Freund and Burak Atakan. "Surrogate model development for hydrogen separation via pressure swing adsorption processes: selection and evaluation of machine learning algorithms". In: *engrXiv* (2022). DOI: 10.31224/2372.

[153] Sol Ahn et al. "Layered two- and four-bed PSA processes for H2 recovery from coal gas". In: *Chemical Engineering Science* 68.1 (2012), pp. 413–423. ISSN: 00092509. DOI: 10.1016/j.ces.2011.09.053.

[154] María Yáñez et al. "PSA purification of waste hydrogen from ammonia plants to fuel cell grade". In: *Separation and Purification Technology* 240 (2020), p. 116334. ISSN: 13835866. DOI: 10.1016/j.seppur.2019.116334.

[155] Dong-Kyu Moon, Dong-Geun Lee, and Chang-Ha Lee. "H2 pressure swing adsorption for high pressure syngas from an integrated gasification combined cycle with a carbon capture process". In: *Applied Energy* 183 (2016), pp. 760–774. ISSN: 03062619. DOI: 10.1016/j.apenergy.2016.09.038.

[156] Mengjing Yu et al. "Combined Hydrogen, Heat and Power (CHHP) pilot plant design". In: *International Journal of Hydrogen Energy* 38.12 (2013), pp. 4881–4888. ISSN: 03603199. DOI: 10.1016/j.ijhydene.2013.02.006.

[157] Dominik Freund, Christoph Horn, and Burak Atakan. "Fuel-Rich Natural Gas Conversion in HCCI Engines with Ozone and Dimethyl Ether as Ignition Promoters: A Kinetic and Exergetic Analysis". In: *Active Flow and Combustion Control 2021*. Ed. by Rudibert King and Dieter Peitsch. Vol. 152. Notes on Numerical Fluid Mechanics and Multidisciplinary Design. Cham: Springer International Publishing, 2022, pp. 47–65. ISBN: 978-3-030-90726-6. DOI: 10.1007/978-3-030-90727-3{\textunderscore}4.

[158] F. Pedregosa et al. "Scikit-learn: Machine Learning in Python". In: *Journal of Machine Learning Research* 12 (2011), pp. 2825–2830.

[159] F. Pedregosa et al. *A random forest regressor*. URL: https://scikit-learn.org/stable/modules/generated/sklearn.ensemble.RandomForestRegressor.html.

[160] Mahler Advanced Gas Systems GmbH. *Gas Generation and Purification*. 2021. URL: https://www.mahler-ags.com/wp-content/uploads/2021/09/Mahler_AGS_Broschuere_0920_A4_view.pdf.

[161] Abdulrahman Alraeesi and Tracy Gardner. "Assessment of Sieverts Law Assumptions and 'n' Values in Palladium Membranes: Experimental and Theoretical Analyses". In: *Membranes* 11.10 (2021). ISSN: 2077-0375. DOI: 10.3390/membranes11100778.

[162] Oluwafemi Omoniyi et al. "Hydrogen Gas Quality for Gas Network Injection: State of the Art of Three Hydrogen Production Methods". In: *Processes* 9.6 (2021), p. 1056. DOI: 10.3390/pr9061056.

[163] Habib Gurbuz. "The effect of H2 purity on the combustion, performance, emissions and energy costs in an SI engine". In: *Thermal Science* 24.1 Part A (2020), pp. 37–49. ISSN: 0354-9836. DOI: 10.2298/TSCI180705315G.

[164] Dominik Schröder and Burak Atakan. "Theoretische Untersuchung der Umsetzung von Biogasen in HCCI-Motoren zur Erzeugung von Synthesegas". In: *29. Deutscher Flammentag* 17.-18.09.2019, Bochum (2019).

[165] A. Carrara, A. Perdichizzi, and G. Barigozzi. "Simulation of an hydrogen production steam reforming industrial plant for energetic performance prediction". In: *International Journal of Hydrogen Energy* 35.8 (2010), pp. 3499–3508. ISSN: 03603199. DOI: 10.1016/j.ijhydene.2009.12.156.

[166] Kenneth Bruninx and Marten Ovaere. "COVID-19, Green Deal and recovery plan permanently change emissions and prices in EU ETS Phase IV". In: *Nature communications* 13.1 (2022), p. 1165. DOI: 10.1038/s41467-022-28398-2.

[167] Martin Roeb et al. *Wasserstoff als ein Fundament der Energiewende: Teil 1: Technologien und Perspektiven für eine nachhaltige und ökonomische Wasserstoffversorgung*. Ed. by Deutsches Zentrum für Luft- und Raumfahrt. 2022. URL: https://www.dlr.de/content/en/downloads/2020/hydrogen-research-study-part-1.pdf.

[168] Chemical Engineering. *The Chemical Engineering Plant Cost Index*. URL: https://www.chemengonline.com/pci.

[169] Gavin Towler. *Chemical engineering design: Principles, practice, and economics of plant and process design*. 2nd ed (Online-Ausg.) Oxford and Waltham, MA: Butterworth-Heinemann, 2012. ISBN: 978-0-0809-6659-5. URL: http://site.ebrary.com/lib/alltitles/Doc?id=10562149.

[170] A2Z Ozone Company. *S-Series Industrial Ozone Generators*. 2021. URL: https://www.a2zozone.com/collections/commercial.

[171] C. Hamelinck et al. "Production of FT transportation fuels from biomass; technical options, process analysis and optimisation, and development potential". In: *Energy* 29.11 (2004), pp. 1743–1771. ISSN: 03605442. DOI: 10. 1016/j.energy.2004.01.002.

[172] Federal Reserve Bank of St. Louis. *Global price of Natural gas, EU*. URL: https://fred.stlouisfed.org/series/PNGASEUUSDM.

[173] European Union. *Eurostat: statistics explained*. URL: https://ec.europa. eu/eurostat/statistics-explained/index.php?title=Natural_gas_ price_statistics#Natural_gas_prices_for_non-household_consumers.

[174] Boqiang Lin and Chongchong Zhang. "Forecasting carbon price in the European carbon market: The role of structural changes". In: *Process Safety and Environmental Protection* 166 (2022), pp. 341–354. ISSN: 09575820. DOI: 10.1016/j.psep.2022.08.011.

[175] World Bioenergy Association. *Global Bioenergy Statistics 2021*. 2021. URL: https://www.worldbioenergy.org/uploads/211214%20WBA%20GBS% 202021.pdf.

[176] R. Rajkumar and C. Kurinjimalar. "Food wastes/residues: Valuable source of energy in circular economy". In: *Handbook of Biofuels*. Elsevier, 2022, pp. 147–163. ISBN: 9780128228104. DOI: 10.1016/B978-0-12-822810- 4.00007-5.

[177] Jacob A. Moulijn, Michiel Makkee, and Annelies E. van Diepen. *Chemical process technology*. 2. ed. Chichester: Wiley, 2013. ISBN: 9781444320244.

[178] Richa Kothari, D. Buddhi, and R. L. Sawhney. "Comparison of environmental and economic aspects of various hydrogen production methods". In: *Renewable and Sustainable Energy Reviews* 12.2 (2008), pp. 553–563. ISSN: 13640321. DOI: 10.1016/j.rser.2006.07.012.

[179] Ibrahim Dincer and Canan Acar. "Review and evaluation of hydrogen production methods for better sustainability". In: *International Journal of Hydrogen Energy* 40.34 (2015), pp. 11094–11111. ISSN: 03603199. DOI: 10.1016/ j.ijhydene.2014.12.035.

[180] Nicolas Abatzoglou and Steve Boivin. "A review of biogas purification processes". In: *Biofuels, Bioproducts and Biorefining* 3.1 (2009), pp. 42–71. ISSN: 1932104X. DOI: 10.1002/bbb.117.

[181] N. P. Komninos and C. D. Rakopoulos. "Modeling HCCI combustion of biofuels: A review". In: *Renewable and Sustainable Energy Reviews* 16.3 (2012), pp. 1588–1610. ISSN: 13640321. DOI: 10.1016/j.rser.2011.11.026.

[182] Jaqueline Daniel-Gromke et al. "Current Developments in Production and Utilization of Biogas and Biomethane in Germany". In: *Chemie Ingenieur Technik* 90.1-2 (2018), pp. 17–35. ISSN: 0009286X. DOI: 10.1002/cite. 201700077.

[183]   Hessamodin Nourbakhsh et al. "A thermodynamic analysis of biogas partial oxidation to synthesis gas with emphasis on soot formation". In: *International Journal of Hydrogen Energy* 43.33 (2018), pp. 15703–15719. ISSN: 03603199. DOI: 10.1016/j.ijhydene.2018.06.134.

[184]   Iván D. Bedoya et al. "Exploring Strategies for Reducing High Intake Temperature Requirements and Allowing Optimal Operational Conditions in a Biogas Fueled HCCI Engine for Power Generation". In: *Journal of Engineering for Gas Turbines and Power* 134.7 (2012), p. 072806. ISSN: 07424795. DOI: 10.1115/1.4006075.

[185]   Iván D. Bedoya et al. "Experimental evaluation of strategies to increase the operating range of a biogas-fueled HCCI engine for power generation". In: *Applied Energy* 97 (2012), pp. 618–629. ISSN: 03062619. DOI: 10.1016/j.apenergy.2012.01.008.

[186]   Iván D. Bedoya et al. "Experimental study of biogas combustion in an HCCI engine for power generation with high indicated efficiency and ultra-low NOx emissions". In: *Energy Conversion and Management* 53.1 (2012), pp. 154–162. ISSN: 01968904. DOI: 10.1016/j.enconman.2011.08.016.

[187]   Darko Kozarac et al. "Experimental and numerical analysis of the performance and exhaust gas emissions of a biogas/n-heptane fueled HCCI engine". In: *Energy* 115 (2016), pp. 180–193. ISSN: 03605442. DOI: 10.1016/j.energy.2016.08.055.

[188]   A. M. Starik, A. N. Korobov, and N. S. Titova. "Combustion improvement in HCCI engine operating on synthesis gas via addition of ozone or excited oxygen molecules to the charge: Modeling study". In: *International Journal of Hydrogen Energy* 42.15 (2017), pp. 10475–10484. ISSN: 03603199. DOI: 10.1016/j.ijhydene.2017.01.179.

[189]   MTU Onsite Energy. *Data sheet "S 400, 50 Hz, Natural Gas"*. URL: https://www.mtuonsiteenergy.com/fileadmin/fm-dam/mtu_onsite_energy/media-all-site/pdf/en/data-sheet/3232571_OE_spec_GN_400_400V_50Hz_1_16.pdf.

[190]   Tadeusz Jozef Kotas. *The exergy method of thermal plant analysis*. Reprint ed. with corr. and new app. G. Malabar, FL: Krieger Pub, 1995. ISBN: 0-89464-941-8.

[191]   Magdalena Mosinska, Malgorzata I. Szynkowska, and Pawel Mierczynski. "Oxy-Steam Reforming of Natural Gas on Ni Catalysts—A Minireview". In: *Catalysts* 10.8 (2020), p. 896. DOI: 10.3390/catal10080896.

[192]   Vasudev Pralhad Haribal et al. "Intensification of Ethylene Production from Naphtha via a Redox Oxy-Cracking Scheme: Process Simulations and Analysis". In: *Engineering* 4.5 (2018), pp. 714–721. ISSN: 20958099. DOI: 10.1016/j.eng.2018.08.001.

[193]   Ilenia Rossetti, Antonio Tripodi, and Gianguido Ramis. "Hydrogen, ethylene and power production from bioethanol: Ready for the renewable market?" In: *International Journal of Hydrogen Energy* 45.17 (2020), pp. 10292–10303. ISSN: 03603199. DOI: 10.1016/j.ijhydene.2019.07.201.

[194]   Steven Wang et al. "Pyrolysis of Natural Gas: Effects of Process Variables and Reactor Materials on the Product Gas Composition". In: *Chemical Engineering & Technology* 42.3 (2019), pp. 690–698. ISSN: 0930-7516. DOI: 10.1002/ceat.201800267.

[195]   Hiroyuki Yamada, Masataka Yoshii, and Atsumu Tezaki. "Chemical mechanistic analysis of additive effects in homogeneous charge compression ignition of dimethyl ether". In: *Proceedings of the Combustion Institute* 30.2 (2005), pp. 2773–2780. ISSN: 15407489. DOI: 10.1016/j.proci.2004.08.253.

DuEPublico

Duisburg-Essen Publications online